Electret Filters,

Production and Properties

1999

Electret Filters, Production and Properties

Proceedings of the International Workshop on Electret Filters, Production and Properties, Warsaw, Poland, January 29 and 30, 1999.

Edited by

J. Ian T. Stenhouse
Loughborough University
Loughborough, Leics., United Kingdom

L. Gradoń
TU Warsaw
Warsaw, Poland

J.C.M. Marijnissen
TU Delft
Delft, the Netherlands

Delft University Press/ 1999

Published and distributed by:

Delft University Press
P.O. Box 98
2600 MG Delft
The Netherlands
Telephone: +31 15 278 3254
Telefax: +31 15 278 1661
E-mail: DUP@DUP.TUDelft.nl

Lay-out: Marco Houben, Rotterdam

ISBN 90-407-1986-1

Printed in The Netherlands

TABLE OF CONTENTS

FOREWORD

Filtration in fibrous filtering structures is a process extensively used to remove suspended particulate matter from a gas stream. Rational design of the filtration process should be based on reliable prediction of the effluent concentration and pressure drop for a given set of operating conditions. Moreover, both of these main filter parameters vary in time when a fibrous structure becomes more and more loaded with deposits. Usually, fibrous filters with a very high porosity can assure a long life-time for a given level of pressure drop and filtration efficiency and therefore the basic issue is an improvement of the clean filter characteristics, that is an increase of filtration efficiency maintaining a low pressure drop. One of the promising methods is an application of electret fibers in the filter structure.

Electret fibers have a „built-in" electric charge and they preserve this charge for a very long time. Due to the electret characteristics of the fibers, additional forces of electrical nature act between them and particles. The collection of submicron particles is considerably improved. Efficient and highly porous electret filters of low flow resistance are preferably used in respirators, clean room filters and ventilating systems.

To stimulate an interdisciplinary discussion, Warsaw University of Technology (Prof.dr.L.Gradoń) and Delft University of Technology (Dr.ir.J.C.M.Marijnissen) organised a Workshop on „Aerosol Filtration in Electret Fibrous Structures". The Workshop was held in the historical Jablonna Palace near Warsaw, Poland, January 28-30, 1999.

This Workshop tried to bring together different disciplines to get a complete view of electret formation, nonsteady-state filtration in electret filters, filter testing and industrial application of electrets. All this information is necessary to produce optimal structures of filters.

This book contains the proceedings of the Workshop, and it includes an additional discussion on the application of biodegradable polymers for fibrous filters formation.

Leon Gradoń, Warsaw University of Technology, the Workshop Chairman

INTRODUCTION

The Workshop "ELECTRET FILTERS, PRODUCTION AND PROPERTIES", was held at the Jablonna Palace, Warsaw, Poland during January 29 and 30, 1999. It was sponsored by Warsaw University of Technology (TU Warsaw), Delft University of Technology (TU Delft), the Gesellschaft fuer Aerosolforschung (GaeF) and 3M Filtrete B.V..

Professor Leon Gradoń of the TU Warsaw was Host and Chairman; the Co-Chairman was Dr. Jan Marijnissen of the TU Delft.

Preface

During the 29th and 30th of January 1999 a group of experts in the fields of filtration and electric charge met in Warsaw at a workshop dealing with the state of the art in the field of electorate filters and electrically enhanced fibrous filtration. Both detailed presentations of new work and reviews were presented and interdisciplinary discussions were held. The theoretical background, methods of production, applications and efficiency measurement were discussed. Proposals for future work were formulated. The workshop is actually the second "Jablonna" meeting, organized by Professor Gradoń ,TU Warsaw and Dr. Marijnissen, TU Delft. The first workshop, on "Aerosol inhalation, lung transport, and deposition and the relation to the environment", was held from September 14 to 16, 1995. This was also a collaborative project between the TU Delft and TU Warsaw.

Genius Loci

The venue for the first workshop, Jablonna Palace near Warsaw in Poland, was so good that it was chosen again for this meeting. In fact the organizers hope that this will be the second of a longer series. A further reason for the location was the proximity to Professor Gradoń's group, which is one of the leading groups on the fundamentals and production of fibrous filters.

Presentations

The opening and welcoming remarks were made by Professor Gradoń and the first presentation was from the inventor of the electret filter, Professor Jan van Turnhout (TU Delft). He gave a bird's eye view of the history and possible future of electret filters.
After this very interesting overview lecture, the presentations could be clearly separated into the following categories: Fundamentals, Production, Applications and Measurements.
The production of permanently charged fibrous filters was considered both from industrial and innovative research perspectives. 3M produces large amounts of electret fibers and filters. The manufacture of the media and some applications which include its use in respirators and medical filters, vacuum cleaners, cabin air filters and filters for improving indoor air quality were described (O. Kievit). In another presentation the manufacture of tribo-electric filters was clearly described (R. Brown). After these already well-established production techniques some new techniques to produce permanently charged fibers for filters were reported: Melt-blown technology for fiber/filter production (T. Ciach and L. Gradoń) and the production of highly charged fibers by electro hydrodynamic atomization (K.B. Geerse and J.C.M. Marijnissen) was described.

The measurement of electret filter efficiency was illustrated from different perspectives. From an industial point of view, 3M showed how they perform efficiency measurements (G Bostock). A more generic and fundamental approach was presented (I. Stenhouse) as were optical and electrostatic measurements of filtration efficiency (W. Szymanski).
A presentation on the influence of particle shape on penetration through fibrous filters (I.L. Tuinman) was made. There was also a more fundamental approach as in the presentation on the efficiency of electrically enhanced filters as a function of loading (D.C. Walsh). This brings us automatically to the presentations of fundamentals. Here different aspects of electrically enhanced filtration were considered, such as the filtration mechanisms, charging of the fibers (H. Fissan and G. Kreis), modeling of the processes (A. Podgorski) and the charging of the aerosol particles (A. Schmidt Ott). One presentation even discussed methods of surface modification of polymer products (W. Fabianowski).
The rest of the papers could be grouped under applications and Other Technical Considerations. A very direct and interesting application is electret filters in face masks (G. Bostock). Under this last item, the following papers can also be categorized: Problems related to regenerable filters (H.J. Rembor), electrified filtration (F. Jordan and H, Fissan) and the measurement of corona discharge aerosols with an Electrical Aerosol Spectrometer (A. Mirme). The workshop finished with a round table discussion on Biodegradable polymers for filter production which was introduced by T.Ciach and G.Rokicki.

Discussion

After each presentation there was a discussion, which was recorded by one of the participants. These discussions are summarized and included in the end of this book.

The papers presented in this book, as well as opinions formed in the discussions, have contributed greatly to the understanding of the field of electrically enhanced filtration. Topics that still need further research also became clear. Finally, the effect of being together socially, the superb Polish hospitality and organization, the beautiful and comfortable Jablonna Palace, all contributed to the excellent atmosphere of this workshop.

Leon Gradoń
Jan C.M. Marijnissen
J.Ian T.Stenhouse

Electret Filters,

Production and Properties

1999

Production and Applications of Split Fibre Electret Filters

O. Kievit
3M Filtrete, European Filtration Products Laboratory
PO Box 2004, 4800 CA Breda, THE NETHERLANDS

KEYWORDS

electret fibrous filter nonwoven

INTRODUCTION

Electrets are either dielectrets or non-conductors containing permanent charges, or dielectrics with a charge polarisation. They have been around for quite some time already, and are used in applications like fibrous filters, microphones, loudspeakers and dosimeters. In 1974, a Dutch patent application was filed by Van Turnhout (NL7403975), suggesting the use of electret fibres in air filtration. The technology described in this patent application forms the basis for the process according to which the Filtrete™ air filter media are manufactured. Although developed 25 years ago, the basic process is still unchanged. This paper will describe how the Filtrete™ air filter media is made, and touch on some of its applications.

ELECTROSTATIC FILTRATION

What makes Filtrete™ air filter media so special? The answer has two main elements: one is that it contains electret fibres, the other is that these fibres are very effective due to their rectangular shape and high charge level (Lathrache et al., 1986).

Fibrous filters capture particles in several ways (Brown, 1993). The process of filtration has been studied extensively, and one can distinguish the following mechanisms:

- sieving
- impaction
- interception
- diffusion

These mechanisms are well-known and active in every fibrous filter. *Sieving* takes place when a particle is larger than the open spaces between the fibres (pores). *Impaction* takes place when a particle is unable to follow the air flow because of inertial effects, which may result in collision with the fibres. *Interception* is a capture mechanism that takes place when the distance between a stream line carrying a particle and the fibre surface is smaller than the particle radius. These three mechanisms dominate for relatively large particles (several micrometers in diameter). Smaller particles (sub-micrometer) are mainly captured by *diffusion*. This mechanism is caused by the Brownian motion of a particle, which makes it move about the flow lines. Due to this so-called random walk, particles may come in contact with the fibre surface and become captured. The listed capture mechanisms are all based on the mechanical properties of fibres and particles, and are thus referred to as mechanical filtration mechanisms. Their combined effect results in a fractional efficiency curve with a typical shape, as shown in Figure 1.

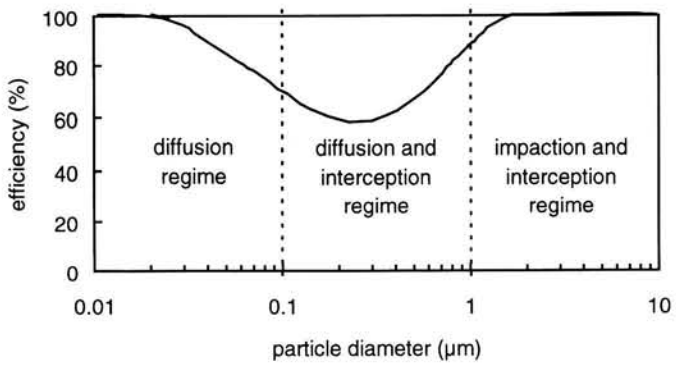

Figure 1. Typical fractional efficiency curve for a mechanical fibrous filter.

Because the effectiveness of the various collection mechanisms is dependent on particle size, the curve contains a minimum efficiency. This point - where the penetration is highest - is usually referred to as most penetrating particle size or MPPS. The MPPS is generally in the range from 0.1 to 0.3 μm.

In the case of Filtrete™ air filter media, the fibres are charged, as will be explained in detail in the next section. This creates additional capture mechanisms, as particles are attracted to the fibre surface due to *electrostatic forces*. The electrostatic mechanism is the combined result of *Coulomb forces* (charged particles are attracted to charged fibres) and *induced-dipole forces* (the electrostatic field around a charged fibre induces a dipole in an uncharged particle, causing it to be attracted towards the fibre). For uncharged fibres the *image force* plays a role (a charged particle induces charge separation in a neutral fibre), but this effect is generally negligible. The electrostatic mechanism greatly enhances the capture efficiency (especially for the smaller particles), without increasing the air flow resistance.

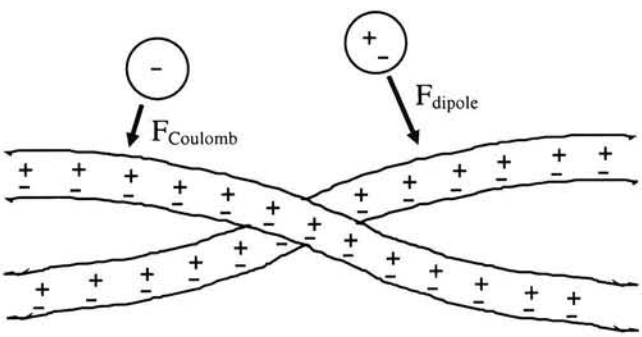

Figure 2. Filtrete™ air filter media contain bipolarly charged electret fibres.

Whereas some electret fibrous filters contain only charges of one polarity, the Filtrete™ air filter media are bipolarly charged. This implies that every fibre carries positive and negative charges, as is schematically shown in Figure 2. Therefore both positive and negative particles can be captured, as well as uncharged particles due to the induced dipole forces. Another advantage of the split fibre process is that it creates fibres with a rectangular cross-section, which results in a highly inhomogenous electrostatic field around the edges. Calculations show that an inhomogeneous field yields the highest capture efficiency.

MANUFACTURING PROCESS

The process for making the Filtrete™ air filtration media contains two steps. In the first step - the tow making - the electrostatically charged fibres are made. These fibres are made into a nonwoven in the second step: the web making. The complete process is schematically shown in Figure 3.

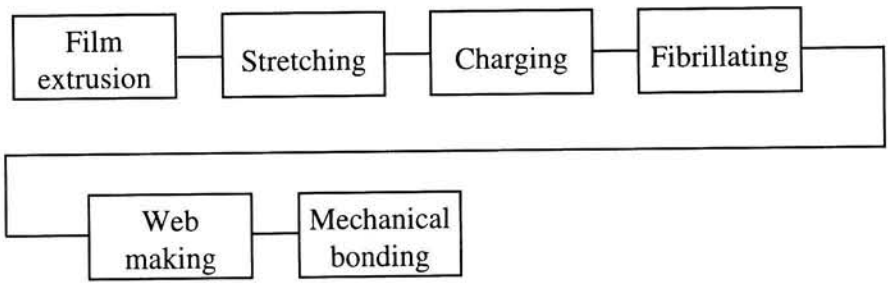

Figure 3. Schematic representation of the Filtrete™ air filtration media process.

The Filtrete™ air filter media are made from 100% pure polypropylene, which is first extruded into a film. This film is stretched, in order to reduce its thickness. Thinner fibres make a more efficient filter media. The stretching also introduces crystalline regions in the polymer, which makes it more susceptible for charging. The charging is done with corona wires, which inject both negative and positive charges deeply into the film. The next step in the process is cutting the film into a large number of fibrils of infinite length. This step is usually referred to as fibrillation, and the sliver or tow created in this way is wound on rolls and stored for further processing.

Before a web can be made out of the tow, this needs to be converted into individual fibres. This is achieved by cutting the tow into pieces of several centimetres, and opening these pieces of chopped tow by mechanical means. The fibres created in this way are fed to a carding machine, where they are airlaid into a nonwoven web. Optionally, the fibres can be combined with a supportive scrim to form a composite construction. The final step in the process is mechanical bonding (needle-punching) which increases the strength of the web.

APPLICATIONS

The electrostatic properties of the fibres Filtrete™ air filtration media result in significant performance benefits. In comparison to conventional mechanical filters, an electret filter has a much lower air flow resistance (pressure drop) for a given performance level. Alternatively, it is possible to achieve much higher efficiencies with an electret filter than with a mechanical filter with an equivalent pressure drop. An additional benefit relates to the loftiness of the Filtrete™ split fibre media. The extremely open structure of the media (solidity 5% or less) ensures that particles are captured throughout the entire depth of the material, which results in a significantly higher dust holding capacity. In practise this translates into an extended filter life, and reduced risk of early clogging.

The low resistance against air flow makes the Filtrete™ split fibre media especially suitable for application in respiratory protection. Nowadays there are several respirators on the market that contain the media, either as primary filtering media or as a prefilter for a second meltblown filter media layer. A related application is the breathing filter. Many hospitalised people depend on automatic breathing systems, which all have filters to prevent cross-contamination between patient and machine. The low pressure drop of an electret filter increases the comfort of the patient, while maintaining adequate protection.

Another successful product is the vacuum cleaner post filter. 3M Filtrete BV has been supplying virtually all major vacuum cleaner OEM's (original equipment manufacturers) with flat post filters for over 15 years now. The post filter cleans the air that is blown from the machine, and thus protects the person vacuuming from particles that originate from the motor or penetrate through the dust bag. A more recent development is the application of pleated filters in vacuum cleaners. A pleated filter has the advantage that it contains more filter media, which results in a lower air flow resistance and better performance.

One of the most important applications for the Filtrete™ air filtration media lies in the automotive industry. People driving in a car can be exposed to various pollutants present on the road, and special filters have been developed for their protection and comfort. Whereas in the beginning only the top models of the more prestigious brands were equipped with these so-called cabin air filters, it is nowadays a standard feature in practically every new car model. The top-line models are already one step further, as they combine the particle filtration media with an activated carbon component. The activated carbon adsorbs gases and vapours, which increases the comfort and safety of driver and passengers.

Finally, Filtrete™ air filtration media are applied for improving the quality of the indoor air. In the United States most houses have air conditioning units that bring fresh air inside. In addition to heating or cooling the air, these units also remove airborne particles with a built-in filter. These so-called furnace filters (Figure 4) are available in various grades, providing different performance levels. Alternatively, the indoor air quality can be improved by using a room air cleaner. This is a device that circulates air and contains some sort of filtering element to remove pollutants. In addition to ionisers and activated carbon elements, Filtrete™ air filtering media is very suitable for this application, as it combines a high particle removal efficiency with a low pressure drop. This will increase the effectiveness of the room air cleaner, by providing a higher Clean Air Delivery Rate (ANSI/AHAM AC-1-1998).

Figure 4. Example of a pleated furnace filter, containing 3M Filtrete™ air filtration media..

SUMMARY

The fibres of an electret filter are electrostatically charged. This makes the filter more efficient than conventional mechanical filters, without increasing the air flow resistance. Filtrete™ air filter media are made by extruding polypropylene into a film, which is consequently stretched and charged by corona. The film is fibrillated to form interconnected fibres of infinite length. The fibres are cut to and opened, and made into a nonwoven in an airlaid carding process. The web strength is increased by mechanical bonding. Applications of the Filtrete™ air filtration media include respirators and medical filters, vacuum cleaner post filters, cabin air filters, and filters for improving the indoor air quality.

REFERENCES

ANSI/AHAM (1988), Method for measuring performance of portable household electric cord-connected room air cleaners, *American National Standard*, ANSI/AHAM AC-1-1998.

Brown, R.C. (1993), *Air filtration*, Pergamon Press, Oxford.

Lathrache, R. and H. Fissan (1986), Enhancement of particle deposition in fibrous filters due to electrostatic effects: Part I, *Proc. 4th World Filtr. Congr.*, April 22-24, Ostend.

Van Turnhout, J. (1974), Werkwijze voor de vervaardiging van een vezelfilter, *Dutch Patent* 7403975

Melt-Blown Technology for Filter Production

Tomasz Ciach and Leon Gradoń
Warsaw Technological University Faculty of Chemical and Process Engineering
00-645 WARSAW, Warynskiego Street 1, POLAND, ciach@ichip.pw.edu.pl

KEYWORDS
electret fibres, melt-blown

INTRODUCTION

The growing needs of high quality products, modern technologies and better working environments necessitate the use of high efficiency filtration materials. A promising method of filter manufacture is melt-blown technology with electrical charging of fibres. The production of fibres by blowing melted polymer, was first described in a military laboratory report [1]. The method is simple and cheap because it is possible to produce non-woven filtering materials directly from the polymer in one step. Additional electrical charging of fibres can increase filtration efficiency of this material. An experimental rig for manufacturing melt-blown electret fibres was constructed. With this the effect of process parameters, such as air and polymer temperatures and flows, on fibre quality could be studied. The influence of those parameters on fibre diameter and filtering bed porosity were investigated and the results are presented here. The possibility of improving the filtration efficiency of melt-blown filters by charging fibres in a corona discharge field was also examined. A simple model of charging fibres in an external electric field is presented. Melt-blown technology provides the potential to manufacture filtering materials with controlled porosity, fibre diameter and fibre charge as a function of depth within the structure. Such a media could be optimised to give high filtration efficiency combined with a much longer lifetime.

MELT-BLOWN FILTER PRODUCTION RIG

A schematic of the rig for obtaining fibres by blowing melted polymer is shown as Figure 1. Granulated polymer is poured into container (1). It is then taken by the extrusion screw (2). The extruder is heated externally in three stages by an electric heater (3). The temperature in those three zones must be precisely controlled. The extruder screw is driven by an electric motor with a gear system (4). The screw rotation speed, which is of the order of a few revolutions per minute, is precisely controlled. Homogenised and melted polymer is pressed into the die. The die is heated and supplied with hot compressed air (6). Melted polymer, extruded through a row of nozzles, is extended by a stream of hot air and forms fibres. These are collected on the cylindrical receiver in a shape of a drum that rotates and moves to-and-fro. Filtering material is thus formed on the surface of this drum.

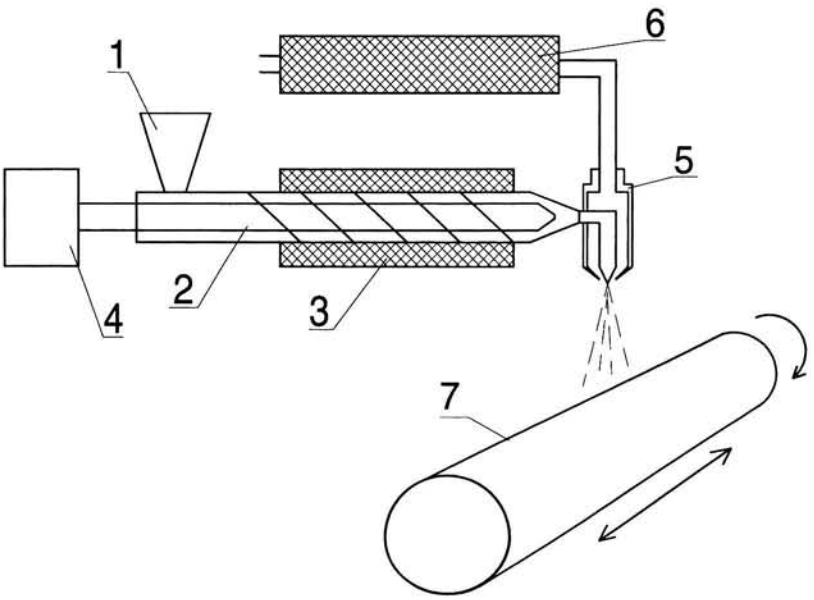

Figure 1.
Stand for melt-blow filters production.

The main problem of this technology is the design of the melt-blow die. It should be manufactured from high quality material and special attention must be paid to the design of the polymer flow channels. Any stagnation zones may cause carbonisation of polymer. A section of the die used in the experiments presented in this paper is shown in Figure 2.

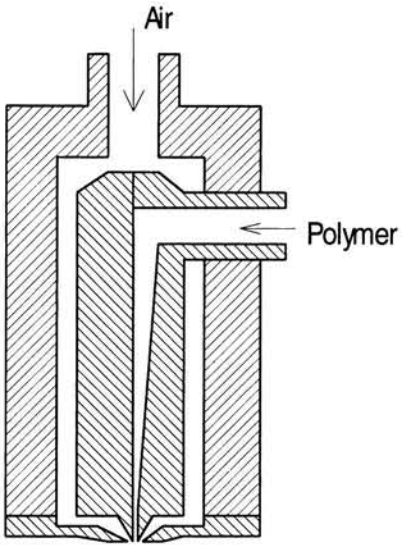

Figure 2.
Melt-blown die section.

The stability of the process is dependent on the properties of the polymer and the shape of the air nozzles. Errors in the design of this region of the die may affect the fibre forming process and droplets of liquid polymer formed under improper conditions can destroy the filtering material even making holes in it.

RESULTS OF EXPERIMENTS

A number of experiments have been carried out to measure the influence of the main process parameters on the geometrical form of fibres obtained from the above set-up. Parameters that were found to have the greatest influence on fibre diameter and filter porosity are:

Polymer flow
Temperature of polymer in the last heated section
Temperature of the die
Air flow
Temperature of the air
Distance between the die and the collecting drum

Fibre diameters were measured with an optical microscope with accuracy of 0.2 μm and are presented as arithmetical averages from ten measurements. The porosity of the fibrous structures was measured by weighting the fabric disk and measuring its geometrical dimensions. Results are presented as arithmetical averages from three measurements. Filtration efficiency was measured using an industrial standard Moore sodium chloride aerosol filter testing device.

The fibre diameter was found to be a function of air flow and air temperature as shown in Figure 3.

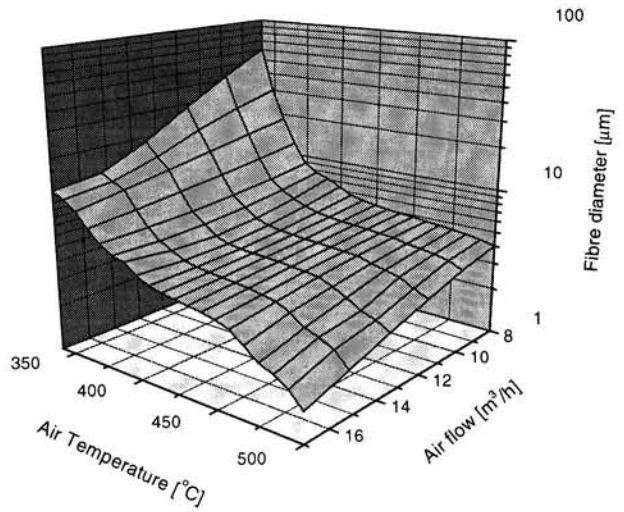

Figure 3. Fibre diameter as a function of air flow and air temperature.

As expected, fibre diameter decreased with increasing airflow. This is due to the higher drag force on the surface of the stretched polymer. Fibres are thinner when the air temperature is higher. This is because of decreasing polymer viscosity. Fibre diameter also decreases with decreasing of polymer flow. When very thin fibres should be obtained another problem appears. Fibres become very short and it is difficult to collect them on the drum. He smallest diameter of fibres that could be collected as a mat was about 0.8 μm.

Other important parameter of filtration material is its packing density. The value of this quantity is affected by most of process parameters. The influence of air temperature and airflow on packing density is presented in Figure 4.

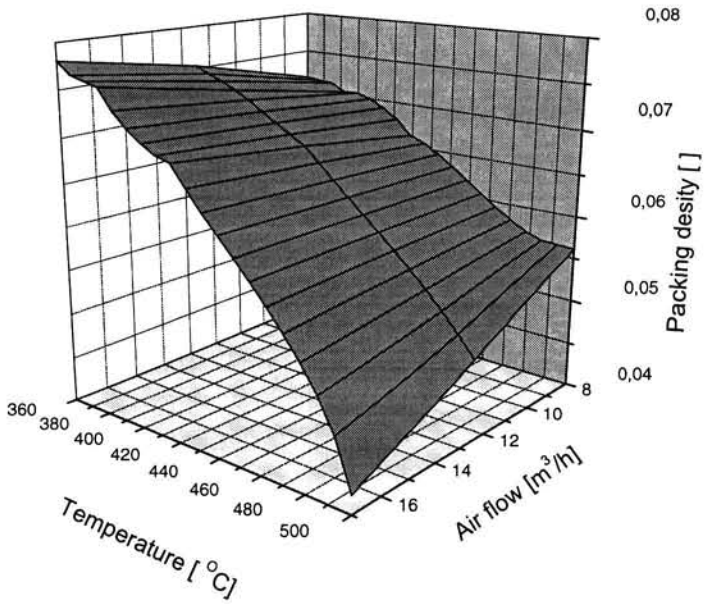

Figure 4.
Packing density as a function of airflow and temperature.

For lower temperatures, an increase in airflow causes an increase in packing density. A different situation occurs at high temperatures when the packing density decreases with airflow. This change is possibly caused by a decrease of fibre diameter at the high temperature. Thin fibres cool down quickly and become more rigid. Thicker fibres need more time to cool down, are more limp and form a better packed bed.

The distance between the die and collecting drum is a parameter which is easy to change and modify the packing density without influencing the fibre diameter. This is very important because it makes it possible to change packing density during filter production. This relation is shown in Figure 5.

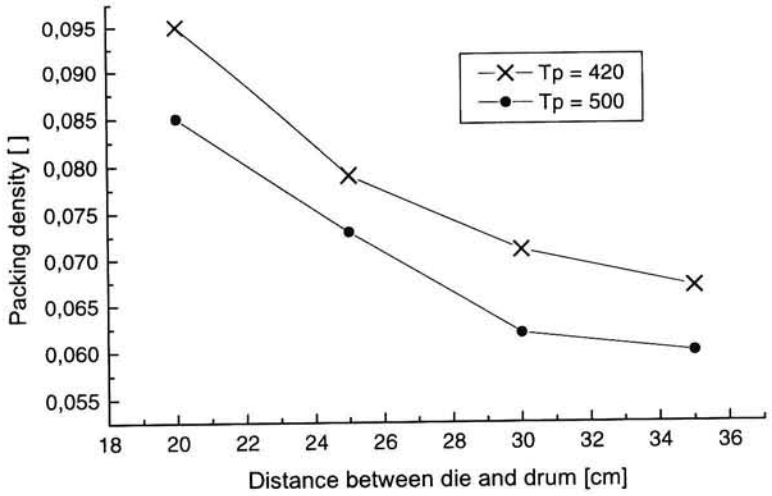

Figure 5.
Packing density as a function of the distance between the die and the drum for two air temperatures.

As can be seen, melt-blown technology makes it possible to obtain filtration materials with different porosities and different fibre diameters. A unique advantage of this technology is the production of structured media with controlled gradients of both porosity and fibre diameter. Such filters can have a high filtration efficiency combined with a long lifetime.

ELECTRICAL CHARGING OF FIBRES

Electrical filtration mechanisms have been applied to enhance the efficiency of melt blown filters. A schematic drawing of the method of using of corona discharge for fibre charging is shown in Figure 6.

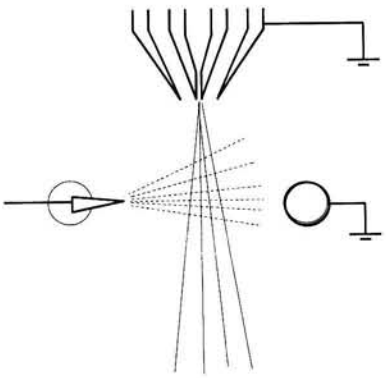

Figure 6.
Fibres charging in corona discharge.

The discharge electrode, on the left, emits electrons or ions in the direction of the earthed counter electrode and earthed die. Electrical charges pass through the stream of fibres and deposit on the liquid filaments of polymer. Then they are trapped inside a polymer structure. A schematic drawing of a fibre in an external electric field and in the stream of ions is shown in Figure 7.

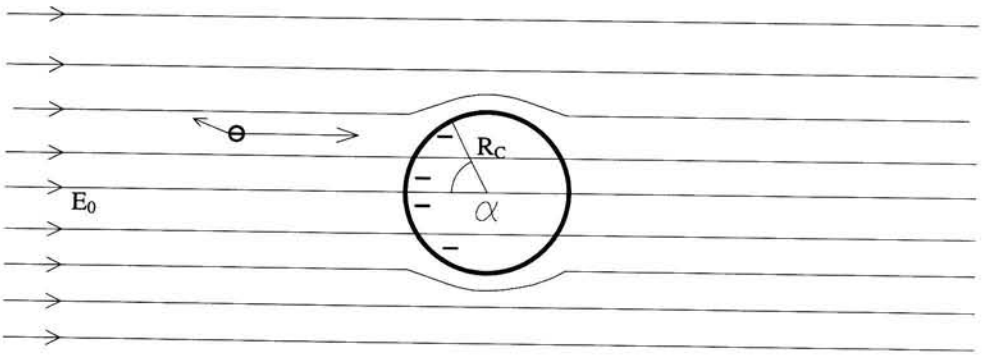

Figure 7.
Charging process of the fibre.

The external electric field is influenced by charges deposited on the fibre. For the conditions of melt blown fibre charging, electrical charges move very quickly compared with the fibre displacement rate. They are driven by two forces: external electric field and repulsive field of deposited charges. Those forces acting on the ion near fibre surface are shown in the Figure 8.

Fo – force of external field
Fe – repulsing force
F_D – resultant force

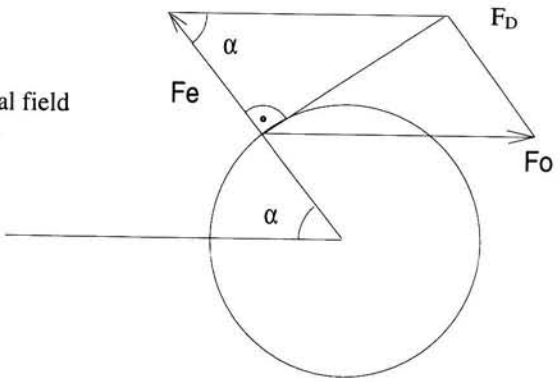

Figure 8.
Forces acting on the electrical charge near fibre surface.

The angle angle of escapement, α, defines the fraction of ion stream that will be deposited on the fibre. This angle can be calculated from Equation 1.

$$\cos(\alpha) = \frac{Fe}{Fo} = \frac{Q}{2 \cdot \pi \cdot \varepsilon_o \cdot R_C \cdot Eo} \tag{1}$$

Q – fibre charge [C/m]

The ion stream per unit length that is deposited on the fibre is expressed by the Equation 2.

$$q = 2 \cdot \sin(\alpha) \cdot Eo \cdot z_i \cdot n_i \cdot R \tag{2}$$

z_i – ion mobility $[m^2 V^{-1} s^{-1}]$
n_i – ion concentration $[m^{-3}]$
q – charge stream $[m^{-1} s^{-1}]$

The fibre charge at the saturation conditions can be expressed by the Equation 3.

$$Q = E_0 \cdot 2 \cdot \pi \cdot \varepsilon_o \cdot R \tag{3}$$

Fibre charge as a function of time can be calculated from Equation 4 and is shown as Equation 5.

$$\frac{dq}{dt} = \sin\left(\arccos\left(\frac{Q}{2\pi\varepsilon_o R E_O}\right)\right) E_O z_i n_i R \tag{4}$$

$$Q = 2\pi\varepsilon_o R E_O \sin\left(\pi - \frac{z_i n_i}{2\pi\varepsilon_o R} \cdot t\right) \tag{5}$$

The time needed for the fibre to obtain a saturation charge can be found from Equation 6.

$$t_S = \frac{\pi^2 \varepsilon_o R}{z_i n_i} \tag{6}$$

For our experimental conditions, at 25 kV corona voltage and 1 mA corona current, this time is very short ($1*10^{-28}$ s). For those conditions, the saturation charge on 3 μm fibres is $4*10^{-11}$C/m. It provides about $5*10^{-6}$ C per gram of polymer. The average value of fibre charge measured in a Faraday chamber for this condition is $0.2*10^{-6}$ C/g. This difference is probably due to charge lose from fibres on the conducting collector and also because of model simplification. Other reason is the attachment of supplementary charges to fibres.

At this point, we also should mention the fibre charge limit due to electrical breakdown of the surrounding media. This maximal charge density is given by Equation 7.

$$Q_C = 2 \cdot \pi \cdot \varepsilon_o \cdot R_C \cdot E_C \tag{7}$$

E_C – critical field intensity, for air has a value $3*10^6$ V/m

For a fibre of 3 μm diameter the maximum linear charge density is $2.5 * 10^{-10}$ C/m.

EXPERIMANTAL RESULTS OF FIBRE CHARGING ON FILTRATION

The filtration quality factor has been used for easy comparison of different filtration materials and to indicate the improvement due to fibre charging. Its definition is given by Equation 8.

$$QF = -\frac{\ln(P)}{\Delta p} \tag{8}$$

P – aerosol penetration

The influence of corona charging of fibres on the filter properties is shown in Figure 9. It is expressed as change of relative quality factor as a function of corona discharge current for different signs of corona and for alternating current at 50 Hz.

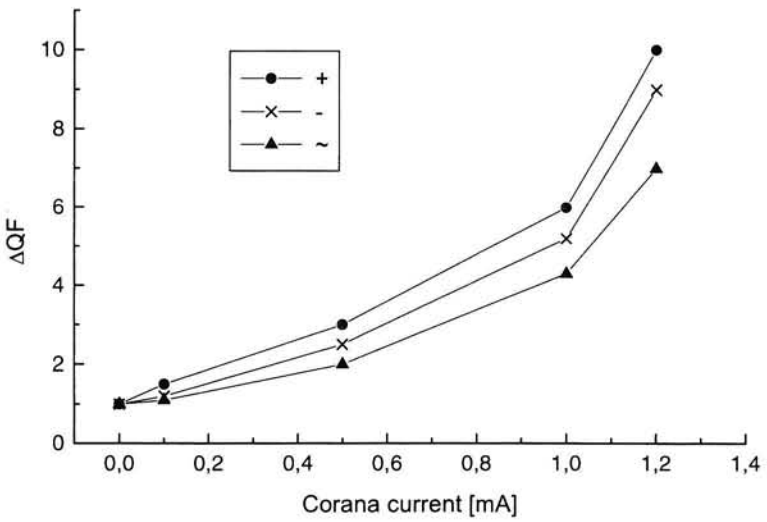

Figure 9.
Change of relative quality factor as a function of corona current.

The penetration was measured with NaCl aerosol particles of mass mean diameter of 0.6 μm using the Moore measurement system at a face velocity of 14 cm/s. Pressure drop was measured simultaneously. As can be seen, the use of alternating current gives the worst results. It is probably because the 50Hz frequency is too high for ions to move far enough. Both positive and negative discharge gives similar results. A very important parameter of the fibre charging procedure is the distance between the corona electrode and polymer nozzle. This is shown in the Figure 10.

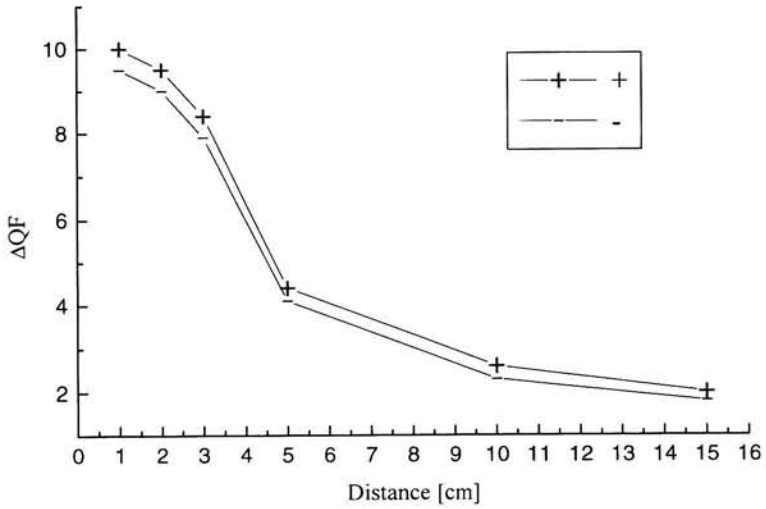

Figure 10.
Change of relative quality factor as a function of distance between corona electrode and polymer nozzle.

The improvement factor of filtration properties of electret fibres falls down with distance between corona electrode and polymer nozzle, despite the use of higher tension for longer distances. This strong dependence is probably because fibres cool down quickly and solidify. Electrical charges adsorbed on a solid polymer surface cannot penetrate easily into the polymer structure. They are weakly bounded to fibres and could be easily removed.

Penetration of electrical charges into fibres and strength of bonds that keep them inside the polymer structure determine the lifetime of the electrets. Charges usually kept in potential wells can be lost with time, especially at higher temperature or humidity. The process of degradation of melt blown electret filters in time, expressed as a change of filtering quality, is shown in Figure 11.

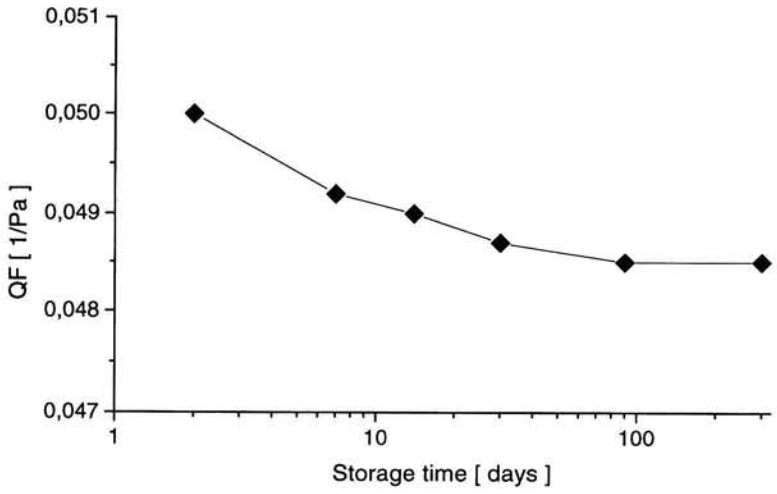

Figure 11
Change in quality factor as a function of storage time.

Changes in quality factor are not very significant and stabilise after three months of storage. It means that filters manufactured using the technology presented here can be stored for at least one year.

SUMMARY

Melt blown technology for electret filter production as presented above is very promising. This method facilitates the manufacture of filtration materials with controlled porosity, fibre diameter and fibre charge in depth within the structure of the filter. Such filtration systems can have much longer lifetimes [3]. Charges are well bounded in the polymer structure and filters can be stored for a long time without significant changes of their filtration properties.

REFERENCES

[1] Report NR 4364; Naval Research Laboratories 1954.

[2] T. Ciach, *Manufacture and Properties of Electret Filters*, **PhD Thesis**, Warsaw University of Technology, 1997.

[3] Podgórski A., Gradoń L., Rudziński M., *Non Steady-State Filtration of Aerosol Particles in the Elctret Filter Structures*. **Chem. Eng. Comm**,Vol151, 125-146, 1996.

Triboelectric Charging of Filters, and Charge Configuration

R C Brown[1] and P A Smith[2]

[1]Health and Safety Laboratory, Broad Lane, Sheffield S3 7HQ, UK; [2]Department of Textile Industries,The University, Leeds LS2 9JT, UK (present address: Unit 28, Newall Hall Park, Otley, LS21 2RD, UK)

KEYWORDS

Filter, electric charge, polymer

INTRODUCTION

The production of filter material carrying a permanent electric charge requires fibres that are made from a good insulator along with a means of charging them permanently. The charge is applied by means of corona discharge in the case of split-fibre electret material, by induction in the case of electrostatically-spun material or by triboelectrification in the case of mixed-fibre material or resin-wool material. A fourth method, that of freezing in of electric polarisation, is feasible but, unlike the other three processes, it is not used in commercially available filter material. Of the three charging mechanisms triboelectrification has the advantage that it can be put into effect by means of normal textile processing techniques; the other charging mechanisms require a high voltage source. The process of triboelectrification can be illustrated on a macroscopic level whereby efficient charging of many textile fibres can be demonstrated. The transfer of this to a microscopic level involves certain technical problems, but the result is a simple material of high filtration efficiency.

TRIBOELECTRIFICATION OF TEXTILE YARNS

The systematic exchange of charge between contacting metals is a process covered by elementary solid state physics (Kittel, 1966). However, when the metals are separated the charge returns to earth. The theory of charging of insulators is more complicated, but triboelectrification of amber rubbed with wool was known to the ancients. Amber is fossilised resin and this example of triboelectrification was almost duplicated in the development of the first electrostatic filter, the resin wool filter (Hansen, 1931; Feltham, 1979).

Since that time, however, the development of polymers has put better insulators at our disposal. Polymer fibres are widely used in textile manufacture, and their propensity to develop an electric charge is a phenonomen that textile scientists have for many years been doing their best to counteract. The normal means of doing this is the application of antistatic agents to the surface of the fibres. Polymer fibres are oleophilic and oily materials have a tendency to spread over the surface forming a very thin layer, which is sufficient to provide a conducting screen over any charge that the textile fibres may develop. If, however, this conducting screen is removed, the charging of the textile fibres can be observed and exploited in the production of a mixed-fibre triboelectrically charged filter material.

Tiriboelectric series

In the early development of the triboelectrically charged material a number of fibre samples of different chemical nature were cleaned and hand-spun into yarns. Short pieces of these were attached to stretchers rather similar to violin bows. In this form two samples of yarn could be rubbed against each other in such a way as to produce contact charge. The friction between the two yarns tended to twist the yarns and so ensure all round contact of the fibres. When this had been carried out the yarns were laid across an earthed plate and the probe of an electrometer was scanned across them. Typically the electrometer would indicate positive as the probe crossed one yarn and negative as it crossed the other. The charge was usually stable for a period of minutes or hours, but on certain occasions only one yarn developed a charge. It was concluded that the unchanged fibre developed a transient charge equal and opposite to that on its companion, for otherwise charge would not be conserved, but the charge leaked rapidly to earth because of the fibre conductivity. The results of experiments of this type enable the fibres to be ranked into a triboelectric series, in which fibres high in the table develop a positive charge when rubbed against fibres lower down. Most of the results obtained, shown in Table 1, were consistent, and there were no repeatable inconsistencies. The results can be compared with other published triboelectric series (Hersh, 1975). Complete agreement is not observed among all authors but this is probably because different fibres with the same generic name but from different sources may be slightly chemically different.

In further experiments yarns were rubbed against samples of various metals. In most instances the fibres developed a charge and in general wool and nylon tended to charge positively with respect to the metals and the other fibres tended to charge negatively. The response shown by the electrometer tended to be considerably smaller and it was assumed that the charge imparting property of the metal was rather lower than that of the fibres.

NATURE OF TRIBOELECTRIC CHARGE

Magnitude of charge

The absolute magnitude of the charge on yarns is difficult to measure, because once the yarn is removed from its stretchers it is strongly attracted to any surface in the vicinity. Rings were, therefore, attached to each end of the yarns, and these were then attached to the stretchers. After charging, the yarn along with the rings could be removed and then dropped into a Faraday ice pail so that an absolute measurement of charge could be made. A correction of the order of 7% had to be made for the rings themselves but it was possible to obtain a reasonable measure of the charge held by the yarns and to relate this to the surface area of the yam and to the breakdown charge that such a yarn could be expected to hold.

Breakdown charge in air is normally considered to be 27 $\mu C\ m^{-2}$. The electric field outside a charged cylindrical object is relatively short in range, and the dielectric strength of air over short distances is relatively high (Harper, 1967). A plot of the charge held by the yarns as a function of diameter is given, against the theoretical magnitude of charge that can be held at breakdown, in Fig. 1. Typically the yarns are able to hold about two thirds of their breakdown charge level.

Stability of charge

A measure of the lifetime of charge on the yarns can be made by charging a yarn, placing it on an earthed surface and then scanning it with an electrometer from time to time and observing the height of the pulse obtained. Although the charge measurement made in this way is not quantitative, the results give a good estimate of the relative charge held by the fibre over a period of time, and indicate a charge lifetime of several days.

TRIBOELECTRIFICATION ON A MICROSCOPIC SCALE

A common process, during textile manufacture for a range of purposes, is carding. During carding fibres are repeatedly combed by rotating drums covered with steel hooks so that a clumped structure is turned into a light and voluminous one with relatively aligned fibres, a fleece. The fleece can be attenuated into yarns which can be woven into textiles. Alternatively, the fleece can be punched with barbed needles which cause the fibres to entangle making the material much more compact and stronger. The resulting structure is known as a needle felt, and is particularly suitable for filter materials. During the carding process considerable contact takes place between the fibres and the material of the carding machine and also between different fibres. The process is also extremely effective in mixing the fibres. If fibres behave like yarns this means that there is much opportunity for triboelectrification to take place.

A large number of different fibre mixtures were carded and needled in this way and their filtration efficiency tested. In order to observe transient effects and short-lived charge, mobile filter test equipment was used to test the materials within two or three minutes of production. Most mixtures developed some electric charge which enhanced the filtration efficiency, but the charge was usually low and fugitive. At first it was thought that mixtures of materials remote in the triboelectric series would produce the best filters, but this was not observed. On the other hand mixtures containing fibres with chlorinated polymers produced filters that had a very high charge level, and filters,containing polypropylene had stable charge; in fact a stable (but low) charge was observed in a polypropylenc-stainless steel mixture. A different type of filter, containing a conductor and an insulator has also been produced (Brown and Blackford, 1983).

A mixture of modified acrylic and polypropylene fibre produced a filter material with a high and stable electric charge (Smith et al, 1988, 1993). The material is in commercial production and is used throughout the world. It exists under a number of different trade names and is made by a number of manufacturers.

ASYMMETRIC CHARGING

If two similar yarns are rubbed together in the symmetrical manner described above, no electric charge will develop. If, however, the yarns are rubbed in the way that a violin bow touches the string of the instrument, i.e a large area of bow contacts a small area of string, this symmetry is broken down and the development of electric charge is not precluded. Experiments have resulted in charge development, but no consistent pattern of magnitude or sign was observed. If, however, this charging process occurs during carding it should be

possible to produce a filter from one fibre type only. Experiments were carried out using the two components of the ideal mixture in different proportions, including the situation in which each was used separately. The filtration performance of these mixtures, measured shortly after production, is shown in Fig. 2. The penetration of a sodium chloride aerosol through the mixture, normalised to a constant area weight, is shown. Neutral material of this structure normally allows about 70% of a sodium chloride aerosol to penetrate. It can be seen that the initially most efficient filter is produced from a mixture of containing about 70% by weight of polypropylene, but since the polypropylene fibres were coarser, there would be approximately equal numbers of fibres of the two types. However, other mixtures also develop charge, as does each component taken separately. This can only be as a result of the asymmetric charging mentioned above. All of the mixtures lose some efficiency on standing but in the case of the polypropylene fibres the efficiency loss is small, in the case of the modified acrylic fibres the efficiency loss is almost complete.

CHARGE LIFETIME

Samples of material produced in the early stages of filter development have been stored for long periods in a laboratory cupboard. The filters were tested within minutes of production, again after a period of about one day and then at increasingly longer intervals, so that between ten and twelve tests were carried out over a period of approximately 14 years. Typical laboratory temperatures during working hours were of the order of 20^0 C and relative humidifies were of the order of 35%.

The results on three filters: A, B and C, which differ only in that A is the thickest and C the thinnest, are summarised in Fig.3, which is a log-log plot. Plotting penetration on a logarithmic scale is good practice because the logarithm of the penetration can be related to more fundamental characteristics like single fibre efficiency or layer efficiency (Brown, 1993), plotting time on a logarithmic scale is necessary because of the long time-scale involved. The filters show a common pattern of behaviour. There is a tendency for penetration to increase with time (apparent decreases are due to instrument behaviour) but this increase is much more rapid in the early stages of the exposure. In fact the fractional increase in penetration is greater in the first day than in the last decade. The reason for this is that the charge exists in bound states with a range of binding energies. The weakly bound charges are lost relatively rapidly whereas a considerably greater exposure is needed for removal of the more tightly bound charge. A simple interpretation of the data is that to give the filtration efficiency of new filters, old filters must be approximately 1.75 times their area weight. If the data in Fig 3 were extrapolated, the graphs would reach a penetration level indicative of the unchanged state only after several centuries.

CHARGE CONFIGURATION

In the simplest model of a triboelectrically charged filter all chemically identical fibres will charge with the same sign, positive in the case of polypropylene and negative in the case of its companion. However, the results above suggests that this can only be an approximation, and this is confirmed by observations. Lathrache (Private communication) scanned three fibres taken from the mixed fibre material and observed considerable spatial variation of charge, with two of the fibres predominately positively charged and the third negatively. At the time that the scans were carried out it was not possible to identify the fibres. However,

they were returned to our laboratory for analysis and when subjected to electron bombardment the presence of chlorine in the fibre that charged negatively indicated that it was modified acrylic. The absence of chlorine in the other two, which charged positively, indicated that these were polypropylene. These measurements therefore confirmed the general picture of triboelectric charging but indicated that the configuration of charge is not uniform.

Our observation showed that polypropylene fibres carded alone developed a charge and so it is very likely that some triboelectrification of split-fibre electret material occurs during carding, complicating the charge configuration. Electrostatically extruded material is normally extruded from an electrode of a single polarity, but Baumgartner et al (1985) scanned fibres from this material and found considerable spatial variation of charge. The charge of sign opposite to that of the extrusion electrode must have been developed by other means, and it is likely that some process akin to triboelectrification is responsible.

Any of the materials mentioned in this paper placed in a Faraday ice pail, will show a low level of macroscopic charge. X-irradiation (Waker and Brown, 1990) measurement shows levels of microscopic charge several orders of magnitude higher. Manufacture of triboelectrically charged material is carried out using fibres without antistatic agent, and so the production of static electricity during carding can be a problem. The use of an ionising source to remove this charge is satisfactory because the macroscopic charge plays no effective role in filtration. At the other end of the scale, the charge on an ionic crystal, though high, is spatially highly variable and of too short a range to be effective in filtration. Only charge with a spatial variation comparable with filter fibres or interfibre spaces can be effective,.

Further confirmation of the complicated nature of charge on electrically charged material follows from two sources, but both rely on some knowledge of the efficiency of filtration as a function of the appropriate dimensionless parameter, N, which is, for charged particles and fibres of most charge configurations, with charge per unit fibre length, Q, and particle charge, q (Brown, 1993)

$$N = \frac{Qq}{6\pi^2\varepsilon_0(1+K_c)\mu d_f R_c U}$$

Capture calculations for charged particles can be worked out relatively easily for uniformly charged fibres or for fibres that have a sinusoidially radially variable charge, and the result is given by Fig. 4. Where the charge is uniform there is a linear relationship between single fibre efficiency, or logarithm of penetration, and dimensional parameter. As the charge becomes more spatially variable this relationship becomes weaker especially as the dimensional parameter becomes larger. Both Lathrache et al (1985) and Fjeld and Owen (1988) have calculated the layer efficiency for split fibre electret material as a function of dimensionless parameter. They observe a relatively weak variation of efficiency with dimensionless parameter, indicating a complex configuration of charge though not indicating exactly what that configuration is.

Confirmation of a complicated charge configuration is also given by the pattern of efficiency loss as a result of X-irradiation. In general, efficiency falls off rapidly for low doses of irradiation and more slowly for high doses, as shown in Fig 5. No functional relationship of the type shown in Fig. 4 would give rise to this variation. In the case of uniformly charged fibres the logarithm of the penetration should approach its minimal value in a relatively linear fashion. If the configuration is more complicated then the approach would be more rapid as the charge is lost.

It is proposed that the configuration of charge consists of a relatively uniform component giving rise to a long-range electric field, to which are added much more spatially-variable components giving rise to electric fields of much shorter range. The long range components will tend to be neutralised first, since they will attract ions from afar, resulting in a considerable loss of filtration efficiency. The residual charge will become more spatially variable. This means that their attraction for the ions will be more limited over space and the resultant loss of charge increasingly slow.

CONCLUSION

Triboelectrification is an attractive method for charging filter material because of both its effectiveness and its simplicity. It requires no additional textile processing stage in its implementation. The separation of materials in the triboelectric series appears to have no relevance to the efficiency of a filter developed from them. It is, however, necessary to have one component that is a good insulator and a second component that exchanges charge effectively. The configuration of charge on the material probably follows the basic simple pattern of one positively and one negatively charged fibre but on this is superimposed a secondary charge distribution of considerable complexity.

ACKNOWLEDGEMENTS

We are grateful to the Health and Safety Executive for sponsoring this work. We would also like to thank our colleagues who helped in the development of the triboelectrically-charged filter material. In particular, at HSE we are grateful to Mr G K Greenough who initiated the work, and to Messrs J Hodges, D Wake and P A Roberts for technical help. At Leeds University we are indebted to Dr G C East for scientific support and Mr E Hampshawe for technical help.

REFERENCES

Baumgartner H, Löffler F and Umhauer H (1985) "Deep bed electret filters. The determination of single fibre charge states and collection efficiencies" *IEEE Trans* El-21 447-486

Brown R C and Blackford D B (1983). "Air filtration by charged filter elements aligned parallel to the airflow", *Filtration and Separation* 20. 349

Brown R C (1993) "Air filtration: an integrated approach to the theory and applications of fibrous filters" Pergaman, Oxford.

Blackford D B and Brown R C (1985) "An air filter made from an electret and a conductor" *IEE Trans* E1-21 471-476

Feltham, J. (1979) "The Hansen filter", *Filtration and Separation*, 16, 370-372

Fjeld R A and Owens T M (1988) "The effects of particle charge on penetration in an electret filter" *IEEE Trans Ind Appl* 24 725-731

Hansen, N.L. (1931) "Method for the manufacture of smoke filters or collector filters", British Patent BP 384052

Harper W R (1967) "Contact and frictional electrification" OUP, Oxford

Hersh S P (1975) in "Surface Characteristics of Filters and Textiles" ed M J Schick, Dekker, New York

Kittel (1966) "Introduction to Solid State Physics" Wiley, New York

Lathrache R, Fisssan H and Neumann S (1986) "Deposition of submicron particles on electrically charged fibres", 17 446-449

Smith P A, East G C, Brown R C and Wake D (1988) "Generation of triboelectric charge in textile fibre mixtures and there use as air filters" *J.Electrostatics,* 21 81-98

Smith P A, East G C and Brown R C (1993) "The development of a new type of electrostatic air filter" *3rd International Textiles Conference*, Lodz, Poland.

Waker A J and Brown R C (1988) "Application of cavity theory to the discharge of electrostatic dust filters by x-rays" *Appl. Radiat. Isot.* 39 (7) 677-684

TABLE 1 *Triboelectric series of textile yarns*

Positive
Wool
Hercosett wool*
Nylon 66
Nylon 6
Silk
Regenerated cellulose
Cotton
Polyvinyl alcohol
Chlorinated wool
Cellulose triacetate
Calcium alginate
Acrylic
Cellulose diacetate
Polytetrafluoroethylene
Polyethylene
Polypropylene
Poly(ethylene terephthalate)
Poly(butylene terephthalate)
Modacrylic
Chlorofibre
Negative

* Hercosett wool is shrink-proof wool, which is first chlorinated, and then coated with nylon as a second process.

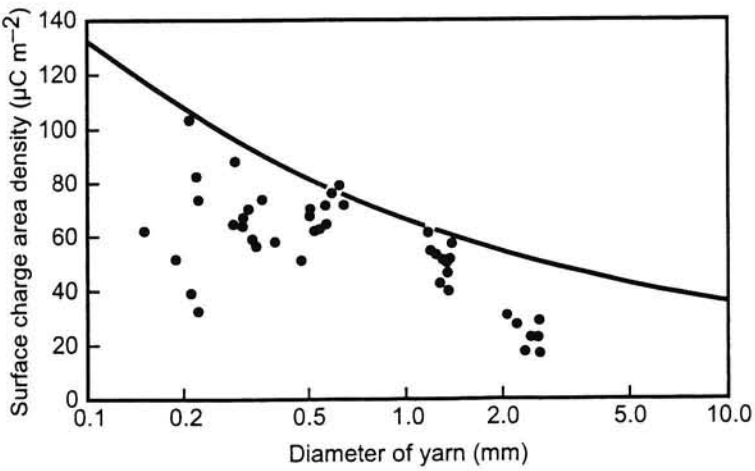

Fig 1. Surface charge density of triboelectrically charged polypropylene yarns

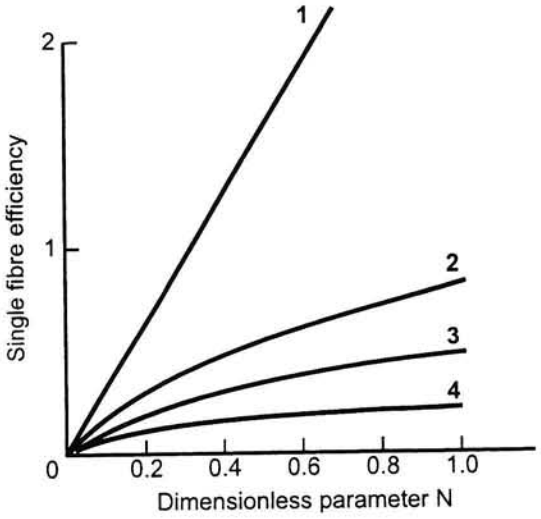

Fig 4. Single fibre efficiency as a function of the relevant dimensionless parameter:
(1) uniformly charged-fibre, charged particle;
(2) uniformly charged fibre, neutral particle;
(3) line dipole charged fibre, neutral particle;
(4) $n = 2$, line quadrupole charged fibre, neutral particle.

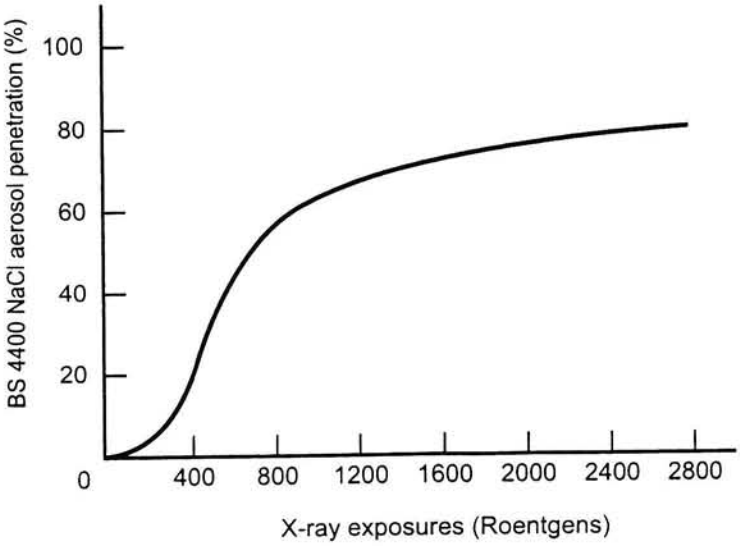

Fig 5. Sodium chloride aerosol penetration through electrically charged filter as a function of integrated radiation dose.

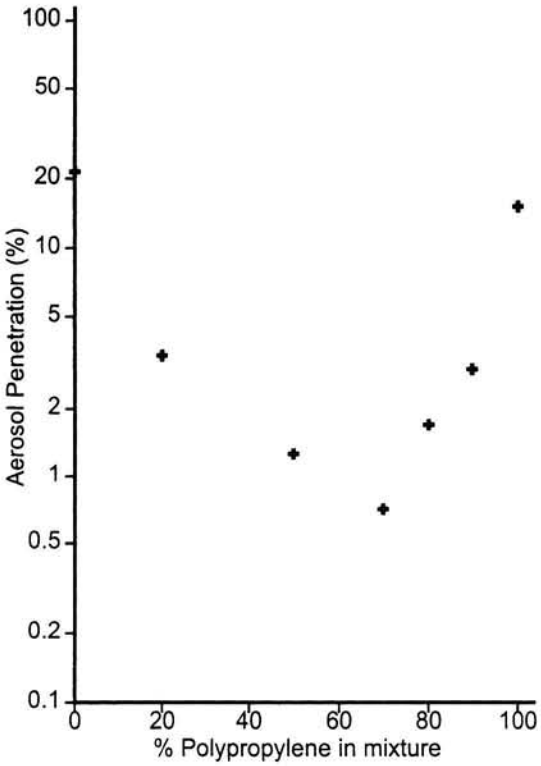

Fig 2. Sodium chloride aerosol penetration through mixed fibre triboelectrically charged filters of different composition

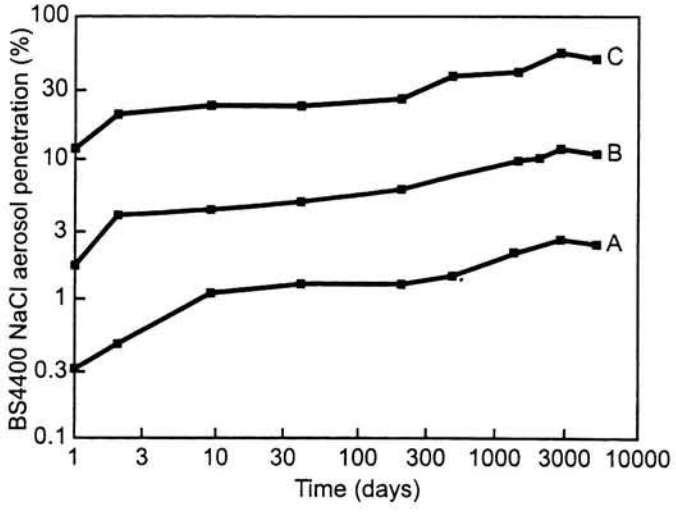

Fig 3. Sodium chloride aerosol penetration through experimental mixed fibre filters stored for extended periods

Morphology of Particulate Structures on Dust Loaded Single Fibres

H.-J. Rembor and G. Kasper
Institut für Mechanische Verfahrenstechnik und Mechanik, Universität Karlsruhe (TH), Germany

Abstract--A Confocal Laser Scanning Microscope (CLSM) was employed to measure the morphology of particulate deposits on single fibres. The CLSM used here for the first time permits perpendicular cross sectional "views" of a dust loaded single fibre by purely optical, and therefore completely noninvasive means. The micrographs from the present study were obtained from deposits in the regime of inertial particle collection, i.e. where particles accumulate mainly on the upstream face of a fibre.

INTRODUCTION

During an ongoing filtration process, the accumulating dust changes local packing densities in a fibrous filter, thereby changing the flow conditions through the medium and hence its filtration behaviour. In order to model and quantify such transient filtration behaviour and be able to predict the clogging of a filter, i.e. the onset of surface filtration, the spatial distribution of the deposited particle mass inside a filter medium must be known. It is known from regenerable filters that dust cakes on the surface of a medium have porosities of 80 - 90 % (Schmidt and Löffler, 1993). One can thus expect that fibrous filters clog as soon as internal particle deposits lead to a comparable porosity in the uppermost layers of the medium. Since local packing densities of a new filter medium have a random distribution laterally, the clogging will tend to happen not at an exactly defined mass loading but in a *clogging regime*. Earlier measurements of mass distributions in dust loaded filter media (Rembor and Kasper, 1998) have shown that gravimetric packing density measurements of different layers in a filter medium are not sufficient to describe or explain the observed increases in pressure drop or filtration efficiency with mass loading, because the spatial resolution, even when using very thin layers, is insufficient. Consequently, the present study focuses on the growth process of particulate structures on single fibres.

It is known (Kanaoka *et al.*, 1986) that different particle collection mechanisms lead to different deposit structures. One must therefore expect that each parameter which influences particle collection must also contribute to some extent to the formation of such structures and hence to the transient filtration behaviour. To reduce the complexity of the problem, the work reported here was limited to one well defined collection mechanism, namely inertial particle deposition.

EXPERIMENTS

The main idea for studying the structure of particulate deposits on dust loaded fibres was to expose a single fibre to an aerosol stream under well defined conditions and to analyse it under a microscope (Schweers *et al.*, 1994). The experimental set up as shown in Figure 1 consists of a series arrangement of an aerosol generation unit, a flow channel with holder for the single fibre, ancillary flow control hardware and a modified optical particle counter

(Umhauer, 1983) permitting in-situ measurements of particle size, number and velocity. A pneumatic nebulizer produces monodisperse polystyrene latex aerosols (1.072 µm, 1.820 µm and 3.135 µm); this aerosol is mixed in a mixing chamber with a second, conditioned air stream to adjust the relative humidity and ensure that no droplets remain in the aerosol. A ^{85}Kr-source (10 mCi) immediately after the generator serves as a particle neutraliser to reduce generally high electrical charges remaining from the nebulizing process to the Boltzmann equilibrium level. Those particles which, in spite of the neutralisation, still carry too much charge are extracted by an electrostatic precipitator (capacitor of two plates with an area of 100 mm x 100 mm, spaced 10 mm apart with an applied voltage of 6 kV). The aerosol then passes a flow rectifier and a pipe whose length and inner diameter (d_i = 16 mm, l = 428 mm) are dimensioned to allow only incompletely developed laminar velocity profiles. This ensures a nearly uniform velocity profile within the direct vicinity of the single fibre and the cross-section of the optical sensing volume, where the aerosol stream traverses in a short free jet zone. The optically defined sensing volume is situated immediately above the fibre. Nominal face velocities ranging from 1.0 to 4.8 m/s are set via a rotameter and a pump installed downstream. Face velocities below 5 m/s ensure that fibres do not vibrate in the gas stream. The actual face velocity just upstream of the fibre was measured very accurately with the OPC from the signal width, which corresponds to the time required for a particle to traverse the sensing volume.

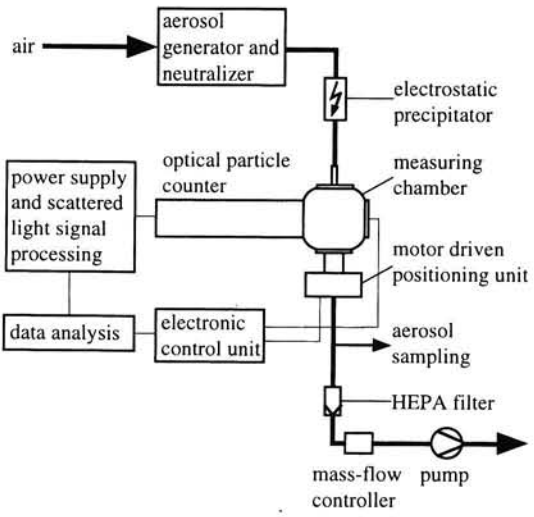

Fig. 1. Schematic diagram of the experimental set-up

The fibre holder can be removed from this set-up and placed in its entirety under a microscope without removing or otherwise handling the fibre. Stainless steel fibres of a diameter D_f = 30 µm are used which do not move or vibrate when exposed to the aerosol flow and any electrical charging effects due to fibre treatment are reduced because of their conductivity. The fibre holder permits rotation of the fibre under a Confocal Laser Scanning Microscope (CLSM) in increments of 15° to the flow direction. The CSLM was applied

because sample preparation for scanning electron microscopy caused particles to move and agglomerate on the fibre surface and therefore lead to false results (Rembor *et al.*, 1999). In addition, the CLSM provides 3-dimensional information of porous structures - such as particulate deposits on a fibre - as well as sectional views of the dust loaded fibre. However, if the loading on the fibre is too high the outer parts of the fibre together with the particulate structures can not be reproduced correctly anymore (see Fig. 2, left side). Therefore the fibre had to be scanned at 7 different angels (at each angle a section of 15° was cut out of the picture) and the micrographs have to be put together by the means of an image processing software (Fig. 2, right side). This quasi-tomographic technique for the first time enables a noninvasive cross sectional "view" of a dust loaded single fibre. The fibres were examined on a length of 100 µm, the cross sections presented here therefore show the projection of all particles collected on the fibre in the range of 100 µm of fibre length and are chosen to be representative for the overall structural shape built on the fibres.

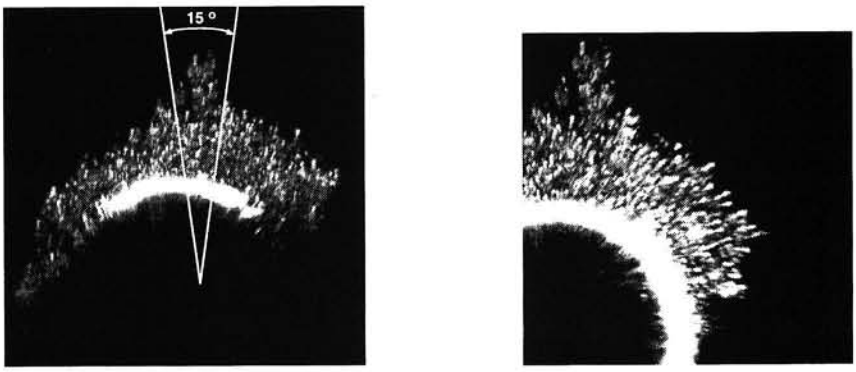

Fig. 2. Full view of fibre cross-section (right) is assembled from 15-degree sections (left) by optical and digital image processing means (fibre diameter D_f = 30 µm, particle diameter d_p = 1.072 µm).

RESULTS AND DISCUSSION

To properly compare the differing deposit structures at different operating conditions, the mass load is a helpful parameter since the structures will change their shape during loading. During the present study various attempts were made to get accurate quantitative data about the mass load on a single fibre. However, the results have not been satisfactory yet, and hence the *growth* of the particulate agglomerates on the fibre was studied by taking micrographs at four different stages of loading. As the single fibre efficiency is expected to change during loading, the particle challenge upstream of the fibre (counted by the optical particle counter) is not a direct measure for loading. In fact, the experiments have shown that very different particle numbers approaching the fibre are necessary at different operating conditions to create *visually* comparable mass loadings. As an example, for the experimental sequences in Figure 3, the growth of agglomerates on a fibre at Stokes number St = 0.27 (definition see below) is shown. In results shown thereafter only one representative

micrograph shall be presented for each series of experiments. However, at all operating conditions a series of experiments with four stages of mass loading was always made and the whole series were compared with each other.

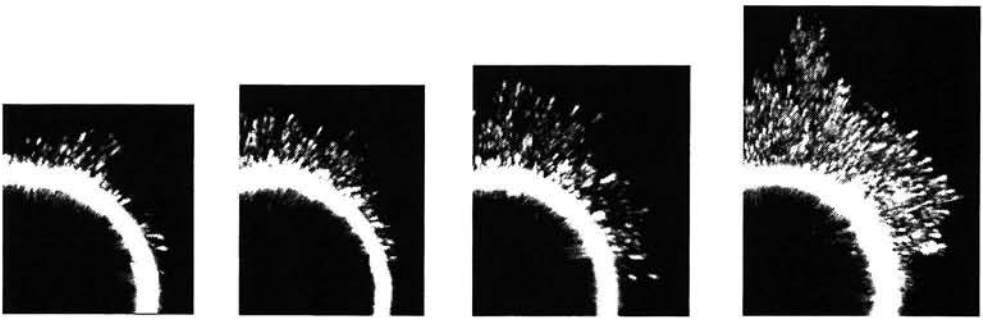

Fig. 3 Growth of particulate deposits on a single fibre at four stages of progressive mass loading (d_p = 1.072 µm, u = 2.2 m/s, St = 0.27, D_F = 30 µm)

Since the metallic fibre reflects the laser beam with much higher intensity than latex spheres, they can be distinguished clearly from the steel fibre. The CLSM resolution suffices to detect PSL spheres used in this study with diameters of d_p = 1.072 µm and above. As can be seen from the series of micrographs in Figure 3, inertial deposition causes particles to accumulate primarily on the upstream face of the fibre. This was also substantiated by visual observation and conventional scanning microscopy. Quantitative data about the limiting angles of deposition (which differ with operational conditions) were also obtained but no clear dependency on St or any of the individual parameters influencing St could be identified yet.

Compared to an earlier SEM study by Kanaoka *et al.* (1986), the present investigation found somewhat different deposit structures. The two main shapes obtained in a range of St numbers between St = 0.27 and St = 3.17 are shown in Figures 4 and 5. On the one hand, at low velocities and low St numbers we observed porous, star-shaped deposits (Fig. 4), presumably because adhesion forces are sufficiently high compared to drag forces to permit the formation of fairly long and thin dendrites. The dendrites in the 45° position may be due to the influence of interception. Higher velocities lead to more compact and rounded structures (Fig. 5); long dendrites are not formed, instead the agglomerates are compressed and thus also more dense optically. This is evident from the dark zones in the micrographs of Fig. 5, where the laser beam cannot penetrate to the highly reflective steel fibre which thus also becomes invisible, as opposed to all other micrograph. This also was confirmed by visual observation of the fibres through the optical microscope.

d_p = 1.072 μm, u = 0.51 m/s, St = 0.063 d_p = 1.82 μm, u = 1.39 m/s, St = 0.49

Fig. 4 Porous, star-shaped particulate structures obtained at relatively low Stokes numbers.

The formation at higher velocities of more compact rather than dendrite-like porous structures occurred at all particle diameters used in the present study but at very differing values of *St*. This again emphasises earlier findings with commercial fibrous filter media (Rembor and Kasper, 1998) that the increase in pressure drop and filtration efficiency with mass loading for the same *St* number reached by different combinations of particle diameter and velocity can be very different. Hence, the *St* number is not the sole parameter required to describe the transient behaviour of fibrous filters with dust load in the regime of inertial particle collection.

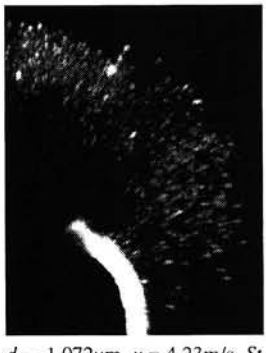

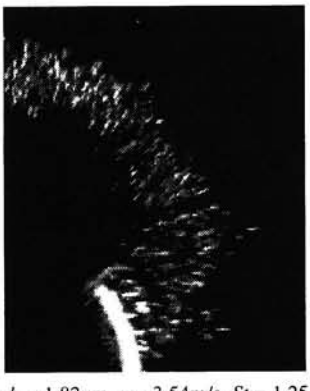

d_p = 1,072μm, u = 4,23m/s, St = 0.51 d_p = 1,82μm, u = 3,54m/s, St = 1.25

Fig. 5 Compact particulate structures obtained at higher Stokes numbers.

Experiments were performed to study the influence of the velocity on the morphology of particle deposits, such that the particle diameter was kept constant while gradually raising the velocity. For all particle diameters used here, a star-like shape of the deposit occurred at ratios of interception parameter R to St number of $R/St > 0.1$. Below, for higher values of

the *St* numbers compact, rounded structures where always observed. These compact and round shapes can undergo further changes with increasing velocity. Figure 6 shows the cross sections of single fibres loaded with particles of diameter of d_p = 3.135 µm. At a velocity of u = 1.23 m/s (left micrograph) the structure has a fairly high lateral expansion. The right micrograph obtained at a higher velocity of u = 3.02 m/s shows a very slimmer shape. This was observed with all particle diameters and generally it can be said that, similar to the findings of Kanaoka *et al.* (1986), the lateral expansion of particulate structures on fibres decreases when the velocity is increased. Again, quantitative information is difficult to give since the particle mass loading on the fibres is not exactly known. However, the phenomenon that the structures become more slim and compact with higher velocities is in contrast to the findings made in an earlier investigation (Rembor and Kasper, 1998). While more compact structures on the fibres with less lateral expansion should lead to a slower increase in pressure drop with mass loading, it was found there that the pressure drop of dust loaded technical filter media rises faster when the velocity is increased.

d_p = 3.135 µm, u = 1,23m/s, St = 1.29

d_p = 3.135 µm, u = 3,02m/s, St = 3.17

Fig. 6 Influence of the velocity on the lateral expansion of the particulate structures on single fibres

With the experimental set-up and particle material described above it was possible to achieve a value of St = 0.5 with three different combinations of velocities and particle diameters. The cross sections obtained are shown in Figure 7. According to these micrographs (which conform with visual observation), the smaller particle diameters lead to more compact shapes but with a higher lateral expansion, while bigger particles extend the fibre contour in the upstream direction which will have lesser effect on the flow and hence the pressure drop. This agrees with earlier findings using fibrous filter media at the same *St* numbers (Rembor and Kasper, 1998). Here, with smaller particles pressure drop and filtration efficiency rose faster than with bigger particles. Furthermore, it can be assumed that the higher specific surface area of comparable mass loads of small particles plays a role, too.

Since with the set of operational parameters applied in this investigation fairly high velocities of up to 4.23 m/s have been reached the behaviour of the agglomerates on the fibres in the flow has been studied. Therefore, after all experimental series the measuring volume of the optical particle counter was positioned directly under the dust loaded fibre and the velocity gradually was increased. The number of particles re-entrained purely as a result of fluid drag was found to be negligible compared to the number of particles ap-

proaching it in the same period of time. Even at very low single fibre collection efficiencies, up to 1000 times more particles are collected during comparable periods of time. However, the way the agglomerates on the fibre are built had considerable influence on the behaviour of re-entrainment. Particles included in more compact structures formed of smaller particles or at higher velocities were blown off even more rarely. Furthermore, it was observed that mainly single particles are re-entrained at all velocities and that dendrites or longer agglomerates only change their direction in the flow instead of being blown off.

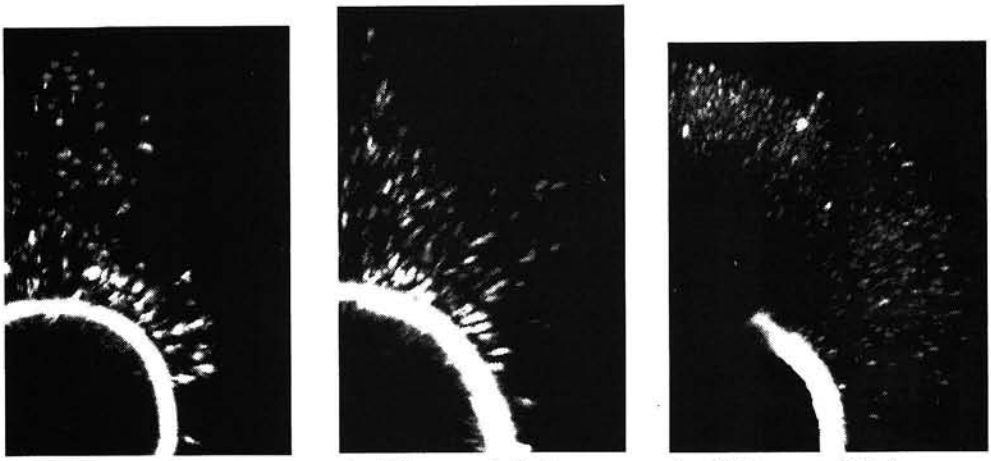

d_p = 3.135 µm, u = 0.46 m/s d_p = 1.82 µm, u = 1.39m/s d_p = 1.072 µm, u = 4,23m/s

Fig. 7 Comparison of particulate deposits at St = 0.5 achieved by different combinations of particle diameter and velocity.

SUMMARY AND CONCLUSIONS

The morphology of porous dust deposits on single fibres was studied with a Confocal Laser-Scanning Microscope (CLSM) to obtain accurate 3-dimensional information. A quasi-tomographic procedure was employed to obtain complete cross-sectional views by purely optically and thus non-invasive means.

The relative growth process was documented with series of such images obtained at progressive mass loadings, each series corresponding to a different set of Stokes numbers, inteception parameters or free stream velocity. However, the absolute particle mass collected at each stage could not be determined exactly.

In the regime of inertial particle collection at St numbers between 0.063 and 3.17, particles are collected only on the upstream face of a fibre. Two main structural shapes were observed. At low velocities (for constant St) the deposits have the shape of a star with fairly long dendrites protruding at an angle of 45° to flow direction. These dendrites seem to be a consequence of the interceptional mechanism of particle collection and occurred only at a ratio of interception parameter R to the St number above 0.1. At higher velocities only compact and rounded shapes were obtained. These structures become "slimmer" at the higher velocities, i.e. have less lateral expansion perpendicular to flow direction.

A comparison of the structures formed at a St number $St = 0.5$ achieved by different combinations of particle diameter and velocity showed that the agglomerates formed of smaller particles tend to have a higher lateral expansion than the ones of bigger particles.

In general, it can be said that models which assume that particles collected in the filter medium lead to a uniform thickening of the fibre diameter or to linear dendrites are probably too simplistic. In reality, just the structures obtained for inertial deposition alone have a much wider range of morphologies which depends on additional quantities beside the Stokes number.

SYMBOLS

$St = \frac{u d_P^2 \rho_P}{18 \mu D_F}$ Stokes number

$R = \frac{d_P}{D_F}$ interception parameter

d_P particle diameter
d_i inner diameter of the pipe
D_f fibre diameter
l length of the pipe
u velocity

REFERENCES

Rembor, H.-J., Kasper, G., Fibrous filters (1998) Measurements of spatial distribution of deposited particle mass, pressure drop and filtration efficiency, World Congress on Particle Technology, Brighton, paper 278

Rembor, H.-J., Kasper, G., (1998) Measurements of spatial distribution of deposited particle mass in fibrous filters, 4th European Symposium Separation of Particles from Gases, Nürnberg, Germany, 223-232

Rembor, H.-J., Maus, R., Umhauer, H., (1999) Measurements of single fibre efficiencies at critical values of the Stokes number, accepted for publication in *Part. Part. Syst. Charact*

Schweers, E., Umhauer, H., Löffler, F., (1994) Experimental investigation of particle collection on single fibres of different configurations. *Part. Part. Syst. Charact.* **11,** 275-283

Schmidt, E., Löffler, F., (1993)Verification of dust cake compression by means of structure analysis and the effect on filtration performance, 6th World Filtration Congress, Nagoya, Japan, 54-59

Umhauer, H. (1983) Particle size distribution analysis by scattered light measurements using an optically defined measuring volume. *J. Aerosol Sci.* **14,** 765-770

Kanaoka, C., Emi, H., Hiragi, S., Mojo, T., (1986) Morphology of particulate agglomeration on a cylindric fibre and a collection efficiency of a dust-loaded fibre, 2nd Intl. Aerosol Conference, Berlin, 674-677

Electrospray, a Possible Way to Produce Charged Fibres?

Kees B. Geerse, Jan C.M. Marijnissen and Brian Scarlett.
Delft University of Technology, Faculty of Applied Sciences, DelftChemTech.
Particle Technology Group.

KEYWORDS
Electrospray, charged fibres, electrohydrodynamic atomisation (EHDA), cone-jet mode.

ABSTRACT

Electrohydrodynamic atomisation (EHDA) is a method of producing very fine droplets from a liquid by using an electric field. Depending on the properties of the liquid, the flow rate of the liquid and the voltage applied to create the electric field, different modes of EHDA can occur.

The mode of most interest is the cone-jet mode. In this mode droplets are produced with a narrow size distribution. Mathematical models to describe this mode are presented.

The use of high viscous liquids, like polymer melts, can lead to the formation of thin fibres instead of droplets, because the normal break up mechanisms do not occur. This fact has lead to the idea of producing thin fibres as a possible application of EHDA. Due to the production mechanism i.e. the use of electrical forces, the fibres produced will have a net electric charge, which offers possibilities for using them in electret filters. These filters are highly effective, especially for small particles, and have a low pressure drop

A full description of EHDA is presented and the production of fibres by this method is described.

INTRODUCTION

The possibility of using electric fields to disperse liquids has attracted much interest from the scientific world. The subject includes a wide variety of applications, numerous experimental configurations and a large array of liquids.

An electrospray refers to the atomisation of a liquid through the Coulombic interaction of charges on the liquid and the applied electric field. The result of this interaction includes both the acceleration of the liquid and subsequent disruption into droplets as well as the buildup of charge. Zeleny (1915, 1917) defined electrospray as the case in which the electric field itself is the cause of the spraying of a liquid into fine droplets. Nowadays, this phenomenon is called *ElectroHydroDynamic Atomisation* (EHDA), to avoid confusion with other spraying techniques using an electric field. This name covers the process of the atomisation of a moving (*dynamic*) liquid (*hydro*) in an electric (*electro*) field.

In this paper different aspects of EHDA will be highlighted. At first, the different modes of electrospray that can occur are described. One of these modes, the so-called *cone-jet* mode is of special interest and will be considered in more detail. Modelling of this mode is carried out

by a number of different research groups and their results will be presented. The potential applications of electrospray as a production method for charged fibres will finally be discussed.

The process of EHDA can take place in various atmospheres (air, inert gas, etc.) using various liquids and experimental conditions, and generate droplets by various production mechanisms. It produces charged droplets in different size ranges (nm-μm) and monodisperse or polydisperse droplet populations in high and low flow rates. Figure 1 shows a typical set-up used for EHDA.

The atomisation of a liquid is a function of both external (experimental configuration, flow rate and atmosphere) and internal (liquid properties) of the system. The important properties are: the electrical conductivity (K), the surface tension (γ), the viscosity (μ) and the density (ρ).

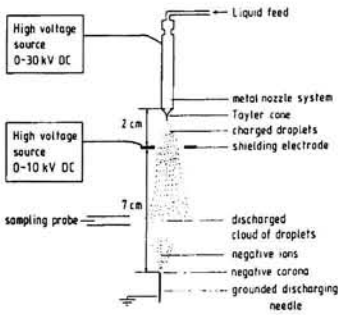

Figure 1. Typical configuration for electrospraying as developed in Delft.[7]

The phenomenon of the electric effect on menisci has been known since the sixteenth century. William Gilbert reported the interaction between a water droplet and a piece of amber, leading to a conical shaped droplet.

Zeleny, at the beginning of this century, showed that liquid menisci subjected to a high enough electric field change to a conical shape and emit a mist of very small droplets.

In the fifties, Vonnegut and Neubauer tried to relate the properties of a liquid to their ability of being sprayed.

Taylor carried out the first mathematical description of the cone by balancing the forces that are present. At the beginning of the nineties, scaling laws for electrospraying of liquids were developed, to predict the characteristics of the spray. Physical models that describe the shape of the cone and the development of the spray were derived by Hartman and are also presented here.

The intention of this paper is to give an overview of the developments in EHDA from the beginning of the nineties until now, with a special emphasis on its potential for the production of charged fibres.

MODES OF EHDA.

Electrohydrodynamic atomisation, also called electrospraying, refers to a process where a liquid jet breaks up into droplets under the influence of electrical forces. Depending on the strength of the electric stresses in the liquid surface relative to the surface tension stress and the kinetic energy of the liquid jet leaving the nozzle, different spraying modes will be obtained.

Several spray modes have been defined by Cloupeau and Prunet-Foch (1994). A brief summary of these spray modes follows. Each mode has multiple characteristics and the transition between modes is not always well defined; consequently, the simple descriptions that follow cannot fully encompass the subtleties of each mode. Figure 2 presents a flow chart describing the modes as a function of the applied potential. In this figure the influence of other parameters on the spray mode can also be seen. Here it is not meant to imply that all liquids under all conditions will follow identically, without deviation, the mode progression through potential space. However, this figure, in general, locates the modes described below in the potential space of the spray.

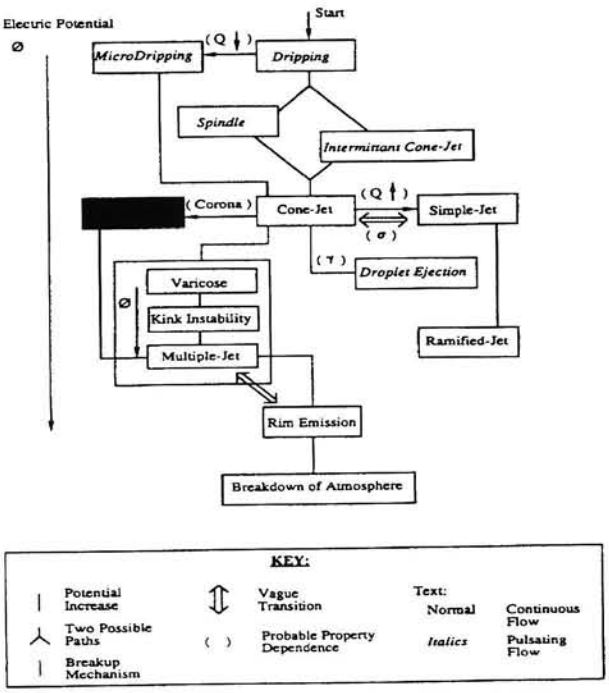

Figure 2. Different modes of EHDA as function of the applied potential.[4]

The modes are separated into two general categories: those that exhibit a continuous flow of liquid through the meniscus and those that do not. The former consists of the simple-jet, the cone-jet and the ramified-jet, while the latter consists of the dripping, the micro-dripping,

the spindle and the intermittent cone-jet modes. The latter are often referred to as pulsating modes.

The dripping mode is characterised by the production of large droplets (usually larger than the capillary diameter) at low frequency (up to several hundreds Hz). The production frequency and the droplet diameter vary directly and inversely, respectively, with the applied potential. The primary droplets are sometimes accompanied by satellite droplets. The microdripping mode occurs at low flow rates and produces droplets smaller than the capillary diameter at a frequency about two orders higher than the dripping mode. Figure 3 shows both modes. The gray areas represent the nozzle.

Figure 3. Dripping mode (left) and microdripping mode (right). (adapted from Cloupeau and Prunet-Foch)[2]

The spindle mode generates two distinct droplet sizes, a large primary droplet and several small satellites. In this mode, a jet extends from the meniscus and collapses into the primary and satellite droplets. The meniscus collapses to the capillary tip and the process is repeated with a regularity depending on the conditions. The intermittent cone-jet mode, as the name suggests, produces an unstable cone-jet. Between the cone-jet occurrences the meniscus collapses to a capillary and several large droplets may be emitted. Previous nomenclature has grouped the spindle and the intermittent cone-jet modes into one mode, the pulsating-jet mode. The droplet diameter differentiates the two modes. The spindle mode produces two diameter classes where the intermittent cone-jet mode produces a multitude of fine droplets with a superimposed, semi-periodic large droplet population.

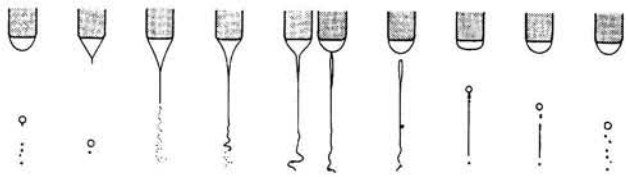

Figure 4. The different stages of the spindle mode. (adapted from Cloupeau and Prunet-Foch)[2]

The continuous modes are described as follows. The simple jet and cone-jet exhibit similar structures. The transition between the two is sharp for high conductivity liquids and vague for low conductivity liquids. Both consist of a single jet drawn from the meniscus by the electrical forces.

In the cone-jet mode, often referred to as the Taylor cone mode, the meniscus forms a conical shape (which has for the limiting case of no flow a half angle of 49.3° as calculated by Taylor).

The jet drawn from the apex of this meniscus breaks up into droplets by two mechanisms as a function of increasing potential. These varicose instabilities where the break-up proceeds as in a natural jet and kink instabilities where the breakup is more disordered due to the large lateral instabilities caused by the high electric forces. Lastly multiple jets appear on the meniscus which break up into droplets.

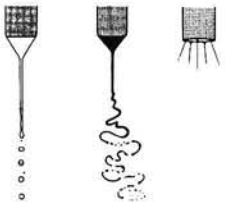

Figure 5. From left to right: varicose instabilities; kink instabilities; multiple jets. (adapted from Cloupeau and Prunet-Foch)[2]

The simple-jet differs from the cone-jet mode in the sharpness of the conical meniscus and in this mode breakup usually occurs via varicose instabilities. This difference is caused by the fact that the kinetic energy of the jet in the cone-jet mode is mainly generated by the electric forces, where in the simple-jet mode the kinetic energy of the jet is mainly generated by the syringe pump. For the cone-jet mode the diameter of the cone base is determined by the outer diameter of the capillary and the jet diameter mainly depends on the liquid flow rate. For the simple-jet mode, the diameter of the cone base is determined by the inner diameter of the capillary. The jet diameter depends on the extra acceleration caused by the electric field. When the electric field is increased over a simple-jet, then the surface charge on the jet becomes larger than a certain threshold value. In that case, the radial electric forces cause the occurrence of several temporal secondary jets issuing from the surface of the primary jet, not just from the apex. This is called the ramified-jet mode.

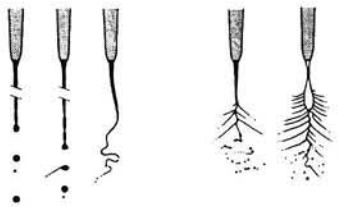

Figure 6. Simple jet (left) and ramified jet (right) mode. (adapted from Cloupeau and Prunet-Foch)[2]

The most reported spray mode is the previously mentioned cone-jet mode. There are actually three reasons for the importance of this mode. First, it allows the production of aerosols within a very large range of droplet sizes, including the submicron range. Secondly, this mode is achievable for a very wide range of liquid properties in terms of conductivity, viscosity and

surface tension. Thirdly, the size distribution of the particles produced can be, depending on the experimental conditions, monodisperse, bimodal or polydisperse.

Figure 7. Photograph of EHDA in the cone-jet mode.

The electrical interaction between polysized, highly charged droplets and differences in inertia are the main cause for a size segregation effect. Small droplets are found at the edge of the spray, while large droplets are found in the spray centre. This makes separation of the main droplets from the smaller secondary droplets possible and a monodisperse spray can be obtained. If the highly charged droplets evaporate, then the Rayleigh limit for droplet charge can be reached. In that case droplet fisson can take place. This effect changes the droplet size distribution.

In the cone-jet mode, a liquid is pumped through a nozzle at a low flow rate. An electric field is applied over the nozzle and some counter electrode. This electric field induces a surface charge in the growing droplet at the nozzle. Due to this surface charge, and due to the electric field, an electric stress is created in the liquid surface. If the electric field, and the liquid flow rate are in the appropriate range, then this electric stress will overcome the surface tension stress. In that case, the electric stresses transform the droplet into a conical shape. The tangential electric field accelerates the charge carriers at the liquid surface toward the cone apex. In a liquid, the charge carriers are mainly ions. These ions collide with the surrounding liquid molecules. This results in an acceleration of the surrounding liquid. As a result, a thin liquid jet emerges at the cone apex. This jet can break up into a number of main droplets with a narrow size distribution, and a number of smaller secondary droplets and satellites, Cloupeau (1989), Gomez (1994), Chen (1995). The number of secondary droplets and satellites can be of the same order of magnitude as the number of main droplets. However, the total volume of these droplets is much smaller than the volume of the main droplets. Due to the excess of surface charge in the liquid cone and jet, the droplets are highly charged.

Depending on the liquid properties, the flow rate and the applied potential, the main droplet size produced ranges from nanometers with production frequencies in the order of 10^9 Hz to hundreds of micrometers with production frequencies of about 10^4 Hz.

Since this cone-jet mode offers many (potential) applications it will be described in more detail.

MODELLING OF THE CONE-JET MODE AND BREAK UP OF THE JET

Several attempts have been made to model the cone-jet mode, including analytical and numerical models. A short review of only the most successful of these follows.

Taylor (1964) was the first to calculate analytically a conical shape, the 'Taylor cone'. For this cone shape the surface tension stress is balanced with the electrical normal stress. Taylor assumed a cone without a liquid jet. Consequently, there was no electrical current or liquid flow through this liquid cone. In Taylor's case the cone had to be a perfect cone. Only the angle at the cone apex could be used as a parameter. For this case Taylor found a cone angle of 98.6°.

Combining dimensional analysis with experimental results, Fernandez de la Morra (1994) and Gañán-Calvo (1997) derived relations for the droplet size and the current as a function of liquid flowrate and liquid properties (conductivity, surface tension, density, viscosity and relative permittivity), the so-called scaling laws.

Using his physical numerical model, Hartman (1998) refined these scaling laws. In the case of a flat radial velocity profile in the jet, he found that the current is given by:

$$\frac{I}{I_0} = b\left(\frac{Q}{Q_0}\right)^a \tag{1}$$

$$\text{where } I_0 = \left(\frac{\varepsilon_0 \gamma^2}{\rho}\right)^{1/2} \text{ and } Q_0 = \frac{\varepsilon_0 \gamma}{K\rho}.$$

For a nozzle with an outer diameter of 8 mm and for n-butanol and ethylene glycol with various conductivities, the scaling law was fitted to current measurements. The results are as follows:

Q/Q_0	a	b
<50	0.493	2.215
50-250	0.518	1.931
>250	0.427	3.203

It should be noted that the current also depends on the electrode configuration and the type of ions used. So, measurements might yield deviations from the scaling laws of up to 30%.

In the developing the droplet size scaling law one of the tools Hartman used was a High Speed Imaging System. The measurements obtained in this work showed that the droplet size produced in the cone jet mode depends on the jet break up mechanism, which was found to depend on the ratio of the electric stress to the surface tension stress. At low stress ratios, the jet breaks up due to varicose perturbations. At higher stress ratios, the jet showed a whipping motion.

He found for the droplet size in the varicose and in the whipping jet break up regime:

$$d_{d,\ varicose} = c\left(\frac{\rho\varepsilon_0 Q^4}{I^2}\right)^{1/6} \qquad d_{d,whipping} = \left(0.8\frac{288\varepsilon_0\gamma Q^2}{I^2}\right)^{1/3} \tag{2}$$

The constant, c, was fitted to the experiments and was found to be 2.05 from the measurements with the camera, and 1.76 from a result of Gañán-Calvo (1997).

The difference can be attributed to the measurement accuracy of the camera system. The droplet size equation (2) that yields the smallest droplet is the one that has to be used. It should be noted that in the whipping jet breakup the size distribution becomes wider with increasing flow rate and that for every liquid a minimum flow rate exists.

Hartman (1998) developed a physical numerical model, based on first principles, Figure 8.

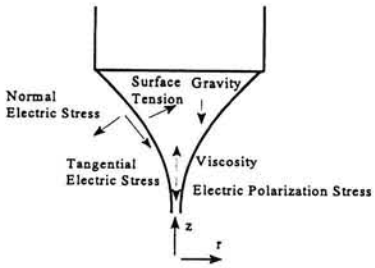

Figure 8. Stresses acting on the cone.[5]

The model is able to calculate the shape of the liquid cone and jet, the electric fields in and outside the cone, and the surface charge density at the liquid surface. The model also estimates the liquid velocity at the cone surface. From these results the current through the liquid cone can be calculated.

As seen already the droplet size produced mainly depends on the liquid flow rate and the liquid properties. The physical model investigates the influence of these parameters on the cone shape, droplet size and droplet charge. The shape of the liquid cone is calculated by solving the Navier-Stokes equation in one dimension, for a steady state situation. To be able to solve these equations, the electric field strengths, the surface charge and the radial velocity profile inside the liquid have to be known. If a certain cone shape is assumed then the electric fields inside and outside the liquid are numerically calculated using Gauss' law. The surface charge follows then from the current balance at the liquid-air interface and from the estimation of the liquid velocity at the liquid-air interface. The one dimensional Navier-Stokes equation is then used to calculate a new cone-shape which is used as input for new electric field, and surface charge calculations. This process is repeated until input cone shape and output cone shape have converged.

The break up of the jet is calculated numerically by using models of Weber and Melcher. The calculations use the previously calculated jet shape. These models yield the jet diameter before break up, the diameter of the combined main and secondary droplet and the droplet velocity just after break up.

THE PRODUCTION OF CHARGED FIBRES USING EHDA

In the previous sections a comprehensive description of the EHDA phenomenon was presented, including physical models of the cone-jet mode. With this knowledge it is possible to use EHDA for the production of tailor made particles, for example for drug production. This section however is not focussed on the atomisation of liquids, but on the production of thin charged fibres by means of EHDA. This is a possible application of EHDA because the fibres produced will have a net electrical charge, if this charge if 'frozen' in the fibre before discharge takes place.

Electret filters are filters made of woven polymer fibres that have a permanent electric charge. Due to this charge, the efficiency of these filters increases substantially, especially for very small particles. The production of the charged polymer fibres is currently done by producing polymer sheets, giving them a charge difference between upper side and underside and splitting the sheets into fibres. The net charge on the fibres therefore is zero. There is only a charge difference and this is what leads to the attraction of particles.

If instead of a low viscous liquid a high viscous liquid is used for EHDA, the normally occurring break up mechanism in the jet that leads to droplet formation, cannot take place. Due to the high viscosity and to solidification, any disturbance on the jet is damped out. This will lead to the production of a fibre with a certain diameter. In his model for EHDA in the cone-jet mode, Hartman (1998), has derived a relation for the diameter and the surface charge for the jet. These relations are given below and are valid for the jet just after the cone tip:

$$d_{jet} = b_{jet} \cdot Q^{a_{jet}} \qquad \sigma = \frac{0.59\, I\, d_{jet}}{4Q} \tag{3}$$

where d_{jet} is the jet diameter, b_{jet} and a_{jet} are scaling constants, Q is the flow rate, σ is the surface charge and I is the current through the jet. The scaling constant a_{jet} is found to be 0.71.

Due to the high shear stresses in a highly viscous liquid, the velocity profile in the jet will be almost flat, i.e. the surface velocity is equal to the centre velocity. In this flat velocity profile case, the current through the jet just after the cone tip is 59 percent due to convection and 41 percent due to conduction. The convectional part of the current is located at the jet surface, leading to the relation for the surface charge as given above. The small charge relaxation time in the jet causes all charges move to the surface almost immediately. For a typical EHDA set up this can lead to surface charges of up to 400 $\mu C/m^2$.

To obtain fibres by EHDA either highly concentrated polymer solutions or polymer melts can be used. Both the solutions and the melts have a low enough viscosity to be sprayed. In case of polymer solutions the solvent, such as acetone, has to vaporise rapidly, so that the fibre can be formed. Polymer melts will stiffen due to the temperature decrease after spraying.

At the beginning of the eighties, Larrondo et al (1981) had already made polymer fibres using an electric field as the only driving force. They used polyethylene and polypropylene melts and solutions in the spray.

Figure 9. Photograph of a cone obtained from a polymer melt.[6]

Despite attempts to model the process, they could not predict the diameter of the fibre produced. However the Hartman models for EHDA in the cone jet mode can also be applied to polymers, to predict jet diameter and surface charge.

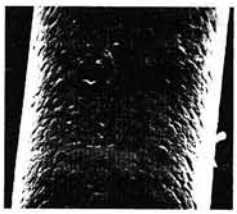

Figure 10. Polypropylene fibre obtained by EHDA, diameter approx. 60 microns.[6]

In the early nineties, polymers were sprayed at Delft University of Technology, producing very long fibres, with a speed up to 10 m/s. The polymer used for these experiments was ATLAC T500, a polymer used by AGFA to produce toner particles for photocopiers. Spraying a solution of this polymer in acetone lead to the formation of small particles. The use of a melt lead to the formation of a thin fibre.

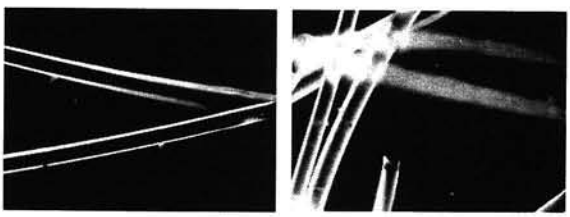

Figure 11. Fibres produced from ATLAC T500 melts.

The surface charge, present on the jet after emerging from the cone apex, remains on the jet during the process. After a certain length the jet will be solidified forming a solid fibre. The charge carriers present will be caught on its surface, so that a surface charge will remain on the fibre. The diameter of the crystallised fibre will be smaller than it was just after the cone apex, decreasing the surface charge. This is because a decrease of the diameter leads to an increase of the equivalent area per unit volume and thus a decrease of the surface charge.

A set-up to produce fibres by EHDA has been built by the Particle Technology Group in Delft. Preliminary results show that the fibres produced are charged and that the charge remains on those fibres.

CONCLUSIONS

Electrohydrodynamic atomisation is a method that can be used to produce very fine droplets. EHDA can occur in different modes, depending on liquid properties, the electric field and the flow rate of the liquid. The mode of most interest is the so-called cone jet mode, producing droplets with a very narrow size distribution. In the last few years, this mode has been very well investigated.

Scaling laws have been developed that predict the droplet size and the current as function of the liquid properties and the flow rate. A fundamental physical model derived by Hartman describes the mechanisms of the cone-jet mode well.

One of the possible applications of EHDA in the cone jet mode is the production of thin fibres with a net electric charge. If this charge remains for a long time on these fibres, they can be used for the production of electret filters. This is under investigation by the Particle Technology Group in Delft.

NOMENCLATURE

a, a_{jet}, b, b_{jet}, c	constants	[-]
d_d	droplet diameter	[m]
d_{jet}	jet diameter	[m]
K	electric conductivity	[S/m]
I	current	[A]
I_0	reference current	[A]
Q	liquid flow rate	[m^3/s]
Q_0	reference flow rate	[m^3/s]
ε_r	relative permittivity	[-]
γ	surface tension	[N/m]
μ	dynamic viscosity	[Pa s]
ρ	density	[kg/m^3]
σ	surface charge	[C/m^2]
ε_0	permittivity of vacuum	$8.85 \cdot 10^{-12}$ $C^2/N\ m^2$

REFERENCES

1. Brunner D.J., (1997), Jet breakup mechanism in the cone-jet mode of electrohydrodynamic sprays, *Graduation thesis*, TUDelft.
2. Cloupeau M. and Prunet-Foch B, (1994), Electrohydrodynamic spraying functioning modes: a critical review. *J. Aersol Sci.*, **25**, No. 6, 1021-1036.
3. Ganán-Calvo A.M.,Dávila J. and Barrero A., (1997), Current and droplet size in the electrospraying of liquid scaling laws. *J. Aerosol Sci.*, **28**, No. 2, 249-275.
4. Grace J.M. and Marijnissen J.C.M., (1994), A review of liquid atomisation by electric means, *J. A.erosol Sci.*, **25**, No. 6, 1005-1019.
5. Hartman R., (1998), Scaling laws for droplet size and current produced in the cone-jet mode. *PhD-thesis*, TUDelft.
6. Larrondo L. et al (1981), Electrostatic Fiber Spinning from Polymer Melts, *Journal of Polymer Science: Polymer Physics Edition*, **19**, 909-940.
7. Meesters G.M.H., (1992), Mechanisms of droplet formation. *PhD.thesis*, TUDelft.
8. Vercoulen P.H.W., (1995), Electrostatic processing of particles. *PhD thesis*, TUDelft.
9. Vercoulen P.H.W., (1990), De produktie van 1 µm druppeltjes met behulp van de Taylor cone., *Graduation thesis*, Delft University of Technology.

Electrified Filtration

F. Jordan and H. Fissan
Process and Aerosol Measurement Technology, Gerhard-Mercator-University Duisburg, Bismarckstraße 81, D-47057 Duisburg, Germany

KEYWORDS
Filtration, electric forces, particles, deposition, diffusion, Brownian motion, single fiber efficiency, enhancement

INTRODUCTION

The filtration efficiency of fibrous filters goes through a deep minimum in the submiron regime. This is caused by the transition from interceptional to diffusional particle capture. In order to improve the filtration efficiency additional electrical forces are applied. Since the electrical forces have no influence on fluid flow, higher filtration efficiency can be reached without increasing pressure drop. This is not the case where mechanical effects are invoked. One type of fibrous filter which uses electrical particle capture mechanisms is the electret filter. This type of filter consists of electrical inhomogeneously charged fibres, which loose their charges with time and particle loading. This disadvantage can by avoided by applying external electric fields to polarise fibres inside the filter media.
In order to estimate the importance of electrostatic effects in the submicron particle size range, the electrical forces have to be considered coupled with the statistical effect of Brownian motion as well as with all known mechanical deposition effects. Models developed to date either neglect deposition by diffusion [6] or diffusion is superimposed [5]. But in parts of the submicron size range, which is of greatest interest, the different deposition mechanisms are of the same order of magnitude. Therefore the coupling effect becomes most important.

FILTER ARRANGEMENT

In order to use external electric fields to improve filter performance, the filter medium has to be placed between permeable electrodes. The arrangement is shown in Figure 1. It is like a plate capacitor with the filter medium inside. The electrodes are a distance, l, apart, which is the thickness of the medium. If a voltage, U, is applied to the electrodes, then macroscopically a homogeneous electric field will appear inside the filter medium. The homogenous field strength can be calculated by equation (1):

$$E_h = \frac{U}{l} \tag{1}$$

It is possible to get a high electric field strength either by applying a high voltage, U, for a given distance, l, or by making the distance, l, very small and keeping the voltage, U, constant. For a thin filter media (l<1mm) only 100V has to be applied to get a field strength inside the filter media in the kilo volt range.

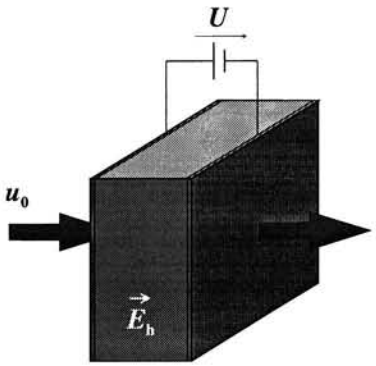

Fig. 1: Fibrous filter media between permeable electrodes

THEORETICAL INVESTIGATIONS

The performance of a filter is macroscopically described by two characteristic parameters: The penetration, P, of particles which get through the filter, and the pressure drop, Δp, across the filter.

The pressure drop can be calculated from the geometric dimensions and the process parameters of the filter. The quantities of equation (2) are thickness, l, of the filter, packing density, α, fiber diameter, D_F, face velocity, u_0, of air, the hydrodynamic factor, Ku, and the dynamic viscosity, μ, of air. The hydrodynamic factor, Ku, can either be fitted by experimental investigations or can be determined theoretically [3].

$$\Delta p = 16 \frac{l \cdot \alpha \cdot \mu \cdot u_0}{D_F^{\,2} \cdot Ku} \tag{2}$$

The penetration, P, is depending on the geometric dimensions of the filter and the single fiber efficiency, η, which has to be investigated microscopically.

$$P = \exp\left(-4 \frac{l \cdot \alpha}{D_F (1-\alpha) \pi} \eta \right) \tag{3}$$

The single fiber efficiency is explained in section 2. It depends on particle parameters, filter parameters, the face velocity and also external forces. These external forces in our case are electric forces. It is interesting to note that the pressure drop is not effected by the electric field, so electric forces only change the single fiber efficiency and reduce the penetration. Electric forces can thus be exploited to increase filter performance without increasing pressure drop.

In section 1 the different deposition mechanisms are explained. To do that, the particle deposition on a single fiber has to be investigated microscopically. The flow field and the electric field around the fibers have to be known. For the description of the flow field the solution of Kuwabara [3] with the extensions of Pich [4] (aerodynamic slip on the fiber

surface) is used. The electric field around a single fiber neglecting the effect of neighboring fibers in a homogenous electric field can be described by equation (4) in polar coordinates.

$$\vec{E}_F(r,\theta) = E_h \cdot \left[\begin{pmatrix} 1+\alpha_F\left(\frac{D_F}{2\cdot r}\right)^2 \\ -1+\alpha_F\left(\frac{D_F}{2\cdot r}\right)^2 \end{pmatrix} \cdot \begin{pmatrix} \cos(\theta)\cdot\vec{e}_r \\ \sin(\theta)\cdot\vec{e}_\theta \end{pmatrix} \right] \tag{4}$$

The dielectric factor, α_F, is a function of the relative permittivity, $\varepsilon_{r,F}$, of the fiber material.

$$\alpha_F = \frac{\varepsilon_{r,F}-1}{\varepsilon_{r,F}+1} \tag{5}$$

1 Deposition Mechanisms

In uniform motion of particles the forces acting on particles are in equilibrium.

$$\Sigma\vec{F} = \vec{0} \tag{6}$$

Here the contributing forces are the inertial force, the drag force, external forces, $\vec{F}_{ext}$, and a random force, $\vec{A}(t)$, due to Brownian motion. Then equation (6) becomes

$$m_p \cdot \frac{d\vec{v}}{dt} + \frac{1}{b_p}(\vec{v}-\vec{u}) = \vec{F}_{ext} + \vec{A}(t) \tag{7}$$

where, m_p, is the mass of the particles, b_p, the mechanical mobility, $\vec{v}$, the velocity of particles and, $\vec{u}$, is the velocity of the fluid at the particle position. The particle mobility, b_p, can be calculated using Stokes law and the slip correction, C_c, where, D_p, is the particle diameter and, μ, is the dynamic viscosity of the fluid.

$$b_p = \frac{Cc}{3\cdot\pi\cdot\mu\cdot D_p} \tag{8}$$

The particle trajectories are determined by integrating equ. (7). These trajectories are later used to calculate single fiber efficiencies. The different mechanical and electrical deposition mechanisms are explained below.

1.1 Interception:

Interception is the deposition mechanism that occurs, when particles follow the streamlines of the fluid and touch the fiber. This only happens if streamlines are close enough to the fiber. If a streamline is closer to the fiber than one particle radius, then the particle touches the fiber and is considered to be captured. The particles are then held by adhesion forces.

1.2 Inertial Impaction

Inertial impaction occurs when the inertial force on a particle is strong enough cause it to leave curved streamlines. The inertial force tries to maintain the direction of the particles. It depends on the particle mass m_p and its acceleration $\dot{\vec{v}}$.

The behavior of impacting particles is shown in Figure 2. In that figure can be seen the influence of the inertia of particles (particles are not able to follow the streamlines) and also the influence of interception.

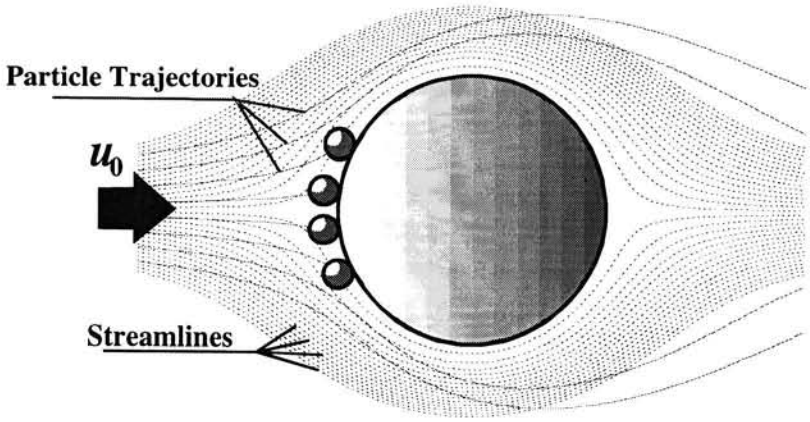

Fig. 2: Particle trajectories and streamlines near a fiber

1.3 Diffusion

Diffusion is the non-deterministic motion of small particles. It is called Brownian motion and is related to the thermal energy of particles. The diffusion process is described by the mean displacement, $\sqrt{\overline{x^2}}$, of particles in a given time, t.

$$\sqrt{\overline{x^2}} = \sqrt{2 \cdot D \cdot t} \tag{9}$$

The diffusion coefficient, D, depends on the mechanical mobility of the particles and their absolute temperature, T.

$$D = b_P \cdot k_B \cdot T \tag{10}$$

To describe a particle trajectory including diffusion, the equation of motion (7) is solved for particle position and velocity. At small timescales, a stochastic walk is added to the particle position and to the velocity. The statistic properties of the random walk and displacement in velocity are published by Chandrasekhar [2].

This capture mechanism is more efficient for smaller particles, because their diffusion coefficient is larger than that of larger particles.

1.4 Deposition Through Dipole Force

In Figure 3 a fiber between two electrodes is shown. The fiber becomes polarized by the applied electric field. The line dipole of the fiber is represented by the separated charges in the middle of the fiber. Also the particles become polarized. The force acting on the particle depends on the particle position. Particle 1 and particle 3 feel an attractive force and particle 2 feels a weaker repulsive force.

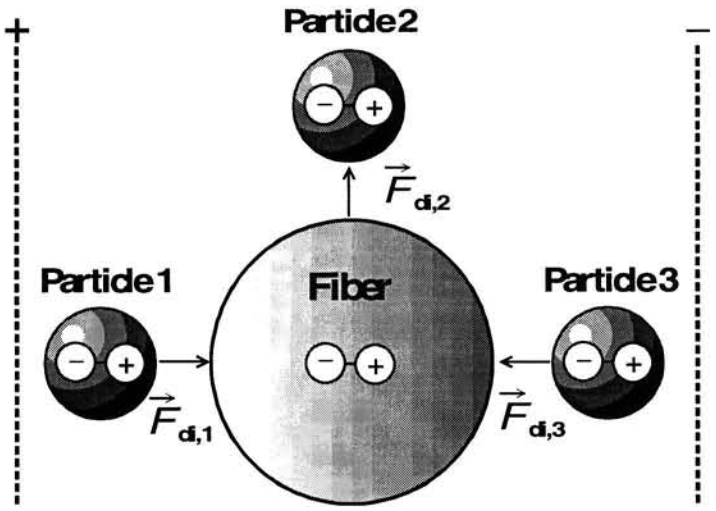

Fig. 3: Dipole force

The magnitude of the force as a function of particle position can be calculated from equation (11).

$$\vec{F}_{di}(r,\theta) = -\frac{2\cdot\pi\cdot {D_P}^3\cdot\alpha_P\cdot\alpha_F\cdot {E_h}^2}{D_F}\left(\frac{D_F}{2\cdot r}\right)\begin{pmatrix}\alpha_F\left(\frac{D_F}{2\cdot r}\right)^2+\cos(2\cdot\theta)\\ \sin(2\cdot\theta)\end{pmatrix}\begin{pmatrix}\vec{e}_r\\ \vec{e}_\theta\end{pmatrix} \tag{11}$$

It shows a cubic dependence on the particle diameter, D_P. The dielectric parameter, α_P, is dependent on the relative permittivity, $\varepsilon_{r,P}$, of the particle material.

$$\alpha_P = \frac{\varepsilon_{r,P}-1}{\varepsilon_{r,P}+2} \tag{12}$$

1.5 Deposition Through Coulomb Force

This deposition mechanism works only for charged particles. The charged particles are effected by the homogenous electric field and they also recognize the induced line dipole in the fiber. This behavior is shown in Figure 4. The flow has the same direction as the electric

field. Positively charged particles are accelerated in flow direction and negatively charged against the flow direction. Near the fiber at the front stagnation point the line dipole causes an attractive force for positively charged particles and at the rear stagnation point a repulsive force. Negatively charged particles are attracted to the positively charged site of the fiber dipole. They will deposit mainly near the rear stagnation point of the fiber.

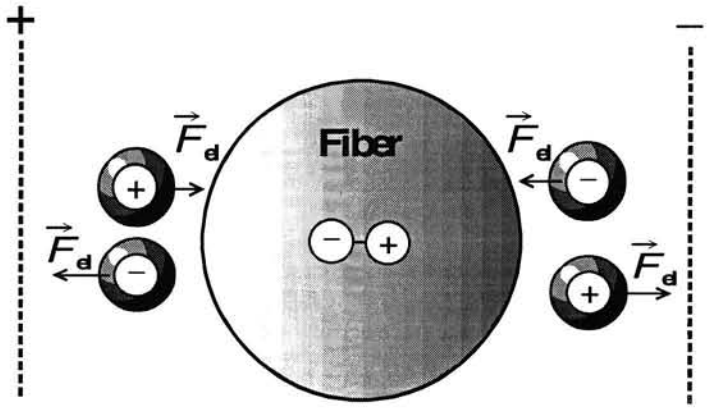

Fig. 4: Coulomb force

The coulombic force on charged particles can be calculated by the following equation.

$$\vec{F}_q(r,\theta) = n \cdot q_0 \cdot \vec{E}_F(r,\theta) \tag{13}$$

In this equation n is the number of elementary charges q_0 and $\vec{E}_F$ is the electric field around the fiber described in equation (4)

2 Single Fiber Efficiency

The forces described in section 1 are introduced in equation (7). This 2nd order differential equation is solved by the Runge-Kutta method to get particle trajectories near the fiber. These particle trajectories are analyzed to evaluate the single fiber efficiency, η, which is used to predict the penetration, P, using equation (3). Figure 5 shows particle trajectories near the fiber. They are determined for different initial starting positions upstream the fiber. The initial position of the limiting trajectory is used to calculate the single fiber efficiency.

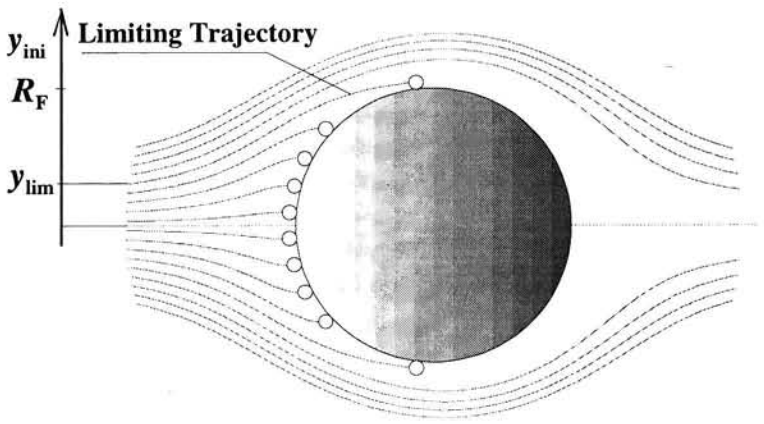

Fig. 5: Particle trajectories neglecting Brownian motion

In the last example diffusion was neglected. To include this mechanism, a random walk of the particles for each small time step, is added to give a new position on the trajectory. Particle trajectories including Brownian motion are shown in Figure 6.

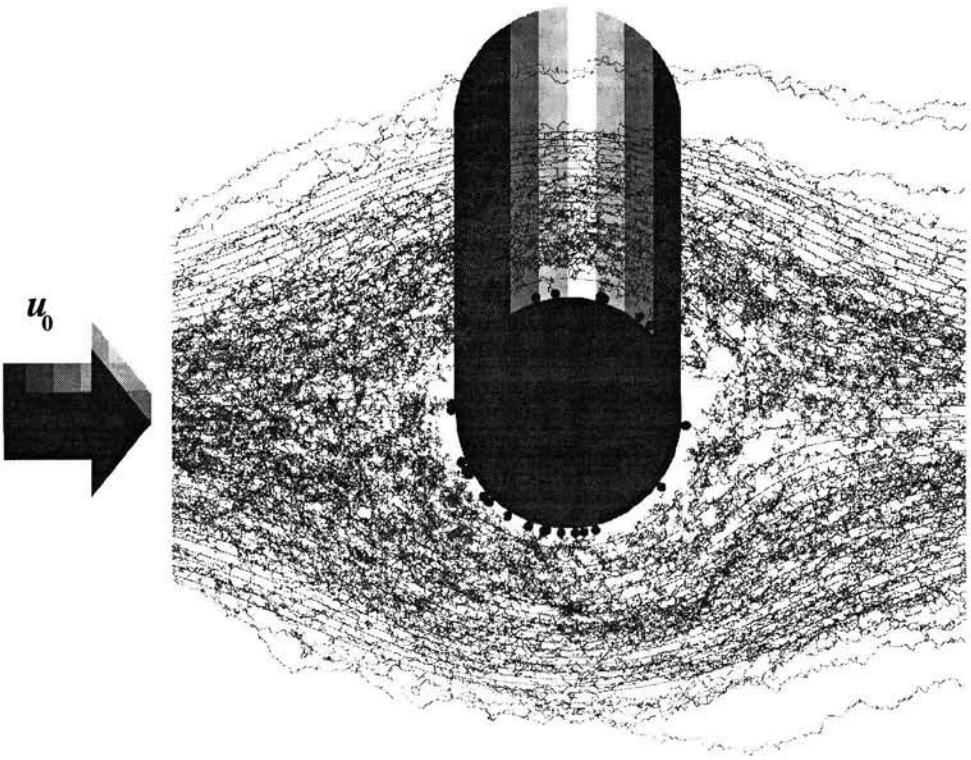

Fig. 6: Particle trajectories including Brownian motion

In the case of diffusion the calculation of the single fiber efficiency is more complicated, because no limiting trajectory exists.

2.1 Single Fiber Efficiency Neglecting Brownian Motion

Each particle has a probability of capture depending on its initial position. When diffusion is neglected, the probability is 1 for initial positions between the centerline of the fiber and the initial position, y_{lim}, of the limiting trajectory. For initial positions outside the initial position of the limiting trajectory the probability of particle capture is 0. The single fiber efficiency is defined in equation (14).

$$\eta = \frac{y_{lim}}{R_F} \tag{14}$$

It is the ratio the initial position of the limiting trajectory, y_{lim}, to the fiber radius, R_F. Only the limiting trajectory has to be found to calculate the single fiber efficiency.

2.2 Single Fiber Efficiency Including Brownian Motion

If Brownian motion is included, there is no limiting trajectory. The single fiber efficiency must be determined by calculating many trajectories. For each initial position only a probability of capture can be found. In Figure 7 the probability of particle capture is shown as function of the initial position (solid line).

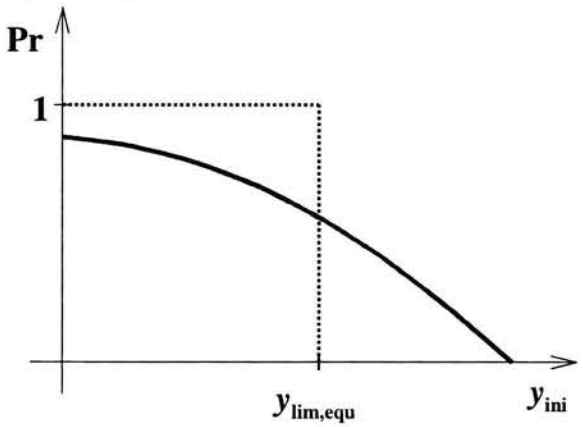

Fig. 7: Probability of Particle Capture as a function of Particle initial Position where Brownian motion is included.

To evaluate the single fiber efficiency, an equivalent limiting trajectory has to be found. This can be done by comparing the areas below the curve of probability functions with and without Brownian motion. The area below the dotted line (probability without diffusion) must be the same as the area below the solid line (probability with diffusion). An equivalent limiting trajectory, $y_{lim,equ}$, is found. Mathematically this can be done by solving the following equation:

$$y_{lim,equ} = \int_0^{\infty} \Pr(y_{ini})\,dy_{ini} \tag{15}$$

The single fiber efficiency is then calculated in the same way as in section 2.2 with equation (14).
This approach was checked by calculating the deposition by diffusion only and comparing it with the results of calculations with continuum approach [1].

3 Deposition Pattern

By analyzing the particle trajectories not only the single fiber efficiency can be determined. Also the positions where the particles deposit can be investigated. The fiber is therefore divided into surface sections and for each section the share of deposited particles is counted, Figure 8.

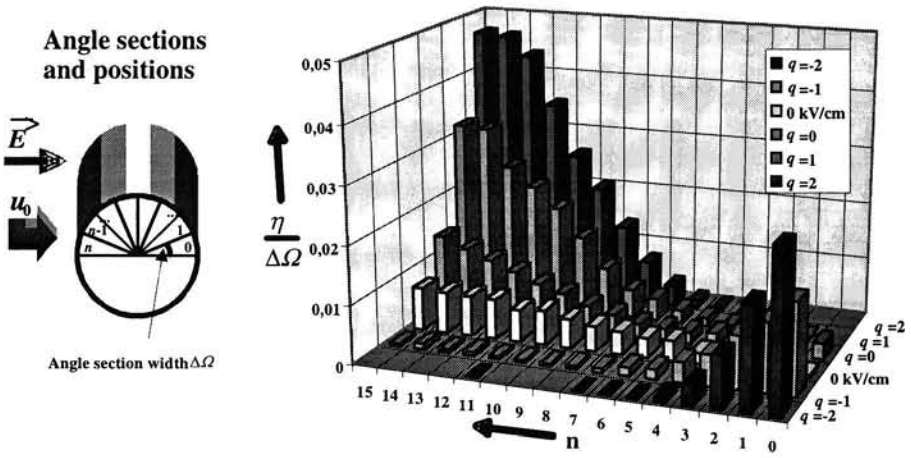

Fig. 8: Location of particle deposition on the fiber for different charged particles

SUMMARY

- Particle trajectories accounting for electric forces as well for Brownian motion and other mechanical forces were simulated.
- Single fiber efficiencies were determined.
- The locations of particle deposition around unloaded fibers were calculated.
- The influence of electrical forces on particle deposition around single fibers was investigated.

REFERENCES

[1] Brown, R.C. (1993) *Air Filtration.* New York: Pergamon Press

[2] Chandrasekhar, S. (1943) Stochastic Problems in Physics and Astronomy Chapter II: The Theory of the Brownian Motion. *Rev. Mod. Phys.* **15**(1):20-44

[3] Kuwabara, S. (1959) The forces experienced by randomly distributed parallel circular cylinders or spheres in a viscous flow at small Reynolds numbers. *Journal of the Physical Society of Japan*, **14**(4): 527 – 532

[4] Pich, J. (1971) Pressure characteristics of fibrous aerosol filtration. *Journal of Colloid and Interface Science*, **37**(4): 912 - 917

[5] Ramarao, B.V.; Tien, C.; Mohan, S. (1994) Calculation of single fiber efficiencies for interception and impaction with superposed Brownian motion. *J. Aerosol Sci.*, **25**(2): 295 - 313

[6] Rao, N.; Faghri, M. (1990) Computer modeling of electrical enhancement in fibrous filtration. *Aerosol Science and Technology* **13**: 127 – 143

ESSENTIAL NOMENCLATURE

b_P	[s/kg]	mechanical mobility
k_B	[J/K]	Botzmann constant
l	[m]	distance
m_P	[kg]	particle mass
q_0	[As]	elementary charge
r	[m]	coordinate
t	[s]	time
$\vec{u}$	[m/s]	fluid velocity
u_0	[m/s]	face velocity
$\vec{v}$	[m/s]	particle velocity
y	[m]	distance
D	[m^2/s]	diffusion coefficient
D_F	[m]	fiber diameter
D_P	[m]	particle diameter
$\vec{E}$	[V/m]	electric field strength
$\vec{F}$	[N]	force
P	-	penetration
R_F	[m]	fiber radius
U	[V]	voltage
α	-	packing density
ε_r	-	relative permittivity
η	-	single fiber efficiency
μ	[kg/(m s)]	dynamic viscosity
θ		coordinate

ACKNOWLEDGEMENTS

These investigations are part of the project „Verbesserung der Abscheideleistung von Luftfiltermedien durch zuschaltbare elektrische Mikrofelder" in cooperation with the Forschungsvereinigung für Luft und Trocknungstechnik (FLT). The authors acknowledge the financial support by the Bundeswirtschaftsministerium and the Arbeitsgemeinschaft industrieller Forschungsvereinigungen, AIF-No. 10526N

Electret Filters For Respiratory Protection

G.J.Bostock
European Laboratory, 3M (United Kingdom) plc., Heighington Lane , Aycliffe, Co.Durham, DL5 6AF, UK.

KEYWORDS

aerosols, filtration, respirator, electrets

INTRODUCTION

Environmental pollution should be controlled such that it is safe for a person to operate in an area. However, in some workplaces this is not possible and it necessary to use personal respiratory protection. The purpose of the protection is to reduce the amount of nuisance and toxic material inhaled and to protect the lungs from the damaging effects of fine aerosols. The human body has its own defence mechanisms to protect the lungs but it is still susceptible to airborne particles of less than about 7 μm. Filters for respiratory protection must therefore be effective down into the submicron range. The filters must also present a low resistance to breathing and be light in weight so not as to unduly burden the wearer. It is in this area that electret filters can offer advantages over filters constructed from glass fibre papers and similar media. Methods of assessing filter performance are discussed.

One of the potential disadvantages of electret filters is their deterioration with use. Advanced filter media are under development that minimise this effect allowing effective particulate respiratory filters to be designed for a wide range of applications.

TEST METHODS

The European Standard EN143:1991 defines performance requirements for three classes of particulate respirator filters based on physiological data and also what is reasonably practical to achieve, Figure 1.

Figure 1: European Standard EN 143:1990
Requirements for particulate filters.

	P1	P2	P3
Penetration NaCl aerosol	20	6	0.05 %
Penetration Paraffin oil	--	2	0.01 %
Pressure Drop at 30 $l.min^{-1}$	0.6	0.7	1.2 mbar
Pressure Drop at 95 $l.min^{-1}$	2.1	2.4	4.2 mbar

The main parameters defined are breathing resistance and filter penetration by two defined aerosols, both of approximately 0.5 μm mass median aerodynamic diameters. The test

aerosols are defined as a sodium chloride solid particulate aerosol formed by the atomisation then evaporation of a 1% aqueous solution of sodium chloride, and a paraffin oil mist formed by the atomisation of a purified mineral oil. A similar Standard, EN149:1991, exists for filtering facepiece respirators, that is respirators which are constructed almost exclusively from filter medium, Figure 2.

Figure 2: European Standard EN 149:1991
Requirements for filtering facepiece respirators

	FFP1	FFP2	FFP3	
Penetration NaCl aerosol	20	6	3	%
Penetration Paraffin oil	--	2	1	%
Pressure Drop at 30 l.min^{-1}	0.6	0.7	1.0	mbar
Pressure Drop at 95 l.min^{-1}	2.1	2.4	3.0	mbar
Exhalation at 160 l.min^{-1}	3.0	3.0	3.0	mbar
Total Inward Leakage	22	8	2	%

This Standard also includes a requirement for total inward leakage and it assesses by determining the sodium chloride aerosol concentration within the respirator as worn.

When various filter media were tested at a realistic face velocity of 0.10 m.s^{-1}, the advantage of electret media could be seen in the low pressure drop combined with low penetration, Figure 3.

Figure 3 Quality Factors

Test Aerosol	Filter Medium	Pressure Drop ΔP mbar	Penetration p %	Quality Factor -Ln(p)/ΔP
NaCl	Glass Fibre Paper	3.19	1.90	1.24
	Electret A	0.20	0.98	23.13
	Electret B	0.30	0.65	16.79
	Electret C	1.17	0.75	4.18
		Pressure Drop mbar	Penetration %	Quality Factor -Ln(p)/p.d
Oil	Glass Fibre Paper	3.05	2.79	1.17
	Electret A	0.28	1.52	14.95
	Electret B	0.26	3.94	12.44
	Electret C	0.94	4.45	3.31

A quality factor based on the logarithm of the penetration can be calculated in order to compare directly the performance of the different media. Also apparent are the different penetrations of the two aerosols through the same medium. This difference can be partially explained by differences in the particle size distribution between the two aerosols. It is also

due to the difference in charge levels on the two aerosols. The penetration of a sodium chloride aerosol through layers of an electret material "C" was measured, Figure 4.

Figure 4: Effect of Ioniser NaCl Aerosol

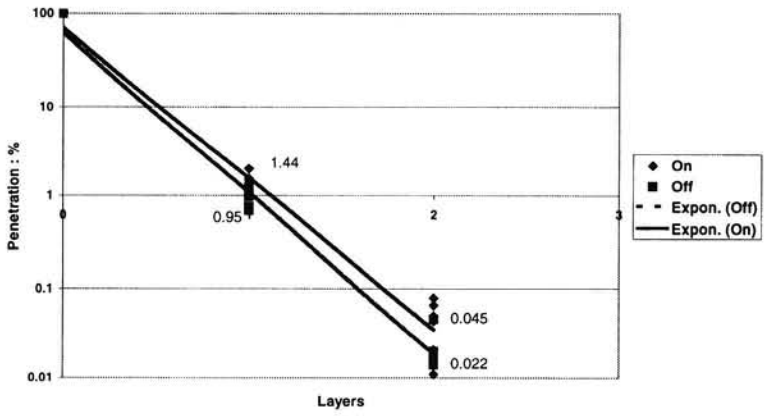

In one set of tests, the aerosol was used as generated. The tests were then repeated after injecting negative and positive ions into the air used to dry the aerosol. It is assumed that the ions combine with the charged aerosol causing the charge to tend towards the equilibrium level. The readings showed that the penetration increased with the ioniser in operation. When the tests were repeated with a glass fibre filter medium the penetration was unaffected. When the tests were performed with an oil aerosol and electret filter medium "C" then the effect was for the ioniser to decrease the penetration, Figure 5.

Figure 5: Effect of Ioniser Paraffin Oil Mist

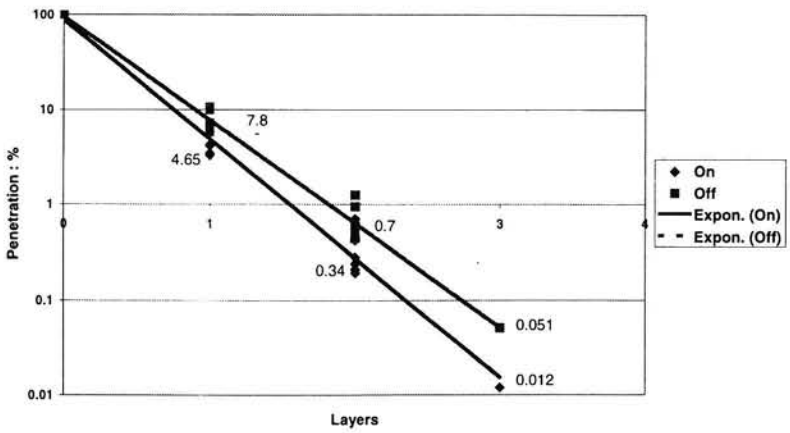

These results are consistent with the charge on the aerosol having little effect on the filtration mechanisms occurring within the glass fibre paper. The penetration of the electret medium is however, affected by the aerosol charge. As the sodium chloride aerosol is generated from an ionic solution, which is then subject to evaporation, it is expected that the aerosol would possess a higher charge than the equilibrium level. The charge level on the aerosol is therefore reduced by the action of the ioniser leading to a higher penetration. The opposite appears to be true for the oil mist generated from the bulk liquid which is an electrical insulator. The oil aerosol has a charge level as generated lower than the equilibrium level and the effect of the ioniser is to increase the aerosol charge level leading to a decrease in the penetration through the electret medium.

The above observation brings into question whether a sodium chloride aerosol generated from an aqueous solution is an appropriate test aerosol to assess respirator filters because of its apparent high charge level. In the test methods currently specified in the United States for respirator filters, when a sodium chloride aerosol is selected it is first subjected to the actions of an ioniser to reduce the charge level. In the proposed revision to the European Standards, all respirator filters are also assessed against an oil aerosol with a low charge level.

When assessing the suitability of a test aerosol it is desirable to have some knowledge regarding the charge levels that might be found on industrial aerosols. Limited experiments had been performed to determine charge levels using an electric field applied across two parallel plates. When coal dust was vigorously dispersed in air, the resulting particles were found to be highly charged when compared to ambient particles which were assumed to have achieved equilibrium. The results for 1μm particles are shown in Figure 6.

Figure 6: Charge on 1um particles

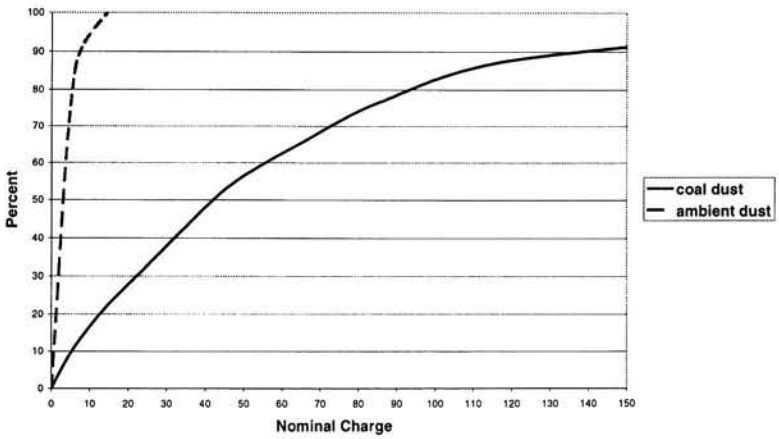

LOADING

If a glass fibre filter paper is loaded with the sodium chloride aerosol, the penetration rapidly decreases and the pressure drop increases, Figure 7.

Figure 7: Glass Fibre Paper Filte, NaCl Aerosol

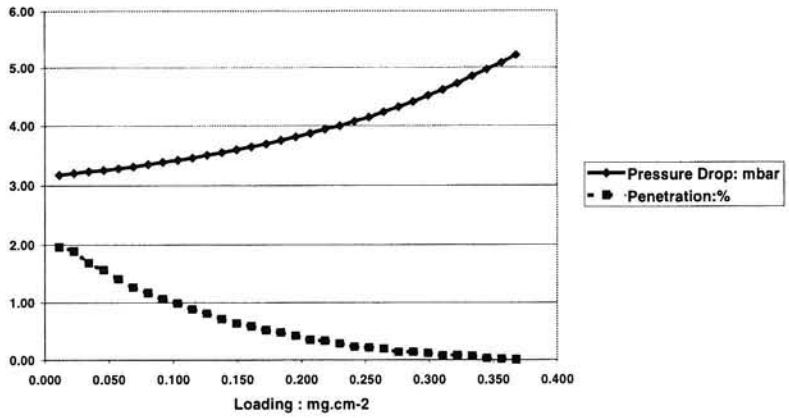

In the case of electret media "A" and "B" the penetration increases as the electric fields are disrupted by captured particles but the pressure drop remains low and almost constant, Figure 8.

Figure 8: Electret Filter Media, NaCl Aerosol

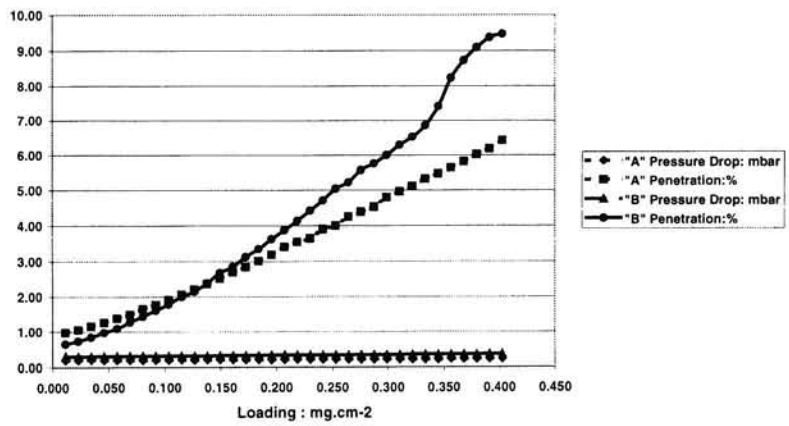

When electret medium "C" is subjected to the same loading test the penetration initially rises but then decreases. The pressure drop shows a small increase, Figure 9.

Figure 9: Electret Filter Medium "C", NaCl Aerosol

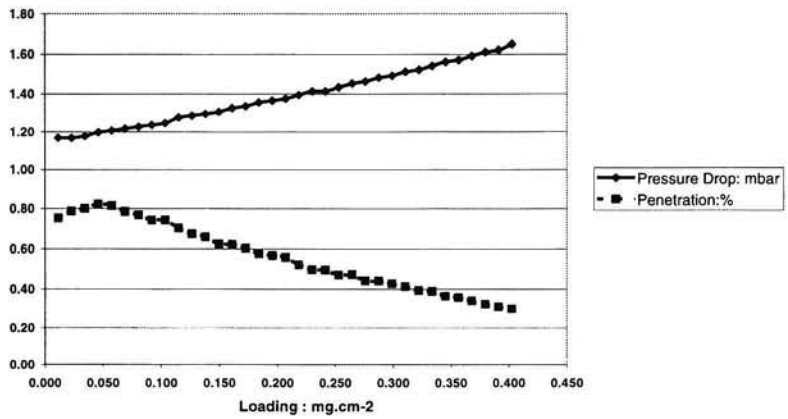

The differing behaviour between materials "A" and "B" and material "C" is that the former materials have an effective fibre diameter of around 30µm while that of material "C" is in the region of 5 µm. By producing electrets with finer fibres it is possible to combine the low breathing resistance of an electret with the resistance to degradation of a glass fibre paper. By laminating coarse and fine fibred electret media of appropriate basis weights it is possible to design filters with low breathing resistances and low rates of degradation to suit various applications, Figure 10.

Figure 10: Composite Laminate, NaCl Loading

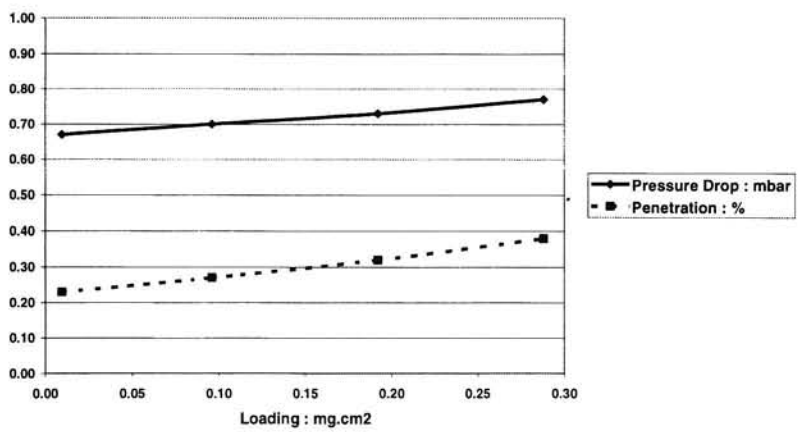

How these laboratory loading tests relate to actual industrial exposure has still to be investigated.

The above loading data were generated with a sodium chloride aerosol. Different results are obtained with a liquid aerosol such as the oil mist. With the glass fibre filter paper, the rate of decrease of the penetration and the rate of increase of the pressure drop is less than with the solid aerosol as the captured particles cannot form agglomerates but flow over the fibre surface, Figure 11.

Figure 11: Glass Fibre Filter Paper, Oil aerosol

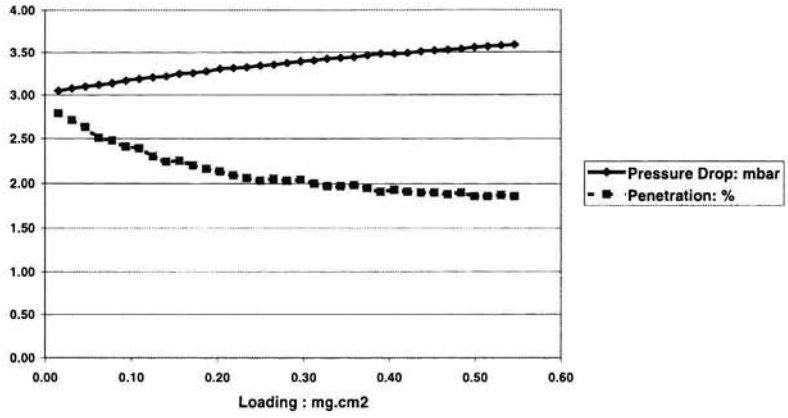

With the fine fibred electret "C" a similar mechanism appears to apply so that the penetration continues to slowly rise but there is little change in the breathing resistance, Figure 12.

Figure 12: Electret Filter Medium "C", Oil Aerosol

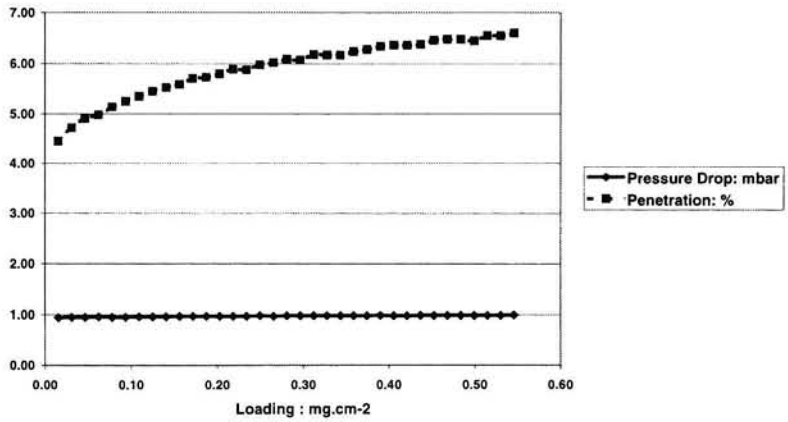

If the observed behaviour is due to the oil flowing over the fibre surface, then it should be possible to modify the surface so that it is not wetted by the oil. If this is done then the change in penetration on exposure to the oil mist is reduced, Figure 13.

Figure 13: Oil Resistant Electret Medium, Oil Aerosol

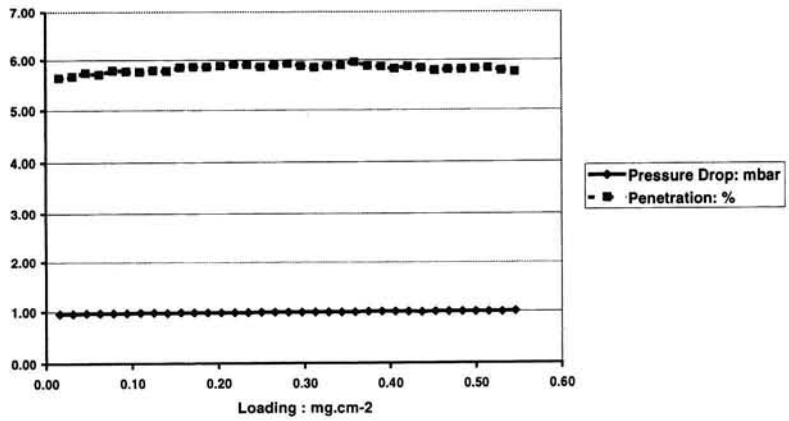

When electret media "A" and "B" are exposed to the oil mist challenge, the rate of loss of performance is markedly different even though the two materials performed in a similar manner when loaded with the sodium chloride aerosol, Figure 14

Figure 14: Electret Filter Media, Oil Aerosol

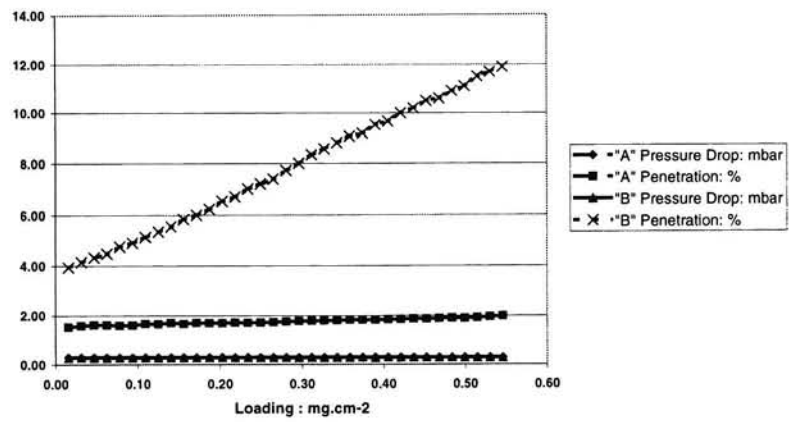

This difference in performance illustrates the difficulties that will be encountered in attempting to devise a laboratory test that will indicate how the respirator filter might perform after extended industrial use.

APPLICATIONS

Electret materials have advantages over glass fibre type materials in manufacturing. As they are frequently manufactured from thermoplastics, they can be readily folded and welded by ultrasonics into three dimensional shapes. It is difficult to form a filtering facepiece respirator from a glass fibre paper as the constant folding can release man made

fibres into the wearer's breathing zone. Pleated paper filters are more robust and easily handled if encapsulated but this will lead to a heavier filter and a more complex manufacturing process. Increasing the effective area of the filter and therefore decreasing the face velocity provides the advantage of reduced penetration for electret filter media, Figure 15.

Figure 15: Effect of Flow Rate

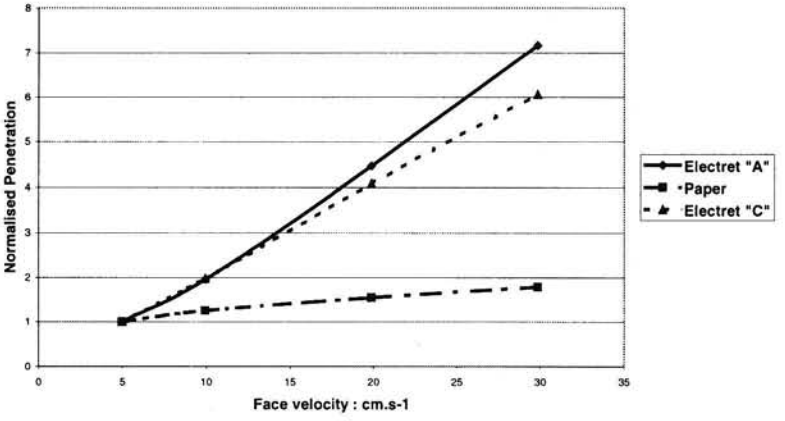

The relative lack of change in the performance of the glass fibre filter paper is indicative of a different filtration mechanism. A large effective area also gives the advantage of a lower breathing resistance and greater resistance to clogging. A large surface area can be achieved, without adversely affecting the wearer's field of view, by using both the front and back surfaces of an unencapsulated electret filter or by welding pleats onto the surface of a filtering facepiece respirator.

In use a low resistance filter will decrease the discomfort of wearing the respiratory protective device although if the pressure drop is below approximately 1 mbar at 95 $l.min^{-1}$ the improvement may be small, Love (1981). A low resistance will also minimise faceseal leakage due to an imperfect fit of the facepiece. The low weight achievable with an electret filter will minimise the strap tensions necessary to keep the facepiece securely against the face and will reduce strain on the neck muscles. Hopefully this will increase the wearer acceptance of the device and increase wear time. However good the filter, the occupational exposure can only be decreased by a factor of two if the operator can only be persuaded to wear the device for half the required period.

One possible disadvantage of electret filter media is that they are frequently good thermal insulators. Precautions should be taken in designing filtering facepiece respirators to minimise the thickness of the webs to prevent undue heat build up and hence discomfort. This can be minimised by the incorporation of a valve to allow for the escape of the warm, humid exhaled air. The exhalation valve needs to be carefully designed to offer a very low resistance or the air will still preferentially flow out through the low resistance filter medium.

REFERENCES

European Standard EN143. Respiratory protective devices - Particle filters - Requirements, testing, marking. CEN 1990

European Standard EN149. Respiratory protective devices - Filtering half masks to protect against particles - Requirements, testing, marking. CEN 1991

Love R.G. (1981) *Respiratory Protection.* (Edited by Ballantyne and Schwarbe) Chapman and Hall Ltd., London

Optical and Electrostatic Measurement of Filter Efficiency

Wladyslaw W. Szymanski

Institute of Experimental Physics, University of Vienna
Boltzmanngasse 5, A-1090 Vienna, Austria

KEYWORDS

fractional filter efficiency, most penetrating particle size, counting efficiency, particle refractive index, charged particles, mean electrical charge, condensation nuclei

INTRODUCTION

Filtration is probably the most widely used technique for particle removal from gases. Filter collection efficiency and most penetrating particle size are important indicators of filter performance, which can be determined with various size-selective detection methods and varying challenge materials [1]. Such an approach is particularly useful when a comparative quantification of various filters, particularly in the initial stages of filtration is needed. The reliability of such measurements however, can be a subject of chosen detection method in connection with the selected particulate material, its electrical condition, size range and concentration. Hence the determination of size dependent filtration characteristics requires instrumentation capable of particle sizing and counting.

Single optical particle spectrometers provide these possibilities, however the sizing accuracy of these devices depends on the particle material and also on the specific instrumental design [2, 3]. Moreover, concentration measurement without dilution devices is possible in rather narrow concentration ranges. At higher particle concentrations the coincidence errors, resulting from presence of more than one particle at a time in the sensing volume will affect the sizing and counting capability of a particle spectrometer and limit its usefulness for filter testing. In contrast to single optical particle spectrometers, the condensation nuclei counters are in principle not size selective instruments. They measure the particle number concentration based on the integral scattered light signal from an ensemble of droplets, which were formed on sub-countable particles (nuclei) by a condensational process. For that reason these instruments are particularly effective for measurement of sub-micrometer particles including even nanometer particle sizes. They are useful for fractional filter efficiency measurement only in connection with a particle size selecting device such as an electrostatic classifier [4]. This instrument segregates aerosol particles based on their electrical mobility. Its operational particle size range is typically limited to sub-micrometer aerosols. Under favorable circumstances an electrostatic classifier provides nearly monodisperse, singly charged particles. Such particles can be also conveniently detected by means of an aerosol electrometer. This instrument detects the charge carried by particles which relates directly to their concentration [5].

In this study the deceiving changes of filtration efficiency were investigated using the above mentioned techniques and various test aerosols. The impact of experimental practices on the shape of filter collection efficiency curves and location of the most penetrating particle size of fibrous and electret filters is presented.

OPERATING PRINCIPLES OF APPLIED TECHNIQUES

The description of the instrumentation used in this study given below is not attempted to be complete and comprehensive. It provides only their main features as far as they are relevant for this contribution.

a. *Single Optical Particle Spectrometer*

Optical particle spectrometers detect the intensity of scattered light from one particle at a time, while the particle is passing through a well defined sensing volume illuminated by a light source such as laser. The practical working particle size range for this group of instruments spans from about 100 nm to 10 μm. Concentration measurements above about $10^3 cm^{-3}$ are prone to coincidence errors.

Depending on the optical configuration, different response of particle spectrometers can be expected with varying refractive index of particles [2]. Response R is a function of particle diameter (d_p), its refractive index (m), the wavelength of illumination (λ) and if applicable also particle shape. For practical reasons it is prevalent to calculate the response based on the Mie theory of light scattering from spheres [6]. If the particle in question exhibits a pronounced non-sphericity, which is the case for e.g. fibrous particles the theoretical prediction of a spectrometer response may fail. The response R is defined here by the scattered light flux normalized to the incident radiation. For an unpolarized laser beam irradiating a particle the response R is given by:

$$R = \frac{\lambda^2}{4\pi^2} \cdot \int_{\theta_1}^{\theta_2} (I_1(d_p, \lambda, m, \theta) + I_2(d_p, \lambda, m, \theta)) \sin\theta \, d\theta \qquad Eq.1.$$

where I_1 and I_2 are scattered light intensities with parallel and perpendicular polarization, respectively. m is the refractive index d_p particle diameter and λ the wavelength if the irradiation. θ_1, θ_2 are scattering angles limiting the light collecting solid angle. Although the calibration of particle spectrometers is usually based on the response characteristics of the instrument to the monodisperse polystyrene latex (PSL) test spheres, calculations presented in this paper were also done for sodium chloride (NaCl). This is based on the fact that NaCl is increasingly popular filter testing material and its refractive index of 1.544 - 0.i is similar to the refractive index for PSL (1.59 - 0.i). This small difference in the real part of the refractive index influences only marginally the response. The non-sphericity of NaCl does not strongly affect the instrument's characteristics [2].

The response shown in Figure 1 represents the sizing performance of a spectrometer used in this study- LAS-X. Its scattering range spans from 35°-120°. For non-absorbing particles the response curve is in general a smooth function of the particle size. Response curve for absorbing particles, however shows basically no sizing sensitivity between about 0.3 μm and 1.0 μm causing a parallel shift of the response above 1.0um. This behavior influences tremendously the sizing capability of LAS-X and is manifested in a considerable under-sizing of absorbing particles above 0.3 μm with reference to the response curve for non-absorbing particles. This has a substantial impact on the filter collection efficiency characteristics as will be shown below.

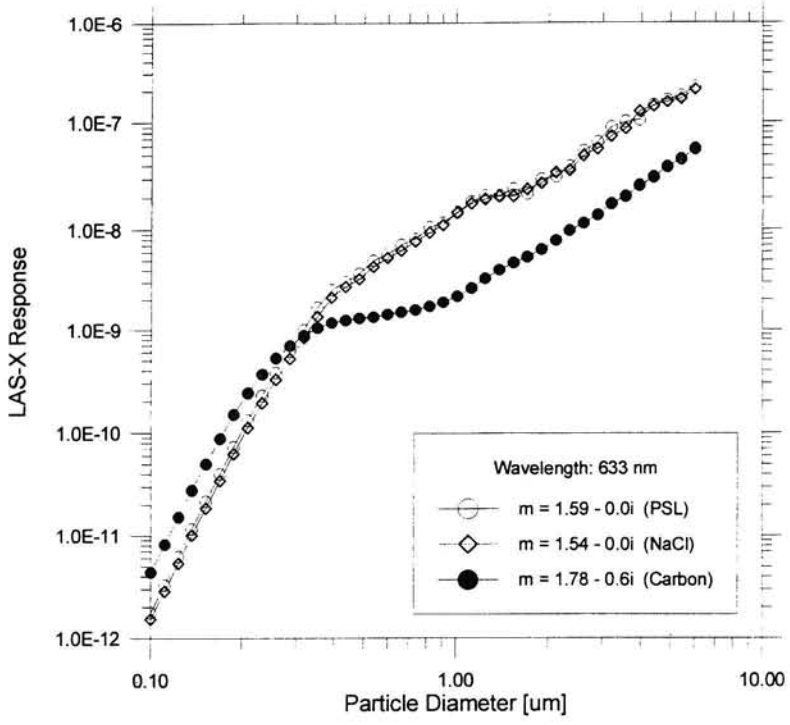

Fig. 1. Response of LAS-X to non-absorbing and absorbing particles

b. Electrostatic Particle Classification and Counting

Quasi-monodisperse aerosol particles with a given electrostatic mobility can be generated by extracting from a polydisperse input aerosol by means of an electric field. The electrostatic mobility is determined by the actual particle size and the number of electrostatic charges carried by the particle in question. The number of charges carried by a particle is determined by the Fuchs-Boltzmann charging probability [7, 8].

Differential Mobility Analyzer (DMA)

The principle of a DMA operation is based on the monotonic relationship between the electrical mobility of charged aerosol particles and particle size when particles are singly charged. To provide the aerosols conditioned in this way the particles are exposed to bipolar ions in the so-called "neutralizer" equipped the radioactive source (Kr^{85}) for the carrier gas ionization. This process known as bipolar charging results in a charge equilibrium with known fractions of neutral, singly and multiply charged particles. The DMA consists of two co-axial cylinders with a variable voltage applied to the inner cylinder, whereas the outer one is grounded. This provides an axial electrical field in which particles of a given electrical mobility can be deflected in a well-defined manner and allow an extraction of a certain mobility fraction.

The DMA is based on a design developed by Liu and Pui [9]. Recently a number of modification were presented extending the working range of DMAs to nano-sized particles [10, 11]. The equation governing the DMA performance is given by:

$$Z_{p,n} = \frac{n \cdot e \cdot C(d_p)}{3\pi \cdot \eta \cdot d_p} \qquad Eq.2.$$

where $C(d_p)$ is the particle slip correction, η the gas viscosity, e the elementary charge value and n the number of elementary charges carried by a given particle. $Z_{p,n}$ is the electrostatic mobility of a particle carrying n elementary charges.

Aerosol Electrometer (AE)

The AE measures the amount of charges carried by particles. These particles are deposited on an "absolute" filter within the unit and the total electrical current resulting from the charge transport by particles is measured by an electrometer. The current measured by the AE can be related to the input aerosol concentration by the equation:

$$I = N \cdot e \cdot Q_A \cdot \frac{1}{K} \qquad Eq.3.$$

where N is the particle number concentration, Q_A the gas flow rate, e the elementary charge value and K a correction factor accounting for the interference effects of multiply charged particles. Physically the value 1/K represents the mean electrostatic charge carried by a particle. K factor equal to unity indicates only singly charged aerosol particles. In such a case the measured current is an absolute indicator of the particle number concentration. The practical working size range of an AE spans from nano-sized particles to micrometer sizes.

Condensational Nuclei Counter (CNC)

The CNC measures the number concentration of particles (nuclei) by optical means. However, in contrast to an optical particle spectrometer particles are not counted directly but rather after passing through a vapor, which condenses then on a particle forming a droplet. Each droplet grows to a final size which is large enough to be detected optically. The final size of droplets is nearly independent on the nuclei size, that is why in CNCs the scattered light signal is a function of number concentration only.

For low concentrations a CNC operates in a similar way as a single particle spectrometer, counting single droplets. The CNC used in this study (TSI, Mod. 3020) operated typically in the photometric mode measuring light scattered from an ensemble of particles. This operation mode allows to measure number concentrations up to about $10^7 cm^{-3}$ within a sub-micrometer size range starting at about 10 nm. Assuming a proper calibration of the optical sensor, particle concentrations can be determined with the accuracy of the sampling flow rate of the CNC.

EXPERIMENTAL ARRANGEMENT AND PROCEDURES

The collection efficiency of glass fiber and electret filters with particles of different materials and varying state of charge was studied in a series of experiments described below. The purpose of these experiments was to measure the actual collection efficiency and to determine the magnitude of possible artifacts influencing such measurement due to specific combinations of challenge material and detection methods. The experimental set-up consists of a stable atomizing unit and allows to control particle size and charge state. In order to avoid differences in instrumental characteristics one instrument strategy for the up- and down-stream measurement was selected. The sampling strategy was optimized [12] to avoid sampling artifacts.

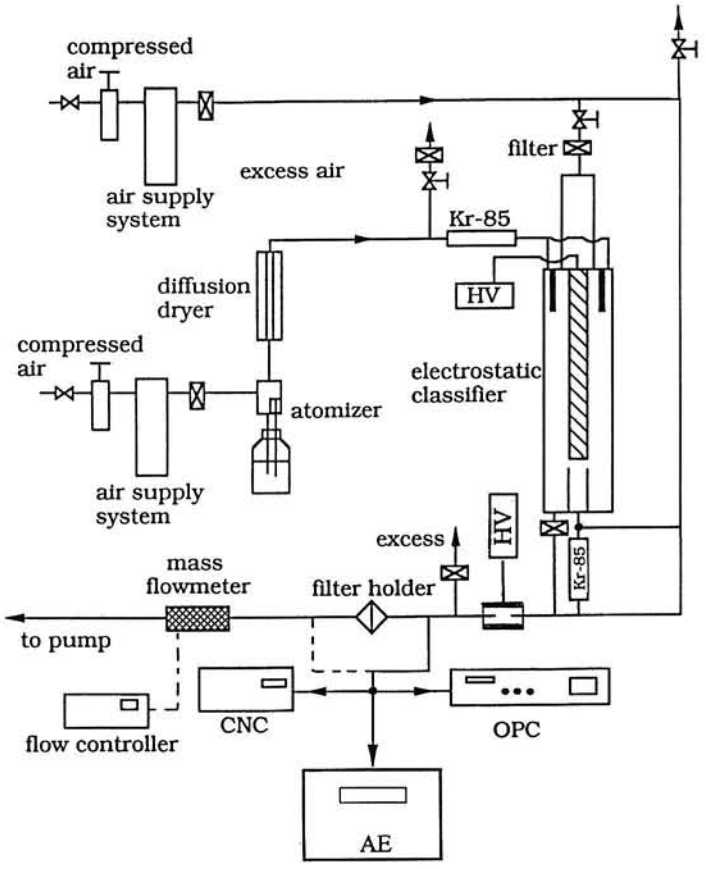

Fig. 2. Schematic diagram of experimental arrangement for fractional filter efficiency measurements with differently conditioned test particles.

Figure 2 presents a schematic diagram of the experimental system used. Primary, polydisperse aerosols were generated from appropriate solutions (NaCl in water, di-ethyl-hexyl-sebbacate (DEHS) in isopropyl alcohol (IPA), carbon in water).

Subsequently these particles were dried in a diffusion dryer and brought to charge equilibrium [7] in the "neutralizer". The so conditioned aerosol was then introduced into a DMA (TSI, Mod. 3071) to generate quasi-monodisperse particles of a given electrical mobility with well-defined sizes based on the Eq.2. For certain operation conditions it can be assumed that this aerosol is singly charged i.e. providing that the amount of particles carrying more than one elementary unit of charge is negligible. This aerosol was then used to study the filter collection efficiency of singly-charged particles with an aerosol electrometer [5]. Next, the singly-charged aerosol particles were passed through a charge neutralizer to obtain an aerosol in the Boltzmann charge equilibrium [7]. Finally, the aerosol directly exiting the DMA was passed through a homogenous electrostatic field in which all charged particles were removed leaving completely neutral test particles. With these particles filter efficiency was measured using the CNC, and in cases when the generated particles were within the measurable size range of the LAS-X, parallel measurement by means of both, CNC and LAS-X were performed. Sizing and counting by means of the single optical particle spectrometers such as LAS-X depends strongly on the fact that only one particle at a time can be present in the sensing volume for a reliable measurement. At higher concentrations this must not be the case and the so-called coincidence errors occur. In such a situation the measured concentration becomes increasingly underestimated and at the same time the measured particle size distribution becomes distorted. In order to determine the coincidence-free measurement range of the LAS-X the aerosol concentration was varied from about 100 to about 50,000 cm^{-3}.

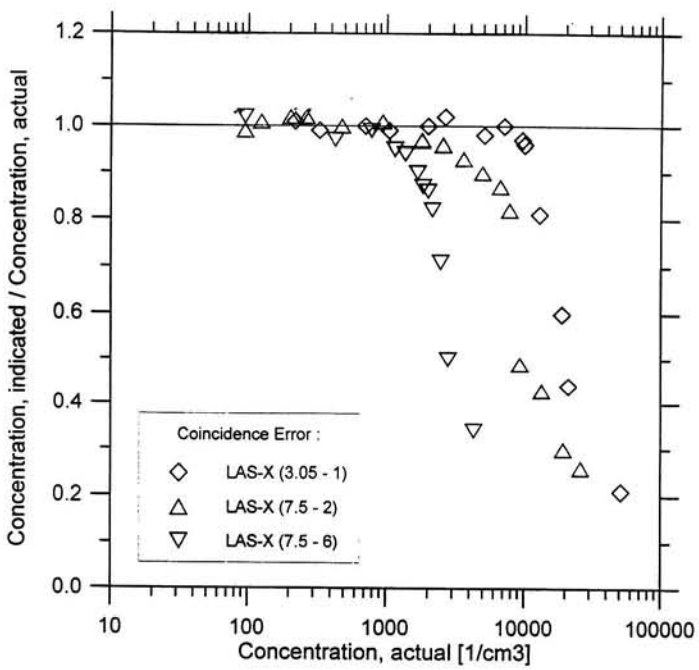

Fig. 3. Experimentally determined coincidence errors for LAS-X.

Figure 3 shows the concentration ratio determined by the LAS-X (indicated concentration) and by the CNC (actual concentration). For concentrations below about 10,000 cm^{-3} this ratio is equal to unity indicating coincidence-free concentration measurement. Above that value an increasing influence of coincidence effects deteriorates the concentration determination by means of LAS-X. This concentration limit is specific for an instrument and has to be taken into account for a reliable measurement. With increasing particle concentrations single particle detection methods fail and either a well-defined particle dilution system or integral measurement methods have to be applied [13].

In order to demonstrate the influence of coincidence conditions on the sizing capability of the aerosol spectrometer monodisperse test particles from a condensational aerosol generator of a La Mer type (di-ethyl-hexyl-sebaccate (DEHS) in an isopropyl alcohol solution with a subsequent electrostatic size classification [14] were used. The nominal particle size was 0.5 µm in diameter with a geometric standard deviation of 1.15. It can be seen in Figure 4 that at relatively low concentration of 1750 cm^{-3} the measured size distribution is basically contained in two channels correctly representing the actual, nearly monodisperse size distribution of particles. Increasing the number concentration to the indicated 20580 cm^{-3} completely changes the picture of the measured distribution. This is caused by the fact that the precondition for the correct measurement with an aerosol spectrometer such as LAS-X - one particle at a time in the sensing volume - fails with increasing concentration. In such a case the size distribution becomes distorted towards smaller particles due to the overlap of signals, and towards larger particles due to simultaneous detection of two or more particles.

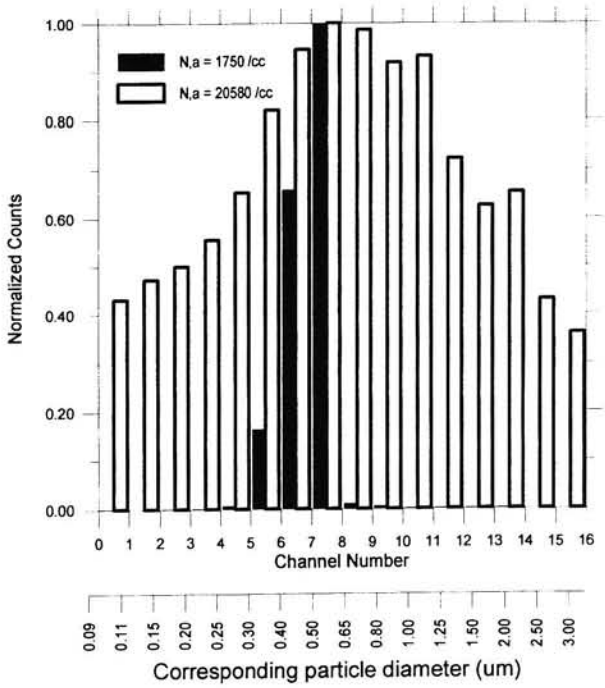

Fig. 4. Virtual change of measured size distribution due to coincidence effects.

RESULTS AND DISCUSSION

Based on the above presented rationale it is evident that an imperceptive application of an aerosol spectrometer for filter efficiency measurement will likely lead to unreliable results which may be caused by sizing error due to the variability of the refractive index of particulate material used for the filter challenge or by erroneous sizing and counting resulting from the optical coincidence.

Filter efficiency measurements with various materials and particle concentrations using LAS-X under rather extreme experimental conditions to scrutinize possible errors and their magnitude were performed [15]. The tested filter was made of a melt-blown electret material. The face velocity was chosen to be 10 cm/sec. As challenge material sodium chloride (refractive index: 1.54 - 0.i) and carbon particles (refractive index: 1.78 - 0.6i) in Boltzmann equilibrium were used. In this case polydisperse aerosol by-passing the DMA was used. The filter efficiency data was obtained at concentrations below 5,000 cm^{-3} which guarantees a coincidence free measurement. The results are presented in Figure 5. The efficiency data obtained with NaCl particles represents the actual filter efficiency curve. In comparison the efficiency data acquired with carbon particles shows quite a different and erroneous filter efficiency curve shape.

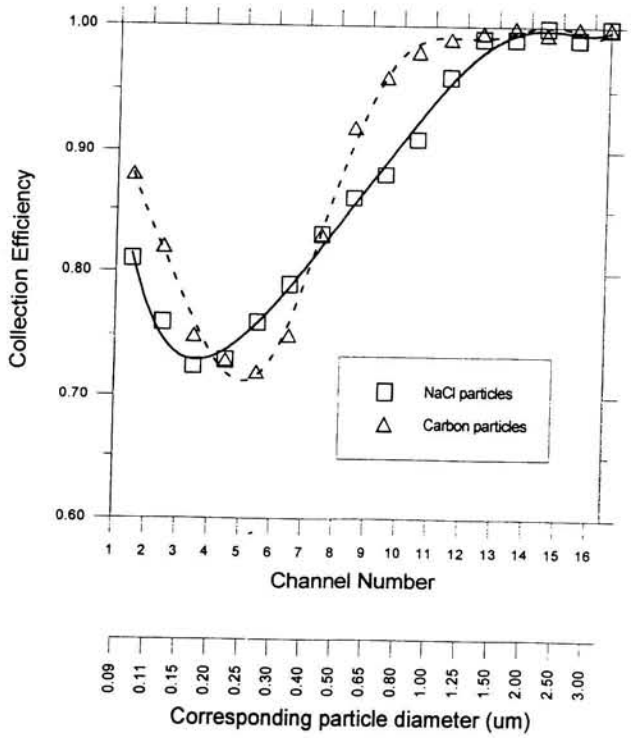

Fig. 5. Change of the collection efficiency due to difference in the refractive index of the filter challenge particles.

The apparently improved efficiency for particles below 0.3 µm results from particle oversizing by the instrument due to their refractive index. Above 0.3 µm the actual response curve of the LAS-X for absorbing particles is nearly flat up to about 1.0 µm. This results in agglomerating of data in lower channels resulting in much steeper apparent increase of the efficiency curve. Both effects have as a consequence a virtual shift of the most penetrating particle size from about 0.15 µm (NaCl) to about 0.3 µm (carbon).

Much more pronounced artifacts can be observed when measuring the filter collection efficiency under severe optical coincidence conditions. The result of such measurements is presented in Figure 6. The seeming decrease of the efficiency (high coincidence curve) is here caused by the false, too low particle concentration determination on the filter upstream side. Due to the actual filter efficiency e.g. at the most penetrating particle size of the order of 70% the concentration of the challenge particulate matter decreases allowing then the proper concentration determination on the downstream side of the investigated filter, hence imitating extremely low filter efficiency. These effects may particularly influence efficiency measurement of filters with higher collection efficiencies.

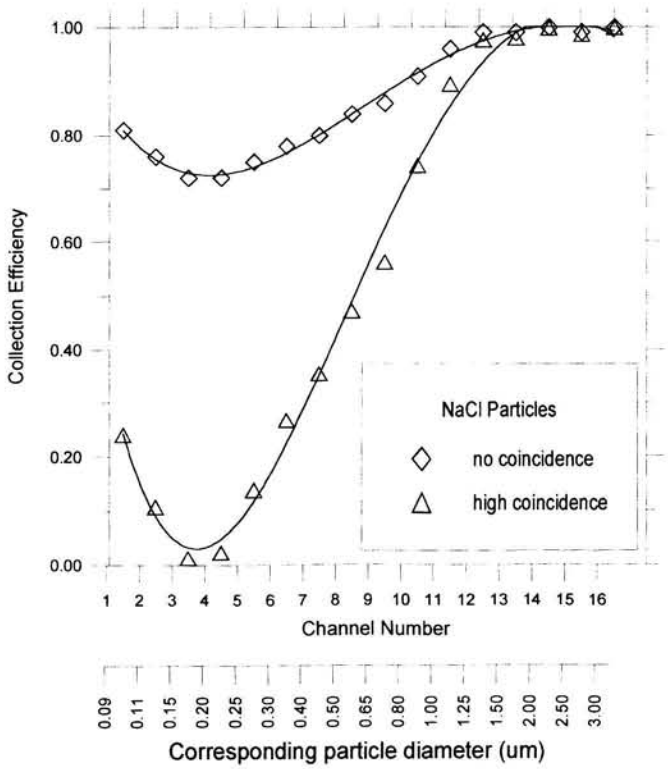

Fig. 6. Unrealistic decrease of the filter collection efficiency curve of a melt blown electret filter caused by coincidence errors.

In the next stage of the study an investigation of the actual monodispersity of a single mobility fraction from the DMA was undertaken in order to understand its impact on the efficiency measurement. Various solutions of DEHS in isopropyl alcohol were atomized and dried before being introduced into the DMA. This resulted in primary polydisperse aerosols with different mean diameter. Depending on the charging probabilities of particles in the bipolar ion atmosphere within the neutralizer and depending on the selected electrostatic mobility from the DMA, quasi-monodisperse aerosols containing not only singly, but also multiply charged particles in non-negligible amounts were generated.

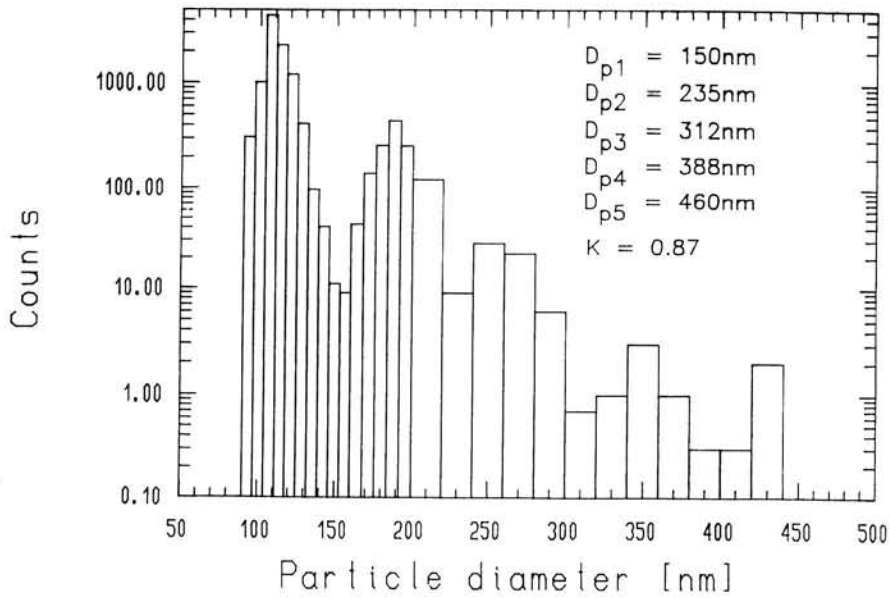

Fig. 7. Quasi-monodisperse aerosol size distribution from a DMA measured by LAS-X.

Figure 7 shows a typical size distribution of such an aerosol. It is obvious that besides singly charged particles with a diameter of 150 nm, even particles carrying 5 elementary charges with a diameter of 460 nm are present. The correction factor K (Eq.3) representing the inverse mean particle charge amounts in this case to 0.87 showing that concentration determination by means of the AE without taking into account the multiply charged particles would result in an error of about 13 %. It has to be emphasized that these effects are a coupled function of the primary aerosol size distribution and the selected electrical mobility interval by means of the DMA. For an experimental system used in this study (Collision atomizer operated at 2 bar pressure, with water or alcohol as solvent, dried and introduced into the DMA) it was found that in order to minimize multiply charged particles, the DMA extraction voltage had to be set to a value corresponding to particle size about 15% larger in diameter than the particle size representing the maximum of the primary aerosol size distribution. In case that only one solution strength is used for generation of the primary aerosol and the DMA operating voltage scans through the various mobility

fractions, multiply charged (hence larger) particles may become a dominant contribution to the size distribution of singly charged particles resulting mean particle charge significantly larger than unity. Figure 8 shows the measured factor K (Eq. 3.) in the particle size range from 10 nm to 380 nm for various strengths of DEHS isopropyl alcohol solutions.

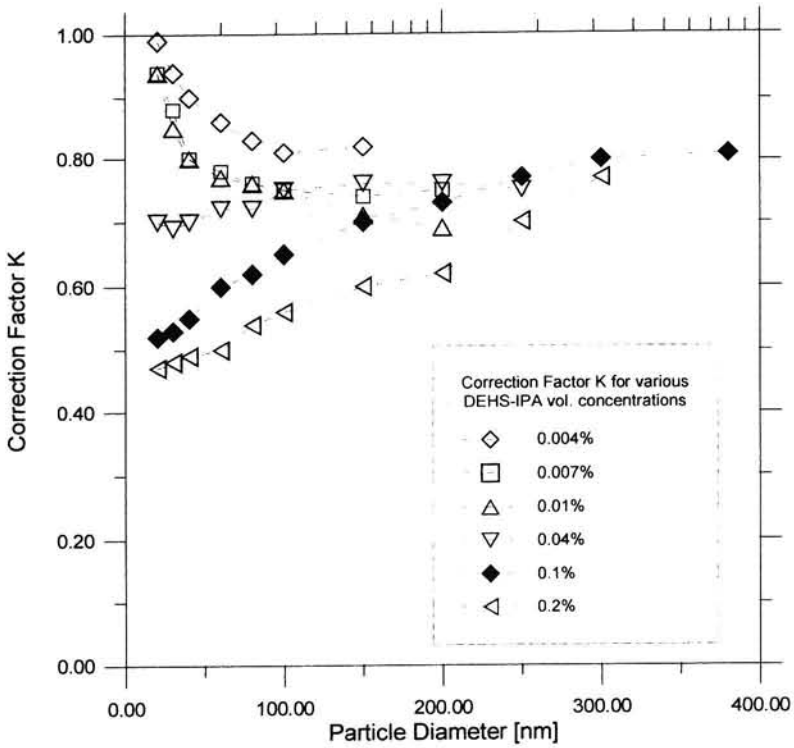

Fig. 8. Measured correction factor K indicating the presence of multiply charged particles for various primary, polydisperse aerosols.

It can be seen that only for the sub-50 nm particles and very diluted solutions (i.e. with the maximum of the primary, polydisperse size distribution in this size range) the factor K can be close to unity. Improper combination of primary, polydisperse aerosol size distribution with the selected electrostatic mobility fraction results in test aerosols far from being monodisperse. This behavior is also illustrated in Figure 9 showing the factor K as a function of selected sizes for singly charged particles and solution strength chosen. It is evident that filter efficiency measurement using instrumental combination of DMA and AE could result in substantial variation of the measured filter efficiency should the above findings be ignored.

To quantify the influence of the above stated effects, the fiber filter efficiency was determined first with optimized quasi-monodisperse DEHS aerosols from the DMA by means of a CNC after the particle neutralization.

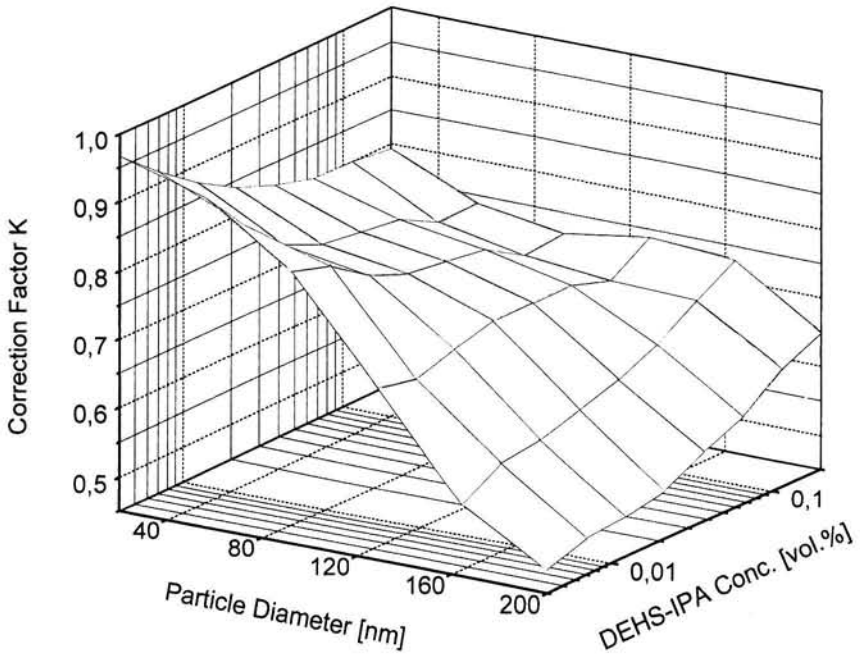

Fig. 9. Measured correction factor K as a function of diameter of singly charged particles and varying atomized DEHS-isopropyl alcohol solution concentration

Next, the experiment was repeated with the quasi-monodisperse aerosol ignoring the presence of a substantial amount of multiply charged particles. Due to the fact that the larger (doubly, and more charged) particle fractions are filtered with different efficiency than particles of the expected, singly charged size extracted from the DMA, an artificial shift of the filter efficiency curve and change in the fractional penetration occurs as can be seen in Figure 10.

In case of electret filter material the efficiency determination will vary depending on the charge state of particles and filter fibers. Previous results of such measurements [16, 17] show differences of data. For that reason electret filter efficiencies with charged and neutral particles were again investigated. Additionally, to emphasize the importance of fiber charge on particle removal, electret filters were exposed to γ radiation of the order of 10 kGy which is known to deteriorate the electrostatic properties of electret filters. The results are summarized in Figure 11. It can be seen that the combination of charged particles and a new, charged electret filter improves the filtration efficiency by over an order of magnitude. The shape of measured curves shows agreement with other results [16]. It is also evident that a discharged electret filter provides rather poor performance. Since with increasing filter load [18, 19] mechanical filtration mechanisms successively dominate the filter performance, it is of a major importance to reliably detemine the initial and usage time dependent filter characteristics.

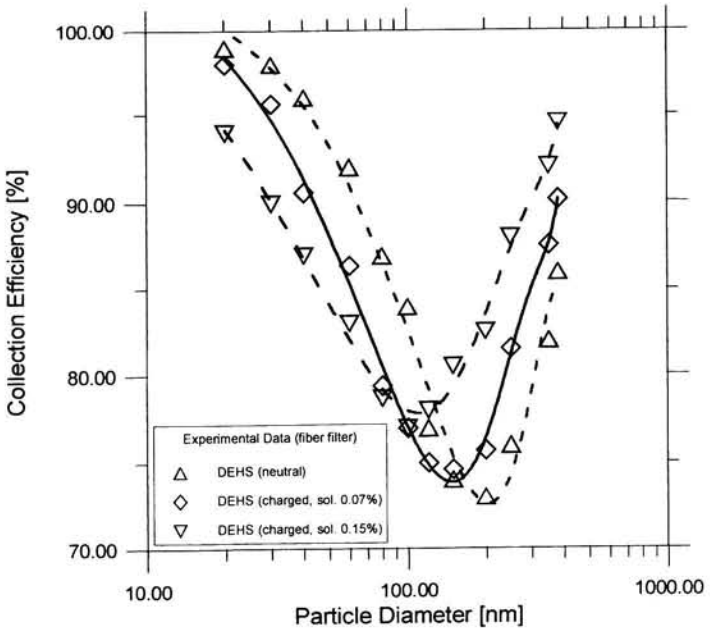

Fig. 10. Impact of multiply charged particles on the collection efficiency curves of a fibrous filter due to measurement with the aerosol electrometer.

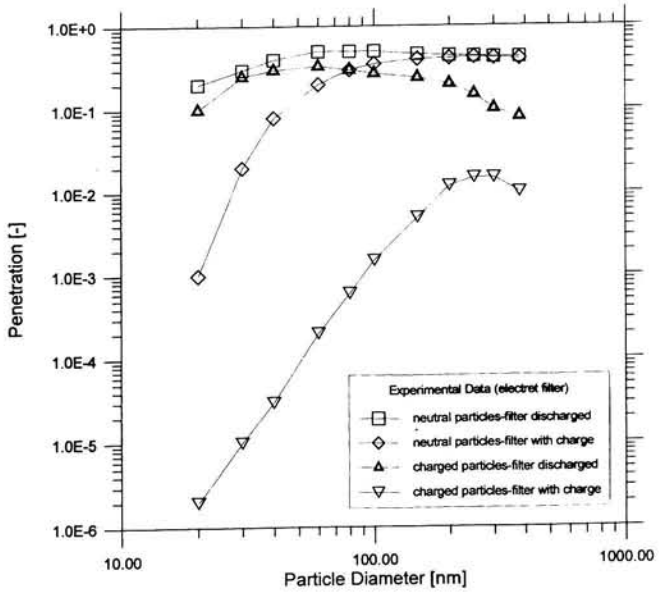

Fig. 11. Influence of the charge state of aerosol particles (NaCl) and of the elctrostatic condition of electret filter on the filtration characteristics.

CONCLUSIONS

The result of this study shows that various real-time, size-sensitive devices allow in principle the realistic indication of fractional filtration efficiency. However, variations of particle material and electrostatic charge, use of very high concentrations and unfortunate combinations of particle generators and detection devices may provide erroneous filtration characteristics in terms of efficiency and most penetrating particle size. Optical spectrometers are useful only within a limited concentration range and are prone to sizing and counting errors with increasing particle concentrations. Electrometer concentration measurement in connection with quasi-monodisperse DMA aerosols is quite sensitive to the presence of multiply charged particles and provides accurate concentration information only if the correction factor for multiple charge interference effects is known. The combination of a DMA and CNC appears to be a satisfactory instrumental approach for filtration efficiency measurement, however it has to be emphasized, that a given electrostatic mobility fraction from a DMA may contain an amount of multiply charged particles which can be substantial, depending on the primary aerosol size distribution and the DMA selected size range. In order to determine the initial, as well as time dependent filter performance, collection efficiency studies with various model aerosols (multi-modal size distributions, specific chemical composition and charge levels, varying humidity and temperature) simulating real life conditions will have to be undertaken. Such studies will provide more complete and representative information regarding the filter media, but also will assert an additional instrumental challenge.

ACKNOWLEDGMENTS

This financial support for this research from the Jubilaeumsfonds der Oesterreichischen Nationalbank, Proj. 5561 and from the National Science Council of the Republic of China is gratefully acknowledged.

REFERENCES

1. Brown, R.C. (1993), *Air Filtration – an integrated approach to the theory and applicactions of fibrous filters*, Pergamon Press, Oxford.
2. Liu, B.Y.H., Szymanski, W.W. and Pui, D.Y.H. (1986), Response of a laser optical particle counter to transparent and light-absorbing particles, *ASRAE Trans.* 92, 518.
3. Szymanski, W.W. and Liu, B.Y.H. (1986), On the sizing accuracy of laser optical particle counters, *Part. Charact.* 3, 1.
4. Knutson, E.O. and Whitby, K.T. (1975), Aerosol classification by electric mobility: apparatus, theory and applications, *J. Aerosol Sci.* 6, 443.
5. Liu, B.Y.H. and Lee, K.W. (1976), Efficiency of membrane and nuclepore filters for submicrometer aerosols, *Environ. Sci. Technol.* 10, 345.
6. Bohren, C.F. and Huffman, R.D. (1986), *Absorption and scattering of light by small particles*, Wiley Interscience, New York.
7. Liu, B.Y.H. and Pui, D.Y.H. (1974), Equilibrium bipolar charge distribution of aerosols, *J. Colloid Interface Sci.* 49, 305.

8. Reischl, G.P., Mäkelä, J.M., Karch, R. and Necid, J. (1996), Bipolar charging of ultrafine particles in the size range below 10 nm, *J. Aerosol Sci.* 27, 931.
9. Liu, B.Y.H. and Pui, D.Y.H. (1974), A submicron aerosol standard and the primary, absolute calibration of the condensation nuclei counter, *J. Colloid Interface Sci.* 47, 155.
10. Zhang, S.H., Akutsu, Y., Russel, L.M., Flagan, R. and Seifeld, J. (1995), Radial differential mobility analyzer, *Aerosol Sci. Technol.* 23, 357.
11. Chen, D.R. and Pui, D.Y.H. (1995), Numerical modeling of the performance of the DMA for nanometer aerosol measurement, *J. Aerosol Sci.* 26, S141.
12. Liu, B.Y.H., Pui, D.Y.H., Rubow, K.L. and Szymanski, W.W. (1985), Electrostatic effects in aerosol sampling and filtration, *Ann. occup. Hyg.* 29, 251.
13. Szymanski, W.W. and Wagner, P.E. (1990), Absolute aerosol number concentration measurement by simultaneous observation of extinction and scattered light, *J. Aerosol Sci.* 21, 441.
14. Szymanski, W.W. Majerowicz, A.E. and Wagner, P.E. (1989), Measurement of Brownian coagulation in monodispersed and bidispersed aerosols, *Aerosol Sci. Technol.* 11, 1.
15. Szymanski, W.W. (1998), Filter efficiency measurement with optical particle counters-limitations and error sources, *Sep. Sci. Technol.* 33, 1225.
16. Trottier, R.A. and Brown, R.C. (1990), The effect of aerosol charge and filter charge on the filtration efficiency of submicrometre aerosols, *J. Aerosol Sci.* 21, S689.
17. Latrache, R. and Fissan, H. (1986), Fractional penetration for electrostatically charged fibrous filters in the submicron particle size range, *Part. Charact.* 3, 74.
18. Stenhouse, J.I.T. and Trottier, R. (1991), The loading of fibrous filters with submicron particles, *J. Aerosol Sci.* 22, S777.
19. Japuntich, D.A., Stenhouse, J.I.T. and Liu, B.Y.H. (1997), Effective pore diameter and monodisperse particle clogging of fibrous filters, *J.Aerosol Sci.*, 28, 147.

Experimental Measurements of Filter Loading Characteristics

J.I.T. Stenhouse[1] and D.C. Walsh[2]
[1]Dept. of Chemical Engineering, Loughborough University, Leics., LE11 3TU, UK.
[2]Dept. of Chemical Engineering, Heriot-Watt University, Edinburgh, Scotland, UK

KEYWORDS

Fibrous filter, loading, electrostatics.

INTRODUCTION

Considerable work has been carried out on the behaviour of filters in the virgin state. Of course this is extremely important. However, there is still much to be done to understand, and quantitatively predict, the behaviour of filters under load. If the lifetime of a filter can be increased then replacement costs will be reduced and the secondary problem of disposal will be alleviated. A severe problem is that the vast bulk of experimental work in this area is difficult to compare with theory. Either the filter properties or the loading aerosol are not adequately described or are too complex for modelling purposes. Ideally filters comprised of monosized fibres should be loaded with monosized aerosol particles which stick perfectly. Data from such experiments could be used to develop or validate theoretical models. These could then be extended to the more complex but practical situations. Some experimental studies have been carried out and these are briefly described in this paper. The experimental method, validation and results of a study of an electrostatically enhanced filter are described

EXPERIMENTAL

The principle of testing was to pass a moderately high concentration of monodisperse aerosol particles through a test filter and continuously record the upstream and downstream concentrations over the duration of a loading run. A high concentration is essential if the tests are to be completed in a reasonable period of time.

A simplified diagram of the experimental rig is shown as Figure 1(Walsh and Stenhouse, 1996). A monodisperse aerosol of stearic acid particles, with a geometric standard deviation less than 1.09, was generated using a MAGE condensation generator (Prodi, 1972). This produces a high concentration of spherical wax like particles, which can be considered to have a negligibly small electrostatic charge. The size range covered in this work was 0.46-1.46 μm diameter. For most of the experiments the aerosol was exposed to ionising beta radiation from a 10 mc ^{85}Kr source for a residence time of about 20 seconds to render it to the Boltzmann equilibrium charge. This was confirmed by measuring the charge distribution. An alternative aerosol of titanium dioxide particles or standard latex was available from a nebuliser via a diffusion dryer. All gas supplies were thoroughly cleaned of particulate and gaseous contaminants. The relative humidity was maintained relatively constant at about 30%. The aerosol was passed through a 0.7m long and 0.07m diameter pipe to provide adequate radial dispersion prior to challenging the test filter in accordance with the ASTM 1215-89 standard.

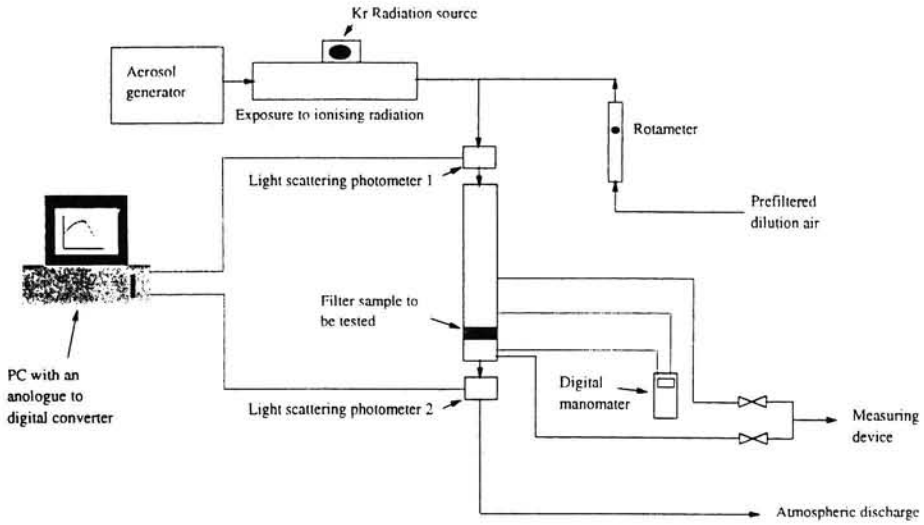

Figure 1. Experimental test rig for measuring filter loading

Light scattering photometers were used to monitor the concentration before and after filtration. One of these is shown in Figure 2. An LED shines light through almost the entire aerosol stream, as it passes through a 10 mm diameter section, and thence into a Rayleigh horn. Scattered light at 60° to the forward angle is measured by a photodiode. By dilution tests it was confirmed that the signals were a linear function of concentration. By comparing the upstream and downstream signals the penetration was continuously monitored. The units were calibrated at the beginning and end of each test and by taking the mass deposit on the filter at the end of the test into account the growth of deposit during the test was monitored. In this way the penetration and pressure drop could be followed as a function of load for the whole test.

The material under investigation here was a mixed fibre media consisting of a mixture of two types of polymer fibre which had become tribelectrically charged during the carding process. Its properties are summarised in Table 1.

Parameter	Value
Fibre diameter	20 μm
Packing density	0.04
Filter depth	3 mm
Fibre charge*	5×10^{-10} C m^{-2}

Table 1. Characteristics of filter media *Back calculated from experimental results using the Kraemer and Johnstone (1955) theory.

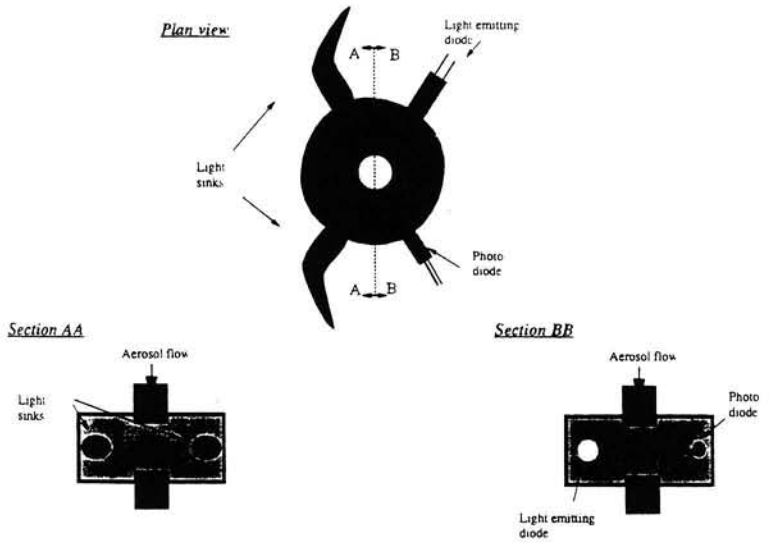

Figure 2. Arrangement of LSP system

The method of testing was found to be sufficiently reproducible for the present work and was sensitive to the second decimal place of fractional penetration. A later version was sensitive to the third decimal place. A considerable increase in sensitivity has more recently been achieved using two 30 mW lasers crossing in the sensing zone instead of the LED. In this case, locating the electronics adjacent to the lasers and photodiode significantly reduced the noise.

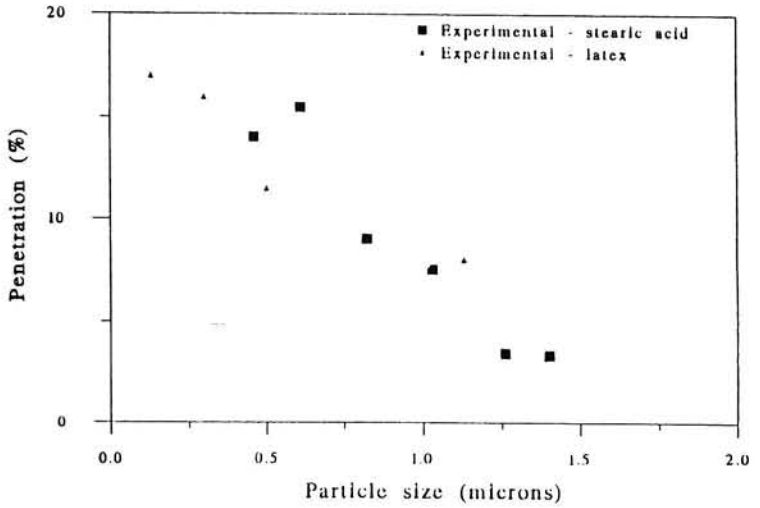

Figure 3. Initial penetration through filter samples challenged with stearic acid and latex particles at 0.1 m s^{-1} (Walsh and Stenhouse, 1997).

Preliminary tests were carried out to study possible effects of aerosol particle concentration on the loading characteristics. The penetration was measured as a function of mass deposit during the initial stages of loading, over a wide range of challenge concentrations, and over an extended period of time. No effect could be detected so it was considered acceptable to conduct the high concentration accelerated tests described here. The initial penetration of the media over the range of particle sizes is shown in Figure 3. Additional validation tests were carried out in which standard latex particles were used. Here the aerosol was sampled upstream and downstream and the concentration of each size measured using a LAS-X particle counter.

RESULTS AND DISCUSSION

It is well known that the penetration of electrostatically enhanced media falls off with loading. This is either due to fibre charge neutralisation (Baumartner and Loeffler, 1987) or a shielding effect (Brown *et al*, 1988). However as dendrites grow within the medium the mechanical efficiency is increased and penetration will eventually fall to zero as the filter is clogged. This is illustrated in Figure 4 in which a number of critical points are defined. It should be emphasised that there are a number of possible definitions for the clogging point. That shown is the simplest. An obvious alternative is the upper point where the pressure drop curve becomes linear i.e. the start of cake formation.

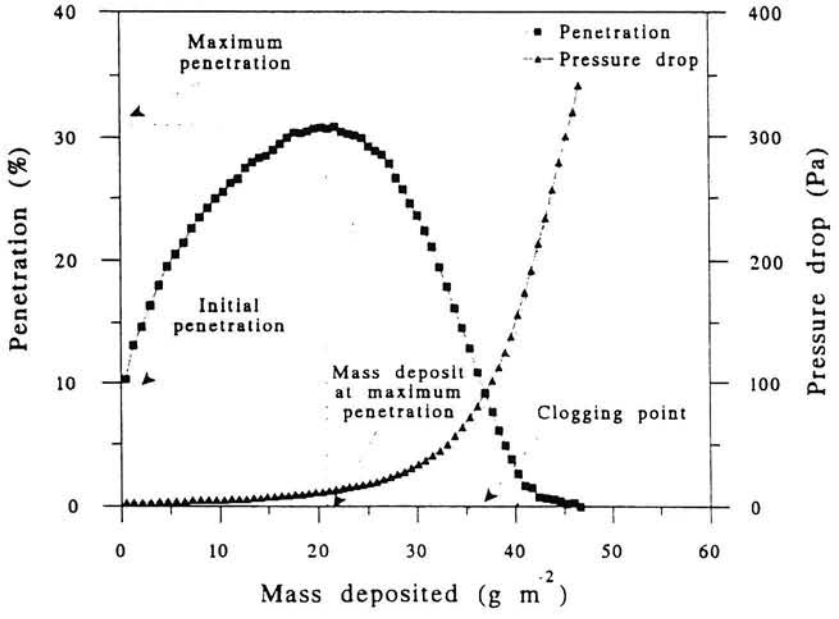

Figure 4. Loading characteristics of electrostatically enhanced media.

Particle size: Figure 5 shows the effect of mass deposit on penetration for six particle sizes and also the pressure drop response. The curves follow the same pattern as shown in Figure 4. The initial penetration is lower for small particles as expected. However, small particles also cause a more rapid degradation in electrostatic efficiency. Dendritic growth

is faster, the maximum is reached more quickly and the clogging point is at a lower mass deposit.

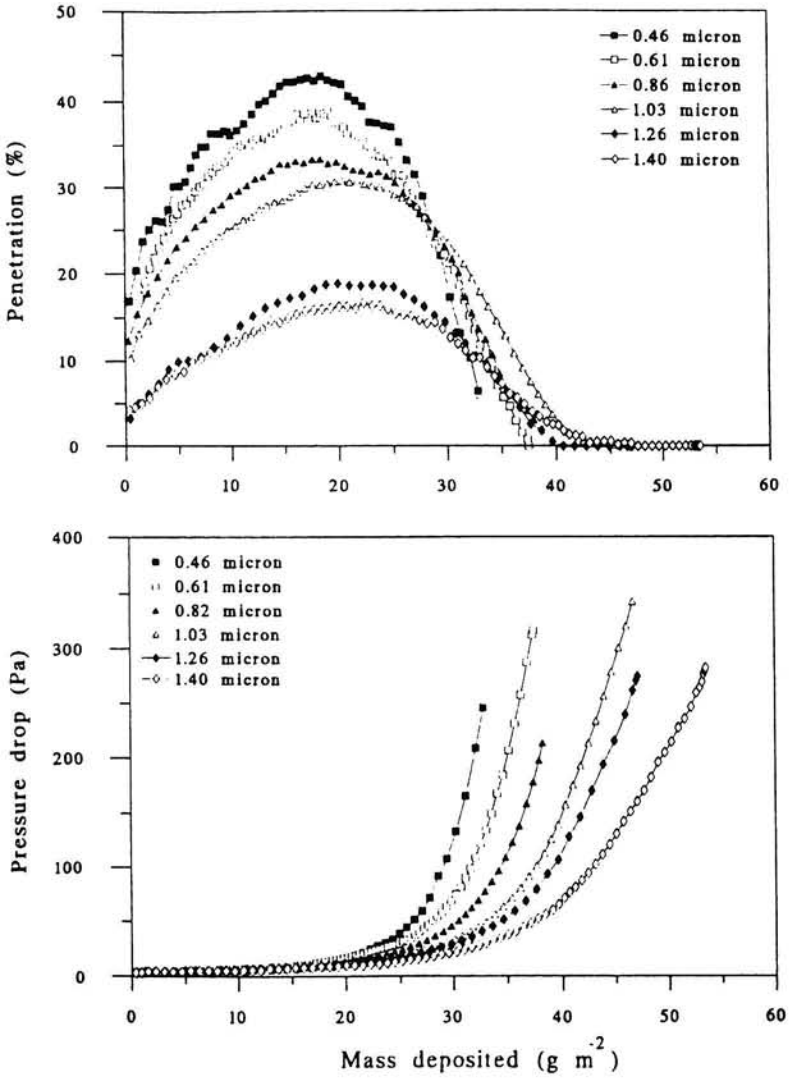

Figure 5. Penetration and pressure drop for filters loaded with stearic acid particles at the Boltzmann equilibrium charge distribution at a face velocity of 0.1 m s^{-1} (Walsh and Stenhouse, 1998).

Face velocity: The face velocity will have an effect on the capture mechanisms and the shape of dendritic structures which build on the fibres. It must therefor have a strong effect on the loading characterisitcs, as is shown in Figure 6. The penetration decreases with velocity as the electrostatic mechanism is diminished. The penetration falls again at the highest test velocity because inertial effects are now significant (Stokes number of

0.23). The pressure drop data show how clogging takes place earlier with high face velocities. With low velocities and high electrostatic forces the whole of the fibre will become evenly coated but at high velocities the front will become preferentially loaded. This unevenness of fibre coating will lead to more rapid bridging and thus clogging. With electrostatics the filter mat will also be more uniformly loaded with depth since the single fibre efficiency, at least in the early stages, falls with loading. With mechanical mechanisms the single fibre efficiency increases with loading so that the front of the filter becomes progressively more efficient and clogs quickly leaving the rest of the filter relatively empty.

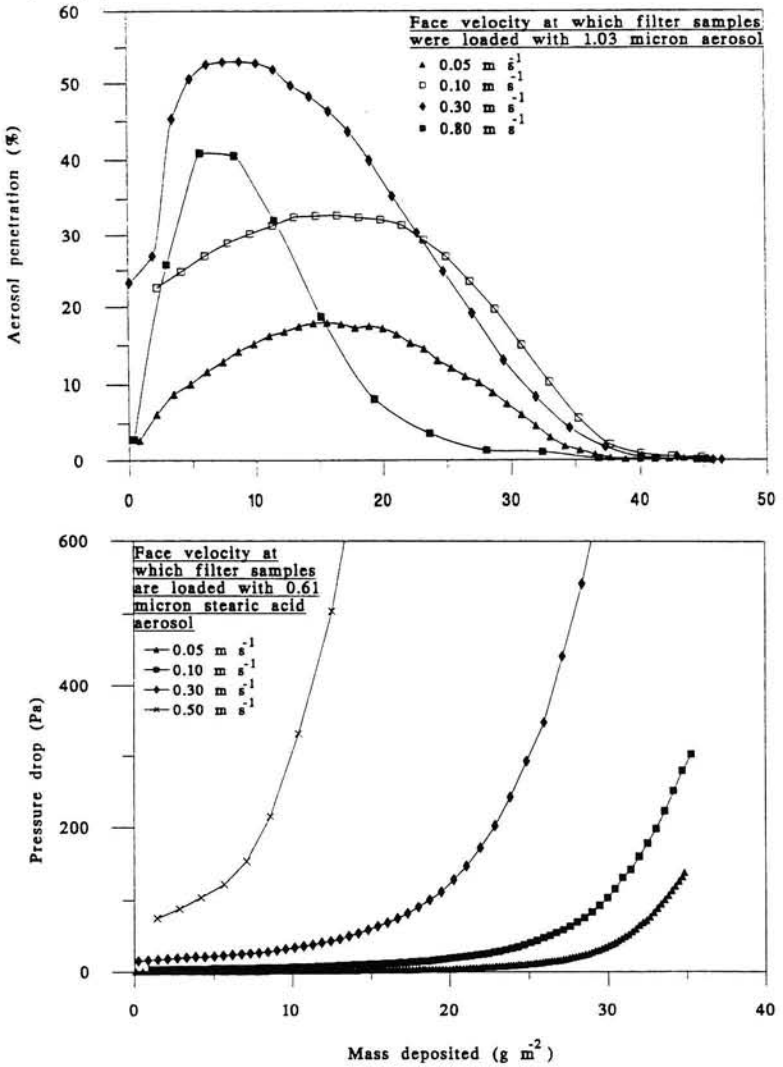

Figure 6. Penetration and pressure drop when filter is loaded with 1.03μm uncharged stearic acid particles at different face velocities.

Filter Charge: The fibre charge on the filters was reduced using two methods. One batch of the material was exposed to ionising radiation (^{241}Am) for 7 days. A second batch was exposed to very high intensity X-rays for 30 minutes. The effects of these exposures on penetration and pressure drop are seen in Figure 7. As expected the penetration is significantly increased and the material clogs more rapidly.

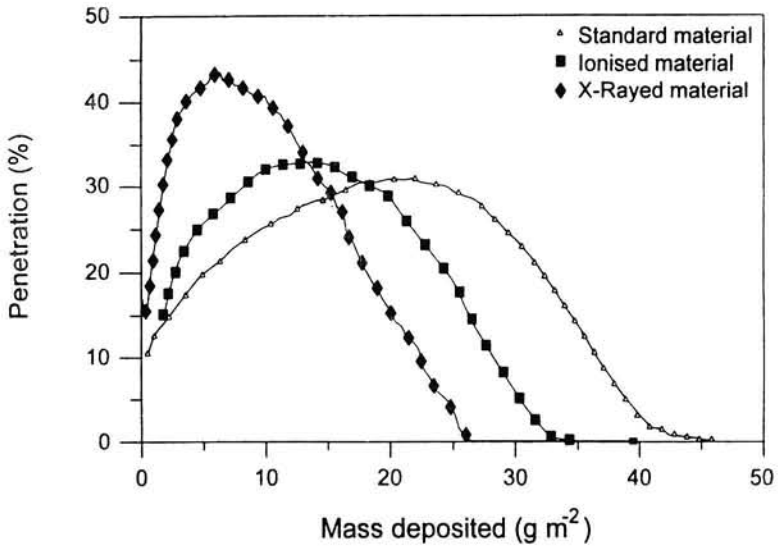

Figure 7 Penetration of filter media of different charge level when faced with 1.03μm stearic acid particles at 0.1 m s^{-1}.

Particle charge: Aerosol particles which had been exposed to ionising radiation and rendered to the Boltzmann equilibrium charge distribution are here considered to be charged. Those fed directly from the condensation generator, without exposure to ionising radiation, have a significantly lower charge and are considered uncharged. The characteristics of the media when faced with this aerosol are shown in Figure 8. The electrostatic effect of the media dies off more rapidly with the uncharged aerosol. This suggests that the degradation in filter efficiency is not a charge neutralisation process, but rather a screening mechanism as suggested by Brown *et al* (1988). The pressure drop data again show that the lifetime of the filter material is enhanced by strong electrostatics. With charged particles both Coulomb and induction forces assist particle capture.

Particle composition: Experiments were carried out with 0.51 μm diameter monodisperse particles of titanium dioxide, which were again rendered to the Boltzmann charge distribution. The results are compared with equivalent stearic acid data in Figure 9. Note that penetration is plotted against volume in this case since the densities of these particles differ by more than a factor of four.

There is a profound difference in the loading behaviour of these two materials. Data shown above on the effect of velocity strongly suggest that this not due to inertia alone. Titanium dioxide particles cause a much more rapid degradation of filter efficiency and clog much more rapidly. This suggests that the electrostatic properties of the filter

deteriorate much more rapidly. There is a notable difference in the electric properties of the two materials – stearic acid has a relative permittivity of 2.2 while that of titanium dioxide is of the order of 90 (Heindricks, 1973). The effect is very pronounced so the experiment was repeated several times with the same result.

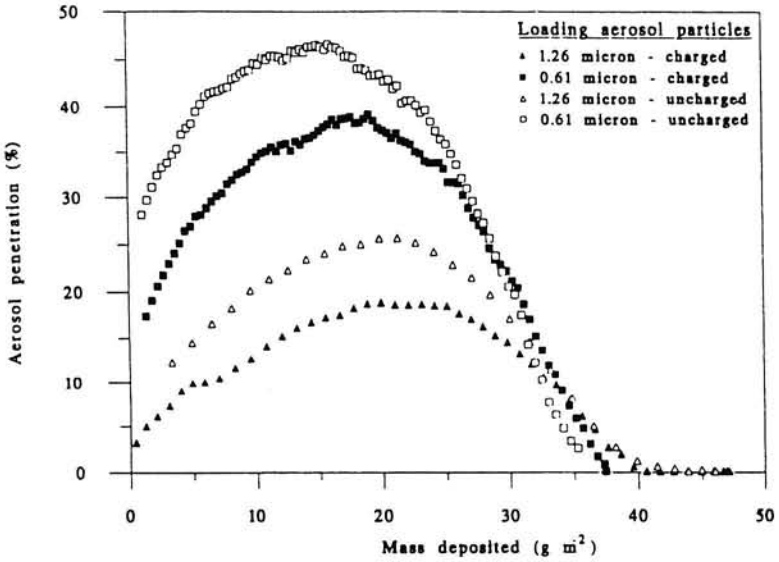

Figure 8 Penetration of standard media with charged and uncharged stearic acid particles face velocity of 0.1 m s^{-1}.

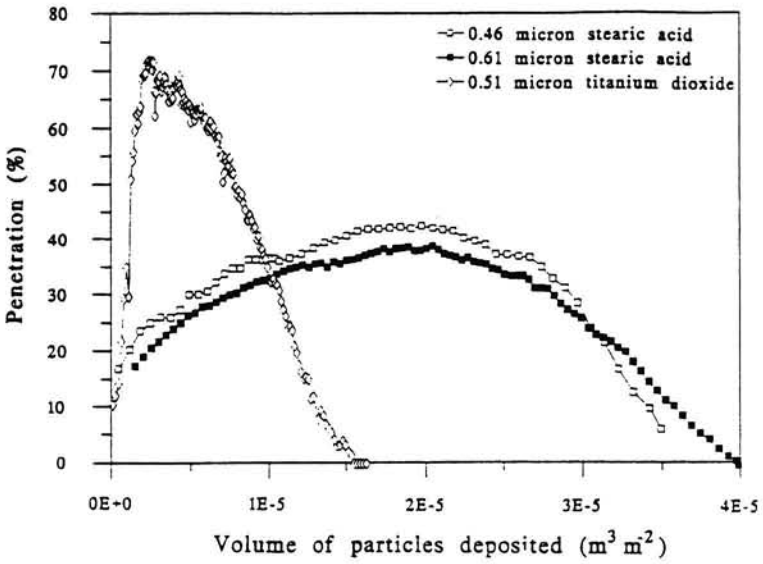

Figure 9 Penetration of media when loaded with Boltzmann equilibrium charged 0.51μm titanium dioxide and 0.46 and 0.61μm stearic acid particles at 0.1 m s^{-1}.

CONCLUSIONS

The fibre charges of the media tested in this work have a strong beneficial effect on collection efficiency. However, there is a degradation of these effects with particle loading. The experimental results suggest that this is due to a charge shielding effect rather than neutralisation. It was also found that the material properties of the particles could strongly influence the rate of degradation.

As loading proceeds mechanical collection on dendritic structures becomes progressively important. The penetration goes through a maximum and eventually the media becomes clogged. When there are strong electrical forces the media holds a much higher deposit before it clogs.

ACKNOWLEDGMENT

The authors would like to acknowledge the support of the Health and Safety Executive who funded this work.

REFERENCES

Baumgartner and Loffler (1987) Particle collection in electret fibres filters a basic theoretical and experimental study. *Filtration and Separation, Sept/Oct.*, 436-351.

Brown R.C., Wake D., Gray D., Blackford D.B. and Bostock G.J. (1988) Effect of industrial aerosol on electrically charged filter materials. *Ann. Occup. Hyg.* **32**, 271-294.

Heindricks C.D. (1973) Introduction to electrostatics. In *Electrostatics and its Applications*. (ed Moore A.D.) Wiley Interscience, New York.

Kraemer H.F. and Johnstone H.F. (1955) Collection of aerosol particles in the presence of electric fields. *Ind. Engng. Chem.* **47**, 2426-2434.

Prodi V. (1972) A condensation aerosol generator for solid monodisperse particles. In *Assesment of Airborne Particles* (ed Mercer T., Morrow P. and Stoeber W.,) Thomas.

Walsh D.C. and Stenhouse J.I.T. (1996) Experimental studies of electrically active fibrous filter loading. *Part. Part. Syst. Charact.* **13**, 47-53.

Walsh D.C. and Stenhouse J.I.T. (1997) The effect of particle size, and composition on the loading characteristics of an electrically active fibrous filter material. *J. Aerosol Sci.*, **28**, 307-321.

Walsh D.C. and Stenhouse J.I.T. (1998) Parameters affecting the loading behavior and degradation of electrically active filter materials. *Aerosol Sci. Technol.*, **29**, 420-432.

Selected Problems in the Modelling of Aerosol Filtration in Fibrous Filters

Albert Podgorski
Department of Chemical and Process Engineering, Warsaw University of Technology, Waryńskiego 1, 00-645 Warsaw, Poland. E-mail: podgorski@ichip.pw.edu.pl

KEYWORDS
fibrous filter; efficiency; modelling; transport equations; loading

INTRODUCTION

Although aerosol filtration in fibrous filters has been studied theoretically for about 70 years (for review see [1], [2]), it cannot be said that a complete and satisfactory theory of the process is available today. Undoubtedly, this is mainly due to the enormous complexity of the internal structure of a fibrous filter, which comprises thousands of (more or less randomly distributed) fibres, making it almost impossible to reasonably reproduce the solid-gas boundary in computer simulations. It is virtually impossible to solve the equation of gas motion for such structure to determine the exact flow pattern. The second source of serious difficulty is the complex nature of motion of an aerosol particle itself, being the result of the action of both slowly varying (deterministic) forces and rapid random fluctuations. Accurate solution of the problem of inertial-diffusive transport is not a trivial issue even for regular flow fields in much simpler geometrical systems. Finally, filtration in fibrous filters is, by definition, a non-steady state process, thus in principle the full "history" of varying conditions should be taken into consideration. This paper presents a short review of selected methods of approach to the theory of aerosol filtration in fibrous filters, but it does not attempt to give the complete overview, reflecting rather the author's interests.

METHODS OF APPROACH: TIME AND LENGTH SCALES

Several characteristic time and length scales may be associated with a fibrous filter depending on the frequency and resolution of our observation and degree of required precision. The roughest approach is to analyse the behaviour of the entire filter considered as a "black-box", i.e. without a detailed analysis of the mechanisms of the process. In this case we are interested in a description of the *filter external characteristics*: its efficiency of removing particles from the gas stream and its resistance (pressure drop). For this *macroscopic approach* the characteristic length scale is the filter thickness, L. The time scale should be small enough to register significant variations of the filter external characteristics (hence, much less than the filter service time, but typically it may be few times the gas mean residence time in the filter). The second extreme is to analyse the "history" of a single aerosol particle or a cloud of particles in the porous spaces of the filter. This group of methods may be termed the *microscopic approach*. The characteristic length of *microscale*, l_μ, must be sufficiently small to enable observation of *local* changes of individual particles' velocities in the inter-fibre spaces; thus l_μ is expected to be of the order of particle diameter and smaller than the average distance between neighbouring fibres. In the microscale one may sample particle motion with various frequencies. Particle displacements may be recorded in time intervals much greater than the average time between the gas molecular collisions, τ_{MC}, (i.e. for $t \gg \tau_{MC} = \lambda_G/|v_{ms}|$, where λ_G is gas mean free path and $|v_{ms}|$ denotes the average molecular speed of gas molecules; this condition means that the fluid molecules are near local equilibrium), but in small enough intervals such that the particle momentum has not relaxed.

The motion of a particle is then superposition of a "smooth" convective displacement and random "jumps" due to Brownian bombardment. This phenomenon is described either by the Langevin equation in the physical space or by the Fokker-Planck equation in the phase space (consisting of position and velocity co-ordinates). The characteristic time scale for this approach is the particle relaxation time $\tau_R=m_P/f$, where m_P is the particle mass and f is the friction coefficient (for a spherical particle in the Stokes regime $f=3\pi\mu d_P/C_C$, where μ is the fluid viscosity, d_P the particle diameter and C_C the slip correction factor; typical values of τ_R for micrometer sized aerosol particles in air are of the order 10^{-6}s). It should be remembered that using this time scale we allow for random fluctuations of particle velocity about its equilibrium value. Let us call this approach the Fokker-Planck limit. The time scale of observation may be increased to $t>\tau_R$, but still small enough to be able to observe variations of the local equilibrium velocity of particles in the microscale. Here we ignore random fluctuations of momentum of individual particles and consider Brownian motion of the cloud of particles as a process of diffusion. This approach can be termed the Einstein-Smoluchowski limit. The "bridge" between the two fundamental methods of analysis of particle behaviour in the microscale, l_μ, and earlier mentioned external characteristics of the entire filter in the macroscale, L, is the mesoscale description, Fig. 1. Using this method we consider the filter medium as a pseudo-continuum matrix composed of fibres (phase σ) immersed in the aerosol stream (phase β) and analyse the variation of some physical quantities related to the averaged concentration of aerosol particles across the filter. The characteristic length for the mesoscale, l_m, should be taken as much greater than the mean inter-fibre distance, but sufficiently small to see variations of averaged quantities. Additionally, it is required that: $L \gg l_m \gg l_\mu$.

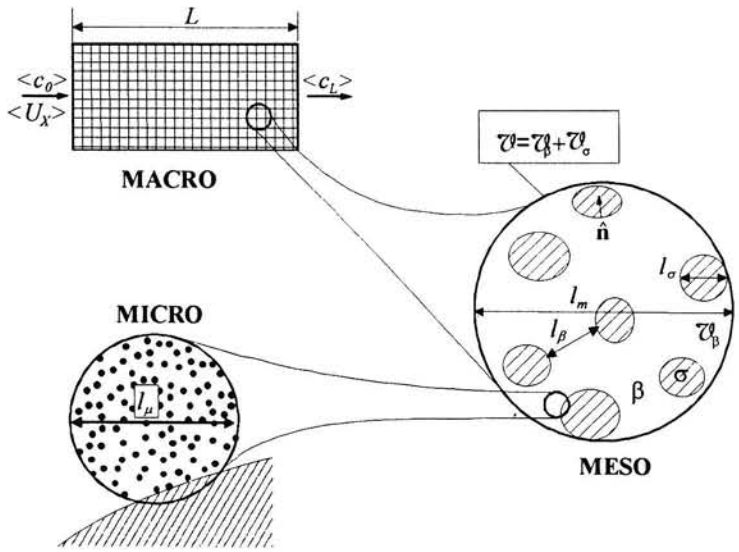

Fig. 1. Macro-, meso- and microscopic representation of the process of aerosol filtration in a fibrous filter and representative length scales.

MODELLING AEROSOL DEPOSITION IN A CLEAN FILTER

MICROSCALE DESCRIPTION

The main filter parameter, the efficiency of removal of particles, is determined by the probability of their collisions with fibres during the flow of aerosol through the filter, and therefore it is a result of the microscopic motion of particles. Generally, this motion is caused by deterministic forces (fluid drag, gravity, inertia, electrostatic forces) as well as by the random ones (Brownian motion and turbulence, the latter one being infrequent event for air filtration). Classical theory of air filtration developed over past decades assumed independent action of these two kinds of mechanisms. Hence, the combined single fibre (or single cell) collection efficiency η was calculated from the partial efficiencies: η_{det} - due to action of deterministic mechanisms only (interception, inertial impaction, sedimentation, electrostatic attraction) and η_B – due to Brownian diffusion only, according to the formula: $\eta=1-(1-\eta_{det})(1-\eta_B)$. The partial efficiencies were estimated by the solving following equations:

- deterministic equation of particle motion which integrated several times enables to find the limiting trajectories and therefore to estimate η_{det}:

$$\frac{d\mathbf{V}}{dt} = \frac{1}{\tau_R}(\mathbf{U}-\mathbf{V}) + \frac{1}{m_P}\mathbf{F}, \tag{1}$$

- simplified (neglecting particle inertia) equation of convective diffusion for the steady-state, which gives profiles of aerosol concentration c around a fibre and hence yields η_B:

$$\nabla\cdot(\mathbf{U}c) = D\nabla^2 c\,. \tag{2}$$

However, the assumption that inertial effects and external forces do not alter particle Brownian motion has no physical basis and the classical approach described above leads to inaccurate results of deposition efficiency when both mechanisms (deterministic and stochastic) are of comparable importance, [3]. It was proposed [4] to include partially inertial effects into the equation of diffusion taking the first order correction in the form:

$$\nabla\cdot[(\mathbf{U}-\tau_R\mathbf{U}\cdot\nabla\mathbf{U})c] = D\nabla^2 c\,. \tag{3}$$

However, this is still too oversimplified an approach because inertial effects are included only partially and the influence of external forces on particle Brownian motion is completely neglected. The latter effect may be of importance when the external force field varies rapidly with position in the microscale, as is commonly the case in electret filters. These difficulties may be avoided if we use the approach based on simultaneous analysis of deterministic and stochastic mechanisms of particle transport, which is discussed below. Two fundamental equations describing these phenomena in the microscale with the time resolution of the order τ_R (thus allowing for particle momentum fluctuations) are:

- (differential) Langevin equation – stochastic equation of particle motion:

$$\frac{d\mathbf{V}}{dt} = \frac{1}{\tau_R}(\mathbf{U}-\mathbf{V}) + \frac{1}{m_P}\mathbf{F} + \mathbf{A}(t) \tag{4}$$

- (phase-space) Fokker-Planck equation – equation of evolution of conditional probability P_{RV} that a particle located at point $\mathbf{R}_0$ and having velocity $\mathbf{V}_0$ at moment t_0 will be located at point $\mathbf{R}$ at time t and will have velocity $\mathbf{V}$:

$$\frac{\partial P_{RV}}{\partial t} + \frac{\partial}{\partial \mathbf{R}}\cdot(\mathbf{V}P_{RV}) - D\frac{\partial^2 P_{RV}}{\partial \mathbf{R}^2} + \frac{\partial}{\partial \mathbf{V}}\cdot\left(\frac{\partial \mathbf{V}}{\partial t}P_{RV}\right) - d\frac{\partial^2 P_{RV}}{\partial \mathbf{V}^2} = \delta^3{}_{\mathbf{R}_0\mathbf{V}_0 t_0} \tag{5}$$

In the above equations $\mathbf{F}$ denotes the vector sum of deterministic forces (other than fluid drag) acting on particle, $\mathbf{A}(t)$ is the stochastic particle acceleration, $\mathbf{V}$ and $\mathbf{R}$ denote vectors of particle velocity and position, $\mathbf{U}$, is the vector of undisturbed fluid velocity and D and d

are coefficients of particle diffusion in physical space and in the velocity space, respectively. For a spherical particle these are given by:

$$D = \frac{k_B T C_C}{3\pi\mu d_P}, \; d = \frac{3\pi\mu d_P k_B T C_C}{m_P^2} \tag{6}$$

where k_B is Boltzmann constant and T – absolute temperature. Although equations (4)-(5) are not useful for straight simulations of aerosol particle deposition, they constitute a basis for further analysis. The stochastic term $\mathbf{A}(t)$ in the Langevin equation (4) cannot be expressed directly in this form. Instead, we can only speak about statistical properties of its value averaged over a period Δt, such that Δt is much greater than the mean time between molecular collisions with the particle, but not much greater than τ_R: $\mathbf{B}(\Delta t) \equiv \int_t^{t+\Delta t} \mathbf{A}(\xi) d\xi$. It has been shown, [5], that the vector $\mathbf{B}(\Delta t)$ has a Maxwellian distribution with an expected value $<\mathbf{B}(\Delta t)>=0$ and variance $<\mathbf{B}^2(\Delta t)>=6D\Delta t/\tau_R^2$ (it means that each component B_i, of $\mathbf{B}$, i=1,2,3, possesses Gaussian distribution with the same, zero expected value and variance $<B_i^2(\Delta t)>=2D\Delta t/\tau_R^2$). Thus, we can perform stochastic simulations of a particle trajectory using the following general scheme presented in Table 1.

TABLE 1. DISCRETE SCHEME FOR BROWNIAN DYNAMICS SIMULATIONS

1. Given: **V**, **R** for time t.
2. Calculate **U**, **F** for (**V**, **R**, t).
3. Compute deterministic components of particle displacement $\Delta\mathbf{R}_{det}$ and change of velocity $\Delta\mathbf{V}_{det}$ during the time interval Δt.
4. Generate random vectors $\Delta\mathbf{R}_{ran}$ and $\Delta\mathbf{V}_{ran}$ for the interval Δt with components which follow multivariate Gaussian distributions with known expected values $<\Delta\mathbf{R}_{ran}>$, $<\Delta\mathbf{V}_{ran}>$ and variances $<\Delta\mathbf{R}^2_{ran}>$, $<\Delta\mathbf{V}^2_{ran}>$.
5. Calculate new vectors **V**, **R** for time $t+\Delta t$: $\mathbf{V}(t+\Delta t)=\mathbf{V}(t)+\Delta\mathbf{V}_{det}+\Delta\mathbf{V}_{ran}$, $\mathbf{R}(t+\Delta t)=\mathbf{R}(t)+\Delta\mathbf{R}_{det}+\Delta\mathbf{R}_{ran}$, etc.

Explicit expressions for $\Delta\mathbf{R}_{det}$, $\Delta\mathbf{V}_{det}$, $<\Delta\mathbf{R}_{ran}>$, $<\Delta\mathbf{V}_{ran}>$, $<\Delta\mathbf{R}^2_{ran}>$ and $<\Delta\mathbf{V}^2_{ran}>$ to perform discrete Brownian dynamics simulations using the integral Langevin method are summarised in Table 2. An alternative approach is based on the Fokker-Planck equation (4) which can be integrated exactly for **a** time interval Δt smaller than the time over which there are significant variations in the fluid velocity **U** and external forces **F** fields, [3], [5], [6]. The resulting expressions for the integral Fokker-Planck method are given in Table 3. Langevin and Fokker-Planck discrete methods are equivalent and should lead to the same results provided that for the former the much smaller time step is used. Indeed, it is easy to prove that formulae given in Table 3 transform themselves to those in Table 2 when the expansion $\exp(-\Delta t/\tau_R)_{|\Delta t/\tau_R<1} \rightarrow 1-\Delta t/\tau_R$ is applied. Both those methods take into account fluctuations of particle position and velocity (the Fokker-Planck method directly, and Langevin method - indirectly for displacement – by means of fluctuating velocity) and they are competitive from the numerical point of view. The Langevin approach is much simpler (no exponential functions, only one random vector to be generated), but it requires a smaller time step than the Fokker-Planck one. The third possible method to simulate Brownian motion of an individual particle can be formulated for the Einstein-Smoluchowski limit, that is for the sampling time $\Delta t \gg \tau_R$. In this case particle momentum is assumed to be near equilibrium, thus only particle displacement has a random component. It is summarised in Table 4. Although this method

may look attractive because of the large time step ($\Delta t \gg \tau_R$), either Langevin or Fokker-Planck schemes should be preferred because of the more realistic reproduction of the idea of Brownian motion, especially where particle inertial effects are important.

TABLE 2. LANGEVIN APPROACH TO BROWNIAN DYNAMICS

$$\tau_{MC} \ll \Delta t < \tau_R$$

$$\Delta \mathbf{R}_{det} = \mathbf{V}\Delta t \qquad \Delta \mathbf{V}_{det} = [(\mathbf{U} - \mathbf{V})/\tau_R + \mathbf{F}/m_P]\Delta t$$

$$\langle \Delta \mathbf{R}_{ran} \rangle = \langle \Delta \mathbf{V}_{ran} \rangle = 0 \qquad \langle \Delta \mathbf{R}^2_{ran} \rangle = 0 \qquad \langle \Delta \mathbf{V}^2_{ran} \rangle = 6D\Delta t/\tau_R{}^2$$

TABLE 3. FOKKER-PLANCK APPROACH TO BROWNIAN DYNAMICS

$$\tau_{MC} \ll \Delta t$$

$$\Delta \mathbf{R}_{det} = (\mathbf{U} + \mathbf{F}\tau_R/m_P)\Delta t - \tau_R[1 - \exp(-\Delta t/\tau_R)][(\mathbf{U} - \mathbf{V}) + \mathbf{F}\tau_R/m_P)]$$

$$\Delta \mathbf{V}_{det} = [(\mathbf{U} - \mathbf{V}) + \mathbf{F}\tau_R/m_P][1 - \exp(-\Delta t/\tau_R)]$$

$$\langle \Delta \mathbf{R}_{ran} \rangle = \langle \Delta \mathbf{V}_{ran} \rangle = 0$$

$$\langle \Delta \mathbf{R}^2_{ran} \rangle = 3D\tau_R[2\Delta t/\tau_R - 3 + 4\exp(-\Delta t/\tau_R) - \exp(-2\Delta t/\tau_R)]$$

$$\langle \Delta \mathbf{V}^2_{ran} \rangle = 3D[1 - \exp(-2\Delta t/\tau_R)]/\tau_R \qquad \langle \Delta \mathbf{V}_{ran} \cdot \Delta \mathbf{R}_{ran} \rangle = 3D[1 - \exp(-\Delta t/\tau_R)]^2$$

TABLE 4.EINSTEIN-SMOLUCHOWSKI APPROACH TO BROWNIAN DYNAMICS

$$\Delta t \gg \tau_R$$

$$\Delta \mathbf{R}_{det} = \mathbf{V}\Delta t \qquad \Delta \mathbf{V}_{det} = [(\mathbf{U} - \mathbf{V})/\tau_R + \mathbf{F}/m_P]\Delta t$$

$$\langle \Delta \mathbf{R}_{ran} \rangle = \langle \Delta \mathbf{V}_{ran} \rangle = 0 \qquad \langle \Delta \mathbf{R}^2_{ran} \rangle = 6D\Delta t \qquad \langle \Delta \mathbf{V}^2_{ran} \rangle = 0$$

Since the methods of Brownian dynamics simulation are based on the generation of stochastic trajectories, they require the use of Monte Carlo techniques. Therefore results from a large number of sampled particles must be averaged – this is their major disadvantage. However, it is likely that the rapidly growing speed of microcomputers will facilitate the use of these methods in the near future.

MESOSCALE DESCRIPTION

Microscopic analysis concerns local motion of aerosol particles in the filter porous space. Neglecting distribution of Brownian particle velocity in the Fokker-Planck equation (5) we obtain the continuity equation describing the variation of aerosol concentration c in the microscale (also referred to as Smoluchowski equation, since the sampling time is much greater than the particle relaxation time):

$$\frac{\partial c}{\partial t} + \nabla \cdot (\mathbf{V}c) - D\nabla^2 c = 0 \tag{7}$$

It should be noted that in Eq. (7) the local (equilibrium) particle velocity, $\mathbf{V}$, is used in contrast to the classical continuity equation which contains the local fluid velocity. It is interesting to analyse the variation of *averaged in the mesoscale* properties of the aerosol stream (concentration, velocity). The governing equation for the aerosol transport in the mesoscale can be obtained using the *method of volume averaging*, [7], [8]. Referring to Figure 1 and the discussion of the length scales, let us choose a characteristic volume for the mesoscale, $\mathcal{V}$, composed of an assembly of fibres of total volume $\mathcal{V}_\sigma$ and of aerosol (gas+particles, considered as a pseudo-homogeneous continuum) of volume $\mathcal{V}_\beta$: $\mathcal{V}=\mathcal{V}_\sigma+\mathcal{V}_\beta$. For any property X related to the aerosol we can define two mesoscale averages: intrinsic $\langle X \rangle^\beta$ and superficial $\langle X \rangle$; they are related to one another by the local filter porosity ε:

$$< X >\equiv \frac{1}{\mathcal{V}} \int_{\mathcal{V}_\beta} X d\mathcal{V}, \quad < X >^\beta \equiv \frac{1}{\mathcal{V}_\beta} \int_{\mathcal{V}_\beta} X d\mathcal{V}, \quad < X >=< X >^\beta \varepsilon. \tag{8}$$

The microscale continuity equation, Eq. (7), may then be averaged applying the following lemmas on averaging accumulation and gradient:

$$\left\langle \frac{\partial X}{\partial t} \right\rangle = \frac{\partial \langle X \rangle}{\partial t} - \sum_\sigma \frac{1}{\mathcal{V}} \int_{A_{\beta\sigma}} X \mathbf{W}_{\beta\sigma} \cdot \hat{\mathbf{n}}_{\beta\sigma} dA, \quad < \nabla X >= \nabla < X > + \sum_\sigma \frac{1}{\mathcal{V}} \int_{A_{\beta\sigma}} X \hat{\mathbf{n}}_{\beta\sigma} dA \tag{9}$$

Let us define the (local in the mesoscale) average rate of particle deposition on the fibres as:

$$-< r >\equiv \sum_\sigma \frac{1}{\mathcal{V}} \int_{A_{\beta\sigma}} [(\mathbf{V} - \mathbf{W}_{\beta\sigma}) c - D \nabla c] \cdot \hat{\mathbf{n}}_{\beta\sigma} dA \tag{10}$$

In the above equations the pair of indices $\beta\sigma$ denotes the fibre-aerosol interface within the mesoscale volume $\mathcal{V}$, $\mathbf{W}_{\beta\sigma}$ is the velocity of this interface, $\mathbf{n}_{\beta\sigma}$ - the unit vector normal to the fibre surface and summation is applied to all fibres present in $\mathcal{V}$. A filter tortuosity vector is introduced $< \mathbf{T} >=\varepsilon < \mathbf{T} >^\beta \equiv \sum_\sigma \frac{1}{\mathcal{V}} \int_{A_{\beta\sigma}} c \hat{\mathbf{n}}_{\beta\sigma} dA$, local (microscale) deviations of aerosol velocity ($\mathbf{V}'$), and concentration (c') from the mesoscale intrinsic averages are defined: $\mathbf{V} =< \mathbf{V} >^\beta + \mathbf{V}'$, $c =< c >^\beta + c'$, and then a total dispersion tensor is introduced $<\mathcal{D}>=D\mathbf{I}+<\mathcal{D}^N>$ with $<\mathcal{D}^N>$ given by: $<\mathcal{D}^N> \cdot[\nabla(\varepsilon<c>^\beta)] = D<\mathbf{T}>-<\mathbf{V}'c'>$. One then obtains the general form of the averaged transport equation in the mesoscale:

$$\frac{\partial \left(\varepsilon < c >^\beta\right)}{\partial t} + \nabla \cdot \left(\varepsilon < \mathbf{V} >^\beta < c >^\beta\right) - < r > - \nabla \cdot \left[< \mathcal{D} > \cdot \nabla \cdot \left(\varepsilon < c >^\beta\right)\right] = 0. \tag{11}$$

This equation contains two phenomenological parameters: scalar deposition rate $-<r>$ and dispersion tensor $<\mathcal{D}>$. They can, in theory, be determined by solving the microtransport equations discussed above or by applying a proper closure scheme [8], [9]. In practice, for typical conditions of aerosol filtration in fibrous filters, equation (11) can be considerably simplified. For this it must be assumed that: a) local aerosol accumulation [first term in Eq. (11)] is negligible; b) the mean aerosol transport through a filter can be considered as one dimensional (say, in x direction); c) the mesoscale averaged intrinsic particle velocity $<V_x>^\beta$ is close to the mean inter-fibre gas velocity $<U_x>^\beta=<U_x>/\varepsilon$ (it does not mean that we neglect local differences in particle and fluid velocity), and d) the main component of the dispersion tensor is the axial one, $<\mathcal{D}_{xx}>$. Hence, a simplified model of aerosol transport in the filter can be written as:

$$< U_x > \frac{\partial < c >^\beta}{\partial x} - \varepsilon < \mathcal{D}_{xx} > \frac{\partial^2 < c >^\beta}{\partial x^2} - < r >= 0. \tag{12}$$

For a clean, macroscopically homogeneous filter it is common to assume that the local mesoscale particle deposition rate is proportional to the averaged flux of aerosol particles crossing a given filter cross-section:

$$-< r(t=0) >=- < r^0 > \; = \; \lambda < U_x >< c >^\beta, \tag{13}$$

where the proportionality constant λ is termed the filtration index. This is related to the classical single fibre efficiency η by: $\lambda=2(1-\varepsilon)\eta/(\pi\varepsilon R_C)$, where R_C is the fibre radius. Equations (12)-(13) can be integrated analytically with Danckwerts' boundary conditions to give:

$$P^0(x) =< c(x) >^\beta / < c_0 >= \frac{4\chi}{(1+\chi)^2 \exp[-\frac{1}{2}(1-\chi)\omega] + (1-\chi)^2 \exp[-\frac{1}{2}(1+\chi)\omega]} \tag{14}$$

where $P^0(x)$ is the penetration of a clean filter as a function of its thickness x, $\chi = \sqrt{1+4/\langle Pe\rangle}$, $\omega = \langle Pe\rangle \lambda x$, and the Peclet number $<Pe>$ for the mesoscale is defined as:

$$< Pe >= \frac{< U_X >}{\varepsilon \lambda < \mathcal{D}_{XX} >} = \frac{< U_X >^{\beta}}{\lambda < \mathcal{D}_{XX} >}. \qquad (15)$$

The solution given by equation (15) is illustrated in Fig. 2, which presents, in the semi-log plot, the initial filter penetration as a function of a dimensionless filter thickness, λx.

Fig.2. Penetration vs. dimensionless filter thickness for various Peclet numbers [mesoscale convection-dispersion–deposition model, Eqs. (12)-(15)].

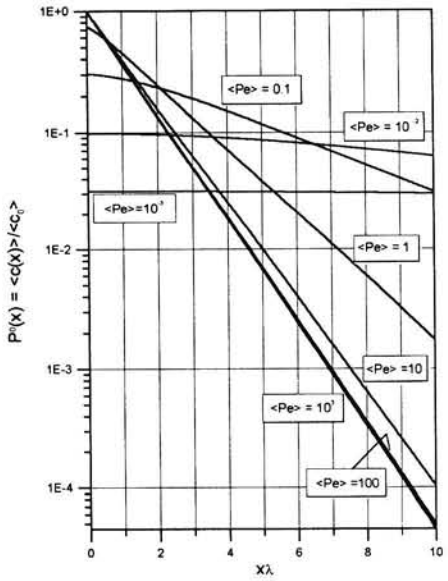

Fig. 3. Penetration vs. filter thickness calculated for staggered model of an electret filter: dashed line – for an assumed constant cell efficiency across the filter; solid line with points – penetration calculated by tracing 20000 trajectories of particles uniformly distributed at the entrance to the first layer. $<U_x>$=2cm/s, d_p=5μm, R_C=10μm, ε=0.97, particle charge=100e, linear charge density of fibres=10^{-10} C/m. Details in [10].

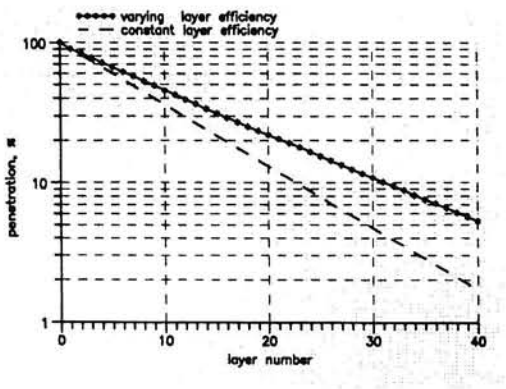

In the limiting case when no dispersion occurs ($<Pe>\to\infty$) equation (15) simplifies to the well known form: P^0=exp(-λx). More interesting is the fact that even in the case of moderate dispersion (see curves for $<Pe>$=10 and $<Pe>$=1 in Fig. 2) the model predicts that the lines of initial penetration, as a function of the filter thickness, are almost straight in the semi-log plot, however, with a different slope. Expanding equation (15) we find the following approximation:

$$\text{For } \langle Pe\rangle \lambda x > 1: \quad P^0(x) \approx \exp(-\lambda_{eff} x), \quad \text{where: } \lambda_{eff} = \lambda \langle Pe\rangle \left(\sqrt{1+4/\langle Pe\rangle} - 1\right)/2 \qquad (16)$$

This means that in practice we can neglect the dispersion term in the mesoscale transport equation, Eq. (12), provided that the effective filtration coefficient λ_{eff} given by Eq. (16) is used in the deposition rate equation, Eq. (13). In such a way the filter structure can be taken into account. Similar results were also obtained using microscopic analysis of deterministic trajectories of 20000 particles for a staggered model of an electret filter, [10]. An example of these results is shown in Fig. 3 – the logarithm of penetration, calculated for a multilayer fibrous structure, is a linear function of its thickness, but with a different slope from that predicted assuming constant layer efficiency.

MODELLING AEROSOL DEPOSITION IN A LOADED FILTER

MICROSCALE DESCRIPTION

As the time of filtration passes, the fibres become progressively covered with particles, and filter efficiency and pressured drop change. The shape of agglomerates formed depends on the predominant mechanism of deposition and the relation between particle and fibre size[11]. For diffusive, and to a less extent electrostatic deposition, distribution of deposits over the fibre surface are much more uniform than when the inertial effect dominates, when particles are mainly collected on the front fibre surface. The larger the fibre, the more porous, chainlike is the structure of agglomerates. Many theoretical studies have been performed to simulate dendrite growth on a single fibre. Among others, analytical models for individual dendrite growth for inertial impaction and interception, [12], and for Brownian diffusion, [13], were formulated. They are based on either the deterministic equation of particle motion, Eq. (1), or on the simplified equation of diffusion, Eq. (2), but do not incorporate Monte Carlo simulations for various starting positions of particles. The latter idea of using random simulations (still, however, based on deterministic transport equations) by computing a large number of trajectories with random upstream starting positions, has also been implemented, [11], [14], [15]. Releasing a particle far from the collector and integrating Eq. (1), each particle trajectory is calculated. If a particle comes in contact with the surface of a collector (fibre covered with deposits) a new collector surface is formed at that place and calculations are repeated for the next incoming particle. Such an approach has been quite successful in predicting qualitatively the shape of dendrites for various conditions of the process. However, one problem is extremely difficult to overcome, and it limits quantitative interpretation of results. When a fibre becomes heavily loaded and the shape of agglomerates formed is irregular, a significant change of local hydrodynamics in its vicinity takes place and it seems to be impossible to account for that adequately in a general case, using classical continuum fluid dynamics. Only in some special cases, when agglomerates of a regular shape are formed, an approximate analysis is possible. For pure diffusive deposition one may assume that deposits are almost uniformly distributed over the fibre, that is the initially cylindrical collector retains its shape during loading, but its effective diameter increases depending on the amount of deposited particles and the packing density of agglomerates. This assumption can be extended for simultaneous moderate inertial and electrostatic deposition, as inertial impaction causes preferential growth of agglomerates on the front side of the fibre. Electrostatic attraction leads to deposition over the entire fibre surface, and for the case of Coulombic attraction, even to a slightly higher degree at a rear surface, where the fluid velocity is smaller and hence local residence time of a particle, is greater. A simplified mathematical model of nonsteady-state filtration in a fibrous electret filter based on the assumption of uniform coverage of fibres in a given cross-section of the filter has been formulated, [16]. It uses a staggered arrangement of fibres and Stokesian flow. Single cell deposition efficiencies due to interception, inertial impaction and the electrostatic mechanisms were calculated by solving the deterministic equation of particle motion, while the efficiency due to Brownian diffusion was estimated from a semi-empirical correlation. These calculations were performed for various diameters of a loaded fibre, thus for various amounts of deposited particles, and change of local hydrodynamics and electrostatic field around the loaded fibre were taken into account. Subsequently, taking the mass accumulation of particles in each layer into account, the governing differential equations describing rate of growth of the loaded fibre diameter in the layer were incorporated, and the time-variation of the aerosol concentration leaving the layer was determined. Instantaneous profiles of aerosol

concentration and filter loading as well as the time-dependency of filter efficiency and pressure drop were calculated by integrating these equations. Two examples of results obtained are shown in Fig. 4 (see caption for explanation). The model formulated correctly predicts the pattern of efficiency variation. When only mechanical mechanisms of deposition act, there is a monotonic increase in the filter efficiency, which can be divided into two stages. There is initially a slow, followed by a more rapid decrease of the logarithm of penetration. For the case of the additional action of electrostatic mechanisms a minimum of efficiency is predicted, since loading an electrically charged fibre with deposits cause two opposite effects. There is a screening of the electric field causing a reduction of attractive electric forces, but simultaneously mechanical capture is enhanced due to the enlargement of the fibre. Both these relationships, for purely mechanical and electret filters, are observed experimentally. However, it should be remembered, that the model proposed will fail for filtration of larger particles, when predominating inertial effect results in complex shapes of unevenly distributed agglomerates. As mentioned above, it seems that dealing with the loading problem under conditions of variable hydrodynamics is impossible in the general case using classical fluid dynamics. An interesting alternative may be the gas-lattice (cellular automata) method, [17], which facilitates the treatment of problems with complex and variable boundaries. This promising approach is, however, still immature, numerically expensive and relatively inaccurate.

A novel issue in the microscopic analysis of nonsteady-state filtration is the question of the mechanical stability of the dendrites formed. Two approaches are possible here namely that based on local stress analysis, or on thermodynamics. The latter approach to describe the filling of void fractions of a fibrous filter structure with deposited particles was recently proposed, [18]. New quantities, like a Hamiltonian, taken for a particular configuration of deposits, compactivity of deposits and effective volume were introduced. Such a description makes it possible to analyse deposit breakage and the displacement of resuspended clusters inside the filter where reemission may be important.

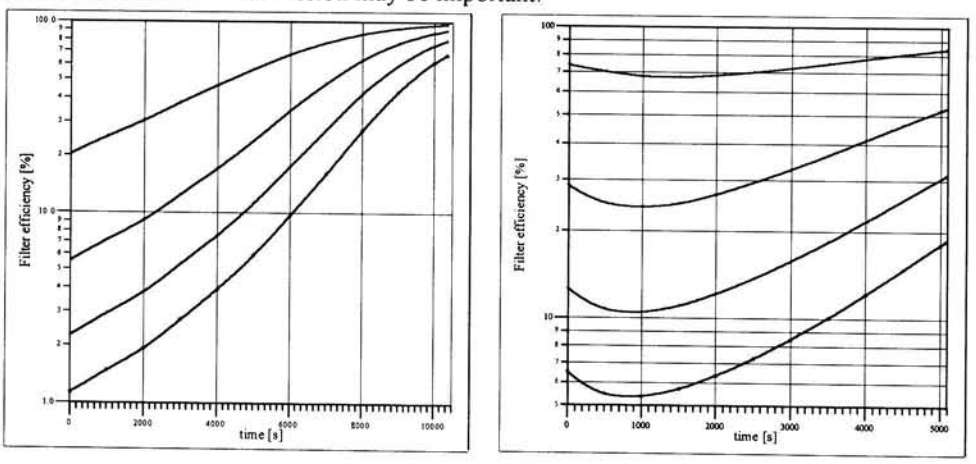

Fig. 4. Results of microscopic simulations of time-variation of filtration efficiency. Staggered model of the filter structure, R_C=10μm, d_P=2μm, $<U_X>$=0.1m/s, inlet aerosol concentration $<c_0>$=0.2g/m^3, particle density 1500kg/m^3, assumed packing density of agglomerates 0.74, initial filter porosity 0.99. Left – no electrostatic interactions. Right – electret filter with uniform linear charge density of fibres 10^{-10}C/m, aerosol particles carry 20 elementary charges of opposite sign. Four curves for filters of various thickness are given (10, 20, 50 and 200 unit layers – from the bottom to the top; for this filter the layer thickness is about 165μm). Details in [16].

MESOSCALE DESCRIPTION

The previously described method of analysis in the mesoscale for a clean filter may be extended to the nonsteady-state case. There is experimental evidence that, in the absence of electrostatic interactions, both filtration efficiency and pressure drop increase with time, showing two regimes of an the initial slow and a later accelerated change, [19]-[22]. During the first stage of the depth filtration aerosol particles are collected on the fibers and previously deposited material due to classical mechanisms. However, when the local filter loading exceeds some critical value, the character of the process undergoes a qualitative change. Particles fill free spaces within and between the dendrites formed, which will eventually link. The sieving effect then becomes important resulting in an increase of the local deposition rate. As this critical loading is reached first in the front layers of the filter, the process gradually changes its character from depth to more and more surface filtration. Subsequently, it may lead to the transition to cake filtration, which is accompanied by formation and growth of an external layer of deposit on the front face of the filter.

As discussed earlier, the macrotransport equation, Eq. (12), may be simplified by neglecting the dispersion term, if the effective filtration parameter, λ_{eff}, given by Eq. (16) is used in the formula for the local deposition rate, Eq. (13). For the nonsteady-state case the effect of local loading $<\sigma>$ (mesoscale averaged volume of deposited particle per unit volume of the filter) on the deposition rate -$<r>$ must be considered. Generally, if reemission of deposits does not occur, the kinetic equation for the deposition rate may be written as:

$$-<r>=\frac{\partial<\sigma>}{\partial t}=\lambda_{eff}<U_x><c>\varphi(<\sigma>) \tag{17}$$

where the function $\varphi(\sigma)$ describes the variation of the deposition rate with local filter loading. A linear form of $\varphi(\sigma)$ has been proposed, [11], [22]. However, such a description would be limited only to the first stage of depth filtration. To account for the transition from the depth to surface filtration mentioned above the following generalization was suggested, [23]:

$$\varphi(<\sigma>)=\begin{cases}1+<\sigma>/\sigma^{*} & \text{for } <\sigma>\le\sigma_c,\\ 1+<\sigma>/\sigma^{*}+a(<\sigma>-\sigma_c)/\sigma^{*} & \text{for } <\sigma>\ge\sigma_c.\end{cases} \tag{18}$$

This equation introduces three phenomenological constants: σ^*, which characterizes loading during the first stage, σ_c, the critical loading at the moment of transition to the second stage and a, a dimensionless factor of acceleration of the deposition during the second period. The analytical solution, $c(x,t)$, $\sigma(x,t)$, of the above problem predicts the following variation of the filter penetration P with time t, [23]:

I STAGE ($t \le t_c$):

$$1/P(t)=1+\exp(\bar{t})[\exp(N_L)-1] \tag{19}$$

II STAGE ($t \ge t_c$):

$$\frac{1}{P(t)}=\left\{\exp\left[N_L(1-\bar{x}_1)\right]\left(1+\frac{1}{\bar{\sigma}_c}\right)-1\right\}\left\{\frac{a\bar{\sigma}_c-1}{1+a}+\left(\frac{1+\bar{\sigma}_c}{1+a}\right)\exp\left[(1+a)(\bar{t}-\bar{t}_c)\right]\right\}, \tag{20}$$

where the dimensionless position of the cross-section separating zones of 2nd and 1st stage, $\bar{x}_1=x_1(t)/L$, (where $\sigma(x_1)=\sigma_c$) moves in time across the filter as:

$$\frac{x_1(t)}{L}=\bar{x}_1=-\frac{1}{N_L(a\bar{\sigma}_c-1)}\ln\left\{1-\left(\frac{a\bar{\sigma}_c-1}{(1+a)\bar{\sigma}_c}\right)\left[1-\exp[-(1+a)(\bar{t}-\bar{t}_c)]\right]\right\}. \tag{21}$$

In the above equations the following notation is used: $\bar{t}=t/t^*$, $\bar{t}_c=t_c/t^*=\ln(1+\bar{\sigma}_c)$, $\bar{\sigma}_c=\sigma_c/\sigma^*$, $t^*=\sigma^*/(\lambda_{eff}<U_x><c_0>)$, $N_L=\lambda_{eff}L$, where L is the filter thickness and $<c_0>$ - inlet aerosol concentration. The model proposed contains 4 phenomenological constants: N_L (or, equivalently, λ_{eff}), t^* (or σ^*), $\bar{t}_c$(or $\bar{\sigma}_c$) and a, which can be easily determined from the experimental data as follows: 1) $N_L=-\ln P_0$, where P^0 is initial penetration; 2) $1/t^*$ as the slope of the curve $\ln[(1-P)/P]$ vs. time during the first stage; 3) t_c as the time, when the curve $\ln[(1-P)/P]$ vs. time starts to deviate from the straight line during the first stage; 4) a by fitting theoretical curve with experimental data for the second stage. Two examples comparing the model with experimental data are shown in Fig. 5. One can conclude that using this simple model it is possible to describe accurately the variation of filter penetration over a very broad range. The key issue for future investigations is to determine the dependence of the model coefficients on the process conditions and aerosol and filter properties.

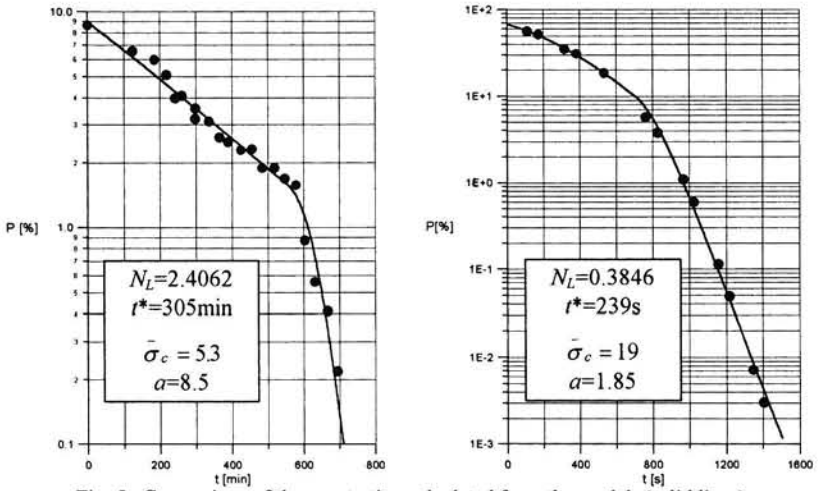

Fig. 5. Comparison of the penetration calculated from the model (solid lines) with experimental data (points): left – data from [22]; right – data from [20].

Description of the filter loading was also extended for the case when deposits may be resuspended in the aerosol stream, [24]. The total loading rate is then a difference between the deposition rate given by Eqs. (17)-(18) and a reemission rate suggested in the form:

$$\left(\frac{\partial<\sigma>}{\partial t}\right)_{reem}=-\kappa<U_X>\psi(<\sigma>),\qquad \psi(<\sigma>)=\begin{cases}0 & \text{for } <\sigma>\le\sigma_R,\\ (<\sigma>-\sigma_R)/\sigma^* & \text{for } <\sigma>\ge\sigma_R.\end{cases} \tag{22}$$

These equations introduce two phenomenological constants, σ_R, and, κ, which have to be determined experimentally. The above discussion did not concern electret filters. In the case where electrostatic interactions occur, a maximum in instantaneous penetration with time is observed, [25], in agreement with the theoretical results given in Fig. 4. To describe this phenomenon, an additional, negative and probably nonlinear term that is dependent on the local loading should be incorporated into the kinetic equations (17)-(18).

CONCLUSIONS

There are still many unresolved problems regarding the theory of aerosol filtration in fibrous filters. In the author's opinion, future studies should be especially focused on:

- *In the microscale analysis*: systematic use of Brownian dynamics methods to establish more realistic correlations for the deposition efficiency resulting from several mechanisms acting simultaneously, including the electrostatic ones; extension of quantitative descriptions for non-spherical particles, especially fibrous ones, [26]; derivation of more realistic models of filter structure and gas flow (a complete generalisation is not expected to be obtained here as each filter has its unique structure); use of new methods of approach (gas-lattice, thermodynamic).
- *In the mesoscale analysis*: verification of kinetic models of filter loading and establishing generalised functional dependencies of these model parameters on filter properties and structure, properties of aerosol and process conditions. This would be of a great practical importance for filter design and optimisation of their use.

Finally, the need for experimental verification of new complex theories should also be emphasised.

REFERENCES

[1] Davies, C.N., *Air Filtration*. Academic Press, London, 1973.
[2] Brown, R.C., *Air Filtration*. Pergamon Press, Oxford, 1993.
[3] Ramaro, B.V., Tien, C., Mohan, S., Calculation of single fibre efficiencies for interception and impaction with superposed Brownian motion. *J. Aerosol Sci.* **25**, 295-313, 1994.
[4] Risken, H., *The Fokker-Planck Equation: Methods of Solution and Applications*. Springer-Verlag, New York, 1989.
[5] Chandrasekhar, S, Stochastic problems in physics and astronomy. *Rev. Modern Phys.* **15**, 1-89, 1943.
[6] Peters, M.H., Cooper, D.W., Miller, R.J., The effects of electrostatic and inertial forces on the diffusive deposition of small particles onto large disks. *J. Aerosol Sci.* 20, 123-136, 1989.
[7] Gray, W.G., A derivation of the equation for multi-phase transport. *Chem. Eng. Sci.* **30**, 229-233, 1975.
[8] Quintard, M., Whitaker, S., Aerosol filtration: an analysis using the method of volume averaging. *J. Aerosol Sci.* **26**, 1227-1255, 1995.
[9] Shapiro, M., Kettner, I.J., Brenner, H., Transport mechanics and collection of submicrometer particles in fibrous filters. *J. Aerosol Sci.* **22**, 707-722, 1991.
[10] Podgórski, A., Gradoń, L., Shadow and ordering effects in fibrous electret filters. *J. Aerosol Sci.* **23** (Suppl. 1), S753-S756, 1992.
[11] Kanaoka, C., Perforfamce of an air filter at dust-loaded condition. Chapter 16 in: *Advances in Aerosol Filtration* (Ed. K.R. Spurny). Lewis Publishers, Boca Raton, 1998.
[12] Payatakes, A.C., Gradoń, L., Dendritic deposition of aerosol particles in fibrous media by inertial impaction and interception. *Chem. Eng. Sci.* **35**, 1083-1096, 1980.
[13] Payatakes, A.C., Gradoń, L., Dendritic deposition of aerosols by convective Brownian diffusion for small, intermediate and high particle Knudsen numbers. *AIChE J.* **26**, 443-454, 1980.
[14] Tien, C., Effect of deposition on aerosol filtration. Chapter 15 in: *Advances in Aerosol Filtration* (Ed. K.R. Spurny). Lewis Publishers, Boca Raton, 1998.
[15] Cai, J., *Fibrous Filters with non-ideal Conditions*. PhD dissertation. The Royal Institute of Technology, Stockholm, 1992.
[16] Podgórski, A., Rudziński, M., Gradoń, L., Nonsteady-state filtration of aerosol particles in the electret filter structures. *Chem. Eng. Comm.* **151**, 125-146, 1996.
[17] Filippova, O., Hänel, D., Numerical simulation of gas-particle flow in filters by lattice Bhatnagar-Gross-Krook model. Chapter 9 in: *Advances in Aerosol Filtration* (Ed. K.R. Spurny). Lewis Publishers, Boca Raton, 1998.
[18] Gradoń, L., Reemission of solid particles from the loaded filter structure. Abstracts AAAR'98 Conference, p.316. Cincinnati, 1998.
[19] Stenhouse, J.I.T., Trottier, R., The loading of fibrous filters with submicron aerosols. *J. Aerosol Sci.* **22** (Suppl. 1), S777-S780, 1991.
[20] Japuntich, D.A., Stenhouse, J.I.T., Liu, B.Y.H., Experimental results of solid monodisperse particle clogging of fibrous filters. *J. Aerosol Sci.* **25**, 385-393, 1994.
[21] Graef, A., Stenhouse, J.I.T., Walsh, D.C., The effect of solid aerosol on prefilter material performance. *J. Aerosol Sci.* **26** (Suppl. 1), S741-S742, 1997.
[22] Brown, R.C., Wake, D., Loading filters with monodisperse aerosols: macroscopic treatment. *J. Aerosol Sci.* **30**, 227-234, 1999.
[23] Podgórski, A., Macroscopic model of two-stage aerosol filtration in a fibrous filter without reemission of deposits. *J. Aerosol Sci.* **29** (Suppl. 1), S929-S930, 1998.
[24] Podgórski, A., Gradoń, L., Luckner, H.J., Investigations on the deposits reemission if fibrous filters. *J. Aerosol Sci.* **29** (Suppl. 1), S931-S932, 1998.
[25] Walsh, D.C., Stenhouse, J.I.T., The effect of particle size, charges and composition on the loading characteristics of an electrically active fibrous material. *J. Aerosol Sci.* **28**, 307-322, 1997.
[26] Podgórski, A., Gradoń, L., Mechanics of a deformable fibrous aerosol particle: general theory and application to the modelling of air filtration. Chapter 10 in: *Advances in Aerosol Filtration* (Ed. K.R. Spurny). Lewis Publishers, Boca Raton, 1998.

Modelling the Loading Behaviour of Electrically Active Fibrous Filter Materials

DC Walsh[1] & C Kanaoka[2]

[1]Lecturer in Chemical Engineering, Department of Mechanical & Chemical Engineering, Heriot-Watt University, Edinburgh, Scotland.

[2]Professor of Environmental Engineering, Department of Civil Engineering, Kanazawa University, Kanazawa, Japan.

KEYWORDS

Filtration, aerosols, loading, electrostatics, electrets

ABSTRACT:

The loading behaviour of electrically active materials has been the subject of considerable research activity in the last twenty years. The reason for such interest is that unlike conventional fibrous filter materials (where the filtration efficiency increases as the material is loaded with particles), in electrically active materials the efficiency usually falls as a function of loading. In this work the authors have integrated semi-empirical models that have been previously employed to describe the degradation of filtration efficiency in electrically active materials [Walsh 1995], and to describe the improvement in efficiency in conventional materials [Kanaoka et al. 1980], in order that the complete loading curve for an electrically active material may be simulated. Fundamental to the integration of these two models has been the assumption that particles that are deposited by electrostatic mechanisms do not contribute to the improvement in collection efficiency by mechanical mechanisms. Using this assumption the effects of particle size, face velocity, and aerosol composition have been successfully modelled.

INTRODUCTION

Studies of the loading behaviour of electrically active materials have generally found filter penetration to increase from an initially low value as the material is loaded, go through a maximum, and finally fall off to zero as a filter cake is formed ([de Haan et. al. 1985], [Baumgartner and Löffler 1986], [Lehtimaki and Heinonen 1994] and [Walsh and Stenhouse 1996]). Two approaches to explain the increase in penetration in the early stages of loading have been proposed. The first concludes that the reduction in efficiency is by some neutralisation process, where the fall in filtration efficiency is attributed to a reduction in the charge of filter fibres by the charge carried by deposited particles [Baumgartner and Löffler 1987]. A second explanation [Brown et al. 1988] concluded that the degradation of the filtration efficiency by deposited particles was not a charge neutralisation process, but rather that the fibre charge was is some way "screened" by the deposited aerosol. It was suggested that the degree to which the filtration efficiency was degraded under a given condition was specific to the loading particles.

Walsh and Stenhouse [Walsh and Stenhouse 1997a] have previously shown that for the filter material used in this study there is a strong relationship between the loading particle's size, charge, composition, and filter loading behaviour. This work showed that smaller loading particles cause penetration to rise more quickly and are more clogging; uncharged particles

cause penetration to rise more quickly and are more clogging than charged particles; and that particles of different composition can have vastly different effects (Titanium dioxide particles are much more clogging, and particles cause penetration to rise more quickly than similarly sized Stearic acid particles). Some of these effects were explained in a later paper where the clogging point, or dust holding capacity, of the filter was shown to be empirically related to the electrostatic parameter describing particle collection by induction (N_{Qo}) [Walsh and Stenhouse, 1997b].

Elsewhere the effects of fluid velocity, fluid humidity, and filter fibre charge on the loading behaviour of this material have been discussed [Walsh & Stenhouse 1998]. A semi-empirical equation was presented allowing the maximum penetration through the filter material over its life to be predicted. This work also presented experiments that allowed the filter degradation process to be described in more detail than had been possible previously, and proved conclusively that the degradation process was not the result of charge neutralisation.

THEORY

Electrically active filters achieve their superior gas cleaning ability by the employment of electrostatic mechanisms that are not possible in conventional materials. These additional mechanisms are achieved by virtue of permanent electric charges stored on the surface of the filter fibres, which allow particles to be collected by Coulombic and induction forces.

The electrostatic parameter for Coulombic collection (N_{Qq}) can be used to quantify the degree to which Coulombic mechanisms exist within the system.

$$N_{Qq} = \left[\frac{Q_f q}{3\pi^2 \varepsilon_g \varepsilon_0 \mu d_p d_f U_0} \right] \qquad \text{(Eq.1)}$$

Similarly a dimensionless parameter (N_{Qo}) can be defined for collection by induction.

$$N_{Q0} = \left[\frac{Q_f^2 d_p^2}{3\pi^2 \mu \varepsilon_0 d_f^3 U_0} \left(\frac{\varepsilon_0 - 1}{\varepsilon_p + 2} \right) \right] \qquad \text{(Eq.2)}$$

The single fibre efficiency due to these mechanisms can then be predicted using equations proposed by Kraemer and Johnstone [Kraemer & Johnstone 1955].

$$\eta_{Qq} = \pi N_{Qq} \qquad \text{(Eq.3)}$$

and

$$\eta_{Qo} = \frac{3\pi N_{Qo}^{1/3}}{2} \qquad \text{(Eq.4)}$$

Thus it is possible to calculate the single fibre efficiency due to either of these mechanisms. If the various collection mechanisms are assumed additive it is therefore possible to predict the clean filter efficiency of an electrically active material. However, the clean filter efficiency of

these materials is of little use as the penetration through the materials usually increases as a function of loading, at least in the early stages. It is therefore necessary to find some way of accounting for this effect of loading on filtration efficiency.

It has been shown experimentally that the reduction in filtration efficiency in these materials is not the result of a charge neutralisation process [Walsh & Stenhouse 1997b, Walsh & Stenhouse 1998], but is rather the result of a screening process, as was first proposed by Brown et al. [Brown et al. 1988]. With this in mind Walsh [Walsh 1995] has proposed a semi-empirical model of the process by which filtration efficiency is degraded in these materials.

The fundamental hypothesis of this model is that the effect of loading on the filtration efficiency can be accounted for by assuming that the permittivity of the space within the filter changes as it becomes loaded, i.e. that the presence of deposited particles dampens the electrostatic forces by having the effect of increasing the permittivity of the gas (ε_g).

This concept is illustrated in Figure 1.

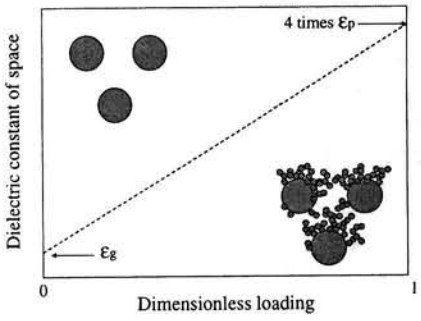

Figure 1: Illustration of the conceptual basis of the varying permittivity model.

Walsh [Walsh 1995] proposed that the penetration at any dimensionless loading ($Pn_{M\_}$) was given by:

$$Pn_{M\_} = \exp\left(\frac{-4\alpha h \eta_{S_{M\_}}}{\pi d_f \xi}\right) \qquad \text{(Eq.5)}$$

where (in a system with negligible mechanical efficiency):

$$\eta_{S_{M\_}} = \pi N_{Qq_{M\_}} + \frac{3\pi N^{1/3}_{Qo_{M\_}}}{2} \qquad \text{(Eq.6)}$$

The electrostatic parameters being calculated at any loading (M_) using Equations 1 and 2, where:

$$\varepsilon_g = \varepsilon_{Air}(1 - M\_) + K\varepsilon_p M\_ \qquad \text{(Eq.7)}$$

The empirical constant of Equation 7 (K) was found to be four, and the dimensionless loading (M_) was defined as the ratio of the mass loading (M_{dep}) to the mass loading required to clog

the filter (M_{clog}):

$$M\_ = \frac{M_{dep}}{M_{\text{Clog}}} \qquad \text{(Eq.8)}$$

In other work [Walsh & Stenhouse 1998] it has been shown that for this filter material, under the conditions described here the mass loading required to clog the filter is given by the empirical equation:

$$M_{\text{clog}} = 50 + 10\log_{10}(N_{Qo}) \qquad \text{(Eq.9)}$$

(Note: The units of M_{clog} in this equation are g m^{-2}, and this empirical equation is only applicable under the conditions from which it was derived.)

So if the characteristics of the filter material, the aerosol particles, and the carrier fluid are known it is possible to predict the initial loading behaviour of the electrically active filter material as shown in Figure 2.

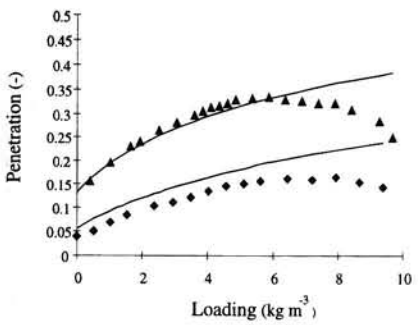

Figure 2: Experimentally derived values for filter penetration as a function of loading compared to values predicted using the filter degradation model [Walsh 1995].

As can be seen in Figure 2 there is good agreement between the predicted values and the experimental data, at least in the early stages. As mechanical effects become important however the predicted values and experimental values diverge. To describe the entire loading curve it is therefore necessary to somehow account for the improvements in mechanical efficiency, which cause the penetration to plateau, and later fall as the filter approaches a clogged state.

As described elsewhere [Kanaoka et al. 1980] it is possible to describe the effect of loading on collection by mechanical mechanisms in filters of similar mechanical structure and similar operating conditions using an efficiency raising factor (λ) type model:

$$Pn_{M_{dep}} = \left[\frac{\exp(-\lambda \frac{4\alpha\eta_o}{\pi(1-\alpha)d_f} M_{faced})}{\exp(-\lambda \frac{4\alpha\eta_o}{\pi(1-\alpha)d_f} M_{faced}) + \exp\left(\frac{4\alpha h\eta_o}{\pi(1-\alpha)d_f \xi}\right) - 1} \right] \qquad \text{(Eq.10)}$$

Incorporation of both models should thus result in a complete description of the loading behaviour of this filter material. The incorporation of these models so as to describe the entire loading curve was thus the stated objective of this work.

SIMULATION OF LOADING BEHAVIOR

In order that the loading behaviour be simulated it was first necessary to estimate the clean filter efficiency using conventional theory. This was achieved by assuming that the single fibre efficiency for the combined collection mechanisms was given by:

$$\eta_S = \eta_{Qq} + \eta_{Qo} + \eta_{Diff} + \eta_{Int} + \eta_{Inertia} \qquad \text{(Eq.11)}$$

This assumes that all collection mechanisms are simply additive. The assumption that no interaction terms existed is an approximation. The electrostatic contribution can then be calculated using Equations 3 and 4 [Kraemer & Johnstone 1955]. The mechanical contributions (diffusion, interception, and inertia) were calculated using the equations of Davies [Davies 1973], Kuwabara [Kuwabara 1959], and Yeh and Liu [Yeh & Liu 1974] respectively, allowing the clean filter efficiency to be predicted.

The loading behaviour was then simulated mathematically by feeding incremental mass loads to the filter and calculating the penetration through the filter. At each mass load a penetration was calculated for both the electrostatic contribution and the mechanical contribution, the total penetration being calculated as the product of the two (i.e. it is assumed the material can be treated as a thin layer, and mechanisms are additive).

$$Pn = Pn_{Elec} Pn_{Mech} \qquad \text{(Eq.12)}$$

Using the varying permittivity model described above the effect of loading on electrostatic contribution to the electrically active material could be calculated as a function of the mass deposited on the filter. However in order to accurately simulate the effect of loading on the mechanical contribution it was necessary to rewrite Equation 10 as:

$$Pn_{M_{dep}} = \left[\frac{\exp(-\lambda \frac{4\alpha\eta_o}{\pi(1-\alpha)d_f} M_{dep_{Mech}})}{\exp(-\lambda \frac{4\alpha\eta_o}{\pi(1-\alpha)d_f} M_{dep_{Mech}}) + \exp\left(\frac{4\alpha h\eta_o}{\pi(1-\alpha)d_f \xi}\right) - 1} \right] \qquad \text{(Eq.13)}$$

Where $M_{depMech}$ is the mass deposited on the filter by mechanical mechanisms.

Thus it was assumed that only material deposited by mechanical mechanisms was able to contribute to any increase in mechanical efficiency. It has been shown previously [Walsh & Stenhouse 1997b] that while material deposited on fibres due to electrostatic mechanisms does so uniformly around the fibre surface, material deposited by mechanical mechanisms is deposited primarily at the front of the fibre. As a result dendritic structures, which can contribute significantly to collection by mechanical mechanisms, are formed more readily when particles are collected by mechanical mechanisms. This is illustrated in Figure 3.

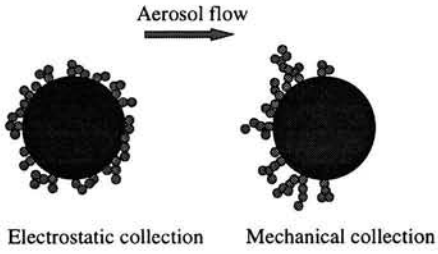

Figure 3: Deposition of particles on a fibre surface by electrostatic and mechanical collection mechanisms.

The resultant model provided a very good approximation of the loading behaviour, as is illustrated by Figure 4. This shows the relationship between mass loading and penetration found experimentally when a sample of electrically active material is loaded with 1.4 μm Stearic acid particles at Boltzmann equilibrium, at a face velocity of 0.1 m s^{-1}. Also shown is the penetration predicted when only mechanical, only electrostatic, and when both electrostatic and mechanical mechanisms are accounted for.

In the early stages of loading particle collection is almost exclusively due to electrostatic mechanisms, with particles being deposited on the fibre surface, and thereby not contributing a great deal to the mechanical efficiency of the material. As loading proceeds however collection due to electrostatics becomes less important as the electrostatic effects are screened by deposited particles. At the same time the mechanical contribution to the overall efficiency accelerates and ultimately becomes the dominant collection mechanism.

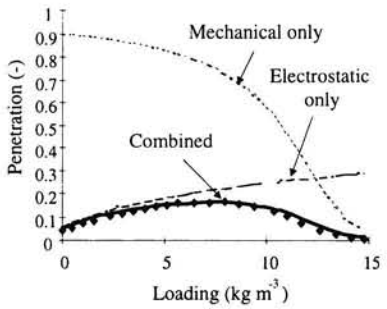

Figure 4: Penetration as a function of filter loading as found experimentally and as predicted.

Clearly a very good agreement is exhibited between the experimental data and the predictions of the model. Such agreement has been found for a range of particle sizes (0.46 to 1.40 μm) and also for a range of face velocities (0.05 to 0.80 m s^{-1}) as is shown in Figures 5 and 6 below.

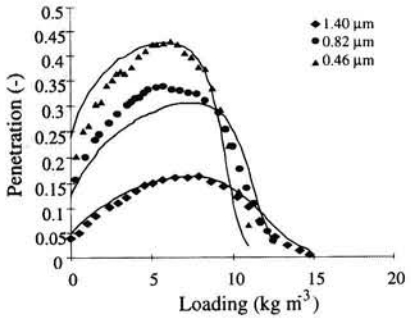

Figure 5: Experimentally derived and predicted penetrations when filter samples are loaded with Stearic acid particles (0.46 to 1.40 µm) at Boltzmann equilibrium, and at 0.10 m s^{-1} face velocity.

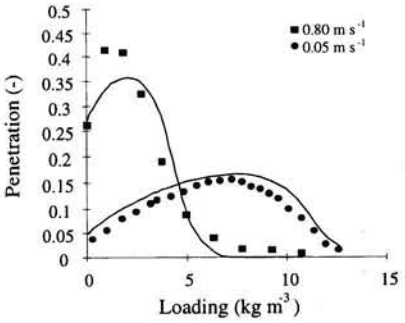

Figure 6: Experimentally derived and predicted penetrations when filter samples are loaded with Stearic acid particles (1.40 µm) at Boltzmann equilibrium, and at 0.05 to 0.80 m s^{-1} face velocity.

As has been discussed previously elsewhere the electrical characteristics of the loading aerosol particles can also have an effect on the materials loading behaviour [Walsh & Stenhouse 1997]. As can be seen from Figure 8 the model described here can also be used to predict such differences in behaviour, although the accuracy of the predicted loading behaviour of titanium dioxide is not nearly as good as that for similarly sized Stearic acid particles.

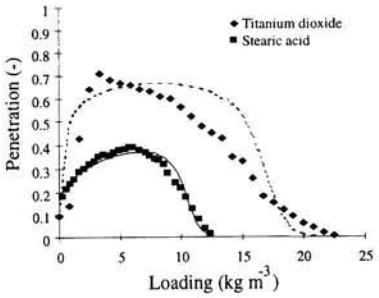

Figure 8: Derived and predicted penetrations when filter samples are loaded with similarly sized Titanium dioxide and Stearic acid particles at Boltzmann equilibrium, and at a face velocity of 0.1 m s^{-1}.

The values of efficiency raising factor used in all these simulations to describe improvements in mechanical efficiency were found using a least squares technique similar to that employed previously for the calculation of the efficiency raising factor in purely mechanical filters [Walsh & Kanaoka 1999]. The values for the efficiency raising factor used to calculate the effect of loading on the mechanical contribution to the filtration efficiency show good

agreement with data from other work as is evidenced by Figure 9.

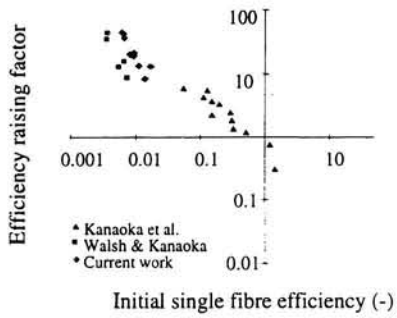

Figure 9: Efficiency raising factor as a function of single fibre efficiency.

The efficiency-raising factor is higher here, but that is unsurprising given the assumption that material deposited by electrostatic mechanisms makes no contribution to the increase in mechanical efficiency.

DISCUSSION

As is evidenced by Figure 10 there is very good agreement between the values of penetration over the filter life using the combined varying permittivity and efficiency raising factor models and those found experimentally.

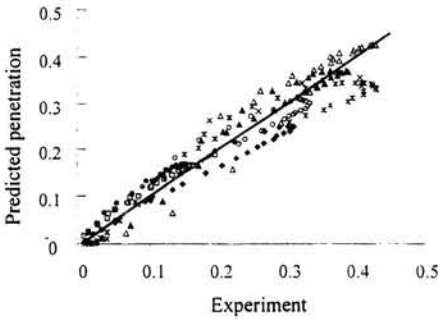

Figure 10: Penetrations calculated using the combined varying permittivity and efficiency raising factor models plotted against penetrations measured experimentally.

In developing this model some fundamental assumptions were made.

I. Degradation of the electrostatic efficiency during loading is due to the effect of the deposited particles on the permittivity of the space within the material.

II. Improvements in mechanical efficiency can be described using an efficiency-raising factor type model.

III. Only material deposited by mechanical mechanisms contributes to improvement of the mechanical efficiency of the material.
IV. All collection mechanisms can be assumed additive.
V. The filter can be assumed as a single layer.

That the presence of deposited aerosol particles in the filter space dampens the electrical effects by increasing the permittivity is conceptually simple, and the varying permittivity model does appears to work very well. It accounts for the difference in filter behaviour when loaded with Titanium dioxide rather than Stearic acid as Titanium dioxide has a much higher permittivity than Stearic acid and one would thus expect it to be more degrading, as has been shown experimentally. However this model requires further verification with aerosol particles of different permittivities. Unfortunately obtaining sufficiently monodisperse particles of sufficiently different permittivities was not possible.

The second assumption, that an efficiency raising factor type model can be employed to describe the improvements in mechanical efficiency has been discussed elsewhere [Kanaoka et al. 1980] where it was found that such a model described loading on a single fibre very well, although experimental values for the efficiency raising factor where typically a lot lower than those derived from theoretical simulations using the Kuwabara flow field [Kuwabara 1959].

For this approach to work it was also necessary to assume that only material deposited by mechanical mechanisms contributes to improvement in the mechanical efficiency. This assumption is based on the observation [Walsh & Stenhouse 1998a] that when electrical forces dominate particle collection, material is deposited uniformly around the fibre surface, and does not form dendritic structures that protrude into the aerosol flow, and thus contribute to the mechanical efficiency, as readily.

The assumption that all mechanisms can be considered additive is considered valid since interaction terms between the mechanisms are not readily available, and any minor differences in the original efficiency calculated will have only a small effect on the efficiency raising factor.

Finally it is also assumed that the filter can be treated as a single layer. Since the filter concerned is relatively thin (0.003 m) this is considered valid, although similar analysis of thicker materials would clearly require incremental multi-layer calculations.

CONCLUSIONS

It has been shown that the degradation of electrostatic effects by aerosol particle loading can be considered to be due to the effect of the deposited particles on the permittivity of the space within the filter, and that the degree to which a given aerosol particle will degrade the filter's efficiency is related to its permittivity.

It has also been shown that, by approximating that only material deposited by mechanical mechanisms contribute to any increase in mechanical efficiency during loading, the varying permittivity model and the efficiency raising factor model can be integrated so as to describe

the entire loading curve for the electrically active material used here at a variety of loading conditions.

Values for the efficiency-raising factor (λ) derived from this approach show very good agreement with previous work, indicating the validity of the approach employed.

ACKNOWLEDGEMENTS

The authors would like to express their gratitude to the Japanese Ministry of Education, Science, Sports and Culture (Monbusho), for the award of a Research Experience Fellowship for Young Foreign Researchers (REFYFR) to Dr. Walsh, which enabled this work to be undertaken.

SYMBOLS & UNITS

d_f	Fibre diameter	m
d_p	Particle size	m
H	Filter depth	m
q	Particle charge	C
K	Constant for Equation 7 (=4)	-
M_	Dimensionless loading	-
M_{dep}	Mass deposited per unit volume of filter	kg m^{-3}
M_{clog}	Mass deposited on filter at clogging point	kg m^{-3}
$M_{depMech}$	Mass deposited on filter by mechanical mechanisms	kg m^{-3}
N_{Qq}	Electrostatic parameter for Coulombic collection	-
N_{Qo}	Electrostatic parameter for collection by induction	-
Pn	Penetration	-
Pn_{Elec}	Penetration when only electrical mechanisms are accounted for	-
Pn_{Mech}	Penetration when only mechanical mechanisms are accounted for	-
Q_f	Fibre charge	
α	Filter packing density	-
ε_o	Permittivity of free space	Farads m^{-1}
ε_p	Dielectric constant of aerosol particles	-
ε_g	Dielectric constant of gas	-
ε_{Air}	Dielectric constant of air	-
η_{Qq}	Single fibre efficiency due to Coulombic mechanisms	-
η_{Qo}	Single fibre efficiency due to induction mechanisms	-
η_{Diff}	Single fibre efficiency due to diffusion	-
$\eta_{Inertia}$	Single fibre efficiency due to inertia	-

η_{Int}	Single fibre efficiency due to interception	-
η_o	Single fibre efficiency of clean filter	-
$\eta_{SM\_}$	Single fibre efficiency of loaded filter	-
λ	Efficiency raising factor	kg m^{-2}
μ	Gas viscosity	Pa s
ξ	Filter inhomogeneity	-

REFERENCES

Baumgartner H., & Löffler F. (1987), Particle collection in electret fibre filters, a basic theoretical and experimental study, *Filtration & Separation*, Sept./Oct. pp.346-351

Brown R.C. et al. (1988), Effect of industrial aerosol on electrically charged filter material, *Ann. Occup. Hyg.*, 32, pp. 271-294

Davies C.N. (1973), *Air Filtration,* Academic Press

de Haan et al. (1985), Fibrous and granular filters with electrically enhanced dust capturing efficiency, *Proceedings of the 5th International Symposium on Electrets, Heidelberg*

Kanaoka C. et al. (1980), Estimation of collection efficiency of an air filter with dust load, *Solid Separation Processes International Symposium, Dublin*, 3, pp. 4/1-4/14

Kraemer H.F., & Johnstone H.F. (1955), Collection of aerosol particles in presence of electrical fields, *Ind. Eng. Chem.*, 47, pp. 2426-2434

Kuwabara S. (1959), The forces experienced by a lattice of elliptical cylinders in a uniform flow at small Reynolds numbers, *J. Phys. Soc. Japan*, 14 (4), pp. 522-527

Lehtimaki M., & Heinonen K. (1994), Reliability of electret filters, *Building and Environment*, 29, pp. 353-355

Walsh D.C. (1995), *The behaviour of electrically active and prefilter fibrous filters under solid aerosol load*, Ph.D. Thesis, Loughborough University of Technology

Walsh D.C., & Kanaoka C. (1999), Modelling the loading behaviour of fibrous filter materials: Part 1 - Prefilter materials, to be submitted to *J. Aerosol Sci.*

Walsh D.C., & Stenhouse J.I.T. (1996), Experimental studies of electrically active fibrous filter loading, *Part. Part. Syst. Char.*, 13, pp. 47-53

Walsh D.C., & Stenhouse J.I.T. (1997), The effect of particle size, charge, and composition on the loading characteristics of an electrically active fibrous filter material, *J. Aerosol Sci.*, 28, pp. 307-321

Walsh D.C., & Stenhouse J.I.T. (1997), Clogging of an electrically active material: Experimental results and 2D simulations, *Pow. Tech.*, 93, pp. 63-75.

Walsh D.C., & Stenhouse J.I.T. (1998), Parameters affecting the loading behaviour and degradation of electrically active filter materials, *Aerosol Science & Technology*, 29, pp. 419-432.

Yeh H.C. & Liu B.Y.H. (1974), Aerosol filtration by fibrous filters, *J. Aerosol Sci.*, 5, pp. 191-217

The Influence of Particle Shape on the Penetration through Fibrous and Electret Filters

I.L. Tuinman
TNO-PML, Lange Kleiweg 137, 228OAA Rij swijk, The Netherlands

KEYWORDS
aerosol filtration, particle shape

Aerosols encountered in reality often differ with respect to shape and size from test aerosols used to certify filters. A typical example is formed by asbestos and ceramic fibres which have high aspect ratios. The group of non-spherical particles discussed here is bacteria and their physical simulants. Bacteria are often rod-shaped with low aspect ratios <5, and many species can form groups or colonies of specific shapes. The penetration of bacteria and some physical simulants through different types of filters are the subject of this study.

EXPERIMENTAL

The test set-up
Four types of filters have been tested:

A. electret filter cloth consisting of smooth (melt blown) fibres,
B. electret filters consisting of rugged (split) fibres,
C. unchanged glass fibre filters, and
D. unchanged, radially folded filters consisting of a mixture of smooth glass fibres and rugged vegetable fibres

The test aerosols consisted of 1) rod-shaped, caffeine particles 2) spherical oil particles, 3) spherical PSL particles, 4) elliptical spores of Bacillus subtilus var. niger or Bacillus globigii, BGspores, and 5) plate-like eicosanoic acid particles and clusters of these. This paper focuses on the first 4 particle types.

The test set-up is shown in figure 1. The BG-spores and PSL particles were aerosolized by spraying them with a Collison 6 nebulizer. The oil, caffeine, and eicosanoic acid particles were generated with a Condensation Monodisperse Aerosol Generator, CMAG (TSI 3470). In this instrument aerosols with several shapes besides the standard spherical oil-particles can be generated as described by Vaughan (1990). First a dilute NaCl solution is sprayed with a nebulizer. The droplets are dried in a diffusion dryer and NaCl crystals of ± 40 nm in diameter remain. The flow is then passed through hot vapour of a certain compound and when the flow cools down aerosol particles are formed by condensation of the vapour on the NaCl nuclei. The particle shape is determined by the condensing compound's crystal structure. The particle size depends on the number of nuclei and the amount of condensing vapour, hence on the temperature of the "oil bath" in which the compound is placed. Examples of the resulting caffeine particles are shown in figure 2. A SEM photograph of the BG-spores is shown in figure 3.

The aerosols are mixed with dry or moisturized, clean air and subsequently led into a test chamber with two exits, one to determine the challenge aerosol concentration and one to determine the particle concentration in the filtered air. The samples are taken iso-axially and (almost) isokinetically. The particle concentration as a function of size is determined with a differential mobility analyzer, a DMA (TSI 3071) for particles < lμm and for particles >0.5 μm with an aerodynamic particle sizer, an APS (TSI 3320).

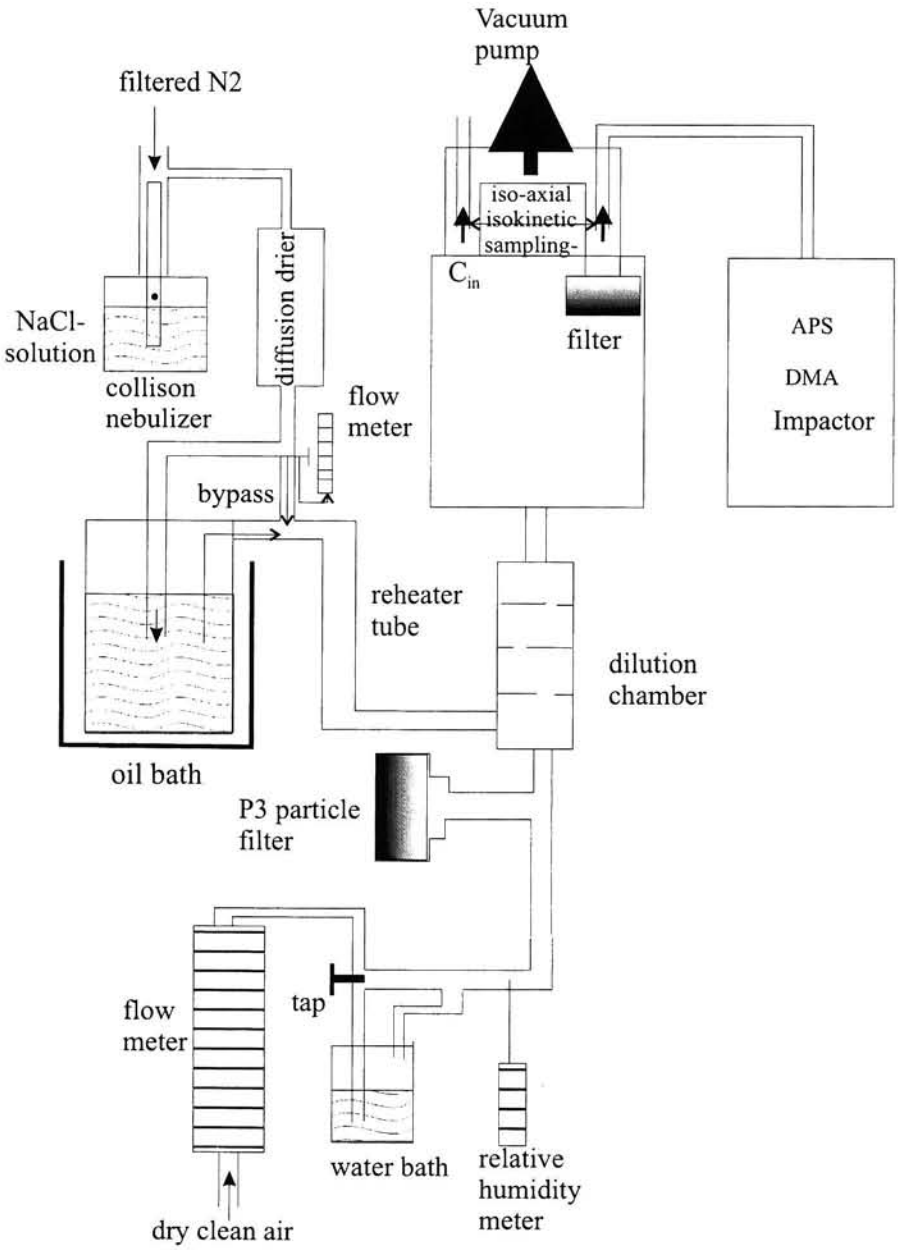

Figure 1 Schematic of the test set-up. The top left section shows the CMAG, the bottom section shows the conditioning of the mixing air.

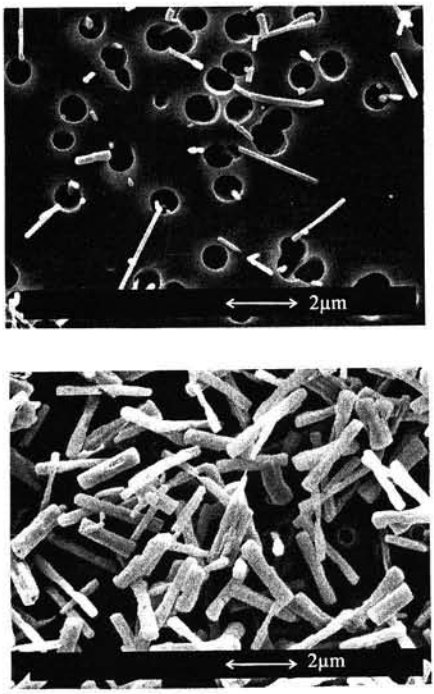

Figure 2 *Caffeine rods produced with increasing T_{ob} (a) 150 °C and (b) 175 °C, T_{RH} 210 °C, and a flow through the oil bath of 100 l/hr in both cases.*

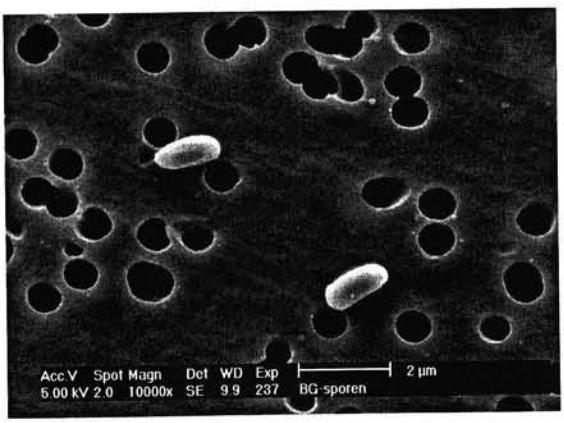

Figure 3 SEM photograph of BG spores

Filtration experiments with the DMA

Earlier we reported that in the size range between 0.2 and 0.9 μm uncharged, folded filters showed a substantially higher efficiency (by a factor of ca. 5) for the rod-shaped caffeine particles than for spherical oil particles with an equivalent size according to the DMA (Tuinman, 1998). Increasing the flow rate through the filter from 20 l/min to 30 and 40 l/min increased the penetration only marginally which is consistent with interception in a Stokes flow. The particle diameter increases with the oil bath temperature T_{ob}, but the particle length is more or less constant under all circumstances. The penetration of caffeine particles does not change significantly with particle size (figure 4) which indicates that particle length is the parameter determining the penetration. Based on these results it can be concluded that interception is probably the main capture mechanism (Brown, 1993).

The type C filter showed penetrations of ca. 12% at 250 nm and 4% at 550 nm for caffeine at 30 l/min; the penetration of PSL particles of 0.330 μm was approximately and 15 %. The type A filter showed penetrations of 2% for caffeine at both 6 l/min and 30 l/min. The penetration of PSL particles of 0.330 μm was approximately 3% at 6 l/min and 5.4 % at 30 l/min. Thus the effect of the aspect ratio on the penetration through the electrically charged filter was less than on the uncharged filters of type C and D.

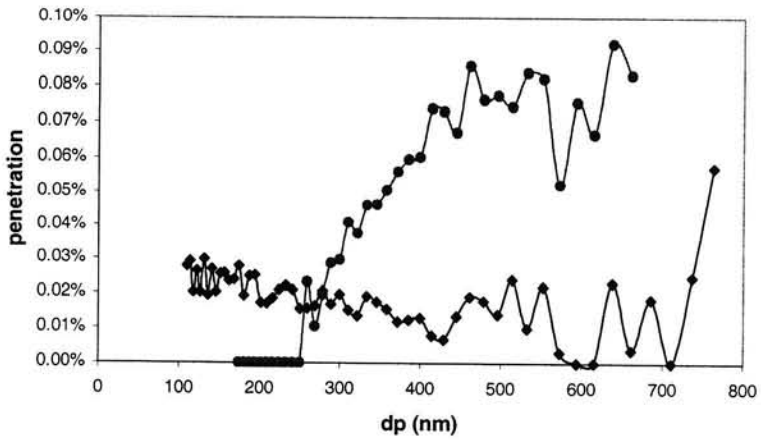

Figure 4 *Comparison of the penetration of caffeine and oil particles through a type D filter. The rod shaped caffeine particles are filtered much more efficiently than oil particles of the same DMA-diameter. C_{in} is 10^4 #/cm^3 at the mode of 0.35 μm.*

Tests with eicosanoic acid particles showed even lower penetrations than those with caffeine particles. New filters show a penetration of eicosanoic acid particles which is about 10 times lower than that of oil droplets. The particle size distribution of an eicosanoic acid aerosol generated at a T_{ob} of 160 °C shows three maxima without charge correction and two after the standard charge correction for spherical particles indicating that these clustered particles carry more charges on average.

Filtration experiments with the APS

At 175°C the larger caffeine particles reach the detection limit of the DMA, whereas the average particle size of caffeine according to the APS is approximately 0.55 μm. Caffeine particles with an aerodynamic diameter of approximately 1 μm according to the APS were produced at the following settings: T_{ob} is 205 °C, the total flow rate through the CMAG is 210 l/hr, of which 100 l/hr is led through the oil bath, and a nucleation solution of 20 mg/l NaCl is used. The penetration of these caffeine particles could be compared with those of BG-spores and oil particles or of PSL particles of the same diameter. The PSL particles are spherical (i.e. aspect ratio = 1) and the BG-spores are egg-shaped and can be considered as rods of aspect ratio 2 (0.75 μm x 1.5 μm). The caffeine particles have an aspect ratio of about 4.

Figure 5 shows the results of such a comparison for a type D filter (uncharged) at a flow rate of 30 l/min. For particles with an aerodynamic diameter of around 1 μm the aspect ratio has little influence on the penetration. This indicates that inertial impaction has become more important than interception as the capture mechanism.

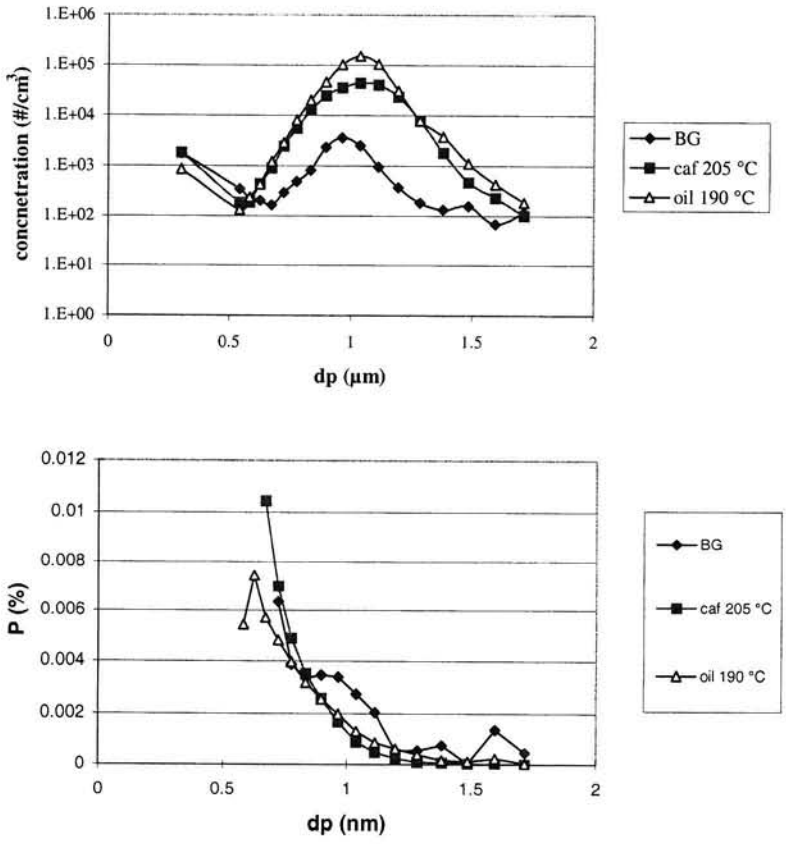

Figure 5 *The penetration of three types of particles through a type D filter with a flow of 30 l/min. The difference in aspect ratio seems to have little influence on the penetration in this size range.*

This comparison was also made for the uncharged type C filter and the two types of electrete filters (results shown in figure 6). Round pieces of flat filter cloth of 88 mm diameter were mounted on a holder and challenged with aerosol at 30 and 80 l/min. The resulting particle velocity in the flat filters is about 10 times the velocity though the folded filter.

The penetration through the type C filter decreased with increasing aspect ratio, so from PSL particles to BG-spores to caffeine. When the flow through the filter was increased the penetration increased with factors of ca. 6, 4, and 2 for caffeine, BG-spores, and PSL particles, respectively, but the penetration still decreased inversely with the aspect ratio.

When challenged with spherical particles both electret filters showed significantly higher penetration than when challenged with BG-spores, as expected. The penetration for caffeine was expected to be lower than that of BG-spores based on theory (Brown, 1993) and on experiments by Willeke et al. (1996). The results obtained with the type B electret material were as expected although there was hardly any difference between the penetration of BG-spores and caffeine at 30 l/min. The type A material, however, shows a reproducible higher penetration for caffeine than for PSL particles. To investigate if this is due to particle charging the experiments with the type A, B, and C filter were repeated with a neutralizer between the aerosol generator and the mixing chamber.

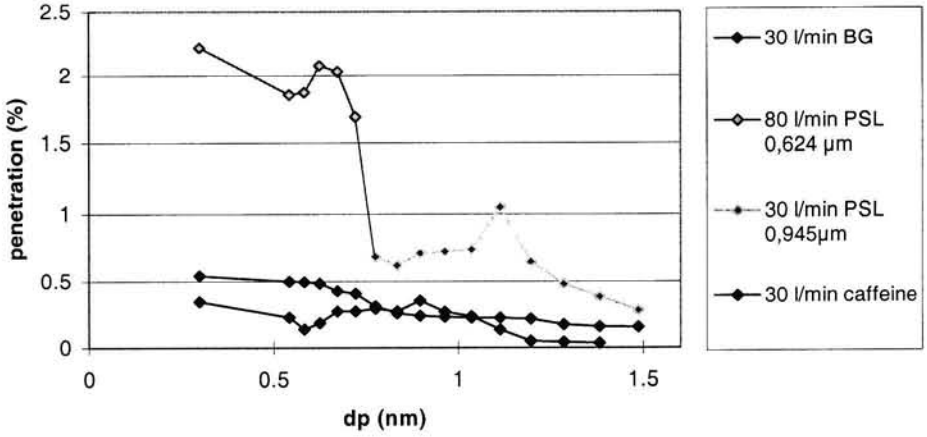

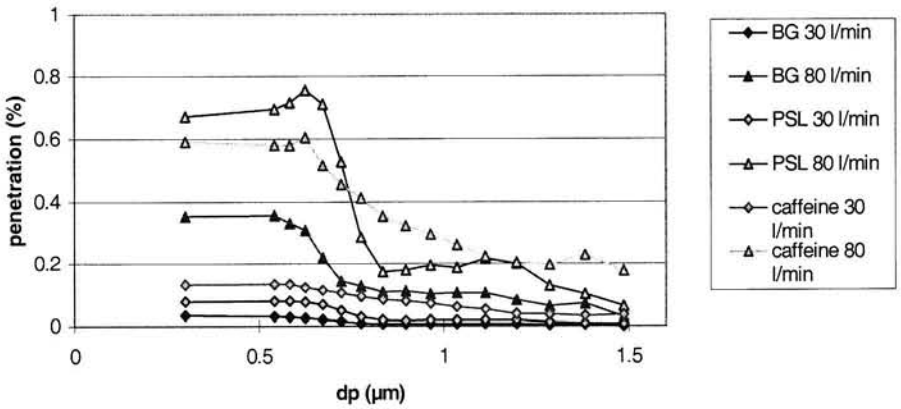

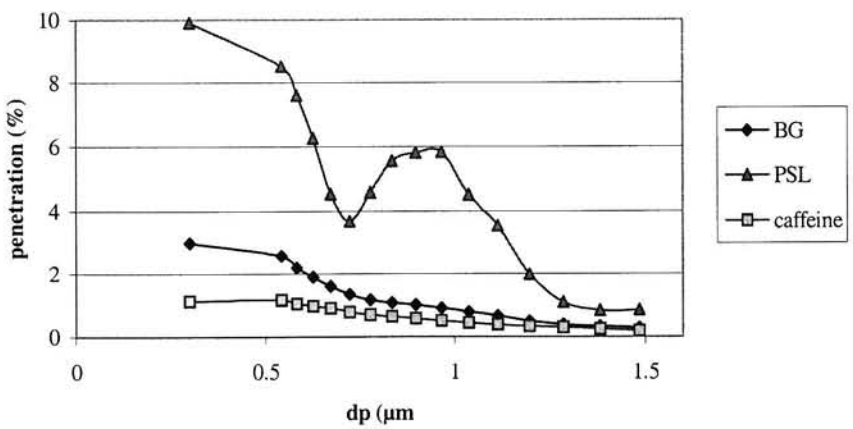

Figure 6 *The penetration of particles of different aspect ratio through type A, B, and C filters*

Generally the penetrations of BG-spores and PSL particles through the type B and C filters increased marginally when the neutralizer was used. The penetration of caffeine particles was influenced more severely, but the overall results with the type B and type C filters showed no significant change.

The penetrations of BG-spores and PSL particles through the type A filter increased more substantially when the neutralizer was inserted, whereas the penetration of the caffeine decreased slightly. The BG-spores are still filtered most efficiently, but the penetration of caffeine particles is next as is shown in figure 7. The PSL particles and BG-spores are probably charged by tribocharging by the nebulizer. The caffeine particles carry few or no charges and receive an equilibrium charge in the neutralizer. The type A electret filter is apparently most sensitive to these particle charges. The effect on the type B electret filter was expected to be similar, but the difference in fiber structure of the two filters is apparently of more influence than the charging of the filters under the experimental conditions.

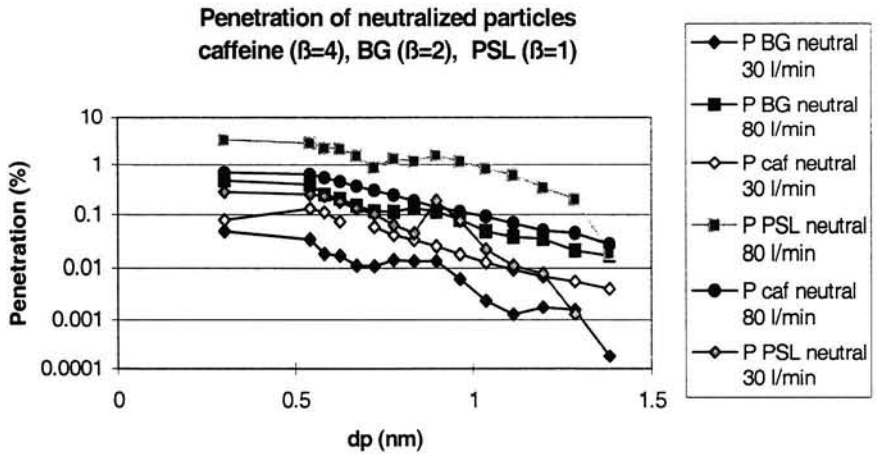

Figure 7 *The penetration of neutralized particles of different aspect ratio through type A filters.*

DISCUSSION

The challenge aerosols used for filtration experiments are more or less monodisperse, i.e. the geometric standard deviation σ_g is usually smaller than 1.25. The monodispersity of the BG-spores was shown by a SEM investigation and also by the exponential variation with depth observed for type A filters. The tail on the side of the smaller particles may be caused by fragments of broken BGspores, unremoved salt in the suspension or different alignments in the measurement section of the APS. The size distribution of the caffeine particles had a geometric standard deviation of 1.15 and was reported by Vaughan (1990) to be fairly monodisperse in both length and diameter. The PSL aerosol is a mixture of monodisperse particles of 0.505 and 0.966 µm. size.

The size distributions of the challenge aerosols must be taken into account when studying the penetration curves. For the highly monodisperse PSL aerosols this results in penetration curves consisting of two levels, one for the small and one for the larger size. The tails of the other aerosols (figure 5, top graph) enable the determination of particle size dependent penetrations over a limited size range. The size distribution of the challenge aerosols provide a relevant size range and a measure for the accuracy of the measurement. Both the DMA and the APS put the particles in channels each

representing a size class and the midpoint diameters of the channels are used to determine the points in the graphs.

The DMA was operated under conditions and with scan times (60 seconds) that enable concentration measurements of the order 1-10 #/cm^3 per channel (=size class) with such accuracy that the trend of the size dependent penetration can still be determined although large fluctuations occur. Longer scan times would yield more accurate results if clogging is insignificant.

The APS can measure concentrations of the order of 10-3 #/cm^3 per size class with scan times of 60 seconds or longer. The lower concentration limit is due to the fact that the APS sizes all penetrating particles that enter the sample flow of 1 l/min during the scan time whereas the DMA first selects a certain size class during a few seconds, counts the number of particles in that size class, and then moves on to the next. As a result, the effective scan time per size class is much shorter in the DMA than in the APS. Because of this the APS can measure lower penetrations than the DMA, but only for larger particles which usually are filtered more efficiently.

CONCLUSIONS

Four types of filters were tested experimentally with aerosols of different aspect ratios. In general the penetration through the filters decreased with increasing aspect ratio. For particles smaller than 0.5 µm this effect was more pronounced than for particles of ca. 1 µm

Particles sprayed with a nebulizer are filtered less efficiently when a neutraliser is inserted between the generator and the filter. This effect was less pronounced for the (caffeine) particles generated with a CMAG. The penetration of caffeine particles through an unchanged filter actually increased when the particles were led through a neutraliser before filtration. A likely explanation is that the caffeine particles carry a charge lower than the Boltzmann equilibrium, so they gain charge in the neutraliser instead of losing it.

REFERENCES

Brown R.C., (1993), *Air Filtration; an integrated approach to the theory and applications of fibrous filters* Pergamon Press, pp 101-106

Tuinman I.L., and Steenweg L., (1998), The influence of particle shape on the penetration through fibrous filters, *J. Aerosol Sci.* **29** Supl. 1,S1163-1164

Vaughan N.P., (1990), The generation of monodisperse fibers of caffeine, *J. Aerosol Sci.* **21**, pp. 453-462

Willeke K., Qian Y., Donnely J., Grinshpun S. and Ulevicius V., (1990), Penetration of airborne microorganisms through a surgical mask and a dust mist respirator, *Am. Ind. Hyg. Ass. J.* **57**, 348-355

	Flow l/hr	Penetration BG-spores	Penetration oil	Ratio P_{oil} / P_{BG}
Filter 1	1200	$1,4*10^{-5}$	$5,1*10^{-5}$	3,6
	1200	$1,2*10^{-5}$	$5,1*10^{-5}$	4,5
	1800	$1,4*10^{-5}$	$5,7*10^{-5}$	4,1
	1800	$1,2*10^{-5}$	$5,7*10^{-5}$	4,8
	3000	$5,0*10^{-6}$	$6,1*10^{-5}$	12,2
	4800	$4,5*10^{-6}$	$9,8*10^{-5}$	21,9
	4800	$5,1*10^{-5}$	$9,8*10^{-5}$	1,92
Filter 2	1200	$5,6*10^{-6}$	$4,1*10^{-6}$	0,73
	1800	$1,8*10^{-6}$	$6,4*10^{-6}$	3,6
	1800	$8,2*10^{-6}$	$6,4*10^{-6}$	0,78
	3000	$1,0*10^{-5}$	$9,9*10^{-6}$	1,0
	3000	$1,5*10^{-6}$	$9,9*10^{-6}$	6,6
	4800	$2,9*10^{-6}$	$1,6*10^{-5}$	5,5
	4800	$5,9*10^{-6}$	$1,6*10^{-5}$	2,7
Filter 3	1200	$6,8*10^{-7}$	$1,9*10^{-6}$	2,8
	1800	$7,9*10^{-7}$	$1,7*10^{-6}$	2,2
	3000	$1,5*10^{-6}$	$1,5*10^{-6}$	1,0
	3000	$4,2*10^{-6}$	$8,0*10^{-6}$	1,9
	4800	$6,8*10^{-6}$	$7,0*10^{-6}$	1,0
Filter 4	1200	$8,0*10^{-6}$	$5,2*10^{-6}$	0,65
	1200	$4,4*10^{-6}$	$5,2*10^{-6}$	1,2
	1800	$8,8*10^{-7}$	$6,4*10^{-6}$	7,3
	1800	$2,0*10^{-6}$	$6,4*10^{-6}$	3,2
	3000	$1,6*10^{-6}$	$6,1*10^{-6}$	3,8
	4800	$8,7*10^{-6}$	$1,1*10^{-5}$	1,3

Basic Considerations in Aerosol Charging by Ion Attachment

A. Schmidt-Ott
University of Duisburg, Institute of Combustion and Gas Dynamics, Lotharstrasse 1, D-47048 Duisburg,Germany

KEYWORDS
charging, diffusion charging, field charging; mobility analysis

INTRODUCTION

The charge state and the size of aerosol particles are of critical importance in a filtration process. Charging prior to filtration can be used to enhance filtration efficiency in some cases. In filtration research, in filter testing and quality control, techniques for measuring particle size and charge distributions upstream and downstream of the filter are required. The most powerful technique for aerosol size analysis and size classification is mobility separation in a so-called differential mobility analyzer (DMA). The particles have to be charged in an appropriate way for determining size distributions or for providing monodisperse aerosol with this device. Particles of well controlled size and charge can be provided by a dual-DMA arrangement (e.g. [1]). The present paper compiles some important features of charging techniques, primarily those based on ion attachment, and points out basic limitations. Those results for which no reference is given are presented for the first time and treated in more detail.

Various mechanisms exist, in which electric charge is transferred to aerosol particles. Mechanisms that have been studied more or less extensively and that are applied in aerosol technology are listed below:

- Ion attachment
    - Diffusion charging
        - Bipolar
        - Unipolar

- Field charging
- Plasma charging (e.g. microwave plasma, combustion, arc discharge, laser ablation plasma)
- Photoelectric charging
- Electrospray
- Triboelectic charging

Ion attachment, the most frequently used charging technique, is based on collision of particles and ions. It is referred to as diffusion charging, if the transport of ions to particles is dominated by Brownian motion of the ions. Bipolar diffusion charging, where ions of both polarities are present, leads to an equilibrium charge distribution, which is usually well defined, since it is independent of the ionization strength of the charger. The term "field charging" is used in charging with unipolar ions, if an external electric field is the driving force for ion transport to the particles. "Photoelectric charging" [1,2,3,4] refers to the effect of photoelectron emission from the particles under ultra violet radiation. This type of charging is material dependent and can thus be used to distinguish between different materials. Particles that emerge from a plasma such as a combustion flame, i.e. an environment with high concentrations of positive and negative ions and reactive molecules, are charged by ion attachment and photoemission by the plasma radiation as well as chemoionization. Usually both polarities occur. Electrostatic dispersion of liquids (electrospray) is based on droplet or jet break-up by electrostatic repulsion and produces very highly charged particles [6,7].

UNIPOLAR DIFFUSION CHARGING
A)THE EFFICIENCY LIMIT IN NANOPARTICLE CHARGING

Diffusion charging is essentially material independent and therefore often used in connection with mobility analysis. Particles a few nanometers in size are most difficult to charge, and considerable effort has been put into the development of efficient chargers for this size range. Some simple considerations below reveal that there is a basic limit to the efficiency of ion attachment in this size regime.

In unipolar diffusion charging, the aerosol is flooded with ions of one polarity. Aiming at the highest possible efficiency, a number of charger concepts have been developed. The charging efficiency is defined as

$$\varepsilon = \frac{N^+}{N_0^0} \quad , \tag{1}$$

where N^+ is the concentration of positive particles coming out of the charger, and N_0^0 is the concentration of neutral particles entering the charger, equal to the total input concentration. Defining efficiency in terms of concentrations is useful for most purposes in aerosol technology such as the connection with mobility analysis, where high concentrations of charged particles are desired.

The following simple model relevant for nanoparticle charging (Diameter D_p<20 nm) reveals the important result that electrostatic dispersion by the space charge of the ions puts an upper limit to any diffusion charging process in that it dilutes the aerosol with respect to charged particles. An aerosol batch is flooded by ions of concentration n during the time t, with no external electric field effective on the particles. The case of applying an alternating electric field as in the charger of fig. .. does not violate this assumption. The following additional assumptions are made:

1)The effective nt-product is independent of the (charged) particle concentration.

This is realistic in most charging situations, where the ion concentration is orders of magnitude higher than the particle concentration. For the same reason

2) the contribution of charged particles to space charge is negligible.

It is further assumed that

3) the particle and ion concentrations are spacially homogenious.

Since it can be shown that electrostatic dispersion does not destroy homogeneity, all concentrations can be regarded as spatially constant. Finally it is assumed that

4) all particles are initially neutral, and

5) there is no multiple charging.

The latter is valid as a consequence of the size range considered. The rate equations for ion attachment including positive ion attachment and electrostatic dispersion can then be expressed as follows.

$$\frac{dN^+}{dt} = n\beta^0 N^0 - N^+ Zn\frac{e}{\varepsilon_0} \tag{2}$$

for particles of a certain size. Here N^+ and N^0 are the concentrations of positive (or negative) and neutral particles, respectively. β^0 is the attachment coefficient for attachment of positive (or negative) ions to neutral particles, n is the ion concentration, Z is the electric particle mobility, e the elementary charge and ε_0 the permittivity of vacuum. The first term in eq. 2 is the attachment rate of ions to neutral particles, and the second one expresses dilution of the aerosol with respect to charged particles due to the space charge field of the ions. It arises from the continuity equation $dN^+/dt = -div\left(N^+\vec{v}\right)$, [8] together with the electric mobility definition $\vec{v} = Z\vec{E}$ and Maxwell's basic equation of electrostatics, $\rho = \varepsilon_0 div\vec{E}$. The charge density is set $\rho = en$ and N^+ is homogeneous in space, according to the assumptions above. The concentration of neutral particles decreases only due to ion attachment, and

$$\frac{dN^0}{dt} = -n\beta^0 N^0 \tag{3}$$

The solution of eq. 3 with $N(0) = N_0^0$ is

$$N^0(t) = N_0^0 \quad e^{-\beta^0 nt} \tag{4}$$

If $N^0(t)$ of eq. (4) is inserted in eq. (2), an analytically solvable differential equation is obtained, and the solution for $N^+(0) = 0$ is

$$\varepsilon(nt) = \frac{N^+}{N_0^0} = \frac{\beta}{\frac{Ze}{\varepsilon_0} - \beta}\left(e^{-\beta nt} - e^{-\frac{Ze}{\varepsilon_0}nt}\right) \tag{5}$$

Note that n and t do not occur separately, and the charging efficiency is a function of the charging parameter nt. Increasing the nt-product increases the number of ions attached to particles, but this is necessarily associated with dilution of the concentration of charged particles by electrostatic dispersion. Fig.1 shows ε as a function of the nt product for distinct particle diameters D_p, according to eq. (5). For $\beta^0(D_p)$ the calculation of Adachi et al.[9], who used the concept of Fuchs [10], was applied. For the ion mass 0.050 kg/mol and for the ion mobility $1.9*10^{-4}$ m²/(Vs) at normal conditions was inserted. For single charging of initially neutral particles Fuchs' approach has been shown to lead to the correct result by Filippov (1993), who carried out a rigorous calculation involving a Monte Carlo simulation. $Z(D_p)$ was calculated according to [11]. Fig.1. clearly shows that there is an optimum nt-product in diffusion charging, which depends on D_p. The value $nt=10^7$ $cm^{-3}s$ is near the optimum for all sizes in the nanometer regime. Figure 2 shows the maximum efficiency vs. The particle diameter. It reveals that 2 nm particles are at best chargeable with a 1% efficiency, and above 20 nm an efficiency close to 100% can, in principle, be attained. Assumption 5) restricts the validity of the calculation above to particle diameters below 20 nm, where double

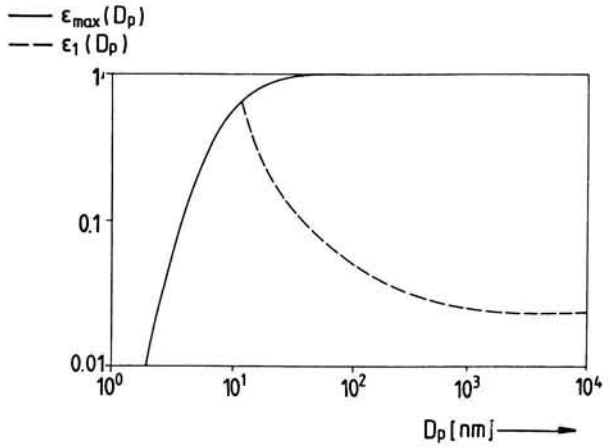

Fig. 1 *Diffusion charging efficiency ε for nanoparticles as function of the nt product.*

charging is essentially avoided by Coulomb repulsion. This restriction practically introduces no error into the solid curve in fig. .., because above 20 nm the maximum efficiency equals 1 with or without inclusion of multiple charging. Practical diffusion charging efficiencies are anticipated to usually be clearly below this limit as in the example shown below, mainly because of particle loss by diffusion to the walls. If an external electric field of non-zero mean is introduced, this further decreases the efficiency through particle loss.

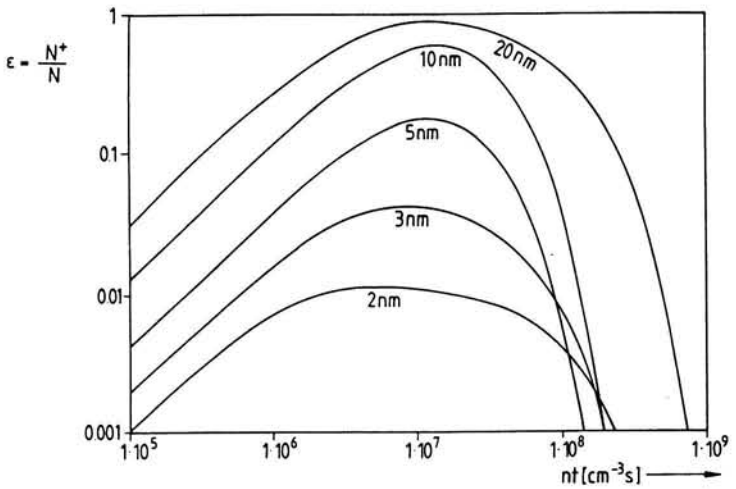

Fig. 2 *Maximum efficiency in diffusion charging ε_{max} and efficiency ε_1, when multiple charging is quenched.*

B) MULTIPLE ION ATTACHMENT IN DIFFUSION CHARGING

Ions are transported to particles by their thermal (Brownian) motion in diffusion charging. A particle already charged will only attach another ion of the same sign, if the kinetic energy of the latter is high enough to overcome the repelling Coulomb force. The higher the kinetic energy of the ions is, the higher is the charge the particles can acquire. The kinetic energies of gas molecules and ions obey the Maxwell distribution [8], according to which zero probability is reached asymptotically with rising kinetic energy, i.e. there is no maximum energy. Accordingly there is no theoretical limit to the particle charge. It will be shown below that there is a practical limit. Hinds [11] gives a useful formula approximating the mean number of elementary charges p for $nt>10^6$ $cm^{-3}s$ and 100 $nm<D_p<2000nm$:

$$p = \frac{2\pi\varepsilon_0 kT}{e^2} D_p \ln\left(1 + \frac{\bar{c}e^2}{8\varepsilon_0 kT} D_p nt\right) \tag{6}$$

where k is Boltzmann's constant, T the absolute temperature, $\bar{c}$ the mean thermal speed of the ions and e the elementary charge Fig. 3 shows the corresponding charge as function of the particle size for room temperature and $\bar{c}$ =2.4*10^{6}m/s with nt as parameter. For large nt the charge is linear with the particle diameter D_p. Since in the continuum regime the mobility is inversely proportional to D_p, the mobility essentially becomes independent of particle size in this regime for high diffusion charging, as seen in fig. 4. Thus high diffusion charging is not suitable in connection with mobility analysis. Another disadvantage concerning mobility analysis is the rather broad distribution of the charge number for a given size.

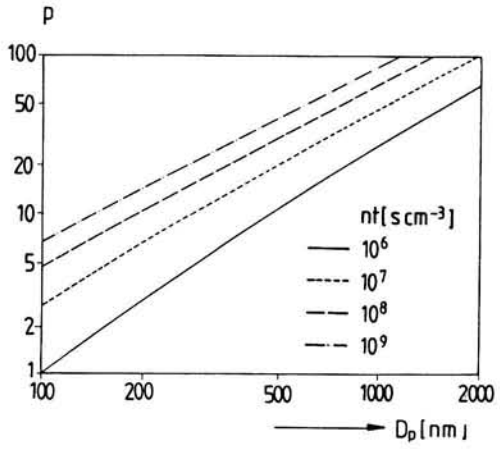

Fig. 3 *Mean charge p per particle in diffusion charging vs. particle diameter D_p (parameter: nt product)*

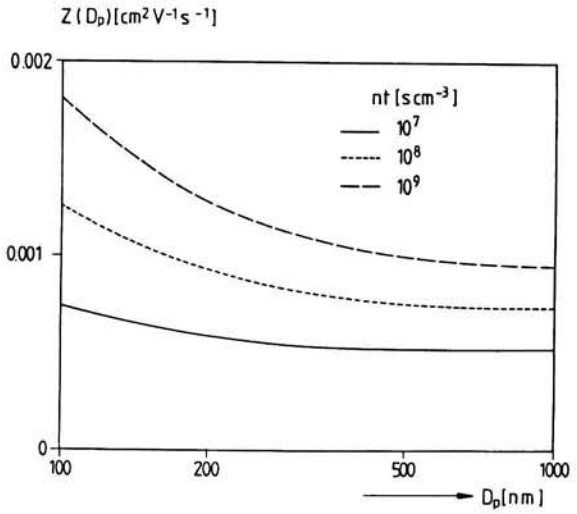

Fig. 4 *Mean mobility in diffusion charging vs. particle diameter D_p (parameter: nt product)*

Again considering dilution by the space charge of the ions, similarly as above, the particle concentration is reduced by a factor of $\frac{N^{p+}}{N_0^0}$ plotted as function of nt for different sizes in fig. 5.

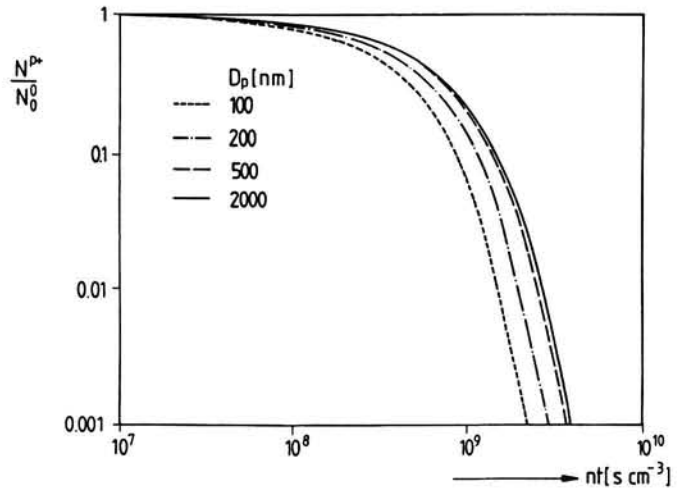

Fig.5 *Factor N^{p+}/N_0^0 by which ionic space charge reduces the particle concentration vs. nt product in diffusion charging.*

The curves show that the dilution becomes independent of D_p above 500 nm, and that nt-products exceeding 10^9 cm^{-3} s lead to very large dilutions, meaning the loss of almost all particles and revealing a *practical* upper charge limit for applications, which is approximately represented by the upper curve in fig. 4.

THE EFFICIENCY OF DIFFUSION CHARGING UNDER SUPPRESSION OF MULTIPLE CHARGING

Reducing the nt-product to a value, where multiple charging is negligible leads to the best size sensitivity of mobility. In addition, this charging mode produces a sharp size-mobility relation for all particle sizes. Multiple charging can be quenched at the cost of efficiency by limiting the nt-product such that the fraction of multiply charged particles occurring in the mobility class of interest does not exceed a certain tolerated value. The efficiency size relation is given by the dashed curve in fig. 1 for a tolerated multiply charged ratio $\frac{N^{m+}}{N^{+}}$ of 5%. This curve is derivable by completing the system of rate equations including multiple charge terms and solving numerically. It has been assumed that the size distribution is uniform.

BIPOLAR DIFFUSION CHARGING

In bipolar diffusion chargers the gas is ionized, usually by the radiation of a radioactive isotope. Molecules of the carrier gas are dissociated into an equal number of positive and negative ions. These attach to the particles and at a high enough nt-product (saturation) an equilibrium charge distribution is established on the aerosol. With the condition of saturation being fulfilled, this distribution is independent of the nt-product, in particular the ionization strength of the charger. Bipolar chargers are also referred to as neutralizers, since in gases containing electronegative molecules like oxygen in air, the mobility of positive and negative carriers is similar, and the charge frequency on particles of a certain size essentially follows a Boltzmann distribution [11] with the mean particle charge zero.

FIELD CHARGING

Field charging occurs, when a stream of ions or electrons drifts through the aerosol, driven by an electric field high enough for electrical drift to dominate over diffusional transport. Field charging is conventionally applied in electrostatic precipitators, where particles are at the same time removed from the gas stream. As a charging method providing charged particles for further analysis in the aerosol state, field charging has not yet become popular, although a study by Büscher and Schmidt-Ott [13] of 19...briefly reviewed below has shown that field charging extends the range of mobility size separation to particles above 1 μm in diameter. The following analytical expression can be given for the mean particle charge:

$$q(jt,E) = q_{\max}\frac{jt}{jt+4\varepsilon_0 E} \qquad q(jt=0)=0. \tag{7}$$

with the ion current density j, the electric field E, the permittivity of vacuum ε_0 and the saturation charge q_{max} given by

$$q_{\max} = \pi\varepsilon_0\frac{3\varepsilon}{\varepsilon+2}ED_p^{\,2} \tag{8}$$

Here D_p is the Particle diameter and ε is the particle dielectric constant. Equation (7) contains jt and E as charging parameters and is derived by a more customary expression containing nt and E instead. The latter is found e.g. in [14] and converted to the form above using $j = enZ_iE$. The advantage of eq. (7) is that the ion mobility Z_i does not enter, and that the current density j and the field are parameters directly accessible to measurement. Saturation of the particle charge arises from compensation of the external field by the particle charge field near the particle surface, avoiding impingement of more ions. Strictly speaking, field charging never occurs in a pure form, because diffusion is present in any case at T>0. Diffusional charging superimposed on field charging typically becomes significant below 1 μm, and the simple equation (7) becomes unprecise here. For particle sizes below 50 nm diffusion charging is always dominant at room temperature. This is because gas breakdown limits the external field E to approximately 10 kV/cm. During the time Δt an ion driven by this field requires to pass a particle of diameter D_p< 50 nm, diffusional displacement ($\propto \sqrt{\Delta t}$)is clearly larger than that particle diameter.

The feature of a sharply defined maximum charge (eq. (8)) leads to a well-defined charge on particles of a certain size in contrast to diffusion charging, where there is generally a broad charge distribution.

CHARGING FOR SIZE CLASSIFICATION AND ANALYSIS VIA THE ELECTRIC MOBILITY

Particles can be classified according to their electrical mobility in a differential mobility analyzer (DMA [15]). In order to determine the size distribution from the mobility distribution, charging process must be applied which establishes a well defined charge distribution on the aerosol. Bipolar diffusion chargers (neutralizers) are conventionally used for this purpose, because they deliver a constant charge distribution without calibration or control. Drawbacks of neutralizers are the restrictions that apply to radioactive material. They are applicable for size analysis, but their usefulness for classification is restricted to the size range below 50 nm. Above this size the particles acquire multiple elementary charges with significant probability, and the size mobility relationship becomes ambiguous. The range of application for classification can be extended to larger particles by using nt products below saturation, if the initial state is neutral for all particles. Another

drawback of the method is the small efficiency in the range of a few nanometers. A 10 nm particle acquires a positive or negative charge only with a 0.3% probability. Another property of neutralizers to be mentioned is the dependence of the charge distribution on the gas composition. Very significant differences occur between air and noble gases, as Wiedensohler [16] showed. The existence of an electronegative component is the most critical point, since without it electrons are the negative carriers vs. ions for the positive polarity, and the mobilities of ions and electrons are typically a factor of 10^3 apart. Thus traces of electronegative impurities in noble gases (O_2, H_2O, SO_2,...) have a large influence, and the results obtained for a noble gas with unknown concentration of these are not of any general value.

The maximum unipolar charging efficiency for nanoparticles is much higher than the equilibrium efficiency of a bipolar charger. Fig. 6 shows a charger concept, which enables comparably high efficiencies [17]. It is a modified version of the diffusion charger introduced by Liu et al. [18]. In the axis of a cylindrical arrangement a corona discharge occurs at the surface of a wire on high positive electric potential with respect to the surrounding cylinder. A fraction of the positive ions produced by the discharge are drawn through the grid section in the cylinder by an electric field. This field is produced by a voltage applied across the aerosol flow, i.e. between said cylinder and the outer one. The major modification with respect to the model of Liu el al. Is that this voltage is not constant but alternates around zero at a frequency f. This enables application of a high electric field amplitude, while the charged particles perform a zigzag motion, but are not precipitated to the walls. In each positive half wave the aerosol flow region adjacent to the grid (charging zone) is flooded by ions. The frequency is chosen such that the ions reach the outer cylinder, but the amplitude of field induced radial particle motion is small compared to the dimensions of the charging zone. Fig. 7 shows the charging efficiency as function of the size achieved with such a charger using an nt-product according to the theoretical optimum (see above) [12]. The optimum is not reached by far, and the main reason are diffusion losses.

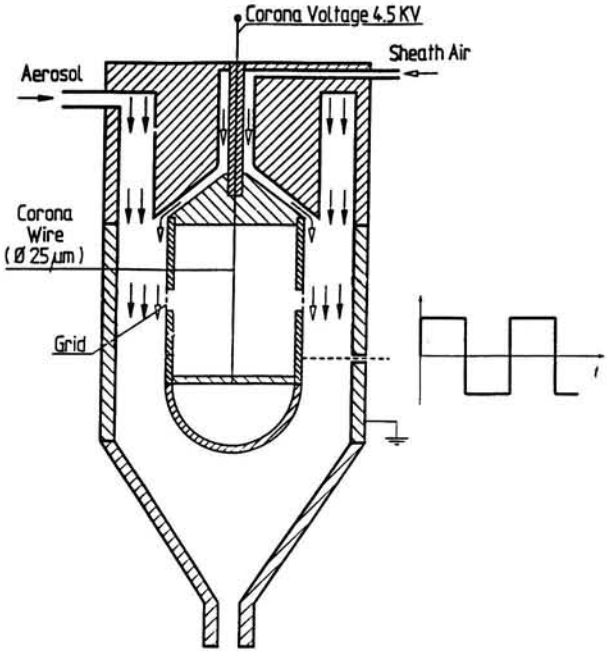

Fig. 6 *Cylindrical diffusion charger according to Büscher and Schmidt-Ott. The grid voltage is a square wave with variable frequency and amplitude.*

An apparent deficiency of the charger is that ions are present in the charging zone only during each half-wave. Other concepts, e.g. by Wiedensohler et al. [19] and by Kruis et al. [20] have tried to overcome this drawback by delivering ions from both sides of the charging zone. This increases the effective nt product, but as shown above, this does not increase efficiency, since the optimum nt product is also easily attainable with the concept of fig. 6. For a charger recently developed by Chen and Pui a charged particle fraction exceeding the maximum efficiency of fig. 2 has been reported [21]. A closer look reveals that the charged fraction is not defined according to the efficiency in eq. (1), which is based in the charged particle concentration.

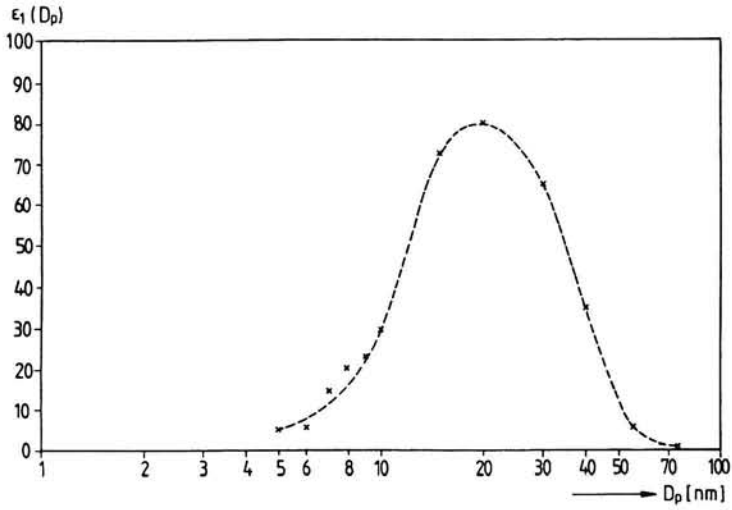

Fig. 7 *Measured single charging efficiency ε_1 (D_p) at optimum nt product with the diffusion charger of fig.6.*

For particles larger than 100 nm the main message of fig. 4 is that the mobility of large particles tends to become size independent when many elementary charges are attached. Reducing the nt-product to a value, where multiple charging is negligible leads to the best size sensitivity of mobility. In addition, this charging mode produces a sharp size-mobility relation. Below 10 nm this condition is always fulfilled even at the optimum nt-product. Multiple charging can be quenched for all particle sizes at the cost of efficiency by limiting the nt-product. In a charger DMA combination (see charger design below) the nt product can be controlled according to the size selected by the DMA [5] such that the fraction of double charges does not exceed a certain tolerated value. The size mobility relation is then given by the lower curve (single charge) in fig.2. A charger enabling control of the nt-product was introduced by Büscher and Schmidt-Ott [13] and is shown in fig. 8. The grid of the charger in fig.6 is replaced by a double grid. the ion concentration n in the charging zone can be controlled by the voltage between the grids.

Saturation field charging can be used for mobility analysis of particles above about 200 nm in size. Since the mobility for single charge, Z_1, is inversely proportional to the particle diameter in this size range, the mobility of field charged particles, $Z=Z_1 q_{max}$ rises proportional to D_p. Thus field charging enables mobility analysis for particles in the micron range. The charger concept of fig. 8 has also been applied for field charging in connection with mobility analysis by Büscher and Schmidt-Ott [13]. The charge distribution obtained above 500 nm was narrow enough to obtain a considerable size resolution comparable to optical counters.

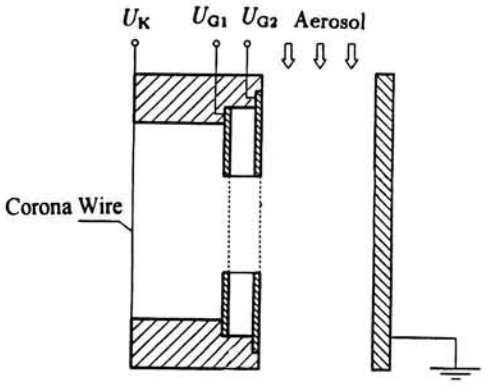

Fig.8 *Double grid modification of the charger in fig. 6. U_K is the corona voltage, U_{G1} and U_{G2} are variable grid voltages.*

REFERENCES

[1] Photoemission by Eximer Lamps, J. Aerosol Sci. 26, 1101 - 1115 (1995).

[2] Photoelectric Charging, J. Aerosol Sci. 25, S531 (1994).

[3] A. Schmidt-Ott, H.C. Siegmann, Photoelectron Emission from Small Particles Suspended in Air, Appl. Phys. Lett. 32, 710 (1978)

[4] H. Burtscher, L. Scherrer, A. Schmidt-Ott, H.C. Siegmann, Probing Aerosols by Photoelectric Charging, J. Appl. Phys. 53, 3787 (1982)

[5] P. Büscher, F. Jordan, A. Schmidt-Ott, International Pat. Application PCT WO 96/06341, Priority Date. 08/23/94

[6] D. Michelson, Electrostatic Atomization, Adam Hilger, Bristol and New York

[7] L. de Juan, J. Fernandez de la Mora, Charge and Size Distributions of Electrospray Drops, J Colloid Interface Sci. 186, 280-293 (1997)

[8] R.B. Bird, W.E. Stewart, E.N. Lightfoot, "Transport Phenomena", Wiley & Sons, N.Y., 1960

[9] M. Adachi, Y. Kousaka, K. Okuyama, "Unipolar and Bipolar Diffusion Charging of Ultrafine Aerosol Particles", J. Aerosol Sci. 16, 109-123 (1985).

[10] N.A. Fuchs, On the Stationary Charge Distribution of Aerosol Particles in a Bipolar Ionic Atmosphere, Geophys. Pura Appl. 56, 185 - 193 (1963).

[11] W.C. Hinds, "Aerosol Technology" p.45, John Wiley, N.Y., 1982.

[12] P. Büscher, Ph.D. Thesis, University of Duisburg, 1994

[13] P. Büscher, A. Schmidt-Ott, A New Compact Aerosol Charger for Unipolar Field-Diffusion Charging, J. Aerosol Sci. 23, S385-S388 (1992)

[14] R.C. Flagan, J.H. Seinfeld, Fundamentals of Air Pollution Engineering, Prentice Hall, New Jersey, 1988

[15] W. Winkelmayr, G.P. Reischl, A.O. Lindner, A. Berner, A New Electromobility Spectrometer for the Measurement of Aerosol Size Distributions in the Size Range from 1 to 1000 nm, J. Aerosol Sci. 22, 289 - 295 (1991)

[16] Wiedensohler, Die Bipolare Diffusionsaufladung von Partikeln in Chemisch Trägen Reinstgasen, Ph.D. Thesis, University of Duisburg, 1989

[17] P. Büscher, A. Schmidt-Ott, A. Wiedensohler, Performance of a Unipolar Square Wave diffusion Charger with Variable nt Product, J. Aerosol Sci. 25, 651-663 (1994)

[18] B.Y.H. Liu, D.Y.H. Pui, "On unipolar Diffusion Charging of Aerosols in the Continuum Regime", J. Colloid Interface Sci. 58, 142 - 149 (1977).

[19] A. Wiedensohler, P. Büscher, H.C. Hansson, B.G. Martinsson, F. Stratmann, G. Ferron, B. Busch, A Novel Unipolar Charger for Ultrafine Aerosol Particles with Minimal Particle Losses, J. Aerosol Sci. 25, 639-649 (1994)

[20] F.E. Kruis, F. Otten, F. Jordan, H. Fissan, A New efficient Unipolar Charger for Nanoparticles, J. Aerosol Sci. 29, S1021-1022 (1998)

[21] D.-R. Chen, D.Y.H. Pui, A Novel Charger for Nanometer Aerosols, J. Aerosol Sci. 29, S1023-S1024 (1994)

Charging of Fibers Orientated Perpendicular to the Electric Field

H. Fissan, G. Kreis, J. Dixkens, and [1]F. Schmidt
Process- and Aerosol Measurement Technology and [1]Chemical Engineering, Gerhard-Mercator-University Duisburg, Bismarckstraße 81, D-47057 Duisburg, Germany

KEYWORDS
Fibers, Field and Diffusion Charging, Orientation of fibers

ABSTRACT
In this paper a theory for fiber charging is reported. The charging rate of fibers depends on two geometrical dimensions (length and diameter) and also on the fiber orientation within the electric field. Until now fiber charging models have assumed that the fibers are orientated perpendicular to the electric field. However, fibers may be orientated in all directions. The two extremes are perpendicular and parallel to the direction of the electric field. A new model has been developed which allows us to calculate the charging rate as a function of time for the case where the fiber axis is perpendicular to the applied electric field. From a practical point of view the interesting information is the charge level n as a function of length L_f of the fiber. Experiments have been performed with fibers with the following properties:
The fiber material was non-conductive glass. These glass fibers (B06, Lauschaer Glaswerke, Germany) have an average fiber diameter of $D_f = 0.6\mu m$, a standard deviation in diameter of $\sigma_D = 1.3$ and a relative dielectricity constant of $\varepsilon_r = 6.5$. To check the new model comparisons with existing fiber charging theories as well as experimental investigations were performed.

INTRODUCTION
Airborne fibers are present in the environment at low concentrations. In some regions they are of natural origin, but often their occurrence is connected with production and application in the building trade. For about 100 years asbestos containing materials were widely used in constructions because of their properties: flame retardancy, thermal insulation, and sound absorption. Several investigations proved that substantial amounts of respirable fibers can be released into indoor and outdoor atmospheres due to vibrations, air movement or mechanical stress. The dangerous potential of these fibers is dependent on the number concentration and the geometric dimensions (length and diameter) of the fibers and less on the chemical composition. Due to the high hazard potential it is necessary to determine the number concentration of the inhaleable fibers. An inhaleable fiber is understood to be any object having a length of $5\mu m < L_F < 100\mu m$, a diameter of $D_F < 3\mu m$ and a length/diameter ratio $L_F/D_F > 3/1$.
For sample preparation analysis instruments are used in which electrically charged fibers are deposited on substrates using electric forces. A commercially available on-line measurement system is the portable fiber monitor RFM 90 (Turnkey Instruments, London [6]). The fibrous aerosol is sucked into a chamber where the fibers are charged unipolarly with a corona charger. These fibers are aligned in the flow direction and deposited onto a glass slide by an electrostatic field. Another well-established technique uses the Scanning Electron Microscope (SEM) to determine the number of fibers deposited on a nuclepore filter (Guideline VDI 4300 Part 1 [9] and VDI 3861 Part 2 [10]). A faster and cheaper off-line fiber analysis is based on

the Dark Field Microscopy (DFM) method, which has been investigated by Schmidt et al [7]. The fibers are charged unipolarly and deposited within an Electrostatic Precipitator (ESP) (Dixkens et al. [2]) on a flat wafer. Since it is important to avoid background scattering from the surface for DFM, a smooth surface is necessary.

Unipolarly charged fibers, monodisperse with respect to the diameter, can be classified according to length in the electric field of a Differential Mobility Analyzer (DMA) (Chen et al. [1]). To investigate the performance of these deposition and classification processes the charge level of fibers charged in a corona discharge has to be known. Up to now in theoretical and experimental investigations the arrangement of fibers was, or was assumed to be, perpendicular with respect to the direction of the electric field. In cases where there is a long residence time in the electric field, this may be doubted. Fibers may align in the direction of the electric field. In this paper we investigate a charging model considering fibers oriented perpendicular to the electric field. The model is based on the three region charging model for spherical particles developed by Smith and McDonald [8]. In a follow up paper [5] we extend the model to fibers orientated parallel to the electric field.

FIBER CHARGING THEORY

The unipolar charging of particles can be separated in two physical mechanisms. Diffusion charging where free ions are transported to the particle surface by Brownian diffusion, and field charging where free ions follow electrostatic field lines which are ending on a particle. Zebel et al. [11] studied the unipolar diffusion charging of fibers in the continuum regime. Their model allows us to calculate the diffusion charging rate of endless fibers. Han and Gentry [3][4] developed a two region model which allows us to calculate combined diffusion and field charging for fibers orientated perpendicular to the electrical field. These models neglect the surfaces at both ends of the fibers.

Cheng et al. [1] showed that fibers will align in the electric field direction if they remain long enough within the field. The case of fibers orientated parallel to the electrical field was not investigated in the literature. For the case that the fiber axis is not perfectly perpendicular to the electric field lines Han and Gentry give a correction factor [4]. However, this solution will not work if the fiber is orientated in the field direction because the face areas of the fibers are neglected.

A new charging model was developed to calculate the charging rate for two extreme fiber orientations (fiber length axis is orientated perpendicular or parallel to the applied electric field). The model described here calculates the charging rate as a function of charging time for fibers oriented perpendicular to the electric field.

In the developed model we assume that the fibers are cylindrical, straight and the fiber material is homogenous. The applied electric field and the ion concentration are homogenous a certain distance from the fiber.

In analogy to the field and diffusion charging theory for spherical particles developed by Smith and McDonald [8], the cylindrical fibers are separated in three regions which are characterised by different ion transport mechanisms to the fiber surface. This theory uses an analytical solution for the resulting electric field which simplifies the calculation.

The case of fibers orientated perpendicular to the electric field (this means in flow direction, see Figure 1) is similar to the well known case of spherical particle charging.

In the case of fibers orientated perpendicular to the E-field the end surfaces can be neglected because the fibers are long. In the first region the ions are transported to the fiber surface due to the applied electric field. This is the zone where only field charging is important because

the electric field lines reach the surface. In region II the field lines bend to the surface but they do not end on the particle and therefore the ions are only transported towards the surface due to the electrostatic field. The ion-transport to the actual surface is caused by diffusion which is reinforced by the electric field. In region III the ion transport is due to diffusion. Analogous to the theory of Smith and McDonald [8] the following theory is derived for cylinders in a

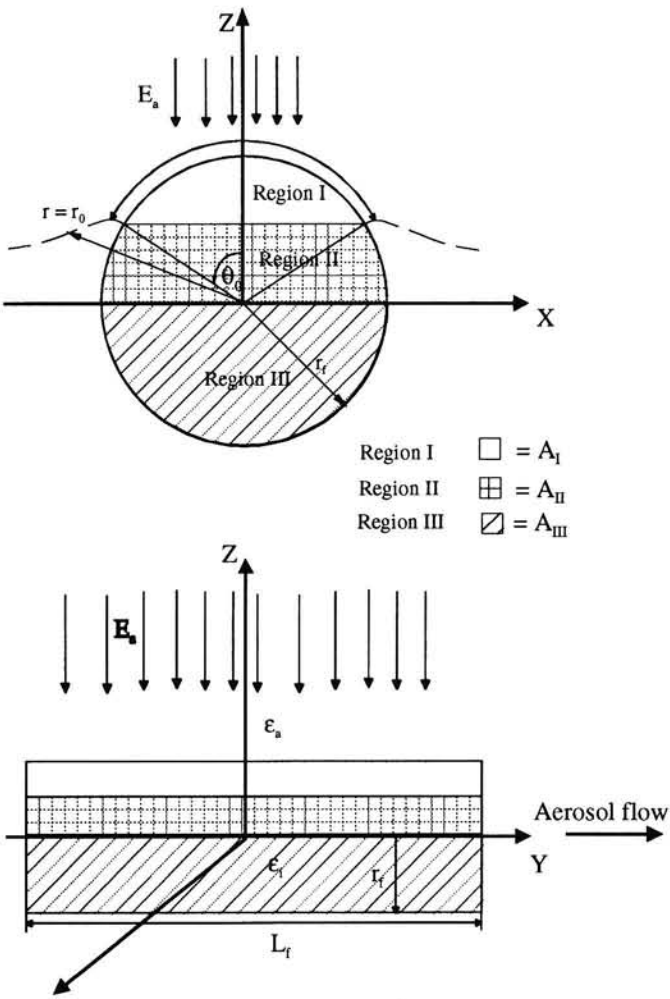

Fig. 1: Three region charging theory for fibers orientated perpendicular to the electrical field

uniform external electrostatic field. The electric field strength E_r near the fiber surface can be described as:

$$E_r = -\text{grad}(\varphi_a + \varphi_g) = -\frac{\partial}{\partial r}(\varphi_a + \varphi_g) \qquad (1)$$

φ_a is the potential of the fiber dipole which is influenced by the applied electrostatic field E_a and φ_g is the counter potential which is caused by the fiber charge. φ_a depends on the applied electrostatic field and the polarisation p_z.

$$\varphi_a = \left(E_a \cdot r - \frac{\vec{p}_z \cdot \vec{r}}{4 \cdot \pi \cdot \varepsilon_a \cdot r^2} \right) \cdot \cos(\theta) \tag{2}$$

Using a proportionality factor β' the dipole moment $p_z \cdot r$ can be written as:

$$\vec{p}_z \cdot \vec{r} = p_z \cdot r = \beta' \cdot E_a \cdot r \tag{3}$$

From this it follows that

$$\varphi_a = \left(E_a \cdot r - \frac{\beta}{r^2} \cdot E_a \cdot r \right) \cdot \cos(\theta) \tag{4}$$

with

$$\beta = \frac{\beta'}{4 \cdot \pi \cdot \varepsilon_a}$$

Since the inner and outer electric potentials are equal at the fiber surface then, $r=r_f$ and the dielectric strength of the inner and outer potentials at the fiber surface are also equal, this leads to the final expression for the proportional factor β.

$$\beta = r_f^2 \cdot \frac{\varepsilon_i - \varepsilon_a}{\varepsilon_a + \varepsilon_i} \tag{5}$$

The counter potential is dependent on the number of charges n on the fiber and can be described as:

$$\varphi_g = -\frac{n \cdot e}{2 \cdot \pi \cdot \varepsilon_0 \cdot L_f} \cdot \ln(r) \tag{6}$$

The counter potential is proportional to the number of charges and decreases the ion transport to the surface with increasing charge level.

Using equations (4), (5) and (6) the electrical field strength E_r near the fiber surface is found.

$$E_r = -\text{grad}(\varphi_a + \varphi_g) = -E_a \cdot \left(1 + \frac{r_f^2}{r^2} \cdot \frac{\varepsilon_i - \varepsilon_a}{\varepsilon_a + \varepsilon_i} \right) \cdot \cos(\theta) + \frac{n \cdot e}{2 \cdot \pi \cdot \varepsilon_0 \cdot L_f} \cdot \frac{1}{r} \tag{7}$$

E_r : radial component of electric field (V/m)
E_a : external field (V/m)
ε_i : fiber dielectric constant
ε_a : dielectric constant of the surrounding gas
r_f : fiber radius (m)
L_f : fiber length (m)

This equation is valid for fibers consisting of non-conductive material.

If equation (7) is set to zero a charge dependent radius r_0, where the counter electrostatic field is equal to the applied electrostatic field, can be determined:

$$r_0^2 + \left(\frac{n \cdot e}{2 \cdot \pi \cdot \varepsilon_0 \cdot E_a \cdot \cos(\theta) \cdot L_f} \right) \cdot r_0 - \frac{\varepsilon_i - \varepsilon_a}{\varepsilon_i + \varepsilon_a} \cdot r_f^2 = 0 \tag{8}$$

The point r_0 where the radial component of the electrostatic field (Eq. 7) must be zero can be calculated for each charge reaching the fiber surface.

If the counter field strength is equal to the dipole field strength the fiber achieves its saturation charge. No field lines end on the fiber surface, θ_0 equals zero and region I vanishes.

The saturation charge n_s can be determined if $n = n_s$, $r = r_f$, and no radial component E_r exists (E_r=0, Eq. 7).

$$n_s = \frac{2 \cdot \pi \cdot \varepsilon_0 \cdot E_a}{e} \cdot \left(1 + \frac{\varepsilon_i - \varepsilon_a}{\varepsilon_a + \varepsilon_i}\right) \cdot L_f \cdot r_f \tag{9}$$

With the knowledge of the saturation charge a charge dependent angel θ_0 which defines region I can be determined:

$$\theta_0 = \arccos\left(\frac{n}{n_s}\right) \tag{10}$$

The areas of regions I and II depend on the charge level of the fiber. Each charge on the fiber causes an electric field which reduces the applied homogeneous electrostatic field E_a. The dashed line $r = r_0$ in Figure 1 shows where the radial component of the electrostatic field E_r is zero. The point of intersection between the dashed line and the fiber surface is described by the angle θ_0 which can be between $0 \le \theta_0 \le \pi/2$. With increasing number of charges on the fiber the angle θ_0 decreases to zero where the charge number is equal to the saturation charge n_s. Region I is between $0 \le \theta \le \theta_0$, region II is between $\theta_0 \le \theta \le \pi/2$ and region III is between $\pi/2 \le \theta \le \pi$.

Our approach is to estimate the probability that ions reach the fiber surface in the three regions and to describe the charging rate dq/dt. The ion concentration near the particle surface N_s (E_a, r_f, θ) can be related to the undisturbed ion concentration N_0.

$$N_s(E_a, r_f, \theta) = N_0 \cdot e^{\frac{\Delta V(E_a, r_f, \theta)}{k \cdot T}} \tag{11}$$

ΔV (E_a,r_f, θ) is the energy difference between the fiber surface and a large distance (r=r') where the average ion distribution is undisturbed. To move an ion from one point in space (r=r') to the fiber surface an energy difference of

$$\Delta V(E_a, r_f, \theta) = \int_{r'}^{r_f} \vec{F} \cdot d\vec{r} = \int_{r'}^{r_f} e \cdot E_r \cdot dr \tag{12}$$

$$\Delta V(E_a, r_f, \theta) = -e \cdot E_a \cdot \cos(\theta) \cdot \left[\frac{r_f \cdot r' \cdot (2 \cdot \varepsilon_a) - r'^2 \cdot (\varepsilon_a + \varepsilon_i) + r_f^2 \cdot (\varepsilon_i - \varepsilon_a)}{r' \cdot (\varepsilon_a + \varepsilon_i)}\right] + \frac{n \cdot e^2}{2 \cdot \pi \cdot \varepsilon_0 \cdot L_f} \cdot \ln\left(\frac{r_f}{r'}\right) \tag{13}$$

must be overcome. With Eq. 11 the ion concentration becomes:

$$N_s(E_a, r_f, \theta) = N_0 \cdot \exp\left[-\left\{\frac{\left[2 \cdot \varepsilon_a \cdot r_f \cdot r' - r'^2 \cdot (\varepsilon_i + \varepsilon_a) + r_f^2 \cdot (\varepsilon_i - \varepsilon_a)\right] \cdot e \cdot E_a \cdot \cos(\theta)}{k \cdot T \cdot r' \cdot (\varepsilon_i + \varepsilon_a)} + \frac{n \cdot e^2}{2 \cdot \pi \cdot \varepsilon_0 \cdot k \cdot T \cdot L_f} \cdot \ln\left(\frac{r'}{r_f}\right)\right\}\right] \tag{14}$$

$$= N_0 \cdot \exp\left[-\{K1 \cdot \cos(\theta) + K2\}\right]$$

$K1$ and $K2$ are abbreviations in equation 14 for parts which are independent of angle θ.

The charging rate is the sum of the rates in each of the three regions under the assumption that the system is in equilibrium and charging can be approximated by a series of steady states.

$$e \cdot \frac{dn}{dt} = \left(\frac{dq}{dt}\right) \Rightarrow \left(\frac{dq}{dt}\right)_I + \left(\frac{dq}{dt}\right)_{II} + \left(\frac{dq}{dt}\right)_{III} \tag{15}$$

Region I

The charging rate is limited to the ion transport rate from outside into the system by the applied extern field. It and can be described as the product of current density and the surface area A_I of region I. The ratio L_F/D_F is always larger than 3 so the ratio of the curved area of the fiber compared with the area of the end faces is greater than 12. Consequently Eq. 15 is solved under the assumption that the flat front and end planes of the fiber can be neglected.

$$\left(\frac{dq}{dt}\right)_I = -\int_{A_I} \bar{j} \cdot dA_I = -Z \cdot e \cdot N_0 \int_{A_I} E_r \cdot dA_I = -2 \cdot Z \cdot e \cdot N_0 \cdot \int_0^{\theta_0} E_r\big|_{r=r_f} \cdot r_f \cdot L_f \cdot d\theta$$

(16)

This leads to the charging rate in region I.

$$\left(\frac{dq}{dt}\right)_I = \frac{Z \cdot e^2 \cdot N_0}{\pi \cdot \varepsilon_0} \cdot [n_s \cdot \sin(\theta_0) - n \cdot \theta_0] \tag{17}$$

(where Z is the ion mobility, e is the electric charge and A is the surface area of the region)

Region II

The charging rate in this region is caused by ion diffusion which is enhanced by the presence of the applied electrical field.

$$\left(\frac{dq}{dt}\right)_{II} = \frac{e \cdot \bar{v}}{4} \cdot \int_{A_{II}} N_s \cdot dA_{II} = \frac{e \cdot \bar{v}}{2} \cdot \int_{\theta_0}^{\pi/2} N_s \cdot L_f \cdot r_f \cdot d\theta \tag{18}$$

(where v is the mean thermal speed of the ions at T=293K; v=240m/s)

Integration of Eq. 18 leads to the charging rate in region II and can be described by the following equation.

$$\left(\frac{dq}{dt}\right)_{II,FI} = \frac{e \cdot \bar{v}}{2} \cdot N_0 \cdot L_f \cdot r_f \cdot [\exp(-K1) - \exp(-K1 - K2 \cdot \cos(\theta_0))] \tag{19}$$

(where K1 and K2 are substitutes in Eq. 14)

Region III

The external electric field and the counter field caused by the fiber charge are in the same direction and there is no point for which the radial component E_r is zero. In region III the effect of the applied field is negligible and the classical diffusion equation for fibers developed by Zebel [11] is used. The ion flux $\dot{N}_f$ to the fiber can be expressed as:

$$\dot{N}_f = 2 \cdot \pi \cdot D_{ion} \cdot N_a \cdot \frac{\frac{2 \cdot J \cdot e}{k \cdot T}}{1 - \left(\frac{r_f}{r_a}\right)^{\frac{2 \cdot J \cdot e}{k \cdot T}}} \tag{20}$$

D_{ion} : diffusion ion coefficient

N_a : ion concentration at any point r_a outside of the fiber ($1/m^{-3}$)

J : charge

If the elementary charge e is uniformly distributed over the fiber a charge number p_f per unit length can be defined.

$$p_f = \frac{2 \cdot J \cdot e}{k \cdot T} = \frac{2 \cdot n_f \cdot e^2}{k \cdot T} = 2 \cdot n_f \cdot d_e \tag{21}$$

(where d_e is the distance between two elementary charges at T=290K, (m))
The value of the fiber charge n_f follows from p_f and can be calculated by using the charging time t_0.

$$t_0 = \int_{n=0}^{n=n_f} \frac{dt}{dn} dn' = \int \frac{1}{\dot{N}_f} dn' = \frac{k \cdot T}{4 \cdot p \cdot e^2 \cdot D_{ion} \cdot N_a} \cdot \int_{p=0}^{p=p_f} \frac{e^{p \cdot \ln\left(\frac{r_a}{r_f}\right)} - 1}{p} dp$$

$$= \frac{1}{4 \cdot p \cdot d_e \cdot D_{ion} \cdot N_a} \cdot \int_{p=1}^{p=p_f} \frac{e^{p \cdot \ln\left(\frac{r_a}{r_f}\right)}}{p} dp \qquad (22)$$

This equation is valid in the range $r_f \leq r_a \leq 10\ r_f$, $r_a/r_f >> 1$ and $r_a/r_f << L_f$.
The final equations (Eq. 17, 19, 22) to describe the time dependent charging rate are solved using a class 5 Runge-Kutta method.

VERIFICATION

1 Comparison with literature data

The model was compared with theoretical results from Han and Gentry [4] and Zebel [11].
In order to calculate diffusion charging of fibers Zebel [11] estimated that his theory is valid between $1 < r_a/r_f \leq 10$ and $r_a/r_f << L_f$. r_a is a distance from the fiber where the ion concentration is undisturbed. Zebel did not mention the ratio explicitly. So we varied the ratio

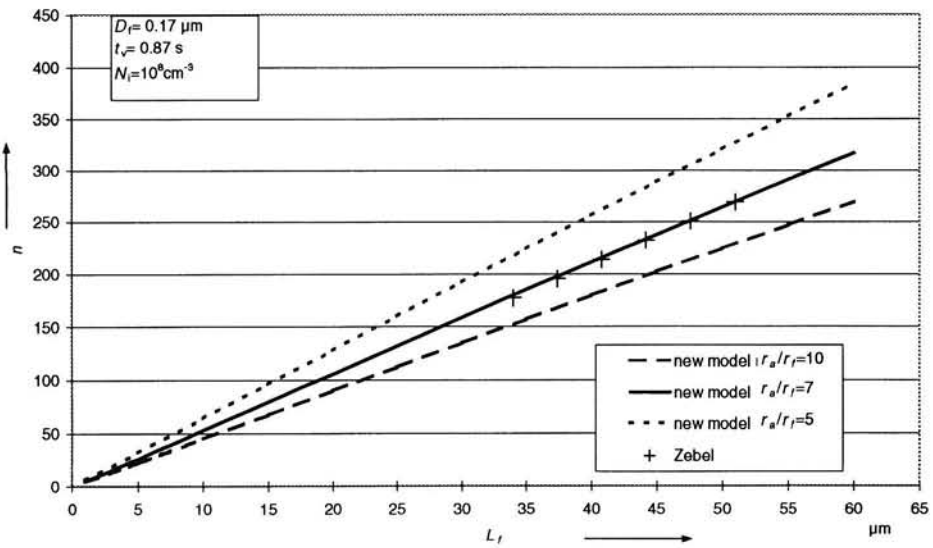

Fig. 2: Diffusion charging of fibers

r_a/r_f and compared our results with the results Zebel [11] published. This investigation indicates that our model will show the same results if the ratio equals $r_a/r_f = 7$ (Figure 2)

Han and Gentry [4] developed a two region model which permits calculation of combined diffusion and field charging for fibers orientated perpendicular to the electrical field as a function of a dimensionless time which includes the integral $N{\cdot}t$-product. The first region is analogous to the regions I and II in our model (field and diffusion charging) and the second region equals region III (only diffusion charging). Using the determined ratio $r_a/r_f = 7$ the combined diffusion and field charging of fibers ($L_f = 10\mu m$, $D_f = 0.4\mu m$) was calculated as a function of charging time and compared with results from Han and Gentry [4]. (Figure 3).

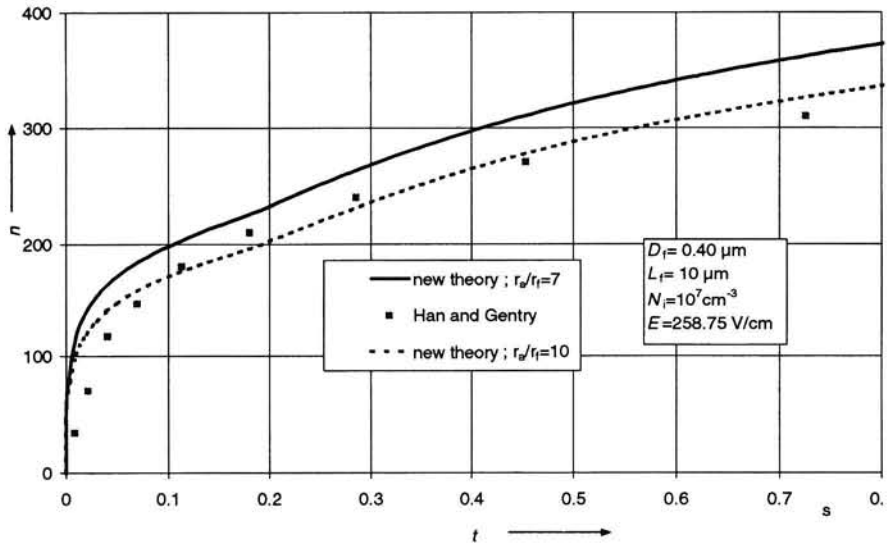

Fig. 3: Field and diffusion charging of fibers orientated perpendicular to the electric field (model developed by Han and Gentry [4] and new theory)

In contrast to Han and Gentry's model the charging time and the ion concentration are regarded as single parameters. The time dependency of the charging rate is thus described in more detail and as a result the new model predicts a faster charging rate than Han and Gentry's model [4] in the first fifty milliseconds. The ion transport to the fiber surface is less if determined with the integral $N{\cdot}t$-product because the flux to the fiber surface is not linear in a time interval but varies exponentially, as in charging a condenser. After a charging time of about $t = 0.05$s the slope of the two functions are nearly the same but there is still a difference between the two models. This leads to the supposition that Han and Gentry may have used a different ratio of r_a/r_f. Using a ratio of $r_a/r_f = 10$ the theoretical results are in a good agreement for a charging time $t > 0.1$s.

2 Experimental investigations

In this section the results of an experimental investigation of fiber charging are introduced. The charging rate was measured as a function of fiber length and compared with the model.

The fibers orientate in direction of the electrical field if the charging time is sufficiently long. Due to the fact that in most chargers particles remain a long time in the electrical field there is a need for a charging model for fibers orientated in the field direction. Only if the charging time is very short will fibers stay aligned in the flow direction, perpendicular to the electrical field.

To check this an experiment with a simple point-to-plate charger was performed. This charger has a charging zone of l_{ch} = 2mm in length and a diameter of D = 6mm. A voltage of U = 5000V and a corona current of i = 5µA was applied at the corona needle. The electrical field in this charger is not homogeneous. The flow rate through the charger was 0.3 l/min. This means that the fibers stay t = 0.0113s in the charging zone. The ion concentration is N = 6.24 $10^6 cm^{-3}$. The experimental set-up used to produce the fibers and to determine the number of charges n as a function of the fiberlength L_f is described in detail in [5]. Figure 4 shows the results of this experiment.

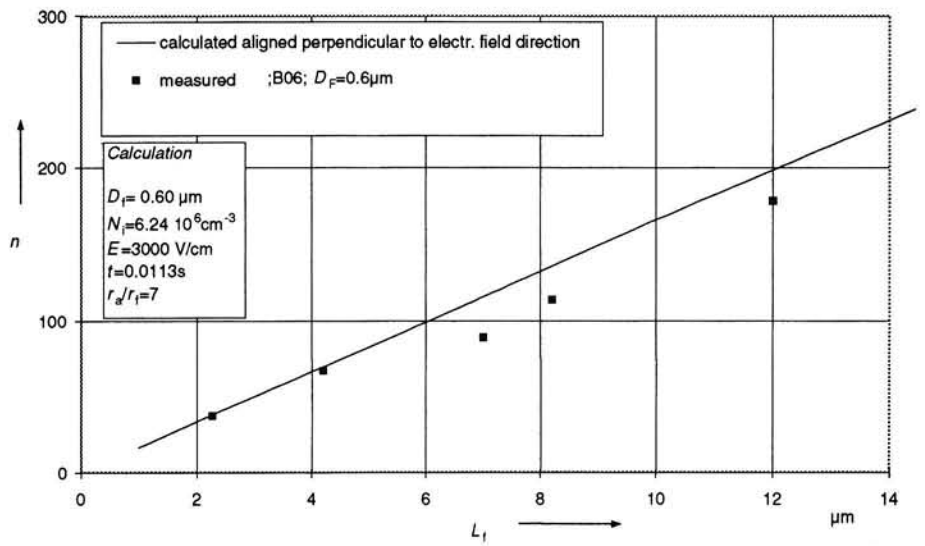

Fig. 4: Average number of charges in dependence of the average fiber length for a charging time of t *=0.0113s measured with a simple point-to-plate charger*

The fibers are mainly orientated perpendicular to the electrical field. This means that most fibers are aligned in the flow direction during the charging process because the charging time is too short to let them change direction.

CONCLUSIONS

We have developed a model to calculate the diffusion and field charging for fibrous particles. This model allows us to calculate the charging rate of fibers which are perpendicular to the field. The model is based on three regions where field charging and diffusion charging occur. The charging rate is not a linear function of charging time so the usual integral $N \cdot t$-product is not included. The number of charges is determined directly as a function of charging time. Comparisons between the results from Han and Gentry [4] and the new model show that the charging rate will be higher if the charging time is considered directly. To check the model experimentally we charged a fibrous aerosol which was nearly monodisperse with respect to diameter but polydisperse with respect to length and separated these fibers with a DMA according to length. After that the charge number was determined as a function of length. The investigations show that the three region charging model is a useful tool to calculate the charging rate of fibers for a combination of diffusion and field charging.

ACKNOWLEDGEMENTS

This work was supported by the Deutsche Forschungsgemeinschaft (DFG).

NOMENCLATURE

Symbol	Dimension	Definition
A_I	m^2	Area of region I
A_{II}	m^2	Area of region II
A_{III}	m^2	Area of region III
C_c	-	Cunningham- correction factor
d_e	m	Distance of 2 elementary charges
D_f	m	Fiber diameter
D_{ion}	$m^2\ s^{-1}$	Diffusions coefficient of ions
$\vec{E}$	$V\ m^{-1}$	Electrical field strength
E_a	$V\ m^{-1}$	applied electrical field strength
Eg	$V\ m^{-1}$	counter electrical field strength
J	C	Charge
$K1$	-	Variable
$K2$	-	Variable
L_f	m	Fiber length
n	-	Charge number
n_s	-	Saturation charge
N	m^{-3}	Ion number concentration
N_a	m^{-3}	Ion number concentration at $r = r_a$
N_S	m^{-3}	Ion number concentration in the vicinity of the fiber surface
N_0	m^{-3}	Undisturbed ion number concentration
$\dot{N}$	s^{-1}	Ion flow rate
p_f		Charge concentration
q	C	Electrical charge
r	m	Radius
r_a	m	Any radius larger than fiber radius
r_f	m	Fiber radius
r_0	m	Radius

r'	m	Radius larger than fiber radius
t	s	Time
t_0	s	Charging time t
T	K	Temperature
U_{DMA}	V	DMA-Voltage
$\bar{v}$	m s^{-1}	average thermal ion velocity
V	J	Potential energy
ΔV	J	Energy difference
x	-	Variable
y	-	Variable
z	-	Variable
z_0	m	Distance from the x-axis
Z	m^2 V^{-1} s^{-1}	Ion mobility
ε_a	-	Dielectricity constant outside of the fiber
ε_i	-	Dielectricity constant in the fiber
φ_a	V	Electrical potential outside of the fiber
φ_g	V	Counter electrical potential
θ	rad	Angel
θ_0	rad	Angel

Indices

f	Fibers
=	in field direction orientated fibers
I	Region I
II	Region II
III	Region III

Constants

e	Elementary charge constant	$1{,}602 \cdot 10^{-19}$ As
k	Boltzmann constant	$1{,}3806 \cdot 10^{-23}$ $AVsK^{-1}$
T_S	Sutherland constant	110,4 K
ε_0	Electrical field constant	$8{,}8542 \cdot 10^{-12}$ $AsV^{-1}m^{-1}$
π		3,1415 ...

LITERATURE

[1] Chen, B. T.; Yeh, H. C.; Johnson, N. F. (1996) Design and use of a Virtual Impactor and an Electrical Classifier for Generation of Test Fiber Aerosol with Narrow Size Distribution, *J. Aersol Sci.*, Vol. 12, No. 1, pp 83-94

[2] Dixkens, J.; Fissan, H. (1997) Design of a Sampling System for Off-Line Particle Analysis of Fine Solid Particles, pp. 214-222, ISBN 3-8265-3050-0, Shaker Verlag

[3] Han, R. J.; Gentry, J. W. (1993) Unipolar Diffusional Charging of Fibrous Aerosols-Theory and Experiment, *J. Aerosol Sci.*, **24**, 211-226

[4] Han, R. J.; Gentry, J. W. (1993) Field and Combined Diffusional and Field Charging of fibrous Aerosols, *Aerosol Sci. and Technol.*, **18**, 165-179

[5] Kreis, G.; Dixkens, J.; Fissan, H.; Schmidt, Charging of Fibers Oriented Parallel to the Electrical Field, Submitted to *J. Aerosol Sci.*

[6] Rood, A.P.; Walker E.J. and Moore D. (1992) Construction of a portable fibre monitor measuring differential light scattering for aligned fibers. *Aerosol Sci. Technol.* **17** ,Nr. 1-8

[7] Schmidt F., Dixkens J., Fissan H. (1998) Measurement of Fibrous Particles Using Dark Field Microscop, *Partec 98*, Preprints II, pp. 685-694, ISBN 3-9211590-53-1

[8] Smith, W. B.; McDonald, J.R. (1976) Development of a Theory for the Charging of Particles by Unipolar Ions, *J. Aerosol Sci.*, **7**, 151-166

[9] VDI 4300 /1 (1995) Indoor-air Pollution Measurement; General Aspects of Measurement Strategy, *VDI-Handbuch Reinhaltung der Luft* Band 5; Beuth Verlag, Berlin

[10] VDI 3861 /2 (1996) Measurement of Inorganic Fibrous Particles in Flowing Clean Exhaust Gas; Scanning Electron Microscopy Method,*VDI-Handbuch Reinhaltung der Luft* Band 4; Beuth Verlag, Berlin

[11] Zebel, G; Hochrainer, D.; Boose, Chr. (1977) A Sampling Method with Separated Deposition of Airborne Fibers and other Particles, *J. Aerosol Sci.*, **8**, 205-213

Characterisation of Corona Aerosol Using an Electrical Aerosol Spectrometer

A.Mirme, P. Paris, Ü. Kikas, M. Laan and E. Tamm

University of Tartu, Tartu, Estonia

KEYWORDS

Corona discharge, Aerosol Spectrometry

INTRODUCTION

An electrical corona is a gas discharge in an inhomogeneous electric field. The ionisation and excitation are concentrated in a comparatively small volume (ionisation zone) near an electrode of small radius of curvature. The energy concentration is high in the ionisation zone and, due to the discharge-surface interaction, sputtering of the electrode material occurs. In the main part of the discharge gap (drift zone) a number of chemical reactions between the ionised/excited particles also takes place.

The corona may exist both in steady and pulsed mode. Due to the space charge fields some forms of pulsed discharge (streamers) may develop. These cross to the opposite electrode where they can also cause chemical reactions and sputtering.

In the case of a DC field a unipolar current prevails in the drift zone. It can be used directly in electric filters to charge aerosol particles. Electrical aerosol instrumentation often uses a corona discharge as a well-controlled source of ions (Whitby and Clark 1966, Keskinen *et al* 1992).

Chemical ion reactions in gaseous media (Luts and Salm 1994) may produce chemical compounds of unpredictable chemical and physical properties which may add to ambient air pollution. The full character of the processes is still not well known. Generation of aerosol particles by corona discharge is a commonly known phenomenon (Nolan and O'Toole 1959, Borra *et al* 1998). The conversion of gases to particles by corona discharge can be used to improve the cleaning efficiency of air filters and to control the pollution of ambient air (Hirsch and Oskam, 1990).

CORONA AEROSOL CHARACTERISATION

From the point of view of aerosol science the formation of aerosol particles by corona discharge is a particular case of particle nucleation.

The study of corona discharge may contribute significantly to the clarification of the processes of aerosol formation in general. Being at the frontier of the aerosol science, corona aerosol study provides a challenge in terms of the techniques used and the instrumentation.

The particle size of corona aerosol is at the lower limit of the size range of most aerosol instruments, where their performance is uncertain. The macroscopic physical properties of

particles may change in that range. The first question is what can be considered as a particle. If a particle is defined as a formation of molecules, that is able to grow by adsorbing vapour molecules from the media, an instrument basing on condensation of vapour to measure particles seems to be most suitable. A commercial instrument of that type is the ultrafine condensation particle counter (UCPC) by TSI, model 3025. The condensation principle has limitations at small particle sizes. An instrument of the lowest size limit - UCPC can count particles down to about 2 nm of size (Mäkelä *et al* 1996). However, the size limit is a little uncertain since condensation is sensitive to chemical composition, vapour supersaturation and other environmental parameters.

Characterisation of corona aerosol by total number count is of limited use in the study of corona aerosol and from measurement point of view. The actual size of particles may be at the edge of the measurement range and the observed effects may be caused merely by the variation of the counting efficiency of the instrument. That information can only be obtained if the particle size distribution is measured.

Instruments that measure aerosol particle size distribution (aerosol spectrometers) are often based on the dependence of particle drift velocity on particle size. Instruments most commonly used in the range of particle sizes below 500 nanometers use electrical phenomena. They classify the charged aerosol particles according to the size by their mobility in an electric field (differentiation by electrical mobility, e.g. Fuchs 1963). A range of differential mobility particle-sizing instruments is produced commercially by TSI (DMPS, UDMPS, SMPS). In these the classified particles are usually detected with condensation particle counters.

The aerosol is exposed to a well-defined ion environment (usually a radioactive neutraliser) before classification. The charging process has been well studied (e.g. Fuchs 1963, Noppel 1983, Pui *et al.* 1988), so the charge distribution is known. The charged fraction of aerosol is a monotonic function of particle size, which is almost independent of other particle properties in that size range. The charging continues down to the size of molecular clusters (below 1 nm) and therefore there is virtually no lower limit to the range of aerosol particles amenable to this measurement technique.

The limitation of the size range imposed by the use of the CPC can be avoided if the electrical charge of the particles is measured instead. The Electrical Aerosol Analyser (EAA by TSI Model 3030) was such an instrument. In contrast to condensation by CPC the electrical detector (Aerosol Electrometer, AE) measures the flux of electric charge carried by particles and is dependent neither on particle size nor on environmental conditions. However the reduced sensitivity of the AE may limit minimal measurable concentration of aerosol.

THE ELECTRICAL AEROSOL SPECTROMETER OF TARTU UNIVERSITY

The University of Tartu, Estonia, has a long tradition of measuring natural atmospheric ions. The experience of ion measurement was applied to the development of an Electrical Aerosol Spectrometer (EAS, Mirme *et al.* 1984, Mirme 1994, Kikas *et al.*1996). The EAS is robust in operation. It can work in ambient conditions for many months continuously without human assistance. With some modification the size range can be extended down to 1.8 nm particle diameter.

Table 1. Technical data of EAS

Operation principle	Full electrical, full parallel, real-time
Particle size range	From 3 nm to 10 μm of particle diameter
Size resolution	4 (up to 8) fractions per decade of particle size
Time resolution	4 second-mean distribution of aerosol of full size range
Aerosol requirement	800 cm^3 per second
Concentration range, (particles per cm^3)	100 to 10^6 at 10 nm size 0.01 to 100 at 10 μm size
Duration of operation In field	Unlimited (six month in ambient downtown conditions)

EAS DESCRIPTION

The EAS utilises an electrical measurement principle. The principle consists of three steps: particle charging, classification and detection. All three steps are made electrically.

Aerosol is introduced into an electrical charger where the particles are exposed to air ions. In this way particles acquire a certain distribution of electrical charges defined by the conditions in the charger. The EAS uses unipolar ions produced by a point-to-cylinder corona discharge.

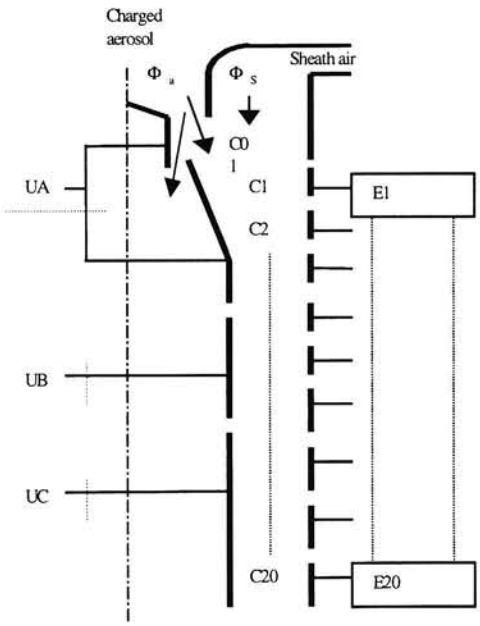

Figure 1. Design of a mobility analyser of EAS.

The charged aerosol is introduced into a cylindrical electrical mobility analyser a schematic of which is presented in Figure 1.

Aerosol, (Φ_a), enters in the form of a coaxial layer around the axial electrode which is biased to a high voltage (UA, UB, UC). The aerosol is surrounded by clean sheath air (Φ_S). The outer electrode consists of a number of cylindrical sections (C1 to C20). The particles are classified in the electric field as the gas passes axially through the system. Those with the highest mobility reach the first section of the outer electrode, the slower ones

to next and so on.

The detection of particles is also performed electrically. Each section of the outer electrode is connected to an extremely sensitive amplifier (electrometers E1 to E20, Fig. 1). A charged particle sticking to a section induces an electric charge in an electrometer equal to the charge carried by the particle. Thus, the electric current of an electrometer is equal to the flux of the particle charge to the respective analyser section.

The EAS has two charging-classification-detection channels (D and E) which work in parallel. In D-channel the charging is performed primarily by thermal diffusion of ions (diffusion charging), so it is effective for small particles less than 0.5 μm. In E-channel the ions are moved by a strong electric field (field charging) and this is effective for large particles greater than about 0.3 μm.

Readings from all electrometers provide an instrument record representing the aerosol particle size distribution via the charged particle electrical mobility distribution. The record is transformed to the size distribution using special mathematical procedures.

The EAS is constructed in such a way that it has proved to be very suitable for long term ambient aerosol monitoring. It does not pollute the environment, contains no consumable parts and needs only very little maintenance.

FEATURES OF THE EAS FOR CORONA AEROSOL STUDY

The EAS has several special features that make it suitable for corona aerosol study (Tamm *et al* 1992). Thanks to a high aerosol flow rate (Table 1) the residence time of particles in the EAS is less than one second - about 0.4 seconds for the smallest particles. That ensures small diffusion losses of particles so that even the ions of 1 nm equivalent size can pass to the analyser. Thus the lower size limit of the EAS is the size of the ions of the charger itself. The small residence time also prevents the formation of measurable secondary particles in the charger. The loss of high mobility particles at the inlet of the analyser is also reduced because there is a low electric field at the inlet (UA is usually below 100 V, Fig. 1). Additionally, the axial part of aerosol, (Φ_a), that might be contaminated by products of corona discharge, is removed at the inlet of the analyser and does not affect the analysis (Fig. 1). Because of simultaneous classification and measurement of all particle sizes the EAS needs only a few seconds for a single distribution measurement. Thus, it is possible to follow fast variations of aerosol distribution e.g. to study the process of filling the maturation volume by corona products (Borra *et al.* 1998).

CHARACTERISATION OF CORONA AEROSOL USING EAS

A study of aerosol formation by corona discharge was performed at Tartu University (Tamm *et al* 1992). The primary purpose was to get data about the possible side effect of corona discharge in nanometer size aerosol measurement. However, it was found that the corona aerosol can have well-controlled parameters and that it can be used as a nanometer size aerosol standard.

SETUP

The measurement set-up has a cylindrical construction (Fig. 2).

The corona discharge was of point-to-cylinder type created by a high voltage biased needle on the axis of a 2.4 cm diameter brass cylinder. The material of the needle was Sn,

although with the Fe and Pt needles the results were similar. The tip of the needle was sharpened to a curvature of less than 10 μm (not controlled).

The discharge was controlled by varying the high tension voltage (HV). The principal discharge parameter was the discharge current measured by a micro-ammeter. If the current is too high it becomes unstable so care was taken to avoid this condition. Thus we can be assured of a glow corona discharge.

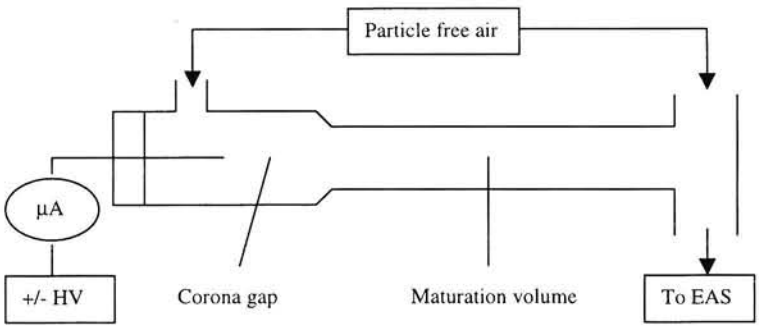

Figure 2. A schematic of corona aerosol study set-up.

The discharge medium was ordinary laboratory air cleaned from particles with an absolute filter. The chemical composition was not controlled. The relative humidity was not controlled but it was around 60%. The air from corona gap was introduced into a cylindrical relaxation chamber (maturation volume, Borra *et al.* 1998). Two configurations of maturation volume have been used.

In Configuration I the volume was 280 cm^3, in an aluminium cylinder of 2.4 cm diameter and 60 cm long.

In Configuration II the volume was 60 cm^3, in a plastic (PVC) cylinder of 0.8 cm diameter and 200 cm long.

The corona medium was diluted by clean air by a factor of 20 or more before the measurement. The dilution prevented changes in the aerosol size. This was confirmed by adding an extra volume with a residence time of about 3 minutes between the diluter and EAS. No change of particle size was registered. Thus all the results are presented for the outlet of the maturation volume.

Aerosol was studied as a function of the following parameters:
corona discharge current,
corona polarity,
air flow via discharge gap and
maturation volume configuration.

The particle number concentration, geometric mean diameter and the geometric standard deviation of the aerosol at the outlet of the maturation volume were measured. This information was used to calculate the number of particles produced per second (particle productivity). The maturation time, i.e. residence time in the maturation volume, was also calculated.

The relative humidity (RH) effect was studied in another experiment (Paris *et al.* 1998). The set-up was similar to that in Figure 2. However the geometrical sizes were larger (the diameter of the cylinder was 6.9 cm) and a streamer corona was used. Here we present the results when the RH was varied over the range from 3 to 90%. None of the other parameters were changed.

RESULTS

The aerosol particles at the outlet of the maturation volume carried almost no electric charge. The particle size distribution appeared to be quite narrow (the geometric standard deviation 1.2-1.3). The other two distribution parameters, mean particle diameter and concentration, were clearly dependent on the parameters of the set-up. The mean particle size varied from below the lower size limit of EAS to 20 nm with increasing corona current and decreasing air flow. The measured concentrations dropped when the distribution shifted beyond the EAS measurement range (smaller than 1.8 nm particle diameter). No threshold effect of particle formation was observed.

After each change of experiment parameters a few minutes were needed to achieve a stable aerosol distribution. This transient, due the residence time distribution in the maturation zone, was not studied in detail.

The effects of maturation time and discharge current on particle production are clear. For negative corona the particle production appears to be proportional to corona current and independent of maturation time (Fig. 3). The proportionality coefficient is not very different for different configurations (Fig. 4).

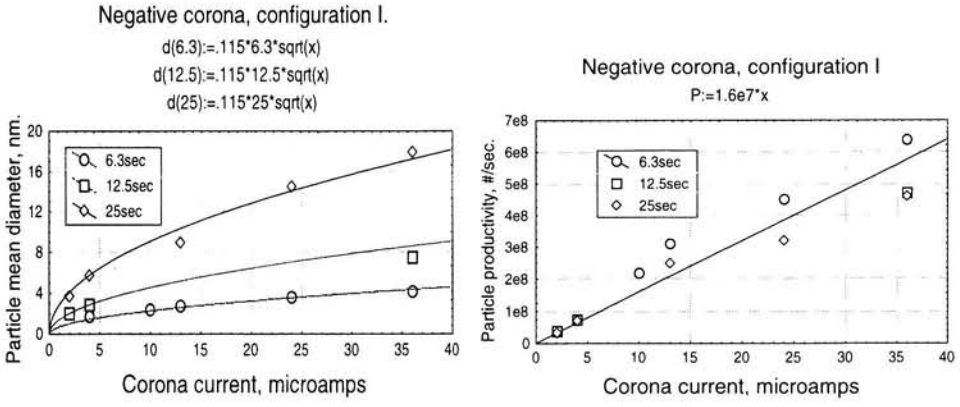

Figure 3. Mean diameter (left) and productivity (right) of particles by a negative corona with the maturation times of 6.3, 12.5 and 25 sec. Configuration I.

The mean particle size seems to be a linear function of maturation time and follows a square root function of corona current for both configurations. However the proportionality constants differ nearly a factor of four.

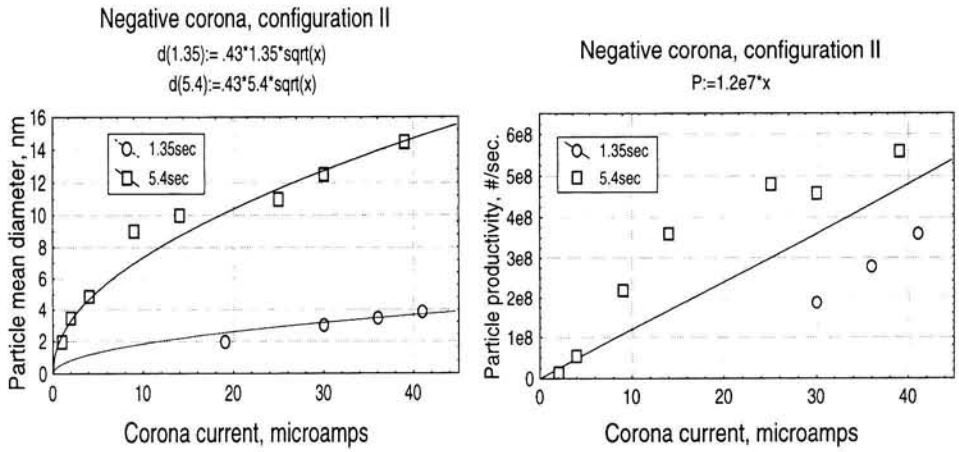

Figure 4. Mean diameter (left) and productivity (right) of particles by a negative corona with maturation times of 1.35 and 5.4 sec. Configuration II.

Positive corona was studied for configuration II. For this case the mean particle size was a linear function of corona current (Fig. 5). The productivity was proportional to the square of corona current.

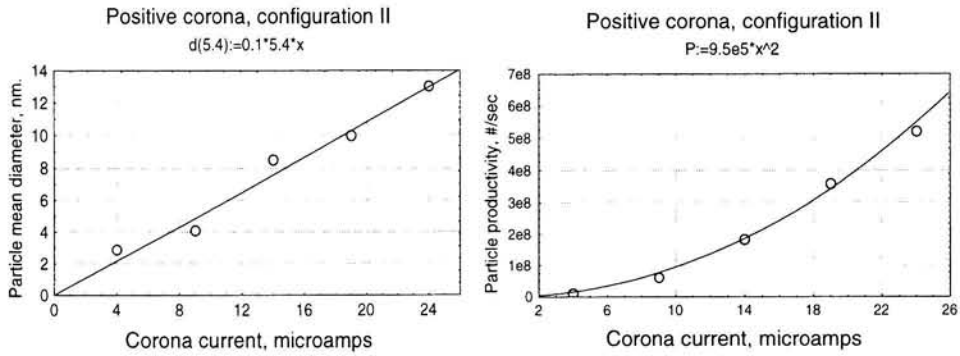

Figure 5. Mean diameter (left) and productivity (right) of particles by a positive corona with a maturation time 5.4 sec. Configuration II.

The humidity seems to have a tremendous effect on aerosol production (Fig. 6).

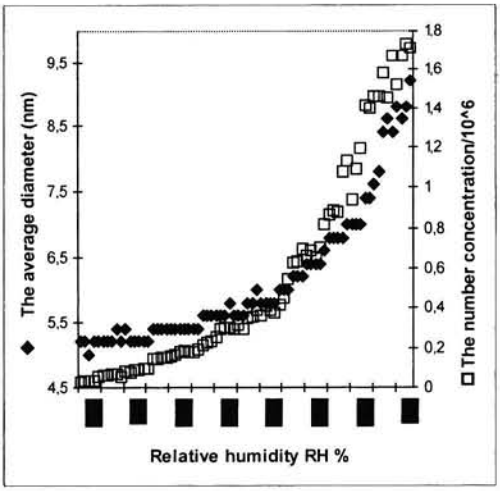

Figure 6. Variation of particle size (left) and concentration (right) with relative humidity.

DISCUSSION

Considering the possible aerosol generation processes, it seems that the particle nuclei are initially formed in the corona gap. The efficiency of nuclei production increases with corona current. Since the negative corona current consists of a series of pulses of constant shape the increase of the current is achieved by an increase of the frequency of pulses, which explains why particle production is proportional to corona current (Fig. 3 and 4). The initial size of the nuclei seems to be small, possibly much smaller than 1.8 nm.

The particles are formed by a condensation process. That is justified by the narrow size distribution, typical for condensation. A competing, coagulation process can be rejected because that would need higher particle concentrations to be effective, also that would lead to a fall of particle concentration with time.

The particle growth results can be explained if it is assumed that the production of condensing vapour is proportional to the production of nuclei, i.e. proportional to corona current in a negative corona and proportional to the square of current in a positive corona. Furthermore, for a given maturation time and particle productivity, the particle sizes also seem to agree between positive and negative coronas (Fig. 4 and 5). That may indicate that the nuclei-to-vapour ratio does not depend on the polarity of the corona (in Tamm *et al.*, 1992 there is a misprint in Table 2C).

The above explanation of the particle formation results requires, however, that the vapour concentration is maintained constant during maturation. That is not possible with normal vapour molecules that should diffuse to the walls of the volume quickly. It may be explained if vapour is created during the maturation (ageing) process by some chemical reaction.

Particle formation depends very strongly on relative humidity. The increase of size with humidity may indicate that the particles adsorb water very well as if they are fully hygroscopic (Fig. 6). However, the parallel increase of particle number concentration is obvious and indicates a direct effect of humidity on particle nucleation in the corona gap.

CONCLUSIONS

Corona discharge is a phenomenon that is not yet fully understood. In particular, the conversion of substances to aerosol particles is a phenomenon that requires further investigation. The electrical aerosol spectrometer facilitates the study of the physics of such corona aerosol formation.

The generation of corona aerosol appears to depend on discharge current, the maturation (ageing) time and relative humidity. However, the results presented here are from a particular study only. Validation by further work incorporating chemical composition analysis is required.

REFERENCES

Borra, J.P., Goldman, A., Goldman, M. and Boulaud, D. (1998) Electrical discharge regimes and aerosol production in point-to-plane DC high-pressure cold plasmas: aerosol production by electrical discharges. *J. Aerosol Sci.* **29**, No. 5/6, pp. 661-674.

Fuchs, N.A. (1963) *Geofis., Pura Appl.* **56**: 185-193.

Hirsch, M.N. and Oskam, H.J. (1990) Gaseous Electronic-Electrical Discharges. Academic Press. New York.

Keskinen, J., Pietarinen, K. and Lehtimäki, M. (1992) Electrical low pressure impactor. *J. Aerosol Sci.* **23**, 353-360.

Kikas, Ü., Mirme, A. and Tamm, E. (1996) Statistical characteristics of aerosol in Baltic Sea region. *J. Geophysical Res.*, **101**, No. D14, pp. 19319-19327.

Luts, A. and Salm, J. (1994) Chemical composition of small atmospheric ions near the ground. *J. Geophysical Res.*, **99**, pp. 10781-10785.

Mirme, A., Noppel, M., Peil, I., Salm, J., Tamm, E. and Tammet, H. (1984) Multi-channel electric aerosol spectrometer. *In Eleventh Int. Conf. on Atmospheric Aerosols, Condensation and Ice Nuclei.* Budapest, **Vol. 2,** pp. 155-159.

Mirme (1994) Electric aerosol spectrometry. *Ph.D. Thesis*, University of Tartu.

Mäkelä, J.M., Mavliev, R. and Jokinen, V. (1996) On the detection efficiency of ultrafine condensation particle counter (UCPC, TSI Model 3025) below 3 nm. *Proceedings of 14th Conf. on Nucleation and atmospheric aerosols*, pp. 643-646.

Nolan, P. and O'Toole (1959) The condensation nuclei produced by point-discharge. *Geofis. Pura Appl.* **42**, pp.117-126.

Noppel, M.G. (1983) About charge distribution of aerosol particles charged with unipolar small air ions. *Acta et Comm.* Univ. Tartuensis, No.648, p. 32-40.

Paris, P., Mirme, A. and Laan, M. (1998) Study of corona discharge aerosol with an electrical aerosol spectrometer. *J. Aerosol Sci.* **29**, S845-S846.

Pui, D.Y.U., Fruin, S. and McMurry, P.H. (1988) Unipolar diffusion charging of ultrafine particles. *Aerosol Science and Technology*, **8**: 173-187.

Tamm, E., Mirme, A. and Kikas. Ü. (1992) Corona discharge as a generator of nanometer-range monodisperse aerosol. Acta et commentations Universitatis Tartuensis, No.947, Air ions and electrical aerosol analysis, pp. 80-88. Translated from Acta et commentations Universitatis Tartuensis, No.824, pp. 123-131.

Whitby, K.T. and Clark, W.E. (1966) Electrical aerosol particle counting and size distribution measuring system for the 0.015-0.1μ range. *Tellus* **18**, p.573.

Methods of Surface Modification of Polymer Products

Wojciech Fabianowski
Department of Chemistry, Warsaw University of Technology,
Noakowskiego 3, 00 664 Warsaw, Poland

KEYWORDS
surface modification, grafting, IPN system, monolayer, multilayers, contact angle

ABSTRACT
Physical and chemical methods of modifying polymeric materials used as membranes are briefly presented. Special stress is placed on the construction of a dense, highly specific surface layer on an asymmetric porous membrane. Surface modifications by graft polymerization on a pre-sensitized surface, the creation of interpenetrating polymer networks and plasma treatment, especially operating under atmospheric pressure are discussed. Methods of surface modification by the deposition of a thin film of thickness less than 1 μm, using the Langmuir-Blodgett mechanism and self-assembly depositions are also described. Properties of tailor-made thin films are compared with natural biological barriers made from phospholipid bilayer. Methods of surface characterization of modified surfaces, especially by contact angle measurements (wettability) are discussed.

INTRODUCTION
In real life we work with mixtures of different materials - liquids, solids, gases. Therefore separation and purification of them is a fundamental problem. Chemistry has developed numerous methods, some of them very elaborated, for purification of materials – *e.g.* distillation, crystallization, phase melting, extraction. All have one thing in common - these methods require high temperatures (or energy input) or aggressive, hydrophobic solvents. On the other hand nature does an excellent separation job at relatively low room, or body, temperature from water based solutions. The mystery of this separation is in the membrane construction, cell bilayer structure. Therefore this is the target of membrane research - to construct highly selective, highly efficient membranes operating at room temperatures from water solutions. From the broad research already performed in membrane processes [1, 2], it can be concluded that research at the present time makes use of existing porous base materials (*e.g.* polypropylene, polycarbonate, polytetrafluoroethylene regenerated cellulose, polysilicone films) and modifies the surface to obtain a dense, highly selective surface skin-like layer [3].
Some methods for surface modifications like graft polymerization on a sensitized surface, plasma treatment and methods for the characterization of surfaces especially by the contact angle measurements (surface wettability) are presented.

PHYSICAL MODIFICATION OF BASE POLYMERIC MATERIALS
The main task of membrane films is to yield elastic but mechanically strong thin support films. The chemical inertness and low resistance to fluid flow should also characterize this reproducible porous structure support which should be obtained at relatively low cost. Celgard® [4, 5] a microporous semicrystalline oriented polypropylene film typifies these requirements. Special polysilicone films (poly[1-(trimethylsilyl)-1-propyne] PTMSP [6]), or

the recently developed Anopore® membranes made from heat and solvent resistant alumina [7] are also available. From the numerous surface modification techniques available two will be discussed in this paper.

Graft polymerization from a pre-sensitized surface is a relatively simple technique resulting in dramatic changes to both surface and permeation character and as such is of considerable importance. Some new and interesting sensitization methods are discussed such as:

a) plasma discharges operating under atmospheric pressure [8];
b) the attachment of an initiator on the surface as a monolayer for free-radical or atom transfer radical polymerization process [9, 10]

But grafting process, as all chemical processes, suffer drawbacks - the presence of solvents, the activation process, contamination of product with homopolymer and ungrafted polymer *etc*. These problems can be partially overcome using the method developed by L. Sperling [11] – the concept of the Interpenetrating Polymer Network. In this relatively simple method a polymer surface can be modified by the *in situ* creation of an additional cross-linked polymer without creating direct polymer bonds between the support membrane and the modifying polymer.

Another method for surface modification, that is still to receive acceptance on a technological level, is discussed here. This method is based on the deposition, on the surface of the support layer, of a thin film, thickness considerably less than 1 μm, composed of polymer multilayers mimicking natural cell membrane bilayer, with embedded "smart molecules" acting as selective channels or carrier molecules. This method, especially when associated with fine organic chemicals separation, hemodialysis and body fluids treatment, [12] shows considerable promise for the future because of its similarity with natural membranes

Some methods for surface characterization with contact angle are also discussed.

GRAFT POLYMERIZATION AND IPN SYSTEMS

In the grafting process side polymer chains are chemically bonded to the main chain of an existing polymer. Usually a support polymer membrane comprising of a hydrophobic polymer is grafted with a hydrophilic monomer resulting in surface modification with increased wettability in aqueous conditions.

By grafting from a pre-sensitized surface the process starts from radicals or other initiator species formed on the backbone of the main polymer chain in contrast to conventional graft polymerization where chains are polymerized in solution and grafting proceeds through active spots on the main polymer chain [9].

In conventional graft systems the thickness of grafted polymer is limited to 1 - 5 nm, since active spots are fast covered with grafted chains and therefore access to active spots is stopped. There is no such a limitation when grafting from a pre-sensitized system since growth proceeds through "living radical polymerization" yielding grafted chains with controlled thickness and polydispersity close to unity [9, 10].

Grafting reaction is characterized by weight gain Δm and grafting efficiency GE calculated as follows:

$$\Delta m = m_2 - m_1 / m_1 \times 100\%$$
$$GE = m_3 - m_1 / m_2 - m_1 \times 100\%$$

where m_1, m_2, m_3 denote mass of the polymer before grafting, after grafting, after grafting and homopolymer extraction respectively. In the formula for GE, $m_2 - m_1$ may be replaced with the mass of monomer used [13].

The GE factor is very important in running the grafting reaction on a technological scale. To increase the GE value some process modifications are used, like performing grafting in the vapor phase of the monomer, reduction of $OH^{\cdot}$ radicals to OH^{-} anions by the Fe^{+2} cations and addition of cross-linking agents such as divinylbenzene, ethylene glycol dimethacrylate. The important issue is formation of active species at the polymer matrix surface. Usually ozone treatment, UV irradiation, high voltage corona discharges, or the more recently proposed surface monolayer with radical/dormant system for Atom Transfer Radical Polymerization (ATRP process) [9, 10], yield active spots. Often surface hydroperoxides, which after decomposition give free radicals attached to the surface. In this way the outer surface, or both surfaces, of the support membrane can be modified. An interesting method for the surface modification of curved surfaces, for example outer or inner surfaces of hollow tubes (catheters), was proposed by S. Okazaki [8]. A dielectric tube is coated with ring shaped high voltage electrodes, which are separated from ground electrodes. The assembly is then placed in a suitable gas mixture (helium) and a frequency over 1 MHz is applied when glow discharges activate the outer surface of the tube.

If the outer side of the tube is wrapped with a spiral high voltage electrode and on the inside of the tube there is a wire ground electrode, when the tube is filled with a helium, argon, nitrogen gas mixture, the inner side of the tube is then activated.

In our own research we have used this method for surface modification of catheters in the form of PCV tubes of 2 mm diameter. The outer side of the tube was filled with a helium/oxygen mixture (Fig. 1). After applying glow discharges for 2 - 5 minutes increased surface wettablity was observed. The contact angle of a water droplet deposited on the tube wall decreased from about 70^0 for an unmodified tube to about 45^0 for modified tubes subjected only to the APG discharges and 54^0 for tubes subjected to the APG discharges in the He/Tetraethoxysilane gas mixture [14].

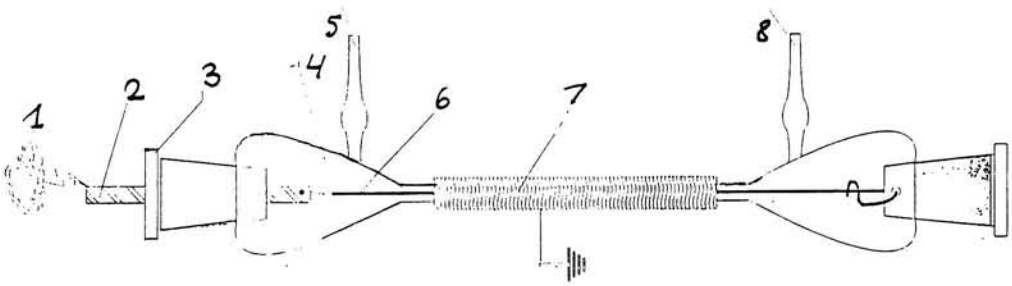

Figure 1. Scheme for APG process for the outer surface modification of catheter
1. high voltage; 2. metal rod-shape electrode; 3. PCV stopper; 4. glass tube (reactor); 5. gas inlet; 6. catheter (with metal electrode inside); 7. copper screen (grounded), 8. gas outlet

L. Sperling [11] proposed an elegant method of polymer modification, as an alternative for graft co-polymerization or polymer blending. If an existing polymer network (A) is swollen by a monomer (B) and a small amount of cross-linking agent (B_1) is added, running co-polymerization of (B) and (B_1) creates a network of polymer ($B\text{-}B_1$) which is finely dispersed in the matrix of polymer (A). In this way, due to the polymer chains entanglements, formation of loops and closed loops, these two polymers (A) and (B) cannot be extracted or separated by physical methods such as extraction with specific solvents, although there is no formation of direct chemical bonds between them. A so-called semi Interpenetrating Polymer Network (semi IPN) is created.
When two monomers (A) and (B) are mixed, with addition of cross-linking agents (A_1) and (B_1), after co-polymerization of ($A\text{-}A_1$) and for example poly-condensation of ($B\text{-}B_1$) systems a complete IPN system is produced. Thus for the surface modification of a porous membrane structure, monomer mixture in solvent which at least partly swells the polymer support a one step process giving a changed wettability with a high Δm and nearly 100% GE is achieved.

MONOLAYERS AND MULTILAYERS AS SEPARATING MEMBRANES

Natural cell walls, built from phospholipid bilayer strengthened with cytoskeleton and retractor proteins, yield not only a physical barrier separating the interior of the cell but also a very specific membrane. Selective and active transport of energetic and metabolic constituent signals to both the interior and exterior of the cell characterize these membranes. Therefore it is not surprising that cell wall construction is attracting considerable attention. Apart from the biologists, researchers involved in the technology of separation and working in the field of Langmuir-Blodgett Transfer, self-assembly thin film preparation, nanotechnology, and even electrochemists, are working with systems which mimic natural biological structures (for example neuron networks) [1, 13].
Membrane built from multilayers is characterized by high selectivity and can be used for the separation of optical isomers [14]. Even when there is a very thin film, in the range of a few nm, it has very good barrier properties. A monolayer built from alcohol molecules of a sufficiently long hydrocarbon chain *e.g.* 1-octadecanol, deposited at the water-air interface reduces the rate of water evaporation and can be used to preserve water in large natural lakes. The barrier properties of the monolayer deposited at the water-air interface are defined according to Langmuir as r - reduction of water evaporation rate [15, 16]:

$$r = A(c_w^{eq} - c_d^{eq})(V_m^{-1} - V_w^{-1})$$

where A - area of water surface
c_w^{eq}, c_d^{eq} - equilibrium water vapor pressure over water phase w and drying agent d hanging over water surface
V_m^{-1}, V_w^{-1} - rate of weight gain of drying agent hanging over water surface with or without spreaded monolayer

For the practical application of the transport properties of monolayers and multilayers several conditions must be fulfilled.
The multilayer must be selective towards the compounds to be separated and be sufficiently robust to withstand the envisaged environment. Therefore monolayer or multilayer, still a very thin and fragile film forming the active part of the membrane, should be deposited on a support membrane, which does not create a large restriction against the flow of solution.

Any restriction should be at least smaller than the restriction of the thin active film. Some of methods applied will be briefly characterized [3].
Membrane selectivity originates from special built in pores made from channel proteins such as cyclodextrines, calixarenes and mixed polyelectrolyte chains [17 - 23]. The mechanical strength of thin films can be increased by their polymerization [24 - 29] or the introduction of bolaamphiphilic compounds (long hydrocarbon chains terminated on both ends with two amphiphilic groups) [3, 30]. Due to cross-linking reaction permeation of ions and water is normally decreased [31 - 33]. Interesting transport phenomena originate from the insertion into the membrane forming bilayer or multilayer of so called "smart molecules" which trigger the transport through the membrane under the influence of a special impulse, such as pH change [34], electric potential change [35].
Numerous research works devoted to the field of Controlled Drug Release (CDR) [36, 37] pay special attention to the selectively triggered transport of molecules. In this work biologically or therapeutically active molecules are linked to a glicolipid of specific length or with two chains from poly(ethylene oxide) $(CH_2CH_2O)_6$ [38, 39]. The steric configuration of the molecules may reduce specific interactions with other cells, for example the use of erythrocyte molecules to prevent blood coagulation [12] or just opposite the selective intrusion into the cell wall following its perforation and the introduction of therapeutic compounds [40]. An example of such an action is the construction of the "umbrella like" molecule consisting of a rigid hydrophobic group, two hydrophilic polyamine groups and side polar groups. This shows strong antifungal activity similar to that of squalamine therefore enabling the destruction of infected cells [41].
Another consideration is the selection of a suitable base to support the thin membrane layer. Because the support cannot be more resistant to the solution flow than monolayer/multilayer system, the active thin films are normallly deposited by the Langmuir-Blodgett Transfer. Possible substrates are microporous teflon [42], Millipore filters [43], platinum screen [35] immobilized between two layers of cellulose acetate [44, 45], microporous polyamide capsule walls [46, 47], porous supports [48, 49] or plasma modified LBT multilayers deposited onto ceramic support made from Si_3N_4 [50]. These substrates are not ideal in that they offer poor properties for technological applications.
When bigger surfaces are used, the number of surface defects starts to be an important issue. The number of defects can be characterized by the measurement of membrane capacity [13]:

$$c_m = c_m^{o}\Theta + (1 - \Theta)c_d$$

where c_m, c_m^{o}, c_d - capacity of support with or without thin membrane layer (3 μF), capacity of defects (30 μF)

Θ - coverage degree of support surface by membrane, closer to the unity indicates higher coverage of support by membrane

A possible solution is the use of polysilicone as a support This was formed from poly[1-(trimethylsilyl)-1-propyne] $[(CH_3)_3SiC{=}C(CH_3)]_n$ which is characterized by a high permeability to gases [6]. On the polysilicone support four monolayers with calix[6]arenes were deposited using the LBT method. For comparitive purposes a copolymer of maleic anhydride-1-octadecane was also deposited. During the period of pressure rise, the membrane with calixarene modification showed higher selectivity of He/N_2 flow ratio (increase from 50 to 80), compared to the control membrane modified with copolymer which maintained the same selectivity ratio in the range of 7 to 6.5.

These results tend to suggest a comparative "easiness" of He flow compared to N_2 flow when higher pressure was applied, leading in turn to a rise in the selectivity ratio.
Research is currently aimed at different methods of surface modifications, such as immobilizing vesicles in the open pores of Nuclepore support membrane, "molecular valves" constructed from calixarenes "corked" with fullerenes C_{60} molecules.

CHARACTERIZATION OF SURFACE PROPERTIES BY CONTACT ANGLE MEASUREMENT

One of the most frequently used methods for the characterization of surface properties is that of contact angle measurement. Contact angle, defined by Young's law nearly 200 hundred years ago, can still be used to elicit new information [51-55].
In Figure 2 the shape of liquid L drop deposited on the surface of solid, S, in the presence of liquid vapor, V, is shown:

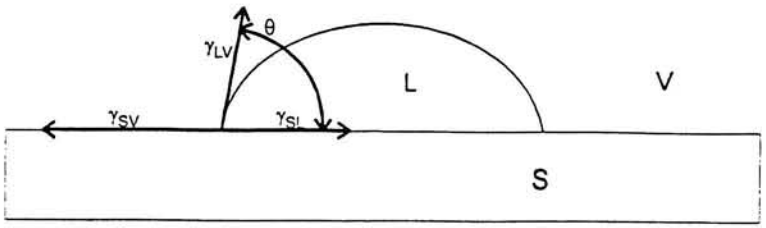

Figure 2. Contact angle Θ resulting from equilibrium between phases S/L/V

From the Young equation describing equilibrium surface energy states at the interphase of S/L/V it can be shown that:

$$\gamma_{SV} = \gamma_{SL} + \gamma_{LV}\cos\Theta \qquad (1)$$

Values of γ_{SV}, γ_{SL}, γ_{LV}, are respectively, surface free energies [mJm^{-2}] of solid S in contact with vapor V; solid S in contact with liquid L and liquid L in contact with vapor V.
In reality, $\gamma_{SV} = \gamma_S + \Pi_L$, where γ_S is surface free energy of solid and Π_L is pressure originating from adsorbed liquid at the surface of solid. The work of adhesion W_{ad} between solid phase S and liquid phase L is equal to the sum of surface free energies of both components less the interphase free energy at the interphase region S/L:

$$W_{ad} = \gamma_S + \gamma_L - \gamma_{SL} \qquad (2)$$

Introducing equation (1) in the form of $\gamma_{SV} = \gamma_{SL} + \gamma_{LV}\cos\Theta$
and assuming, that $\Pi_L \cong 0$; $\gamma_L = \gamma_{LV}$, it follows that

$$W_{ad} = \gamma_S + \gamma_L + \gamma_{SL} = \gamma_S + \gamma_L - \gamma_{SV} + \gamma_{LV}\cos\Theta = \gamma_L(1 + \cos\Theta) \qquad (3)$$

This equation is basic to the calculation of surface free energies of solids, polymers and to establishing surface compositions of copolymers of both hydrophilic and hydrophobic units [56-58]. In the latter case the Cassie equation can be applied[59]. The contact angles, Θ_1 and Θ_2 , for the separate components 1 and 2 respectively, are related to the contact angle Θ on copolymer with the following formula:

$$\cos\Theta = f_1\cos\Theta_1 + (1 - f_1)\cos\Theta_2 \qquad (4)$$

f_1 and f_2 are the fractional compositions of 1 and 2 on the surface.
In the case of measured values of contact angles for mixed monolayers and multilayers, according to Gee and Israelachvili [60] the Cassie equation should assume average geometric interactions, not simple linear additivity in the form of $W_{ad} = f_1W_1 + f_2W_2$ which is the basis of equation (4). Therefore in the case of monolayers and multilayers built from different amphiphilic compounds 1 and 2 the Cassie equation should be expressed as follows:

$$(1 + \cos\Theta)^2 = f_1(1 + \cos\Theta_1)^2 + (1 - f_1)(1 + \cos\Theta_2)^2 \qquad (5)$$

The volume of the deposited drop and therefore measured value of contact angle Θ depends on several factors [61, 62].
By slowly adding, using a syringe needle, new portions of liquid L to the already deposited drop one can see that a rapid change of measured contact angle value takes place once the threshold value (Θ_a) is crossed giving, what is called, an advancing contact angle value (Fig. 3). Similarly by removing small portions of liquid L from an already deposited drop one can see a diminishing value of measured Θ contact angle value up to the threshold value (Θ_r) - the receding contact angle value. After reaching the lowest Θ_r contact angle value a rapid change of surface covered with the liquid drop is again observed.
Additional information can be obtained from hysteresis measurements. Hysteresis defined as $\Theta_a - \Theta_r$, where Θ_a and Θ_r are respectively the advancing and receding contact angles (the highest value of contact angle measured after slow increase of deposited drop volume and the lowest value of contact angle measured after withdrawal of water from deposited water drop, respectively). Hysteresis is a measure of surface roughness, r, defined as the ratio between real surface area and geometric area [61, 62]. Hysteresis has been also attributed to the Acid-Base (A-B) interaction [63] at the liquid-solid surface interface region. Another advantage of contact angle measurements is their sensitivity to the A-B character of surfaces, which can be determined by the so-called three liquid probes method [64, 65]. Contact angle measurements are sensitive to chemical changes taking place at the solid surface within the distance of 5 C-C bonds in hydrocarbon chain (0.6 nm). When polar groups, formed during plasma modification or monolayer deposition on polymer surface, are available low contact angle values are measured (high wettability). When these polar groups are not available (they are buried in the rising substrate or hidden by being coated with hydrocarbon chains of longer molecules from another constituent of mixed monolayer) immediate changes in the contact angle values (increase of contact angle value, lower wettability) are observed [66, 67].

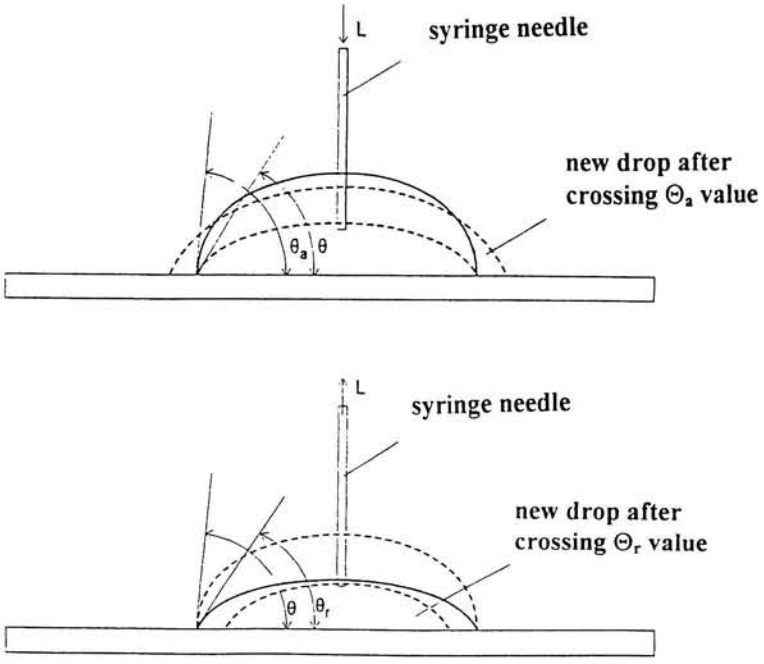

Figure 3. Advancing Θ_a and receding Θ_r contact angle values

CONCLUSIONS

Several methods of surface modification like grafting, IPN-systems, monolayer and multilayer deposition have been characterized. Of particular interest are surface modifications of porous support films with tailor-made multilayers deposited in a self-assembly procedure suitably modified with "smart" supramolecular compounds. These systems, mimicking natural membranes, should be characterized by permeation methods, and also by simple contact angle measurements which yield valuable information about modified surfaces.

ACKNOWLEDGEMENT

The author wishes to thank A. Elliot, The Technicon, Natal, South Africa, for valuable discussions in the preparation of this paper.

LITERATURE

1. Narębska Aet al., (1998) Membranes and membrane separation techniques, *supported by Tempus Project JEP-04720PL, Wydawnictwo Uniwersytetu Mikołaja Kopernika, Toruń.* (in Polish)
2. Narębska A, (1998) Membranes, in Chemistry of Polymers, vol. III, (ed. Z. Florjańczyk and S. Penczek), Oficyna Wydawnicza Politechniki Warszawskiej, 193-218 (in Polish)
3. Fabianowski W. (1997) *Polimery,* **42** 1-9 (in Polish)
4. US Patent 3,558,764 (Jan. 26, 1971) *Process for preparing microporous film*
US Patent 3,679,538 (July 25, 1972) *Novel open-celled microporous film*
GB Patent 1 287 504 (31 August 1972)

5.Takahara H. and Kawai H. (1968) *Jour. Soc. Fiber Science* and Process for producing microporous film *Techn. Japan*, **24** (1968) 311-322
Takahara H., Kawai H., Yamaguchi, Y. and Fukushima A. (1969) *ibid* **25** 60-72, and references cited
6. Lee W., Hendel R., Dedek P., Janout V. and Regen S. (1995) Jour. *Amer. Chem. Soc.*, **117,** 10599-10600.
7. ANOPORE Inorganic Membranes, Technical Bulletin #136, Alltech Associates, Inc
8. Okazaki S.and Kogoma M., (1993) *Jour. Photopolym. Sci. and Tech.,*. **6,** 339-342
9. Prucker O., Ruhe J. (1998) *Langmui,,r* **14,** 6893-6898
Husemann M., Hawker C., Hedrick J., Russell T., Malstrom E., Mate M., McNamara M., Mansky P. and Huang E., (1998) *Proceedings of MacroIUPAC Congress*, Brisbane 144
10. Matyjaszewski K., (1966) *Polym. Preprints,* **37,** 325-326
Patten T., Xia J., Abernathy J.and Matyjaszewski K., (1996) *ibid,* **37,** 575-576
Beers K., Gaynor S.and Matyjaszewski K., (1996) *ibdi,* **37,** 571-572
11. Sperling L., (1974) *Recent Advances in Polymer Blends, Grafts and Blocks, Polymer Science and Technology*, Plenum Press, New York, 4
12. Sackmann E., (1996) *Science*, **271,** 43-48
13. Bard A., (1994) *Integrated Chemical Systems, A Chemical Approach to Nanotechnology*, John Wiley & Sons Inc., Chichester, Brisbane, Toronto, Singapore
14. Aoki T., Shinohara K. and Ockara E., (1994), *MAKROAKRON'94, 35 IUPAC Int. Symp. Macrom.*, Akron, USA, 358
15. Barnes G., Gostin I., Hunter D. and Saylor J., (1980), *J. Inter. Sci.* **78,** 271
16. Barnes G. and Hunter D., (1990) *J. Coll. Inter. Sci.*, **136**, 198
17. Dreamer D. and Bramhall J., (1986) *Chem. Phys. Lipids,* **40,** 167
18. Kikuchi Y.and Kubota N., (1985) *Makromol. Rapid Comm.*, **6**, 387
19. Kunitake T., Tsuge A.and Takarabe K., (1985) *Polym. Jour.*, **17,** 633
20. Montal M., (1987) *J. Membr. Biol.*, **98,** 101
21. Ganhema H., Johansson G., Percec V.,and Möller M., (1994) *MAKROAKRON'94, 35 IUPAC Int. Symp,*. Macrom., Akron, USA, 383
22. Tsukruk V., (1994) *Langmui,* **10,** 996
23. Conner M., Janout V., Kudelka I., Dedek P., Zhu J.and Regen S., (1993) *Langmuir,* **9,** 2389
24. Laschewsky A., Ringsdorf H.and Schneider J., (1986) *Die Angew. Makr. Chem,*. **145/146**, 1
25. Laschewsky A., Ringsdorf H., Schmidt G. and Schneider G., (1987) *J. Am. Chem. Soc.,*. **109,** 788
26. Kock H., Laschewsky A., Ringsdorf H.and Teng K., (1986) *Makrom. Chem.*, **187,** 1843
27. Elbert R., Laschewsky A.and Ringsdorf H., (1985) Jour. Amer. Chem. Soc., **107,** 4134
28. Stefely J., Markowitz M.and Regen S., *J. Amer. Chem. Soc.*, **108,** 7789
29. Ariga Y.K.and Seki T., (1998) *J Amer. Chem. So.,*. **110,** 2495
30. Fuhrhop J.and Fritsch D., (1986) *Acc. Chem. Res.*, **19,** 130
31. Chung V.and Regen S., (1993) *Langmuir*, **9,** 1937
32. Dorn K., Klingbiel R., Specht D., Tyminski P., Ringsdorf H.and O'Brien T., (1984) *J. Amer. Chem. Soc,*. **106,** 1627
33. Drummond C., Elliot P., Furlong D.and Barnes G., (1992) *Thin Solid Films*, **210/211,** 69
34. Okahata Y., Noguchi H.and Seki T., (1987) *Macromol*, **20,** 15

35. Okahata Y., Maguchi K. and Seki T., (1985) *J. Chem. Soc. Chem. Comm,* **116,** 1122
36. *Controlled Drug Delivery: Fundamentals & Applications*, (ed. J. Robinson, W. Lee, Dekker), (1987) New York
37. *Controlled Drug Release of Drugs*, (1989) (ed. M. Rosoff), VCH Publishers, New York
38. Stadler E., Dedek P., Yamashita K. and Regen S., (1994) *J. Amer. Chem. Soc.*, **116,** 6677
39. Service R., (1994) *Science,* **265,** 316
40. Jayasurija N., Fabianowski W. and Regen S., (1989) *Biochem. Biophys. Res. Comm,* **159,** 566
41. Sadownik A., Deng G., Regen S., Bernard E., Kikuichi K. and Armstrong D., (1995) *J. Amer. Chem. Soc.*, **117,** 6138
42. Kaiyama T., Kumano A., Takeyanagi M. and Kunitake T., (1984*) Chem. Lett.*, **6,** 915
43. Hiroyama O., Tanaka N. and Kuroni Y., (1987) *Agric. Biol. Chem.*, **51,** 1203
44. Shimomura M. and Kunitake T., (1984) *Polym. J.*, **16,** 187
45. Higashi N. and Kunitake T., (1984) *ibid,* **16,** 583
46. Okahata Y., (1986) *Acc. Chem.Res.,* **19** 57
47. Okahata Y., Iizuka N. and Seki N., (1985) *J Chem. Soc. Perkins Trans. II* , **10,** 1591
48. Stroeve P., Vasquez V., Rabolt J. and Coelho M., (1995) *VII Int. Conf. Org. Molec. Films,* Numana, Italy, 123
49. Hoffmann D. and Ulss P., (1994) *MAKROAKRON'94, 35 IUPAC Int. Symp. Macrom.,* Akron, USA 1039
50. Messel V., Keil M., Petemple P., Terpstra R., Eijk J., Heijde M., Smid J., Festag R. and Vendorff J., (1995*) VII Intern. Conf. Org. Molec. Films*, Numana, Italy, 10599
51. *Surface and Interfacial Aspects of Biomedical Polymers*, vol. 1 *Surface Chemistry and Physics*, (ed. J. Andrade), (1985) Plenum Press, New York, London
52. Packham D.E., (1983) in *Adhesion Aspects of Polymeric Coatings*, (ed. K. L. Mittal), Plenum Press, New York, London 19
53. Janczuk B. and Bialopiotrowicz T., (1989) *J. Coll. Interf. Sci,.* **127,** 59
54. Janczuk B. and Bialopiotrowicz T., (1989) *J. Coll. Interf. Sci.,* **129,** 189
55. Lloyd T., (1994) *Coll. & Surf. A: Physicochem. & Ener. Asp.* **93,** 25
56. Kuczyński J., (1990*) Polimery - Tworzywa Wielkocząsteczkowe,* **35,** 219
57. Anastasiadis S., Chen J., Koberstein J., Sohn J. and Emerson J., (1986*) Pol. Eng. Sci.*, **26,** 1410
58. Lin F., Gardner D. and Wolcott M., (1995*) Langmuir,* **11,** 2674
59. Nakagawa O., Ashok S., Sheen C., Mărtenson J. and Allara J., (1991) *Japan Jour. Appl. Physics,* **30,** 3759
60. Israelachvili J. and Gee M., (1989) *Langmuir,* **5** 288
61. Ponter A. and Yektar-Fard M., (1985*) Coll. & Pol. Sci.*, **263** 673
62. Schwartz L. and Garoff S., (1985) *Langmui,r* **1,** 219
63. Lloyd T., private communication
64. Fowkes F., (1967) Chapter 8 in *Surface and Interfaces, I. Chemical and Physical Characteristics,* (ed. Burke J., Reed N. and Weiss V.), Syracuse University Press,
65. Janczuk B. and Zdziennicka A., (1993) *Indian J Techn.*, **31,** 136
66. Troughton E., Bain C., Whitesides G., Nuzzo R., Allara D. and Porter M., (1988) *Langmuir*, **4**, 365
67. Bain C., Evall J. and Whitesides G., (1989*) J. Amer. Chem. Soc.*, **111,** 7155

Electret filter Workshop

Discussion Session

Biodegradeable Filters

It is necessary to dispose of used filters so in the interests of environmental sustainability it would be desirable to recycle old filters or introduce the use of biodegradeable materials. This matter was the subject of an extended discussion, which was introduced by three speakers:

Dr. Ciach pointed out that the commonly used fibrous materials based on polypropylene persist in the environment and that the environmental impact associated with their disposal is therefor significant. Even if the filters are incinerated this will lead to a redistribution of the contamination. It is sensible therefor to consider the use of biodegradeable polymeric materials. Some materials are already available such as used in the manufacture of waste bags. The polymer could be treated to include cellulose and other blocks which would accelerate degradation. It would mean the introduction of a shelf life management systems for filters since degradation would start at the point of manufacture. Storage conditions would be important.

Professor Rokicki briefly described the polymer chemistry involved in the production of biodegradable fibres. Potentially there is a very wide range of materials to chose from. Selection of the most appropriate material, for both (electically assited) filtration effectiveness, and biogradeability, requires considerable research invesment.

A general discussion ensued. It will be necessary to describe and define the rate of degradation so that the shelf live, useable life and method of disposal can be specified. The method of initiating, or accelerating degradation, such as exposure to ultra-violet radiation, must also be specified. It may also be possible to use the loaded filters as fuel or recycle the material. The method of disposal used will depend on the specific application and especially on the potentially hazardous nature of the contaminant. The possibility of secondary pollution should be borne in mind. Media currently used has been developed over many years to provide excellent filtration properties. Less effective fibrous material will suffer from the disadvantage that more will have to be used to achieve the same result. This will diminish to some extent any environmental benefit from using degradable fibres. A life cycle analysis, which includes the energy used in manufacture, should be carried out on any proposal to ensure that a real benefit to the environment will result.

Aerosol charge level for standard testing

Aerosol charge obviously has a significant effect on penetration but this does not appear to be considered in standard test procedures. The question arises as to which charge level should be used in for example standard flat testing.

It was considered that in about 90% of aerosols encountered in practice are at the Boltzmann charge equilibrium. Coagulation aerosols have a lower charge than this and clean room

aerosols have been found to be less than the Boltzmann level. However most industrial aerosols have higher charges. More field work is required to further characterise aerosols and dust in a range of situations particularly with respect to charge.

It would at first sight seem reasonable and safest to specify the test aerosol charge to be equivalent to the worst case. However, in the case of respirable filters, flat testing under these conditions could lead to over specification of the media. This would increase the media resistance causing increased leakage and an overall reduction in performance. It is important to consider the end use and optimise on that. It is generally true that the work place protection factor is lower than that measured in the laboratory. Hence it is best that testing should be carried out under conditions which are as realistic as possible. Electret media deteriorates with loading. It should thus be tested over a range of loadings.

Penetration of very fine nanometre particles

It is well known that filter penetration falls with particle size as the diffusion coefficient increases rapidly. It is also clear that molecular species are not removed. There must therefor be some lower particle size limit where filters cease to be effective. Since the particle fibre collision efficiency is very high this limit must be associated with the ability of the particles to stick. Molecules are thrown from surfaces with an energy which is associated with the thermal translational energy of the surface. With larger particles this is not strong enough to overcome the London Van der Waal's energy and the particles are retained. The magnitude of the energies involved depend on the physical and chemical properties of the particle and substrate, so it is difficult to predict the limit. Certainly this is below any experimental sizes used in tests to date, (authors note: this matter is further dealt with in e.g.:

Kops J.A.A.M., Scholten L.C., Kema N.V., Deworm J.P. and Zeevaert T., Penetration of ultra-fine particles through HEPA filters. (1985) *Commission for European Communities, "Gaseous Effluent Treatment in Nuclear Installations", Conference held Luxemburg, 14-18 Oct.* pag. 73-85.

Wang H.C. and Kasper G. (1991) Filtration efficiency of nanometer-size particles. *J. Aerosol Sci.*, **22**, 31-42).

KEYWORD INDEX

LIST OF AUTHORS

ISBN: 90-407-1986-1

Delft University Press